Investigation of the molecular basis of symbiosis between *Epichloë festucae* and perennial ryegrass

---

A thesis presented in partial fulfillment of the requirements for the degree of

Doctor of Philosophy

In

Genetics

at Massey University, Palmerston North

New Zealand

Milena Mitić

2011

Abstract

The symbiosis between the endophytic filamentous fungus *Epichloë festucae* and its plant host, perennial ryegrass (*Lolium perenne*), is a highly regulated mutualistic interaction which represents a good model system for the investigation of plant-fungal mutualism. Fungal signalling pathways play a crucial role in regulation of this interaction. While genes involved in the production of reactive oxygen species (ROS), as well as a member of the MAP kinase signalling pathway, have been shown to regulate maintenance of the mutualistic interaction, the signalling pathways responsible for regulation of this symbiosis are still relatively poorly understood.

In pathogenic fungi, members of calcium signalling pathways, such as Ca^{2+}/calmodulin-regulated kinases (CaMKs) and phosphatase (calcineurin), are required for normal host-pathogen interactions. Three genes encoding multifunctional CaMKs, *cmkA*, *cmkB* and *cmkC*, were identified in *E. festucae*, as well as one gene encoding the catalytic subunit of calcineurin, *cnaA*. Targeted replacements of these genes have identified a novel role for the fungal *cmkB* in the regulation of ion homeostasis and an important role for calcineurin for both culture growth and symbiosis maintenance. However, unlike the pathogenic fungi, *E. festucae* CaMKs do not appear to have a role in the regulation of the mutualistic interaction.

In order to identify new genes regulating the symbiosis, T-DNA mutagenesis was used to generate symbiotically defective *E. festucae* mutants. Two mutants, Ag51 and Ag212, with both in culture and *in planta* phenotypes, were identified. A detailed molecular analysis showed that Ag51 had a complex T-DNA insertion while Ag212 had a deletion of ten genes. Ag212 failed to establish plant infection and complementation experiments using cosmids identified candidate genes for both the in culture and *in planta* phenotype. Analysis of the colonization process showed that this mutant is defective in establishing a specific interaction between hyphal and plant cell walls, essential for the plant colonization.

This work provides new insights into calcium signalling in fungi and increases our understanding of plant-fungal mutualism.

Acknowledgments

Firstly, I want to thank my supervisor Barry Scott. When I look back on this PhD, to all tough times, all weird or no results years – I honestly believe you were the best supervisor I could imagine. Sometimes, when things were going very, very badly, your guidance, experience and reassurance were the only anchors I was holding onto. Thank you for that. To my co-supervisor Jasna Rakonjac, thank you for providing the "out-of-the-field" view of my work and special thanks for your help when I had just arrived to New Zealand and had no idea of how everything works here.

I am grateful for the funding that made this project possible. It was founded through Marsden Grant by the Royal Society of New Zealand with additional funding from the Lincoln Bioprotection CoRE.

Thank you, to people who, through their work, provided support to this project. Thanks to Chris Schardl for providing the *E. festucae* 2368 genome sequence. Thanks to Mike Christensen, Anouck de Bonth and Wayne Simpson from the AgResearch, for looking after my plants and always helping with a good advice. Thanks to people from the Manawatu Microscopy and Imaging Centre for their help with the microscopy part of the project. Special thanks to Doug and Jianyu for being helpful and patient with my difficult TEM samples. The big 'Thank you' to Murray Cox for his help with bioinformatics and for the fantastic work on the cosmid sequence assembly.

To past and present members of the Scottbase lab – I cannot thank you enough for your help and friendship. To Michelle and Ruth, special thanks for your help with the experimental work in the very beginning of my PhD. To Yvonne, Matthias, Matt, Aiko, Sanjay, Kim, Sarah – thank you for listening to me about my experiments and results, and for your advice and suggestions. To Carla, Emma, Gemma, Daniel – thank for your help in the lab, but above all, thank you for being there when I just needed someone to listen to my complaints about how things are going.

To everyone at IMBS who was there when I needed advice or technical help – thank you.

Thanks to Kezia for providing the non-scientific feedback on this thesis.

There are many people who haven't been involved in this project but without whom it would still be impossible for it to happen. To my Mum Zorica, thank you for making me who I am, for supporting me to be who I am and for being happy for me to be who I am (and I know none of this is easy). Thank you for always supporting my choices, from being one of the few who supported my choice of a 'risky' university degree, to supporting my decision to leave for the other side of the world. To my brother Marko, well, thank you for somehow, suddenly, growing up and becoming someone I can talk to about the life, the universe and everything. I have to admit I have no idea how that happened but I'm glad it happened ☺. To my best friend Milena – Misho, it would take too long to thank you for everything I would need to, so you'll have to take just one, general "thank you". Sadly, some people are not with us any more, but I will carry their influence with me for the rest of my life. To a remarkable woman, my grandmother Radica Milenković, thank you for being who you were in a place were it was not easy and for inspiring me in my very young years to pursue my views of life. To Mihajlo Miša Elezović, thank you for your immense support during my undergrad years and during my move to NZ. I wish you were here to see the result and I know you would've been proud.

John, thank you for everything.

Contents

List of figures

List of tables

Abbreviations

A	Adenine
Amp^R	Ampicillin resistant
AMT	Agrobacterium mediated transformation
ATP	Adenine triphosphate
BLAST	Basic local alignment search tool
BLASTN	Nucleotide database search using a nucleotide query
BLASTP	Protein database search using a protein query
BLASTX	Protein database search using a translated nucleotide query
bp	Base pair(s)
BSA	Bovine serum albumin
Ca^{2+}/CaM	Ca^{2+}/calmodulin
CaMK	Ca^{2+}/calmodulin-dependent kinase, protein
CaMKK	Ca^{2+}/calmodulin-dependent kinase kinase
cmk	Ca^{2+}/calmodulin-dependent kinase, gene
cDNA	Complementary DNA
CDS	Coding sequence
CIAP	Calf intestinal alkaline phosphatase
DAB	3-3'Diaminobenzidine
DAG	Diacylglycerol
DIC	Differential interference contrast
DMSO	Dimethyl sulfoxide
dNTP	Deoxynucleotide triphosphate
EC	Ectopic
EGFP	Enhanced GFP
EGTA	Ethylene glycol tetraacetic acid
FGI	Fungal Genome Initiative
Gen^R	Geneticin resistant
GFP	Green fluorescent protein
GPCR	G protein-coupled receptor
HR	Hypersensitive response
Hyg^R	Hygromycin resistant

IM	Induction medium
ip	inoculation point
IP3	Inositol trisphosphate
Kan^R	Kanamycin resistant
Kb	Kilobases
KO	Knock-out
LB	Luria-Bertaini medium
LB	T-DNA left border
MAPK	Mitogen activated protein kinase
Mb	Megabases
mRNA	Messenger ribonucleic acid
NADPH	Nicotinamide adenine dinucleotide phosphate (reduced form)
NBT	Nitroblue tetrazolium
NCBI	National centre for biotechnology information
Nox	NADPH oxidase
PCR	Polymerase chain reaction
PD	Potato dextrose
Phl^R	Phleomycin resistant
PKC	Protein kinase C
PLC	Phospholipase C
RB	T-DNA right border
REMI	Restriction enzyme mediated integration
RG	Regeneration medium
RNA	Ribonucleic acid
ROS	Reactive oxygen species
rpm	Revolutions per minute
RT	Room temperature
RT	Reverse transcriptase
RT-PCR	Reverse transcriptase-polymerase chain reaction
SAM	Shoot apical meristem
TAIL-PCR	Thermal asymmetric interlaced-polymerase chain reaction
TBLASTN	Translated nucleotide database search using a protein query
T-DNA	Transfer DNA
TEM	Transmission electron microscopy

tRNA	Transfer RNA
WA	Water agar
WT	Wild-type
w/v	Weight/volume ratio

1. Introduction

1.1. Symbiotic associations of plants and fungi

The associations between fungi and plants are of great ecological and evolutionary significance. Most of the plants in natural ecosystems are involved in some kind of interaction with fungal species. These interactions range from antagonism to mutualism and some are of great importance from an economical aspect since they involve plants used in agriculture. One of the best studied plant-fungal interactions is the association between plants and mycorrhizal fungi. Mycorrhiza are mutualistic associations between fungi (*Glomeromycota*) and underground tissues of plants, where fungal hyphae form various types of interactions with plant roots. In this mutualistic association the fungus increases the host supply of water and nutrients while being provided with plant-fixed carbon (Parniske, 2008). About 90% of terrestrial plants, including crop plants, belong to families that form mycorrhizal associations (Buscot *et al.*, 2000). Other fungi form antagonistic associations with plants, some of which are being extensively studied since they involve major pathogens of crop plants. Based on whether they feed on living or dead plant tissue, plant pathogens are classified as biotrophs, hemibiotrophs or necrotrophs. Biotrophs feed on living tissue and rather than killing host cells they establish a feeding relationship, employing specialized structures like haustoria (Perfect & Green, 2008). The stem rust fungus, *Puccinia graminis*, is an obligate biotroph inducing disease in wheat, barley, oat and rye (Leonard & Szabo, 2005). Hemibiotrophs start their life cycle as biotrophs, by growing on living plant tissue, but will continue to grow and feed once the tissue has died, thus establishing sequentially biotrophic and necrotrophic or saprobic stages. *Colletotrichum* species represent important hemibiotrophic pathogens of food crops (Munch *et al.*, 2008). Necrotrophic fungi kill living tissue and feed on dead plant tissue. Therefore, they have evolved a variety of toxins and enzymes able to induce host death. The grey mold fungus, *Botrytis cinerea*, is a nectrotroph that induces host death using toxins, production of reactive oxygen species (ROS) and induction of host-produced oxidative burst (Choquer *et al.*, 2007).

Filamentous fungi called endophytes form associations with plants where fungal hyphae grow in the intercellular spaces of plant aerial organs, without penetrating or causing any damage to neighbouring plant cells. Symbiotic associations between the endophytes of *Epichloë* and *Neotyphodium* species and cool season grasses (family Poaceae) are

one of the most important ecologically and economically plant-fungal associations (Scott & Schardl, 1993, Schardl, 2001).

1.2. Plant-endophytes association

Epichloë endophytes belong to the family Clavicipitaceae, phylum *Ascomycota*. The type of symbiotic association that epichloë endophytes have with their grass host depends on the endophyte mechanism of transmission and the associations range from antagonistic to mutualistic. These systems provide a good opportunity to study evolution of mutualistic symbiosis between plants and fungi (Schardl, 1996).

1.2.1. Endophyte lifecycle and associations with plants

The type of association that epichloë endophytes have with the grass host depends on the means by which the fungus reproduces. These endophytes are taxonomically classified into two main groups: the genus *Epichloë*, which includes species able to reproduce both sexually and asexually, and the genus *Neotyphodium*, which includes strictly asexual species (Glenn *et al.*, 1996) (Fig 1.1). The asexual life cycle leads to vertical transmission of the fungus, where the fungus is transmitted by colonization of the seeds of the host plant, following hyphal invasion during floral development. In this case, no damage is caused to the host and the fungus is transmitted to the next plant generation. The sexual life cycle culminates in horizontal transmission. The fungal hyphae switch to epiphytic growth, forming a stroma around the flag leaf of the developing inflorescence. This causes abortion of inflorescence development, a disease known as “choke” (Schardl, 2001). In nature the sexual cycle is facilitated by *Botanophila* flies which transfer spermatia between the stroma of two mating types, allowing mating and spore formation (Bultman *et al.*, 1995). Spores generated on mature stromata are ejected and land on the surface of the grass floret where they germinate and colonize the ovules and seeds, resulting in the vertical transmission of the fungus (Schardl, 2001). As a consequence of their mode of transmission, those species that undergo the sexual life cycle and horizontal transmission will exhibit antagonistic interactions with plants, and, conversely, species that have only asexual reproduction will form mutualistic symbiotic

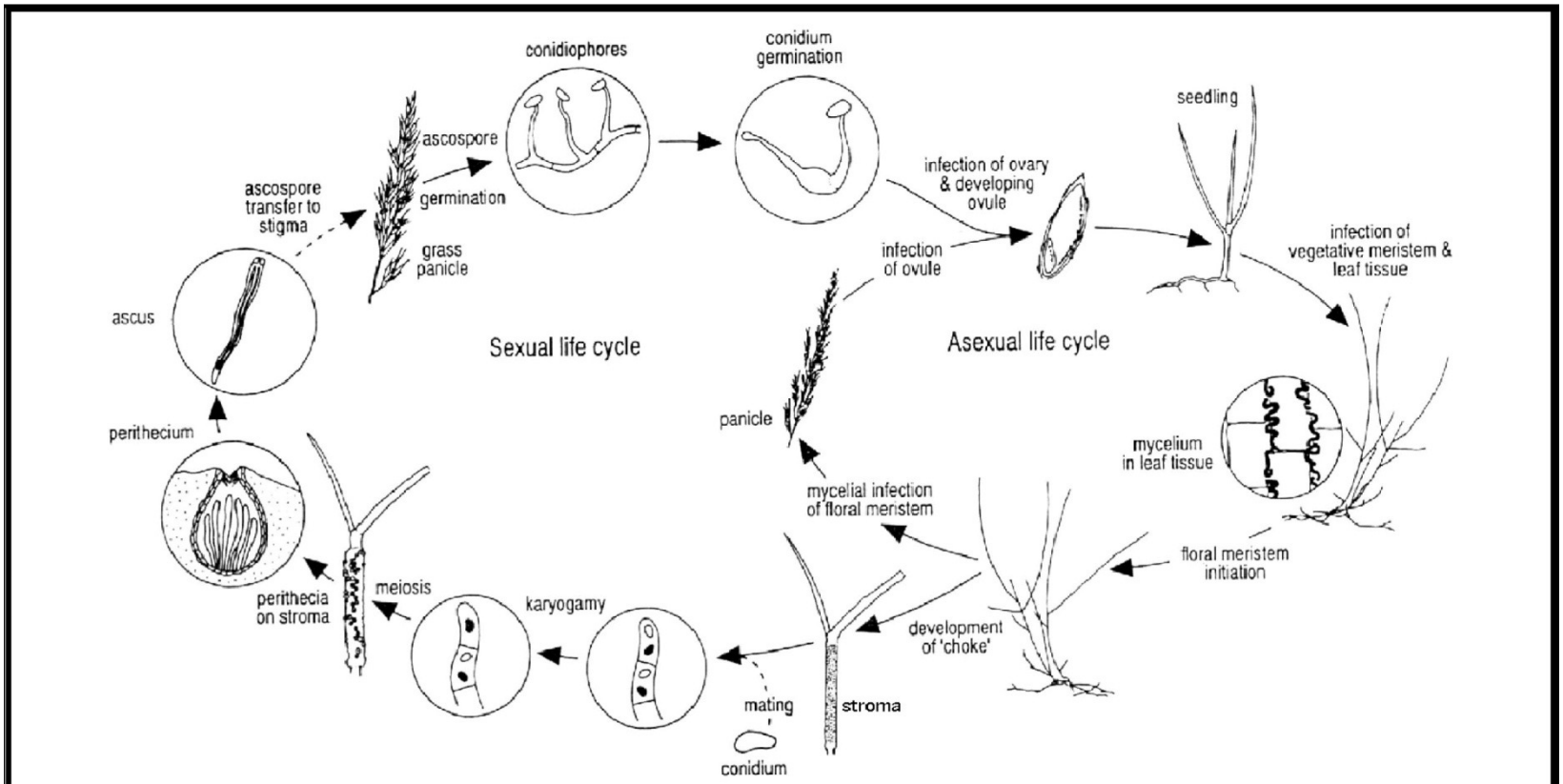

Figure 1.1. Schematic representation of sexual and asexual life cycles of epichloë endophytes.
Asexual life cycle results in the asymptomatic, vertical transmission of the endophyte, achieved by endophyte colonization of the host seed. In the sexual life cycle, the fungus forms a stroma around the developing inflorescence, preventing the opening of the inflorescence which is known as 'choke disease'. When the stroma is formed, horizontal transmission of the fungus occurs as follows: Botanophila flies transfer spermatia produced on the stroma surface to stroma of the opposite mating type which results in developing and maturation of ascospores. Ejected ascospores germinate on the stigmas of the grass florets which leads to colonization of seeds. Reproduced from Scott & Schardl (1993). Trends Microbiol. 5:196-200.

associations. *Epichloë* species show a spectrum of interactions. Some species, like *E. typhina*, are highly antagonistic, causing sterilization of all host tillers. Other species show a variable level of antagonism with both vertical and horizontal transmission, which may lead to sterilization of only some of the host tillers while others remain asymptomatic and continue development. The latter form of interaction with alternative life cycles of the fungus is referred to as a pleiotropic symbiosis and is represented by the associations between *Epichloë festucae* and its host grass *Festuca rubra*. Fungi with pleiotropic interactions represent good model systems for studying the evolution of mutualism in plant-fungal interactions.

In contrast to the dual mechanism of transmission exhibited by *Epichloë* species, species use only vertical transmission. Many *Neotyphodium* species evolved as hybrids of two or more *Epichloë* spp. and lost the ability to enter the sexual life cycle, therefore forming obligate mutualistic associations with their host grasses. Some other species, such as *N. loli*, show no evidence of hybridization. Investigations of *N. loli* suggest that it has evolved from *E. festucae* by the loss of the sexual cycle (Schardl & Craven, 2003, Moon *et al.*, 2004).

In the mutualistic associations between plants and the endophytes that propagate mainly by vertical transmission, both symbiotic partners benefit from the interaction. In this association, the plant host provides nutrients, a stable environment for fungal growth and transmission through the seeds (Schardl *et al.*, 2004). The fungus confers on the host enhanced tolerance to various biotic and abiotic stresses. Infection with endophytes provides the host with enhanced drought tolerance (Hahn *et al.*, 2008, Arechavaleta *et al.*, 1989) as well as an enhanced ability to grow on phosphorus-deficient soils (Malinowski & Belesky, 1999). Increased tolerance to biotic stresses is the result of the production of alkaloids toxic to mammalian species (indole-diterpenes and ergot alkaloids) and insect species (lolines and peramine) (Schardl, 2001). The indole-diterpene alkaloid lolitrem B is produced by some *Epichloë* species and is the causal agent of the livestock disease ryegrass staggers (Gallagher *et al.*, 1984), making grass-endophyte associations important for agriculture and farming.

1.2.2. *E. festucae* as an experimental model system for genetic analysis of plant/endophyte symbiotic associations.

For experimental work on endophytes, *Epichloë festucae* has some very important advantages over other endophytic fungi. One of the main problems in experimental research of mutualistic associations of plants and endophytes is the slow growth rate of these fungi in axenic culture. *E. festucae* is relatively fast growing in culture, forming colonies of 1.5 cm in diameter on potato dextrose agar plates in around two weeks. Also, with a simple procedure, hyphae of *E. festucae* may be converted into protoplasts that can be used for genetic manipulations, such as gene replacement. The frequency of homologous recombination depends on the locus and size of the flanking sequences used to make the construct for gene targeting and varies from 1% to 25% of the total number of transformants (Scott *et al.*, 2007). *Epichloë festucae* is a haploid organism, which is another advantage in genetic studies, with a genome of ~29 Mb (Kuldau *et al.*, 1999), which has recently been sequenced (http://csurs.csr.uky.edu/biodb-testbed/).

E. festucae genetically manipulated in culture can be artificially introduced into perennial ryegrass *Lolium perenne*, thereby allowing a functional analysis of the genes involved in regulating the symbiosis. Inoculation of grass seedlings is performed by insertion of fungal hyphae, grown on agar plates, into the region of the apical meristem of the seedling. This procedure usually gives a high rate of infection (80-90% for wild-type). Studies over the years have shown that artificially introduced fungi have the same growth pattern as endophytes in naturally infected grasses.

1.2.3. *E. festucae* growth *in planta*

The main characteristics of the association formed between *E. festucae* and its plant host is the highly regulated growth displayed by the fungus. The fungus grows systemically in the aerial tissues of the plant, without eliciting any obvious signs of a host defense reaction. Fungal hyphae grow in the intercellular spaces, aligned parallel to the leaf axis, with infrequent branching. The growth rate of the hyphae matches that of the leaf: hyphae grow only while the leaf grows and cease growth when leaf growth ceases (Christensen *et al.*, 2002, Schmid *et al.*, 2000). Epiphyllous hyphae can sometimes be

found on the surface of the infected leaves (Moy *et al.*, 2000). A recent study demonstrated that hyphae in leaves are firmly attached to the walls of neighbouring plant cells (Christensen *et al.*, 2008). In contrast to the growth seen in the leaves, in the shoot apical meristem (SAM) of the plant hyphae appear to form a highly branched network growing in all directions. It is assumed that hyphae switch to highly regulated growth upon invasion of the leaf primordia, formed in the SAM, and attach to the differentiated plant cell. This model, however, is in contrast with the widely accepted model of hyphal growth which proposes that hyphae grow exclusively by tip growth. If that were the case for *E. festucae* growth *in planta*, hyphae in the leaves would be torn apart by the mechanical stress induced by elongating plant cells. A new model has been proposed (Christensen *et al*., 2008) for the endophyte colonization of the plant based on measurement and observation of hyphal growth *in planta*. This model involves intercalary growth of fungal hyphae where hyphae are growing by extension between septa. By this model, colonization of plants involves two stages of hyphal growth. Firstly, hyphae in the SAM, where there is no extension of plant cells, grow by tip growth with frequent branching. Once hyphae invade the leaf primordia, hyphae become attached to the walls of rapidly extending plant cells, where they are subjected to mechanical stretch. To overcome this stress, hyphae grow by intercalary extension and, consequently, avoid being torn apart. This model, therefore, suggests that stretch activates the transition from apical to intercalary growth and explains how the growth of the hyphae matches that of the leaf in terms of growth rate and polarity.

1.2.4. Role of molecular signaling in the regulation of the *E. festucae*-plant association

The importance of fungal growth regulation for the maintenance of mutualism between *E. festucae* and the host was recently demonstrated by a functional analysis of fungal genes involved in signal transduction (Scott *et al*., 2007, Eaton *et al.*, 2010). These studies have shown that disruption of only one gene can lead to a transition from a mutualistic interaction to an antagonistic interaction.

Using insertional mutagenesis as an unbiased genetic approach to study genes involved in regulation of symbiosis, Tanaka *et al*. (2006) identified an *E. festucae* mutant that

was unable to establish a mutualistic association with perennial ryegrass. Infected plants had a stunted phenotype and premature senescence. Microscopic analyses showed that the mutant had unregulated hyphal growth *in planta* with increased hyphal biomass, hyper-branching and loss of growth synchronization with the leaf cell. Analysis of the site of plasmid insertion showed that the mutant was disrupted in a gene encoding a key catalytic component of the ROS production enzyme NADPH oxidase (Nox) complex, *noxA*. The NADPH oxidase complex from the mammalian neutrophils, responsible for the oxidative burst of ROS in response to pathogen invasion, is the best studied Nox complex. However, ROS produced by NADPH oxidases are also known to have a regulatory role in growth and differentiation responses, induced by environmental signals, of various tip-growing cells such as pollen tubes (Liu *et al.*, 2009a), root hairs (Foreman *et al.*, 2003) and fungal hyphae (Semighini & Harris, 2008). Disruption of the two other regulatory components of the Nox complex, *noxR* and *racA*, lead to similar defects in the plant-fungus interaction (Takemoto *et al.*, 2006, Tanaka *et al.*, 2008). Detailed analysis of ROS production in culture showed that it is disruption of ROS localization, rather than the level of the production, that is responsible for breakdown of the mutualistic interaction (Takemoto *et al*., 2006). Furthermore, experiments in which Pooid grasses other than perennial ryegrass were inoculated with the Δ*noxA* strain of *E. festucae* confirmed the role of ROS as a signalling regulator. Perennial ryegrass, tall fescue and meadow fescue infected with the *noxA* mutant all showed a stunted phenotype. However, in meadow fescue, microscopic analysis showed fungal growth that was very similar to wild-type. This suggests that an increase of fungal biomass is does not result in stunting of the host plant (Tanaka *et al.*, 2007a). This is further confirmation of the hypothesis that the stunting phenotype is caused by disruption of normal signalling between the fungus and host plant.

A recent study performed by Eaton *et al.*, 2010, showed that the stress-activated mitogen-activation protein kinase *sakA* has an essential role in the establishment and maintenance of the mutualistic interaction. As for *noxA*, a mutant deleted for the *sakA* induces stunting and premature senescence of the host plant and exhibits an increased biomass and hyper-branching. Furthermore, plants infected with the mutant strain show development of bulb-like structures at the base of the tillers that lack anthocyanin pigments normally formed in plants infected by wild-type. High-throughput mRNA sequencing analysis, used to compare the transcriptomes of wild-type and mutant

associations, revealed dramatic changes in both fungal and plant gene expression, confirming an essential role of this signaling pathway for the maintenance of the mutualistic association (Eaton *et al*., 2010).

Taken together, these findings suggest that the mutualistic symbiotic association between *E. festucae* and perennial ryegrass is tightly regulated by signaling, both within and between the two partner organisms that compose the symbiosis.

1.3. Calcium signaling

One of the best-studied signaling pathways of living cells are calcium (Ca^{2+}) signaling pathways. Calcium is an almost universal secondary messenger involved in a broad range of processes from gene expression to muscle contraction and apoptosis (Bootman *et al.*, 2001) and is proposed to be the most versatile biological messenger known (Cheng & Lederer, 2008).

1.3.1. Generation and decoding of calcium signals

The concentration of calcium in cell cytoplasm is maintained at a very low level (100 nM – 500 nM) compared with that in the extracellular spaces and internal depots (1 mM - 5 mM) (Permyakov & Kretsinger, 2009, Halachmi & Eilam, 1989). A calcium signal is generated when the cytoplasmic Ca^{2+} concentration increases and when this increase is perceived by the effectors regulated by Ca^{2+}. Tight regulation of calcium signaling relies on the fast changes of intracellular calcium concentration enabled by the concentrations of Ca^{2+} in the cytoplasm and extracellular spaces and intracellular depots. In most cases, the "calcium signal" is an elevation of the cytoplasmic concentration of Ca^{2+} ions by influx from the extracellular space or intracellular depots. Localization and amplitude of these fast calcium influxes is very important for the generation of calcium signals. These elemental Ca^{2+} entries can lead to the generation of calcium spikes, which are rapid and highly localized elevations of Ca^{2+} involved in fast responses, or global, often repetitive, calcium intracellular waves, involved in regulation of slow responses (Berridge *et al.*, 2003, Putney & Bird, 2008). For effective calcium signaling there must be a large difference in Ca^{2+} concentration between the different

compartments of the cell. At any time, the calcium level in the cytoplasm is determined by the balance between activity by many mechanisms of calcium entry in the cytosol and depletion from the cell (Cui *et al.*, 2009b). Calcium influx is facilitated by various transporters, channels, exchangers and calcium ATPases on the plasma membrane or membranes of intercellular calcium depots. In animal cells, the main intracellular depots of calcium ions are the endoplasmic reticulum and mitochondria, whereas in plant and fungal cells there is also the vacuole. Calcium entry may be triggered by various stimuli from outside or inside the cell. These stimuli may result in depolarization of the plasma membrane, triggering influx through voltage-operated calcium channels, mechanical stress of the membrane, activating stretch-activated Ca^{2+} channels, depletion of intracellular calcium stores, activating store-operated calcium channels, and various extracellular agonists and intracellular messengers. Mechanisms involved in removing calcium ions from the cytoplasm include various calcium cytosolic buffers, calcium pumps and ion exchangers (Berridge *et al*., 2003).

Once elicited, the calcium signal has to be precisely decoded by the cell. This is achieved by various proteins that act as calcium sensors and respond to changes to calcium concentration. These proteins are classified as relays and responders (Sanders *et al.*, 2002). Relays undergo a calcium-induced conformational change that is then relayed to an interacting partner. The partner then responds with some change of its activity or structure that leads to a cellular response to the calcium signal. An example of this type of calcium sensor is calmodulin, a small cytoplasmic protein that undergoes a conformational change upon binding of Ca^{2+} ions. This change enables calmodulin to interact with other enzymes and to change their activity (Chin & Means, 2000). Calcium responders are those enzymes that undergo conformational change upon calcium binding. This intramolecular change is sufficient for the activation of these enzymes. Examples of these proteins are enzymes that are directly regulated by calcium binding, as is the case for some types of NADPH oxidases (Kawahara *et al.*, 2007).

An important requirement for versatility of calcium signals is cross-talk with other signaling pathways. Many stimuli that initiate calcium release into the cytoplasm function through phospholipid signaling pathways, which start with the activation of phospholipase C (PLC). Phospholipase C catalyzes the release of diacyl glycerol (DAG) and inositol-1,4,5-triphosphate (IP3) from phosphatidyl inositol-4,5-bisphosphate, a

phospholipid occurring at low concentrations in the membrane. There are several isoforms of PLC that differ in their mechanism of activation. They are activated by G-protein coupled receptors (PLCβ), tyrosine-kinase-coupled receptors (PLCγ), an increase in Ca^{2+} concentration (PLCδ), or through Ras (PLCε) (Fukami, 2002). IP3 released into the cytoplasm acts as a second messenger inducing activation of IP3-operated calcium channels on the membranes of organelles that serve as the intracellular calcium depots. Together with DAG generated by PLC, Ca^{2+} ions released into the cytoplasm activate protein kinase C (PKC), an enzyme with many different and important functions in eukaryotic cells (Shirai & Saito, 2002). Like PLCs, PKCs are regulated in many different ways and it is interesting to note that fungal PKCs appear not to be regulated by calcium ions (Schmitz & Heinisch, 2003).

Cross-talk between calcium and ROS signaling pathways has been shown in many organisms. Interactions between Ca^{2+} and ROS signaling systems are very complex and may be both stimulatory and inhibitory, depending on the type of target proteins, the ROS species, the dose, duration of exposure, and the cell context (Yan *et al.*, 2006, Mori & Schroeder, 2004). While many ROS generation processes are calcium-dependent, calcium signals themselves may be regulated by the redox-state of the cell. Some of the NOX enzymes have Ca^{2+} binding regulatory domains and are directly regulated by calcium. This is the case with mammalian NOX5 (Jagnandan *et al.*, 2007) and DUOX1 and DUOX2 isoforms of NADPH oxidases (Lambeth, 2004). All NOX enzymes in plants are directly regulated by calcium (Torres *et al.*, 1998). In the social amoeba *Dictyostelium discoideum*, signalling of NOXA and NOXB, homologues of the gp91phox subunit, is regulated by alg-2B, a calcium binding protein (Lardy *et al.*, 2005). NOXC isoforms present in some fungi also contain calcium binding domains (Takemoto *et al.*, 2007). Crosstalk of calcium and ROS signaling is proposed to occur in nodule development in the symbiotic interaction between legumes and nitrogen-fixing rhizobial bacteria, but this remains to be demonstrated (Oldroyd & Downie, 2004, Lohar *et al.*, 2007). In mammalian cells PKC is directly involved in ROS signaling (Lassegue & Clempus, 2003).

A schematic representation of the calcium signaling machinery in a eukaryotic cell is given in Figure 1.2.

1.3.2. Calcium and polarized cell growth – importance for hyphal growth

Calcium is widely recognized as a crucial molecule in signaling pathways regulating polarized growth. Polarized growth has been studied in animal, plant and fungal cells, as it is a form of growth crucial for differentiation and development in most organisms. Studies of the neuronal elongation process established localized calcium gradient as a necessary requirement for the axogenesis (Mattson, 1999). The motility of the neuronal growth cone depends on a localized increase of cytoplasmic Ca^{2+}, induced by cell adhesion molecules through lipid signaling (Dunican & Doherty, 2000). Calcium regulates the processes of directional cell movement where an increase of Ca^{2+} is mediated through a stretch-activated Ca^{2+}-permeable channel and inositol-1,4,5-trisphosphate receptors as a response to membrane tension and chemoattractant signal transduction (Wei *et al.*, 2009). The extreme examples of polarized cell growth are tip-growing cells like pollen tubes, root hairs or fungal hyphae. Root hairs and pollen tube cells have been established as model systems for the studies of tip growth in plants (Yang, 1998). Calcium ion gradients and fluxes have a crucial role in regulation of pollen tube growth (Feijo *et al.*, 2001). The importance of a tip-high calcium gradient for the growth of the root hair is well documented (Wymer *et al.*, 1997). Furthermore, a close connection with ROS signaling has been established. *Arabidopsis thaliana rhd2* mutants are defective in calcium uptake and their root development is severely impaired, exhibiting stunted roots and short root hairs. It was shown that *rhd2* encodes an NADPH oxidase and that ROS accumulates in wild-type growing root hairs but are absent from the *rhd2* mutant cells. A direct link between ROS and calcium signaling was established when it was shown that addition of ROS to *rhd2* mutant cells stimulates the activity of plasma membrane hyperpolarization-activated Ca^{2+} channels (Foreman *et al*., 2003).

In the polarized growth of fungal hyphae, a role for a tip-localized Ca^{2+} gradient is not yet well established, mostly due to the lack of reliable and routine techniques for the measurement of the cytosolic Ca^{2+} concentrations. Some studies suggest that a Ca^{2+}

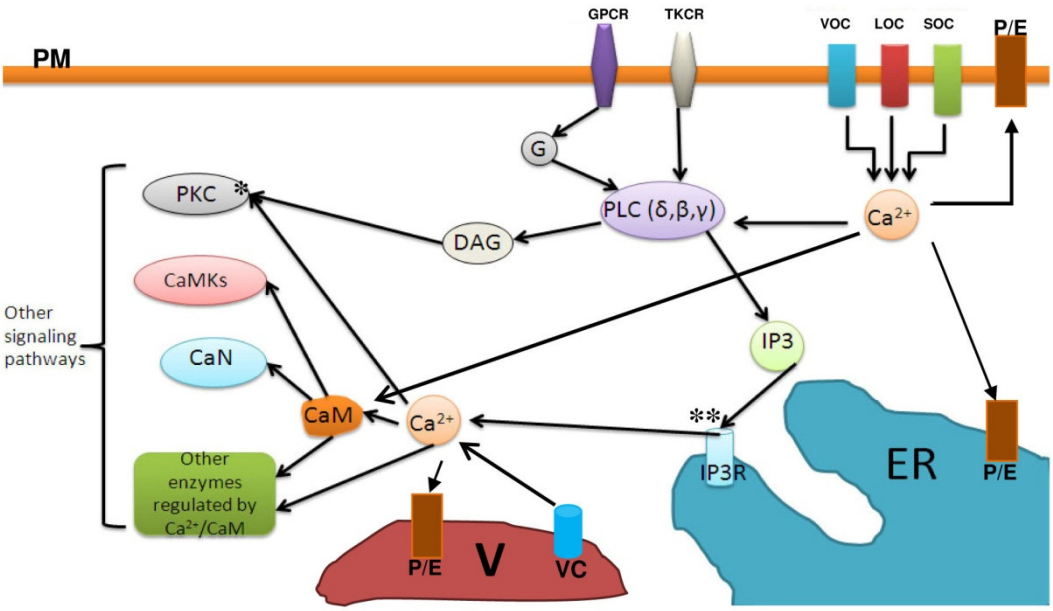

Figure 1.2. Simplified presentation of calcium signaling in eukaryotic cells.
Calcium ions enter the cytoplasm from the extracellular spaces and intracellular depots through the system of Ca^{2+} channels and are actively transported out of the cytoplasm through various Ca^{2+} pumps and exchangers. In the cytoplasm, Ca^{2+} regulates activity of various enzymes like phospholipase C, protein kinase C, Ca^{2+}/calmodulin regulated kinase and phosphatases, and others (more details in the text). GPCR – G-protein-coupled receptors; TKCR- tyrosine-kinase-coupled receptors; VOC- voltage-operated calcium channels; LOC - ligand operated calcium channels; SOC – store operated calcium channels; PLC (Δ, β, γ) – phospholipase C isoforms; IP3 - inositol-1,4,5-triphosphate; DAG – diacyl glycerol; ER – endoplasmic reticulum; V- vacuole; VC – vacuolar channels; IP3R – IP3-operated calcium channels; P/E – pumps and exchangers; PKC – protein kinase C; CaMKs – calcium/calmodulin dependent kinases; CaN – calcineurin, calcium/calmodulin dependent phosphatases; PM – plasma membrane; G – G protein subunits.
* Fungal PKCs characterized so far are not regulated by Ca^{2+}
** IP3-operated Ca^{2+} calcium channels have not been characterized in fungi, although studies strongly suggest that these channels are present (Silverman-Gavrila & Lew, 2002).

gradient at the hyphal tip is essential for hyphal growth (Silverman-Gavrila & Lew, 2003, Silverman-Gavrila & Lew, 2002) but more studies are needed in order to fully understand the role of the tip-high Ca^{2+} in the hyphae. However, while a role for a Ca^{2+} gradient in hyphal tip growth still remains unclear, the role of calcium signaling pathways in hyphal growth and branching pattern is well documented (Jackson & Heath, 1993, Torralba & Heath, 2001). In *Neurospora crassa*, disturbance of the intracellular calcium concentration caused hyperbranching of the growing tip (Schmid & Harold, 1988) whereas high concentrations of exogenous calcium induced restoration of the wild-type phenotype in hyperbranching mutants (Kawano & Said, 2005). Furthermore, disruption of calcineurin, a Ca^{2+} regulated phosphatase, induced hyperbranching in *N. crassa*, dissipation of the tip-high Ca^{2+} gradient and eventually growth arrest, suggesting that calcineurin is essential for the normal tip growth (Prokisch *et al.*, 1997). In the dimorphic human pathogenic fungus, *Candida albicans*, a role for calcium signaling in hyphal orientation has been clearly demonstrated. Inhibitors of stretch-activated and voltage-gated calcium channels impaired hyphal thigmotropism in this organism (Watts *et al.*, 1998). Mutants deleted for the *C. albicans* homologues of the stretch-activated Ca^{2+} channel Mid1 and the voltage-gated Ca^{2+} channel Cch1 exhibited a similar phenotype with disruption to both thigmotropism and galvanotropism (Brand *et al.*, 2007).

1.3.3. Calcium signaling in fungi

The components and dynamics of calcium signaling in fungi are best understood for the budding yeast *Saccharomyces cerevisiae* and less in filamentous fungi. However, yeast appears to have a calcium signaling machinery that is less complex than that of filamentous fungi (Zelter *et al.*, 2004).

1.3.3.1. *Calcium channels*

Three Ca^{2+} permeable channels have been characterized in *S. cerevisiae*: the voltage-gated channel Cch1p, the stretch-activated Mid1p channel and the transient receptor potential-like Ca^{2+} channel Yvc1p. Disruption of *mid1* induces loss of cell viability after

pheromone-induced cell differentiation. It has been shown that Δ*mid1* mutant has low Ca^{2+} uptake and the loss of a viable phenotype can be restored by incubating the Δ*mid1* mutants with a high extracellular Ca^{2+} concentration (Iida *et al.*, 1994). The Δ*cch1* mutants had phenotypes identical to the Δ*mid1* mutants, leading to the conclusion that Cch1p and Mid1p are components of the same Ca^{2+} permeable channel, Cch1pMid1p (Paidhungat & Garrett, 1997). Besides a role in the pheromone response, the Cch1pMid1p channel has a role in the regulation of responses to ion stress as well as to low temperature stress (Peiter *et al.*, 2005). The Yvc1p channel is located in the vacuolar membrane (Palmer *et al.*, 2001). This channel is mechanosensitive and involved in the calcium response triggered by hyperosmotic shock (Zhou *et al.*, 2003, Denis & Cyert, 2002). In the human pathogen *Cryptococcus neoformans*, Cch1 is important for growth under conditions of low extracellular Ca^{2+} (Liu *et al.*, 2006). Functional analysis of Ca^{2+} signaling proteins in *Magnaporthe oryzae* showed that a knock-down mutant of the Cch1p homologue had reduced sporulation and appressorium formation but retained the ability to infect the host plant. A knock-down of the Mid1p homologue had a mild reduction of the same processes as a Cch1 knock-down mutant, while the knock-down of Yvc1p strongly affected conidia and appressoria formation (Nguyen *et al.*, 2008). A deletion mutant of Cch1 in *Gibberella zea* had a reduced growth rate in culture and an inability to forcibly discharge spores (Hallen & Trail, 2008). A particulary interesting phenotype was observed for the Δ*mid1* mutants of the rye pathogen *Claviceps purpurea*. While mutants had a reduced growth rate in culture, polarity and branching pattern were unaffected. This culture phenotype could be rescued by addition of extracellular Ca^{2+}, as for the *S. cerevisiae* mutant. However, the Δ*mid1* mutant had a complete loss of pathogenicity, produced appressoria-like structures, which are unusual for *C. purpurea*, with multiple apical branches. These results suggest that Mid1 is essential for the generation of the mechanical force required for penetration of the cuticle (Bormann & Tudzynski, 2009).

1.3.3.2. *Calcium ATPases and exchangers*

The role of the Ca^{2+} ATPases (Ca^{2+} pumps) and exchangers is to maintain low cytoplasmic Ca^{2+} concentrations by actively removing Ca^{2+} from the cytoplasm. Calcium pumps and exchangers in yeast and other fungi operate together with

calcineurin in regulating the response to stress induced by high salt concentration. Disruption of the gene encoding Ca^{2+} ATPase PMR1, which is located on the Golgi membrane, causes a growth defect in *S. cerevisiae* in a low Ca^{2+} environment. Disruption of this gene also increases salt tolerance as a consequence of the constantly high cytoplasmic Ca^{2+} concentration which maintains calcineurin in a highly active state (Park *et al.*, 2001). The vacuolar Ca^{2+} ATPase PMC1 is required for growth under conditions of high Ca^{2+}, a phenotype that is suppressed by inactivation of calcineurin. Under conditions of high Ca^{2+} the active form of calcineurin inhibits the vacuolar H^{+}/Ca^{2+} exchanger, VCX1, thus preventing calcium removal from the cytoplasm (Cunningham & Fink, 1996). PMR1 homologues in *Aspergillus niger* and *Aspergillus fumigatus* are required for maintaining Ca^{2+} homeostasis in these fungi (Yang *et al.*, 2001a, Pinchai *et al.*, 2010). However, while the Δ*pmrA* mutant of *A. fumigatus* had disrupted ion homeostasis and cell wall defects, it retained its pathogenicity. Silencing of three homologues of PMC1 and two homologues of PMR1 found in *M. oryzae* resulted in severe conidiation defects and a slow growth rate (Nguyen *et al*., 2008). However, because of the high sequence similarity between Ca^{2+} pumps, it was noticed that these genes were silenced simultaneously, so the phenotypes observed in attempts to silence single genes are most likely the consequence of simultaneous silencing of more than one gene.

1.3.3.3. *Phospholipase C*

Fungal phospholipase C enzymes show the highest similarity to the mammalian phospholipase C isoform PLCδ. In *S. cerevisiae*, deletion of *PLC1* was shown to have pleiotropic effects, including variable rates of survival depending on the genetic background (Yoko-o *et al.*, 1993). Viable mutants of *PLC1* showed sensitivity to osmotic stress, temperature stress and utilization of carbon sources other than glucose (Flick & Thorner, 1993). PLC1 works together with the Gpr1p/Gpa2p G-protein-coupled receptor (GPCR) to transduce the glucose-induce calcium signals (Tisi *et al.*, 2002, Flick & Thorner, 1993). In *C. neoformans* one of the two PLC genes found in this organism, *plc1*, is involved in regulating several crucial steps in the infection process including melanin production, growth at 37°C and secretion of phospholipase B1 (Plb1). Inactivation of this gene results in loss of pathogenicity in mice. In Δ*plc1* strains,

cleavage of the membrane-bound Plb1 was impaired resulting in the accumulation of this enzyme at the plasma membrane. The pathogenicity phenotype of Δ*plc2* strain was identical to wild-type (Chayakulkeeree *et al.*, 2008). In *C. albicans*, *CaPLC1*, one of the three PLC genes identified in this fungus, is essential for viability. A conditional mutant of *CaPLC1* was sensitive to osmotic and temperature stress and was unable to grow on several carbon sources, other than glucose (Kunze *et al.*, 2005), phenotypes similar to those found for *S. cerevisiae*. In the plant pathogen *M. oryzae*, disruption of *plc1* resulted in a pathogenicity defect presumably due to disturbance of calcium fluxes essential for the infection processes. Interestingly, the PLC-Δ1 gene from mice was able to restore calcium flux in *M. oryzae*, demonstrating high evolutionary conservation of this regulation (Rho *et al.*, 2009). In *Botrytis cinerea*, knock-down of *plc1* led to down-regulation of expression of several genes regulated by calcineurin and the G-alpha subunit BCG1 showing that PLC1 is a component of these signaling pathways (Schumacher *et al.*, 2008b).

1.3.3.4. *Calmodulin*

Calmodulin is involved in many cell processes through the regulation of its targets such as the Ca^{2+}/calmodulin-dependent protein phosphatase, calcineurin or Ca^{2+}/calmodulin-dependent protein kinases. The single gene encoding calmodulin in *S. cerevisiae*, *CMD1*, is essential for viability (Davis *et al.*, 1986). Interestingly, beside the Ca^{2+}-dependent functions, the yeast calmodulin regulates an internalization step of endocytosis in a Ca^{2+}-independent manner (Kubler *et al.*, 1994). Expression of the *M. oryzae* calmodulin gene is upregulated during appressorium formation (Liu & Kolattukudy, 1999). Preferential localization of calmodulin to germ tubes and appressoria, rather than aerial hyphae, provides further support for a role for calmodulin in the infection process (Ma *et al.*, 2009).

1.3.3.5. *Ca^{2+}/calmodulin-dependent protein kinases*

An important group of calcium-dependent enzymes are the Ca^{2+}/calmodulin-dependent protein kinases (CaMKs). CaMKs are serine/threonine protein kinases with an amino-

terminal catalytic domain and a carboxy-terminal regulatory domain. The regulatory domain consists of an autoinhibitory domain and the Ca^{2+}/calmodulin (Ca^{2+}/CaM) binding domain. The autoinhibitory domain regulates the activity of the enzyme by interacting with the catalytic domain in a way that prevents substrate binding or causes distortion of the catalytic sites. The autoinhibition is overcome when calmodulin, following binding of Ca^{2+}, interacts with the calmodulin-binding domain, causing a conformational change that releases the catalytic domain. However, regulation of Ca^{2+}/CaM kinases is more complex. After the initial activation the enzyme may remain active independently of the presence of Ca^{2+}/CaM. Furthermore, the enzyme may require additional modification, such as phosphorylation, for full activation. The enzymes of the CaMK family are usually classified in two groups, based on their substrate specificity. In the mammalian system, the first group consists of multifunctional kinases including CaMKK, CaMK I, II and IV. These kinases have broad substrate specificity and each kinase has multiple downstream targets. The CaMKs of the second group are substrate specific kinases, such as myosin light chain kinase, which has just one phosphorylation target. The best studied CaMK is the mammalian CaMKII, due to its important role in neurological processes such as synaptic plasticity and memory. CaMKII is the only CaMK that has an association domain and in its active form functions as a twelve subunit complex. CaMKK, CaMK I, and IV are members of the so-called CaMK cascade. CaMKK is a kinase kinase whose substrates are CaMKI and CaMKIV. Phosphorylation by CaMKK is necessary (but not sufficient) for the activation of the other two kinases and this activation step occurs after the Ca^{2+}/CaM binding. CaMKI is a cytosolic protein whose exact function is still not known but the cAMP response element binding protein (CREB) is a known substrate. CaMKIV is found both in the cytosol and nucleus where it is known to regulate the activity of CREB, serum response factor and histone deacetylase 4 (reviewed by (Swulius & Waxham, 2008) and references therein).

Fungal homologues of the mammalian multifunctional CaMKs have important roles in fungal development as well as interactions with other organisms. In *S. cerevisiae* there are two CaM kinases, CMK1 and CMK2 (Ohya *et al.*, 1991). They are involved in thermotolerance (Iida *et al.*, 1995) and survival of the pheromone-induced cell cycle arrest in which they function independently of calcineurin, another CaM responsive enzyme important for this process (Moser *et al.*, 1996). Just one CaMK (CMK1) has

been identified in the fission yeast *S. pombe*. Hyperactivation of this gene caused cell cycle arrest and morphological defects (Rasmussen, 2000). In the dimorphic human pathogen *Sporothrix schenckii*, inhibition of SSCMK1 blocked the mycelium to yeast transition (Valle-Aviles *et al.*, 2007). In the filamentous fungus *Aspergillus nidulans* three Ca^{2+}/CaM-dependent protein kinases, CmkA, CmkB and CmkC, have been reported. CmkA and CmkB were identified as bona fide CaMKs whereas CmkC was shown to be a CaMKK which phosphorylates CmkB *in vitro*. Disruption of either *cmkA* or *cmkB* is lethal while expression of CamkA constitutively active form prevents spores from entering the first nuclear division cycle (Dayton & Means, 1996, Joseph & Means, 2000, Dayton *et al.*, 1997). Disruption of CaMKs in other filamentous fungi results in less dramatic phenotypes. In *N. crassa*, CAMK-1 was shown to regulate the circadian clock protein FREQUENIN. Deletion of the gene encoding CAMK-1 induces a transient slow growth phenotype (Yang *et al.*, 2001b). MoCMK1 deletion mutants of *M. oryzae* have delayed spore germination and appsessorium formation and display a reduced ability to infect the host plant (Liu *et al.*, 2009b). CaMK inhibitors block the *Colletotrichum gloeosporioides* infection process suggesting CaMKs have a key role in pathogenicity (Kim *et al.*, 1998). Homologues of *A. nidulans* CmkA, CmkB and CmkC were identified in *Stagnospora nodorum*, a wheat phytopathogenic fungus. Disruption of these three genes (*cpkA*, *cpkaB* and *cpkC*) showed that none of them are essential. No phenotypic difference was detected between the *cpkB* mutant and wild-type. Disruption of the *cpkA* gene affected vegetative growth *in vitro* and sporulation, while disruption of *cpkC* delayed lesion development and sporulation during plant infection by *S. nodorum* (Solomon *et al.*, 2006).

1.3.3.6. *Calcineurin*

Calcineurin signaling pathways are probably the best-studied calcium signaling pathways in fungi. Calcineurin is a Ca^{2+}/calmodulin-dependent protein phosphatase (PP2B) and is a heterodimer of a 57 to 71 kDa catalytic subunit (CnA) and a 18 to 20 kDa regulatory subunit (CnB). The catalytic subunit is a polypeptide with four different domains: a catalytic domain, a CnB binding domain, a Ca^{2+}/CaM binding domain and an autoinhibitory domain. As for CaMKs, the autoinhibitory domain inhibits the enzyme activity and this inhibition is relieved by Ca^{2+}/CaM binding (Rusnak & Mertz,

2000). Calcineurin signalling through its phosphorylation target, calcineurin-responsive transcription factor CRZ1, is important for regulation of ion stress response, cell wall integrity, hyphal growth and a number of other developmental processes (Stie & Fox, 2008). Of particular interest for this study are findings that calcineurin signaling pathways are involved in regulation of plant-fungal associations. In *Ustilago maydis*, the causative agent of corn smut disease, calcineurin is a crucial factor for virulence. Mutants of the calcineurin catalytic subunit gene fail to induce tumors in inoculated plants (Egan *et al.*, 2009). In *M. oryzae*, pharmacological studies using cyclosporin A, an immunosuppressant of calcineurin, indicate that calcineurin has a key role in appressorium formation. This was confirmed by RNAi experiments where it was shown that mutants with reduced levels of *MCNA*, the *M. oryzae* homologue of calcineurin A, have significantly lower rates of appressorium formation (Choi *et al.*, 2009b). Disruption of the *M. oryzae* CRZ1 homologue, *MoCRZ1*, confirmed that calcineurin signaling is required for the infection process. Although the Δ*Mocrz1* mutants did form appressoria, only a small percentage of them developed infectious hyphae (Choi *et al.*, 2009a). Although *M. grisea crz1* mutants formed appressoria, the turgor pressure was much lower than that of WT, suggesting this was the likely cause of the attenuated pathogenicity (Zhang *et al.*, 2009). *B. cinerea crz1* mutants were defective in the penetration step of the infection process, a phenotype that could be rescued by addition of Mg^{2+}. Under these conditions, mutants were able to complete the infection cycle like wild-type (Schumacher *et al.*, 2008a). These studies demonstrate that the calcineurin signaling pathway plays an important role in plant fungal interactions.

1.4. Agrobacterium mediated mutagenesis as a tool for understanding the symbiosis

With the increasing number of fungal genomes available, there is a growing need for rapid and reliable methods of generating large numbers of random mutants in order to identify and study genes that encode functionally important proteins. Agrobacterium-mediated T-DNA mutagenesis has been established in recent years as a particularly useful tool for random mutagenesis of fungi.

1.4.1. Agrobacterium-mediated transformation (AMT) in nature

AMT naturally occurs between plants and Gram-negative bacteria of the genus *Agrobacterium* in the process of inducing crown gall disease of plants. Transfer of the T-DNA (Transfer DNA) region of the Ti plasmid from *Agrobacterium* to the plant nucleus and integration into the plant genome is crucial for establishment of tumourgenesis. The T-DNA carries genes required for tumour induction and other plant induced functions. T-DNA transfer from *Agrobacterium* to plant cells requires excision and transfer of the single-stranded T-DNA, a process involving numerous Vir (virulence) proteins. Besides Vir proteins, a necessary requirement for transfer to occur is presence of two 25 bp sequences on each end of the T-DNA, named left (LB) and right (RB) border. Direct repeats at the LB and RB are recognition signals for binding of DNA cleavage complex, VirD,which is required for initiation of the transfer (Gelvin, 2003).

1.4.2. Adaptation for use in the laboratory

There are two requirements for the T-DNA transfer: LB and RB repeats and Vir proteins. This has enabled adaptation of the T-DNA transfer as a tool in genetics research. Vir proteins can be provided *in trans* and the sequences between the LB and RB are not important for the transfer to occur, allowing for tumorgenesis genes to be replaced by sequences of interest. This has lead to the development of binary vector systems in which two plasmids, one carrying the *vir* genes without the T-region (called "disarmed Ti plasmid") and the other carrying T-DNA with the sequence of interest sub-cloned between the borders, are together in the same bacterial cell. This binary vector system allows for easy genetic manipulation of the T-DNA located on a small plasmid (binary vector). T-DNA transfer starts with induction by various compounds such as acetosyringone, which is perceived by one of the Vir proteins, VirA. VirA activates VirG which acts as a transcriptional activator of other *vir* genes located on the disarmed Ti plasmid. VirD1/VirD2 proteins are responsible for excision of single-stranded T-strand which will be transferred to the recipient. Generation of a single strand starts at the 3'OH of the RB and terminates at the LB. Transfer and integration are facilitated by numbers of others Vir proteins (Fig. 1.3) (Michielse *et al.*, 2005).

1.4.3. Agrobacterium mediated mutagenesis in fungal research

Since the discovery that *A. tumefaciens* can transfer T-DNA into fungal cells, AMT has been widely adapted for fungal research. AMT has a number of advantages over other insertional mutagenesis procedures such as restriction enzyme-mediated integration (REMI) (Brown & Holden, 1998). REMI tends to generate a large number of non-tagged insertions (Michielse *et al.*, 2005) which can pose serious problems in phenotype analysis of the generated mutants.

Since the development of the method in yeast (Piers *et al.*, 1996), ATM has been used for mutagenesis in a wide range of fungal species, from the entomopathogenic fungus *Beauveria bassiana* (Leclerque *et al.*, 2004) to the ectomycorrhizal fungus *Lacarria bicolor* (Kemppainen *et al.*, 2005). A systematic analysis of insertion sites identified on *M. oryzae* suggested that there might be a preference for the T-DNA to integrate into promoter regions of the genes and other noncoding regions (Li *et al.*, 2007). A preference for insertion in promoter regions was found in a screen of *Cryptococcus neoformans* mutants for genes involved in melanization (Walton *et al.*, 2005). However, AMT was successfully used in a large-scale screen for genes involved in pathogenicity. In the tomato pathogen *F. oxysporum*, 111 potential pathogenicity genes were discovered using AMT (Michielse *et al.*, 2009). A novel gene required for suppression of host defense was discovered in *M. oryzae* using AMT mutagenesis (Chi *et al.*, 2009).

In *E. festucae*, a method for T-DNA mutagenesis has been developed (Tanaka *et al.*, 2007b) and it was shown that ~60% of the insertions were single-copy insertion mutants. These results suggest that AMT is a useful tool to screen for mutants disrupted in mutualistic symbiotic interaction between *E. festucae* and perennial ryegrass.

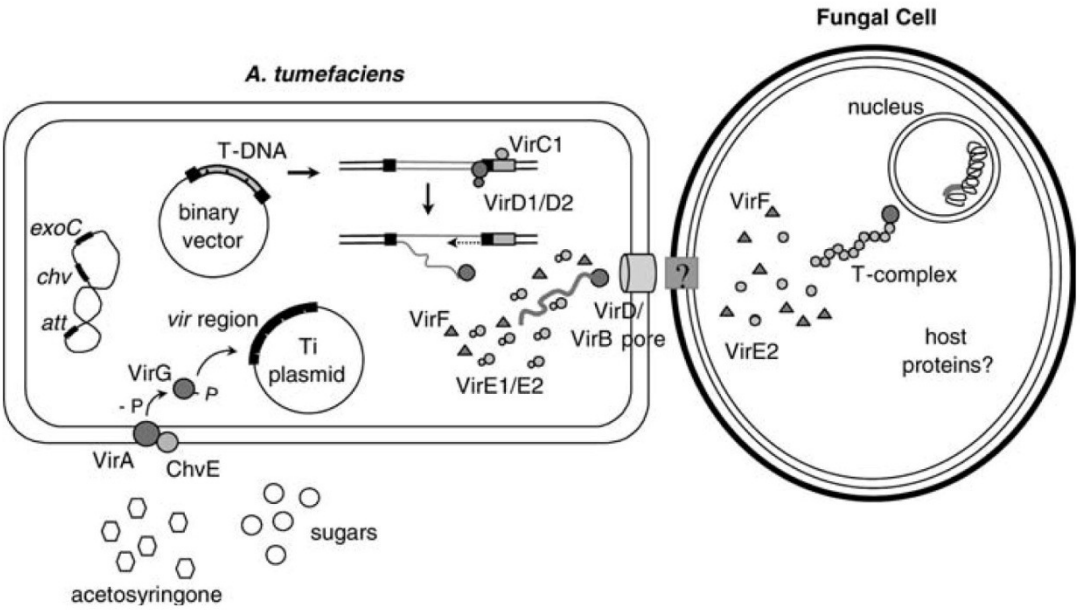

Figure 1.3. Overview of the binary vector T-DNA transfer system from *A. tumefaciens* into a fungal cell

Products of the *vir* genes, located on the Ti plasmid, together with the chromosomally located genes (*exoC*, *chv*, *att*) facilitate generation, transfer and integration of the T-DNA, located on a binary vector. Phenolic compounds, such as acetosyringone, activate a two-component regulatory system composed of VirA and VirG proteins. Chromosomally encoded ChvE interacts with VirA and enhances the activation. VirG then activates transcription of other *vir* genes on the Ti plasmid. VirC and VirD1/D2 generate a single-stranded T-DNA from the binary vector and VirD2 remains attached to the T-strand. Transfer to the fungal cell is facilitated by a pore made of VirD4 and VirB. Together with the VirD2/T-strand, VirF and VirE proteins are also transferred to the host cell (VirE is thought to coat the T-strand). Once in a host cell, T-strand is directed to the nucleus by the nuclear localization signal present on the C-terminus of VirD2, which is followed by stable integration into the host genome. Reproduced from Michielse *et al.*, (2005.).

1.5. Aims of this research

The main goal of this research was to increase our understanding of the molecular basis of the symbiotic interaction between *E. festucae* and perennial ryegrass. Based on the importance of signaling pathways in the regulation of the *E. festucae*-perennial ryegrass association, this study adopted two genetic approaches in order to discover new genes involved in the regulation of this mutualistic association.

Firstly, a reverse genetic approach was used to identify the role of the calcium signaling components in the plant-fungal interaction. This approach included two main objectives:

1. Identification and functional analysis of genes encoding three multifunctional Ca^{2+}/calmodulin-dependent kinases of *E. festucae*, *cmkA*, *cmkB* and *cmkC*.

In this objective, single-deletion mutants of each kinase gene, as well as a double-deletion mutant of *cmkA/cmkB* were generated to determine weather CaMKs have a role in regulation of fungal growth in culture and in the symbiosis.

2. Identification and functional analysis of the gene encoding *E. festucae* calcineurin A, *cnaA*.

In this objective a deletion of the *E. festucae* calcineurin A gene was generated to test the importance of calcineurin for growth in culture and symbiosis.

Secondly, a forward genetics approach using *Agrobacterium* mediated T-DNA mutagenesis was adopted in order to identify new candidate genes responsible for the regulation of the symbiosis.

2. Materials and methods

2.1. Biological materials

Fungal and bacterial strains and plant material used in this study are listed in Table 2.1. Plasmids and cosmids are listed in Table 2.2.

Table 2.1 Fungal strains, bacterial strains and plant material

Biological material	Relevant characteristics	Reference
Fungal strains		
Epichloë festucae		
Fl1 (PN2278)	Wild-type	(Young *et al.*, 2005b)
E2368 (PN2734)	Wild-type; genome sequenced	Chris Schardl
WG11 (PN2467)	Fl1/pPN82; Hyg^R	(Tanaka *et al*., 2006)
Δ*cmkA8.4* (PN2751)	Fl1/*cmkA*::*PtrpC-nptII-TtrpC*; Gen^R	This study
Δ*cmkA15.2* (PN2729)	Fl1/*cmkA*::*PtrpC-nptII-TtrpC*; Gen^R	This study
Δ*cmkA15.4* (PN2727)	Fl1/*cmkA*::*PtrpC-nptII-TtrpC*; Gen^R	This study
Δ*cmkB1.3* (PN2725)	Fl1/*cmkB*::*PtrpC-nptII-TtrpC*; Gen^R	This study
Δ*cmkB10.5* (PN2750)	Fl1/*cmkB*::*PtrpC-nptII-TtrpC*; Gen^R	This study
Δ*cmkB14.2* (PN2726)	Fl1/*cmkB*::*PtrpC-nptII-TtrpC*; Gen^R	This study
Δ*cmkC19.2* (PN2749)	Fl1/*cmkC*::P*trpC-hph*; Hyg^R	This study
Δ*cmkC19.3* (PN2724)	Fl1/*cmkC*::P*trpC-hph*; Hyg^R	This study
Δ*cmkC40.3* (PN2728)	Fl1/*cmkC*::P*trpC-hph*; Hyg^R	This study
A1	Δ*cmkA15.2*/pMMI7; Hyg^R; Gen^R	This study

A2	Δ*cmkA15.2*/pMMI7; Hyg^R; Gen^R	This study
Ba1	Δ*cmkB1.3*/pMMI5; Hyg^R; Gen^R	This study
Ba2	Δ*cmkB1.3*/pMMI5; Hyg^R; Gen^R	This study
Bb1	Δ*cmkB1.3*/pMMI6, pAN7-1; Hyg^R; Gen^R	This study
Bb2	Δ*cmkB1.3*/pMMI6, pAN7-1; Hyg^R; Gen^R	This study
Bc1 (PN2755)	Δ*cmkB10.5*/pMMI6, pAN7-1; Hyg^R; Gen^R	This study
Bc2 (PN2756)	Δ*cmkB10.5*/pMMI6, pAN7-1; Hyg^R; Gen^R	This study
Bc3	Δ*cmkB10.5*/pMMI6, pAN7-1; Hyg^R; Gen^R	This study
Bc4	Δ*cmkB10.5*/pAN7-1; Hyg^R; Gen^R	This study
C1	Δ*cmkC19.2*/pMMI8, pII99; Hyg^R; Gen^R	This study
C2	Δ*cmkC19.2*/pMMI8, pII99; Hyg^R; Gen^R	This study
Δ*cmkAB16* (PN2752)	Δ*cmkA15.4*/ *cmkB*:: P*trpC-hph*; Hyg^R; Gen^R	This study
Δ*cmkAB28* (PN2753)	Δ*cmkA15.4*/ *cmkB*:: P*trpC-hph*; Hyg^R; Gen^R	This study
Δ*cmkAB31* (PN2754)	Δ*cmkA15.4*/ *cmkB*:: P*trpC-hph*; Hyg^R; Gen^R	This study
AB-A1 (PN2757)	Δ*cmkAB16*/ pMMI7, pAN8-1; Hyg^R; Gen^R; Phl^R	This study
AB-A2 (PN2758)	Δ*cmkAB16*/ pMMI7, pAN8-1; Hyg^R; Gen^R; Phl^R	This study
AB-B6 (PN2759)	Δ*cmkAB16*/ pMMI6, pAN8-1; Hyg^R; Gen^R; Phl^R	This study
AB-B7 (PN2760)	Δ*cmkAB16*/ pMMI6, pAN8-1; Hyg^R; Gen^R; Phl^R	This study
AB-AB2 (PN2761)	Δ*cmkAB16*/ pMMI7, pMMI6, pAN8-1; Hyg^R; Gen^R; Phl^R	This study
AB-AB3 (PN2762)	Δ*cmkAB16*/ pMMI7, pMMI6, pAN8-1; Hyg^R; Gen^R; Phl^R	This study

Δ*cnaA*12 (PN2763)	Fl1/*cnaA*:: P*trpC-hph*; Hyg^R	This study
ΔcnaA13 (PN2764)	Fl1/*cnaA*:: P*trpC-hph*; Hyg^R	This study
Δ*cnaA*19	Fl1/*cnaA*:: P*trpC-hph*; Hyg^R	This study
Δ*cnaA*27	Fl1/*cnaA*:: P*trpC-hph*; Hyg^R	This study
Ag51 (PN2723)	Fl1/pBSYT6; Hyg^R	This study
Ag212 (PN2730)	Fl1/pBSYT6; Hyg^R	This study
212GFP (PN2767)	Ag212/pPN83, pII99; Hyg^R; Gen^R	This study
12-1 (PN2765)	Ag212/12G8, pII99; Hyg^R; Gen^R	This study
12-2	Ag212/12G8, pII99; Hyg^R; Gen^R	This study
12-7	Ag212/12G8, pII99; Hyg^R; Gen^R	This study
17-1 (PN2766)	Ag212/17G5, pII99; Hyg^R; Gen^R	This study
17-4	Ag212/17G5, pII99; Hyg^R; Gen^R	This study
17-11	Ag212/17G5, pII99; Hyg^R; Gen^R	This study

Bacterial strains

Escherichia coli

DH5α	F^-, φ80*lacZ*, ΔM15, Δ*lacZYA-argF*), U169, *recA1*, *endA1*, *hsdR17* (r_k^-, m_k^-), *phoA*, *supE44*, λ^-, *thi-1*, *gyrA96*, *relA1*	Invitrogen
TOP10	F^-, *mcrA*, Δ(*mrr-hsdRMS-mcrBC*), φ80*lacZ*ΔM15, Δ*lacX74*, *deoR*, *recA1*, *araD139*, Δ(*ara-leu*)7697 *galU*, *galK*, *rpsL*(Str^R), *endA1*, *nupG*	Invitrogen

Agrobacterium tumefaciens

EHA105 (PN1828)	pTiBo542; Rif^R	(Hood *et al*., 1993)
EHA105/pBSYT6 (PN1975)	pTiBo542, pBSYT6; Rif^R, Kan^R	Aiko Tanaka

Plant material

Lolium perenne

G3196	*Lolium perenne*/Fl1	This study
G3231	*Lolium perenne*/Fl1	This study
G4009	*Lolium perenne*/Fl1	This study
G4060	*Lolium perenne*/Fl1	This study
G4080	*Lolium perenne*/Fl1	This study
G4163	*Lolium perenne*/Fl1	This study
M472	*Lolium perenne*/Fl1	This study
M659	*Lolium perenne*/Fl1	This study
M708	*Lolium perenne*/Fl1	This study
M713	*Lolium perenne*/Fl1	This study
M730	*Lolium perenne*/Fl1	This study
M833	*Lolium perenne*/ WG11	This study
G3056	*Lolium perenne*/Ag212	This study
G3562	*Lolium perenne*/Ag212	This study
G4010	*Lolium perenne*/Ag212	This study
G4074	*Lolium perenne*/Ag212	This study
G4162	*Lolium perenne*/Ag212	This study
M660	*Lolium perenne*/Ag212	This study
M714	*Lolium perenne*/Ag212	This study
M834	*Lolium perenne*/212GFP	This study
M835	*Lolium perenne*/212GFP	This study
G3324	*Lolium perenne*/Ag51	This study
G4073	*Lolium perenne*/Ag51	This study

G4161	*Lolium perenne*/Ag51	This study
G4062	*Lolium perenne*/Δ*cmkA8.4*	This study
G4077	*Lolium perenne*/Δ*cmkA8.4*	This study
G4168	*Lolium perenne*/Δ*cmkA8.4*	This study
G4061	*Lolium perenne*/Δ*cmkA15.2*	This study
G4085	*Lolium perenne*/Δ*cmkA15.2*	This study
G4166	*Lolium perenne*/Δ*cmkA15.2*	This study
G4063	*Lolium perenne*/Δ*cmkA15.4*	This study
G4082	*Lolium perenne*/Δ*cmkA15.4*	This study
G4165	*Lolium perenne*/Δ*cmkA15.4*	This study
G3315	*Lolium perenne*/Δ*cmkB1.3*	This study
G4076	*Lolium perenne*/Δ*cmkB1.3*	This study
G4167	*Lolium perenne*/Δ*cmkB1.3*	This study
G3317	*Lolium perenne*/Δ*cmkB10.5*	This study
G4078	*Lolium perenne*/Δ*cmkB10.5*	This study
G4164	*Lolium perenne*/Δ*cmkB10.5*	This study
G3316	*Lolium perenne*/Δ*cmkB14.2*	This study
G4079	*Lolium perenne*/Δ*cmkB14.2*	This study
G4169	*Lolium perenne*/Δ*cmkB14.2*	This study
G4084	*Lolium perenne*/Δ*cmkC19.2*	This study
G4172	*Lolium perenne*/Δ*cmkC19.2*	This study
G4011	*Lolium perenne*/Δ*cmkC19.3*	This study
G4081	*Lolium perenne*/Δ*cmkC19.3*	This study
G4171	*Lolium perenne*/Δ*cmkC19.3*	This study
G4012	*Lolium perenne*/Δ*cmkC40.3*	This study

G4083	*Lolium perenne*/Δ*cmkC40.3*	This study
G4170	*Lolium perenne*/Δ*cmkC40.3*	This study
M473	*Lolium perenne*/Δ*cmkAB16*	This study
M709	*Lolium perenne*/Δ*cmkAB16*	This study
M474	*Lolium perenne*/Δ*cmkAB28*	This study
M710	*Lolium perenne*/Δ*cmkAB28*	This study
M711	*Lolium perenne*/Δ*cmkAB28*	This study
M475	*Lolium perenne*/Δ*cmkAB31*	This study
M716	*Lolium perenne*/Δ*cmkAB31*	This study
M712	*Lolium perenne*/Δ*cmkAB31*	This study
M729	*Lolium perenne*/Δ*cnaA12*	This study
M724	*Lolium perenne*/Δ*cnaA13*	This study
M723	*Lolium perenne*/Δ*cnaA19*	This study
M728	*Lolium perenne*/Δ*cnaA27*	This study
M661	*Lolium perenne*/12-1	This study
M715	*Lolium perenne*/12-1	This study
M720	*Lolium perenne*/12-2	This study
M721	*Lolium perenne*/12-2	This study
M719	*Lolium perenne*/12-7	This study
M662	*Lolium perenne*/17-1	This study
M716	*Lolium perenne*/17-1	This study
M717	*Lolium perenne*/17-1	This study
M722	*Lolium perenne*/17-4	This study
M718	*Lolium perenne*/17-11	This study

Table 2.2 Plasmids and cosmids

Name	Relevant characteristics	Reference
Cosmids		
36H7	pMO-cosX clone Fl1 genomic DNA cosmid library containing the *cmkA* gene	This study
41B6	pMO-cosX clone Fl1 genomic DNA cosmid library containing the *cmkB* gene	This study
15H5	pMO-cosX clone Fl1 genomic DNA cosmid library containing the *cmkC* gene	This study
2C5	pMO-cosX clone Fl1 genomic DNA cosmid library containing the *cnaA* gene	This study
12G8	pMO-cosX clone Fl1 genomic DNA cosmid library containing genes deleted in Ag212	This study
17G5	pMO-cosX clone Fl1 genomic DNA cosmid library containing genes deleted in Ag212; sequenced	This study
8B1	pMO-cosX clone Fl1 genomic DNA cosmid library, false positive for gene 1006-3	This study
46D1	pMO-cosX clone Fl1 genomic DNA cosmid library, false positive for gene 1006-3	This study
Plasmids		
pPN83	pBlueScriptII® KS(+) with P*gpd*-EGFP-T*trpC*; Amp^R	(Takemoto *et al*. 2006)
pII99	P*trpC-nptII*-T*trpC* ; Amp^R/Gen^R	(Namiki *et al*. (2001)
pSF15.15	P*trpC-hph* ; Amp^R; Hyg^R	S. Foster
pSF13.5	P*trpC-hph* ; Amp^R; Hyg^R	S. Foster
pSF17.8	P*trpC-nptII*-T*trpC* ; Amp^R; Gen^R	S. Foster
pUC118	Amp^R	(Vieira & Messing (1987)
pGEM-T Easy	Amp^R	Promega
pCR4-Topo	Amp^R, Kan^R	Invitrogen

pAN7-1	P*trpC-hph*; Amp^R, Hyg^R	(Punt *et al.*, 1987)
pAN8-1	Amp^R, Phl^R	(Punt & van den Hondel, 1992)
pBSYT6	Kan^R, Hyg^R	A. Tanaka
pMMI1	PN4057; pSF17.8 containing *5'cmkA*-P*trpC-nptII*-T*trpC-3'cmkA*; Amp^R, Gen^R	This study
pMMI2	PN4058; pSF17.8 containing *5'cmkB*-P*trpC-nptII*-T*trpC-3'cmkB*; Amp^R, Gen^R	This study
pMMI3	PN4059; pSF15.15 containing *5'cmkC*-P*trpC-hph-3'cmkC*; Amp^R, Hyg^R	This study
pMMI4	pSF15.5 containing *5'cnaA*-P*trpC-hph-3'cnaA*; Amp^R, Hyg^R	This study
pMMI5	pSF13.5 containing 3.3 Kb *Hind*III/*Eco*RV *cmkB* fragment ex 41B6; Amp^R, Hyg^R	This study
pMMI6	pUC118 containing 9.2 Kb *Bam*HI *cmkB* fragment ex 41B6; Amp^R	This study
pMMI7	pSF13.5 containing 3.3 Kb *Sst*I/*Bam*HI *cmkA* fragment ex 36H7; Amp^R, Hyg^R	This study
pMMI8	pUC118 containing 11.2 Kb *Sma*I *cmkC* fragment ex 15H5; Amp^R	This study
pMMI9	pSF15.15 containing *5'cmkB*-P*trpC-hph-3'cmkB*; Amp^R, Hyg^R	This study
pMMI10	plasmid obtained by plasmid rescue using *Xho*I genomic digest of Ag212; Amp^R	This study
pMMI11	plasmid obtained by plasmid rescue using *Sst*I genomic digest of Ag212; Amp^R	This study

2.2. Media and growth conditions

All media were prepared with milli-Q and sterilized at approximately 121°C for 15-20 min.

2.2.1. Luria-Bertani medium (LB)

LB medium (Miller, 1972) contained 0.5% (w/v) NaCl, 1% (w/v) tryptone and 0.5% (w/v) yeast extract; pH 7.0 – 7.5. For preparation of LB agar plates, agar was added to LB medium to a final concentration of 1.5% (w/v).

2.2.2. SOC medium

SOC media (Dower *et al.*, 1988) contained 20 mM glucose, 2.5 mM KCl, 10 mM $MgCl_2$, 10 mM $MgSO_4.7H_2O$, 10 mM NaCl, 2% (w/v) tryptone and 0.5% (w/v) yeast extract.

2.2.3. Induction medium (IM)

Induction medium was prepared with 20% (v/v) of 5x Minimal Salt solution (0.05 M $K_2HPO_4.3H_2O$; 0.05 M KH_2PO_4; 0.01 M NaCl; 0.2 mM $FeSO_4.7H_2O$; 94.5 mM $(NH_4)_2SO_4$), 0.4 M MES (pH 5.3), 1M glucose, 1 M $CaCl_2$, 1 M $MgSO_4$ and 0.5% (w/v) glycerol. For preparation of agar plates, agar was added to the final concentration of 1.5% (w/v).

2.2.4. Potato dextrose (PD) medium

PD media was prepared with 2.4% (w/v) potato dextrose broth (Difco). PD agar was prepared by addition of agar to a final concentration of 1.5% (w/v).

2.2.5. Regeneration medium (RG)

RG media contained 2.4% (w/v) potato dextrose (Difco) and 0.8 M sucrose. pH was adjusted to 6.5. RG agar was prepared by addition of agar in final concentrations of 1.5% (w/v) (for plates) or 0.8% (w/v) (for overlays).

2.2.6. Water agar plates (WA)

WA plates were prepared with 3% (w/v) agar added to milli-Q water.

2.2.7. *E. coli* growth conditions

E. coli strains were grown on LB agar plates or in LB broth (with shaking at 200 rpm) at 37°C, overnight. For the selection of ampicillin-resistant (Amp^R) cells, ampicillin was added to the medium to a final concentration of 100 µg/ml. Cultures were stored at -80°C in 50% (v/v) glycerol.

2.2.8. *Agrobacterium tumefaciens* growth conditions

A. tumefaciens used for T-DNA mutagenesis were grown in 1.5 ml LB broth, overnight at 28°C, shaking at 180 rpm. To maintain selection for plasmids, rifampicin and kanamycin were added, both to a final concentration of 50 µg/ml. Cultures were stored at -80°C in 50% (v/v) glycerol.

2.2.9. *Epichloë festucae* growth conditions

E. festucae strains were grown on PD agar at 22°C for 6-8 days or in PD broth, with shaking at 150 rpm, for 4-10 days. *E. festucae* protoplasts were regenerated after

transformation by growing them on RG media at 22°C for 10 to 28 days. Cultures were stored at -80°C in 15% (v/v) glycerol and working stock was maintained at 4°C.

2.2.10. *Epichloë festucae* growth tests

In order to assess growth phenotypes of different *E. festucae* strains under stress conditions in culture, plugs of mycelia, 0.5 cm in diameter, were inoculated onto PD agar plates containing various stress agents. For the induction of osmotic stress, PD agar plates contained 0.4 M, 0.6 M or 0.8 M NaCl. Oxidative stress was induced by addition of 1 mM hydrogen peroxide. Cell wall integrity was tested by addition of 0.01% (w/v) SDS. For Mg^{2+} and Ca^{2+} sensitivity tests, PD agar plates contained 0.4 M, 0.5 M, 0.6 M or 0.8 M $MgCl_2$, 0.4 M. 0.5 M or 0.6 M $CaCl_2$, and both 0.4 M $MgCl_2$ and 0.4 M $CaCl_2$. Growth under conditions of low calcium concentration was assessed by addition of 1 mM EGTA to the PD agar plates. For induction of temperature stress, cultures were grown on PD agar plates at 30°C.

2.2.11. *Lolium perenne* growth conditions

Lolium perenne seedlings were grown on WA plates for three weeks. Two weeks after the inoculation, seedlings were planted in root trainers containing potting mix. After screening for infection with fungal strains, plants were repotted in larger pots containing potting mix and Confidor® Insecticide (Bayer). Plants were watered regularly and sprayed with insecticide and fungicide when required.

2.3. DNA isolation and manipulation

2.3.1. Plasmid DNA Isolation

Plasmid DNA was isolated using the High Pure™ plasmid isolation kit (Roche Diagnostic) according to the manufacturer's instructions. Cultures for plasmid isolation were grown overnight in 5 ml LB broth containing the appropriate antibiotic, at 37°C.

2.3.2. Cosmid DNA isolation

For isolation of cosmid DNA, *E. coli* cultures were grown overnight at 37°C in 5 ml LB broth containing antibiotic. Cells were harvested by 5 min centrifugation at 13,000 rpm. Harvested cells were resuspended in 100 µl of cold Solution I (50 µM glucose, 25 µM Tris-HCl pH 8.0, 10 µM Na_2EDTA; stored at 4°C). In order to induce cell lysis, 0.5 mg of lysozyme was added and cells incubated at room temperature for 5 min. After incubation, 200 µl of fresh Solution II (0.4 N NaOH, 2% SDS (w/v)) was added, followed by 5 min incubation on ice. Neutralization of solution II was achieved by addition of 150 µl of cold Solution III (3 M potassium acetate, 11.5% (v/v) glacial acetic acid; stored at 4°C) and incubation on ice for a further 5 min. The mixture was then centrifuged at 13,000 rpm for 10 min in order to pellet the cellular debris. The supernatant was transferred to a new tube and RNaseA (Sigma-Aldrich) added to a final concentration of 20 µg/ml in order to remove RNA contamination. After 20 min incubation at 37°C the supernatant was purified by chloroform extraction. In order to precipitate cosmid DNA from the aqueous phase, 40 µl of 3 M sodium acetate together with 1 ml of 95% ethanol was added and the mixture incubated at -20°C for 10-20 min. DNA was pelleted by centrifugation at 13,000 rpm for 10 min. After centrifugation, the pellet was washed in 70% ethanol, air-dried and resuspended in 50 µl milli-Q water.

Cosmid DNA used in sequencing reactions was purified using the High Pure™ plasmid isolation kit (Roche Diagnostic) according to the manufacturer's instructions.

2.3.3. Fungal genomic DNA isolation

Fungal genomic DNA was isolated using the method of (Byrd *et al.*, 1990). Cultures were grown in PB broth for 4 days, with shaking. Mycelia was collected and freeze-dried for 48 h. 20-30 mg of freeze-dried mycelia was grounded in liquid nitrogen and resuspended in 800 µl of extraction buffer (150 mM EDTA, 50 mM Tris-HCl, 1% SLS; pH 8.0; stored at room temperature). Protein was removed by addition of proteinase K to a final concentration of 2 mg/ml and incubation at 37°C for 20 min. Cellular debris

was pelleted by centrifugation at 13,000 rpm for 10 min. The aqueous phase was taken through three phenol-chloroform extractions, using a 1:1 phenol-chloroform mixture. The aqueous phase from the final phenol-chloroform extraction was extracted with an equal volume of chloroform in order to remove the residual phenol. DNA was precipitated by addition of an equal volume of isopropanol and incubation at RT for 10 min or -20°C for 2 h. DNA was then pelleted by centrifugation at 13,000 rpm for 10 min. The pellet was washed with 70% ethanol, air-dried and resuspended in milli-Q water.

2.3.3.1. *Crude DNA isolation*

For the purposes of PCR screening, fungal DNA was isolated from a small amount of mycelia (1 cm^2) grown in 150 µl PD broth, at 22°C, for three days, with shaking. Mycelia were collected by centrifugation and ground in 150 µl lysis buffer (100 mM Tris, 100 mM Na_2 EDTA, 1% SDS; pH 8.0; stored at room temperature). The mixture was incubated at 70°C for 30 min, followed by addition of 150 µl of 5 M potassium acetate and further 10 min incubation on ice. Samples were then centrifuged at 13,000 rpm for 10 min. Supernatant was transferred to a new tube and 0.6 volumes of isopropanol were added in order to precipitate DNA. After 15 min centrifugation at 13,000 rpm, pelleted DNA was washed in 70% ethanol, air dried and resuspended in 20 µl milli-Q water.

2.3.4. DNA quantification

Fungal genomic DNA was quantified using DyNA Quant 200 Fluorometer (Hoefer) according to the manufacturer's instructions. All other DNA was quantified using Nanophotometer (Implen) as per the manufacturer's instructions. Both the quantity and quality of DNA was checked using agarose gel electrophoresis (Section 2.3.12). An aliquot of the DNA sample together with a range of DNA standards of known concentration was separated by electrophoresis on a 0.8% agarose (w/v) gel at 100 V for ~1.5 h. Gels were then stained with ethidium bromide and the concentration of DNA of interest determined by comparing band intensity to those of the standards.

2.3.5. Restriction endonuclease digestion of DNA

Plasmid and cosmid DNA was digested for 2-3 h at 37°C, using 3 units of restriction enzyme/µg of DNA, 1x commercial buffer provided with the enzyme and milli-Q water to a final volume of 50 µl. Genomic DNA for Southern blot analysis was digested at 37°C overnight, using 1.1 µg of DNA, 30 units of enzyme, 1x commercial buffer provided with the enzyme and milli-Q water to a final volume of 50 µl.

2.3.6. DNA purification

Inactivation/removal of enzymes or other impurities, as well as purification of PCR products and fragments excised from agarose gels, was achieved by DNA purification using the Wizard® SV Gel and PCR Clean-up System (Promega) as per manufacturer's instructions.

2.3.7. DNA concentration by ethanol precipitation

In order to concentrate DNA in samples of low concentration, samples were mixed with 2.5 volumes of 95% ethanol and 0.1 volumes of 3 M sodium acetate and DNA was precipitated at -20°C for 2 h. DNA was then pelleted by centrifugation at 13,000 rpm for 10 min, washed with 70% ethanol, air-dried and resuspended in milli-Q water.

2.3.8. Gel extraction

DNA bands of interest were excised from ethidium bromide stained agarose gels visualized under the UV light and DNA was extracted using the Wizard® SV Gel and PCR Clean-up System (Promega) as per manufacturer's instructions.

2.3.9. Calf intestinal alkaline-phosphatase (CIAP) treatment of vectors

In order to prevent religation of vectors treated with restriction endonucleases, vectors were treated with calf intestinal alkaline-phosphatase (CIAP; Roche Diagnostics) by incubating 2-5 µg of digested vector with 1 unit of CIAP per picomole of DNA ends in a dephosphorylation buffer provided with the enzyme and milli-Q water to a final volume of 40 µl, at 37°C for 60 min. Samples were then purified by column purification (Section 2.3.6).

2.3.10. Ligation

Ligation of fragments of interest into CIAP-treated vectors was performed by incubating 20 ng of vector DNA with insert DNA (1:3 molar ratio) with 1 unit of T4 DNA ligase (NEB) and 1x ligation buffer supplied with the enzyme in a final volume of 20 µl, overnight, at 4°C. Ligation of A-tailed PCR products into pCR4-Topo (Invitrogen) and pGEM-T easy vectors was done as per manufacturer's instructions. PCR fragments generated with proof-reading enzymes were A-tailed (Section 2.3.11) before ligation into pCR4-Topo or pGEM-T easy.

2.3.11. A-tailing

A-residues were added to the PCR products lacking terminal A-residues in order to facilitate cloning into pCR4-Topo and pGEM-T easy. A-tailing reaction was performed using ~200 ng of purified PCR product, 5 units of Taq DNA polymerase (Roche Diagnostics), 1x Taq DNA polymerase buffer and 200 nM dATP in a total volume of 10 µl. The reaction mixture was incubated at 72°C for 10 min.

2.3.12. Agarose gel electrophoresis

Agarose gels for electrophoresis were prepared in 1x TBE buffer (89 mM Tris; 89 mM boric acid; 2.5 mM Na_2EDTA, pH 8.2). Agarose was added to the buffer and melted in

a microwave oven. The solution was allowed to cool to 55°C before pouring into gel trays. The percentage of agarose in gels varied depending on the size of DNA fragments to be separated. 0.7% agarose gels were used to separate fragments between 3 Kb and 25 Kb, 1% agarose gels for fragments between 1 Kb and 7 Kb, 1.6% agarose gels for fragments between 0.2 Kb and 3 Kb and 2% agarose gels for fragments between 0.1 Kb and 0.2 Kb. All DNA samples, except genomic and cosmid DNA digests used for Southern blot analysis, were separated at voltages of 90-130 V, for 1-2 h. Separation of genomic and cosmid DNA digests for Southern blots was done at 30 V, overnight. After electrophoresis, gels were stained with ethidium bromide (1 µg/ml in milli-Q water) for 15-30 min. The DNA fragments were visualized and photographed using a UV transilluminator Gel Documentation system (Bio-Rad).

2.3.13. Southern blotting

E. festucae genomic and cosmid DNA digests separated by gel electrophoresis, stained and visualized as described in Section 2.3.12, were transferred to positively charged nylon membranes using a modification of the method of Southern (1975). Gels were prepared for blotting as follows: depurination by gentle agitation in blotting solution I (0.25 M HCl), for 15 min; denaturation by gentle agitation in blotting solution II (0.5 M NaOH, 0.5 M NaCl), for 45 min; neutralization by gentle agitation in blotting solution III (2 M NaCl, 0.5 M Tris, pH 7.4), for 60 min. Upon neutralization, the gel was washed for 2 min in 2x SSC (0.3 NaCl, 0.03 M trisodium citrate) and assembled onto a blotting stand which was assembled as follows: two 3MM paper wicks soaked in 20x SSC (3 NaCl, 0.3 M trisodium citrate); covered with plastic wrap except for a surface area slightly smaller than the gel; gel was placed on top of the assembly and covered with the nylon membrane presoaked in 2x SSC; two 3MM papers presoaked in 2x SSC and two dry 3MM papers were placed on top of the membrane, followed by a stack of paper towels and a weight. The blot assembly was left overnight to allow DNA to transfer. Upon transfer, the membrane was washed in 2x SSC for 5 min and DNA was crosslinked to the membrane using an Ultraviolet crosslinker Cex-800 (120,000 lJ/cm^2; Ultra-Lum Inc.).

2.3.13.1. *Radioactive probe labeling and hybridization*

The DNA fragments used in Southern blot analyses were radioactively labeled as follows: DNA fragments were denaturated by boiling for 3 min and placing directly on ice; fragments were then radioactively labeled using [^{32}P]-dCTP (3,000 Ci/mmol; Amersham Biosciences) and High Prime kit (Roche Diagnostics) as per the manufacturer's instructions. The membranes were prehybridized in 10x Denhardt's solution (0.4 M Hepes buffer (pH 7.0), 3x SSC, 0.02 mg/ml *E. coli* tRNA, 0.1% SDS, 0.2% Ficol, 0.2% BSA, 0.2% PVP, 0.0018% phenol extracted herring sperm DNA) for at least 2 h at 65°C in glass hybridization tubes (Amersham Biosciences). The labeled probe was denaturated by boiling, placed on ice for 5 min and added to the hybridization tube. Hybridization was performed overnight at 65°C. Upon hybridization, membranes were washed in 2x SSC containing 0.1% SDS (w/v). Hybridized bands were detected by exposure to X-ray film (Fuji) at -80°C. The length of exposure varied depending on signal intensity. Films were developed in a 100Plus™ automatic X-ray processor (All-Pro Imaging Corp.).

2.3.13.2. *Stripping of radioactive membranes*

Hybridized membranes were striped by adding boiling 0.1% (w/v) SDS solution to the blots, which were agitated until the solution cooled to RT. This was repeated at least three times and stripped membranes were checked using a Geiger counter to ensure all radioactive labeled probe was removed.

2.3.14. DNA sequencing

Sequencing of plasmids and PCR generated DNA fragments was carried out by the Massey Genome Service, Massey University Palmerston North, New Zealand, using BigDye™ Terminator (version 3.1) Ready Reaction Cycle Sequencing Kit (Applied Biosystems). Samples for sequencing were prepared as per facility's instructions: the reaction mixture of 15 µl contained 300 ng of plasmid DNA or 2 ng/ 100 bp of PCR

products and 3.2 pmol of primers. Sequence data was analyzed using MacVector™ Assembler (Accelrys) or SEQUENCHER version 4.5 (Gene Codes).

2.3.15. Cosmid sequencing

Cosmid DNA was isolated using High Pure™ plasmid isolation kit (Roche Diagnostic) according to the manufacturer's instructions and the sample containing 5 µg of cosmid DNA in 100 µl DNase-free water (provided with the kit) was sent to the Massey Genome Service, Massey University Palmerston North, New Zealand. Cosmid from the clone 17G5 was sequenced by the Illumina Genome Analyzer IIx (informally known as Solexa) with version 1.6 of Illumina's data analysis pipeline. Sequence data was assembled by Dr Murray P. Cox, using the de Bruijn graph assembler *ABySS* (version 1.2.0).

2.3.16. Plasmid rescue

Plasmid rescue was performed using genomic DNA of T-DNA mutants. 1 µg of genomic DNA was digested using the appropriate enzyme, overnight at 30°C. The digest was then purified by phenol : chloroform extraction and precipitated with isopropanol (Section 2.3.15.1). The purified DNA was ligated at a final concentration of 10 ng/µl, using 1x T4 DNA ligase buffer (New England Biolabs) and 40 units of T4 DNA ligase (New England Biolabs) in 20 µl, 40 µl, 60 µl, 80 µl and 100 µl reactions. After overnight ligation, each reaction was transformed into *E. coli* TOP10 cells and Amp^R colonies were screened for the presence of the appropriate plasmid (Section 2.5.1.1).

2.3.16.1. *Phenol-chloroform purification of DNA*

DNA was purified by adding equal volumes of phenol and chloroform, vortexing and spinning for 10 min at 13,000 rpm. Residual phenol was removed by addition of equal

volume of chloroform, vortexing and spinning for 10 min at 13,000 rpm. DNA was then precipitated with isopropanol, washed with ethanol and resuspended in milli-Q water.

2.3.17. Screening of *E. festucae* cosmid library

For the purposes of the cosmid library screen, radioactive labeling of probes, hybridization, washing and stripping of filters were performed as described in Section 2.3.13.1, with the following differences: filters were hybridized in (360 mM Na_2HPO_4, 50 mM NaH_2PO_4, 7% (w/v) SDS, 1% (w/v) BSA, 1 mM EDTA pH 8.0) instead of 10x Denhardt, in plastic boxes, without shaking at 65°C. Radioactive probes were stripped from the filters by three 10 min incubations in a stripping solution (0.1 M NaOH, 10 mM EDTA pH 8.0, 0.1% (w/v) SDS), followed by a single milli-Q water rinse and a 10 min wash in 5x SSPE (75 mM NaCl, 50 mM $NaH_2PO_4.H_2O$, 6.25 mM Na_2EDTA).

2.4. RNA isolation and manipulation

2.4.1. RNA isolation and quantification

Total RNA was isolated from ~100 mg of fungal mycelia or pseudostem of endophyte infected plants. Plant tissue or mycelia from liquid culture was ground in liquid nitrogen using a mortar and pestle and resuspended in 1 ml of TRIzol. Samples were centrifuged at 9,700 rpm for 10 min, at 4°C. 200 µl of chloroform was added to the supernatant, mixed for 15 sec and incubated at RT for 3 min, followed by centrifugation at 9,700 rpm for 15 min, at 4°C. RNA was precipitated by mixing the aqueous phase with 500 µl of isopropanol, incubation at RT for 10 min and centrifugation at 9,700 rpm for 10 min, at 4°C. The pellet was washed in 75% ethanol, air-dried and resuspended in DEPC-treated water.

2.4.2. RNA agarose gel electrophoresis

The quality of the isolated RNA was assessed by agarose gel electrophoresis, using 1.4% agarose 0.3% SDS gel. Electrophoresis was performed at 110 V for 1.5 h.

2.4.3. DNAse treatment

In order to eliminate DNA contamination, RNA samples were treated with DNaseI using Amplification Grade DNase I (Invitrogen), as per manufacturer's instructions.

2.4.4. RT-PCR

Total RNA isolated as described in Section 2.4.1 and treated with DNaseI as described in Section 2.4.3 was used for cDNA synthesis using Super-Script™ First Strand Synthesis system for RT-PCR (Invitrogen) as per manufacturer's instructions.

2.5. Cell transformation

2.5.1. *E. coli* transformation

Chemically competent TOP10 cells, commercial (Invitrogen) or prepared in the laboratory, were transformed by addition of 2-5 µl of ligation mixture or 1 ng of control plasmid to one vial of cells (50 µl for commercial cells, 100 µl for cells prepared in the laboratory). Cells were then incubated on ice for 5 min, heat-shocked at 42°C for 30 sec, gently mixed with SOC and incubated at 37°C for 1 h with shaking. Upon incubation, cells were plated on LB agar plates containing appropriate antibiotic. Chemically competent DH5α cells were transformed by addition of 2-5 µl of ligation mixture or 1 ng of control plasmid to 100 µl of cells. Cells were then incubated on ice for 20 min, heat-shocked at 42°C for 60 sec, gently mixed with 900 µl of SOC and incubated at 37°C for 1 h with shaking. After incubation, cells were plated on LB agar plates containing an appropriate antibiotic.

2.5.1.1. *Screening of* E. coli *colonies for presence of the plasmid*

The presence of the correct plasmid in the transformed colonies of *E. coli* was confirmed using CloneChecker™ System (Life Technologies) as per manufacturer's instructions.

2.5.2. *E. festucae* transformation

2.5.2.1. *Preparation of protoplasts*

Fungal protoplasts were prepared from 7-day-old mycelia grown in liquid culture, at 22°C. Mycelia were harvested, washed first in milli-Q water then in OM buffer (1.2 M $MgSO_4.7H_2O$, 10 mM Na_2HPO_4, pH 5.8, adjusted using 100 mM $Na_2HPO_4.2H_2O$) and weighed. Filter sterilized glucanex (Chemcolour; 10 mg/ml) was added to give a final ratio of ~10 ml per 1 g of mycelia (wet weight). The mixture was incubated at 30°C for 4-5 h, with shaking at ~80 rpm, in order to digest the cell walls. Undigested mycelia were removed by filtering samples through a nappy liner and protoplasts were harvested from the filtrate by overlaying with 2 ml of ST buffer (0.6 M sorbitol, 100 mM Tris-HCl, pH 8) and centrifuging at 4,000 rpm for 5 min. The band of protoplasts formed at the interface of the glucanex-ST layer was collected and protoplasts were washed at least three times with STC buffer (1 M sorbitol, 50 mM $CaCl_2$, 50 mM Tris-HCl, pH 8). In each washing step, protoplasts were collected by centrifugation at 4,000 rpm for 5 min. After the final washing step, protoplasts were resuspended in STC buffer to the final concentration of 1.25×10^8 protoplasts/ml. For long-term storage, 80 µl aliquots of protoplasts were mixed with 20 µl PEG buffer (40% PEG 4000, 50 mM $CaCl_2$, 1 M sorbitol, 50 mM Tris-HCl, pH 8) and stored at -80°C.

2.5.2.2. *Transformation of protoplasts*

Fungal protoplasts were transformed following the method of Itoh *et al*. (1994). Aliquots of 5 µl heparin (5 mg/ml), 2 µl spermidine (50 mM) and 5 µg of DNA were

added to a mixture of 80 µl protoplasts and 20 µl PEG buffer (described in Section 2.5.2.1). Samples were gently mixed and incubated on ice for 30 min, before addition of 900 µl of PEG buffer, mixing and incubation on ice for further 15-20 min. Aliquots of 330 µl were then added to the 3.5 ml of molten 0.8% agar RG medium and the mixture was spread on the 1.5% agar RG plates. Plates were incubated at 22°C for 24 h and then overlaid with 5 ml molten 0.8% agar RG containing hygromycin, geneticin or zeocin, to final concentrations of 150 µg/ml, 200 µg/ml and 160 µg/ml, respectively. Plates were incubated at 22°C for 10-28 days and transformants growing through the antibiotic overlay were subcultured onto PD agar plates containing an appropriate antibiotic. These transformants were then taken through 3 rounds of nuclear purification by subculturing 2 mm^2 piece of mycelia from the edge of the colony to a fresh plate.

2.5.3. *A. tumefaciens* mediated T-DNA mutagenesis

A. tumefaciens mediated T-DNA mutagenesis of *E. festucae* strain FL1 was performed using *A. tumefaciens* strain EHA105/pBSYT6, together with EHA105, containing disarmed agropine plasmid pTiBo542, as a control. *A. tumefaciens* strains were grown overnight in 1.5 ml of LB containing rifampicin for strain EHA105 and both rifampicin and kanamycin for strain EHA105/pBSYT6. Cells were harvested by centrifugation at 4,000 rpm and resuspended in 100 µl induction medium (IM). Resuspended cells were then grown for 6 h in 1 ml IM containing 200 µM acetosyringone, in a 30 ml culture tube, at 28°C, with shaking (200 rpm). After the incubation, 100 µl of the *Agrobacterium* culture was mixed with fungal mycelia prepared as follows: a 2 cm^2 block of mycelia was finely ground in 30 ml PD broth and 4 ml aliquots were grown in universal bottles for 6 days, at 22°C. Mycelia were harvested by centrifuging at 3,500 rpm for 5 min and resuspended in 5 ml IM. The mixture of mycelia and bacterial culture was spread over a sterile nitrocellulose membrane placed on the IM agar plates containing 200 µM acetosyringone. After a 48 h incubation period at 22°C, the membranes were transferred to PD agar plates containing 150 µg/ml hygromycin and 200 µg/ml cefataxime, in order to select for Hyg^R fungal transformants. Plates were incubated at 22°C for 8-20 days and Hyg^R transformants were subcultured onto PD plates containing hygromycin. Transformants were then taken through 3 rounds of nuclear purification.

2.6. PCR reactions

Oligonucleotide primers used in this thesis are listed in Table 2.3. All primers were synthesized by Invitrogen or Sigma Aldrich. Primers were resuspended in sterile milli-Q water to concentration of 100 pmol/µl. Primers used in PCR reactions were diluted to a final concentration of 10 pmol/µl. All stock was stored at -20°C.

Table 2.3 Primers used in PCR reactions

Name	Sequence	Designed for
MI1	TCGAGTTCACCAACGATG	*cmkC*
MI2	CGCATATTGTCAGCCTTG	*cmkC*
MI3	TCGCAGGAATGCTCAACC	*cmkA*
MI4	TCCTTGGCATCTTGACTG	*cmkA*
MI5	CGAATCTGCCGCAAAGGGTC	*cmkB*
MI6	TGCGTCGGGCGTTGAAGTTC	*cmkB*
MI13	ATCACCGTTTGTGGCGACG	*cnaA*
MI14	TCTCGCAGCACCTGGAACAC	*cnaA*
MI15	TTCCTCGGCGATTACGTCG	*cnaA1*
MI16	GCCCACCAGACGCAATTTTG	*cnaA1*
MI59	TACTTGGTACCACACCTGTGTCG	*cmkA* 3'flanking sequence
MI60	CGGGTCTGTCTCACAGCAG	*cmkA* 3' flanking sequence
MI66	TTGTCCTGCAGATCATCAATTCCATC	*cmkC* 5' flanking sequence
cna1372F	CACGCTGAGCCTAACCTCGT	*cnaA1*
cna1372R	CAGGACACATTCAACGCTAAA	*cnaA1*
1372-1 F	TGGCTGAAGGCTACCGTTGTG	*cnaA1*
1372-1 R	CTGATGCTGTCCTAACCAAGTTTTC	*cnaA1*
1327-2 F	CTGAGGTCTGACGAAACG	*cnaA1*
1372-2 R	CCAACTGGCTACTTACGG	*cnaA1*
cna2 F	CGAGTCGGATTTGTCAACAC	*cnaA1*

cna2 R	CAGTGGTGGTGGTATTTGG	*cnaA1*
1006ppF	CGATAATAACAGTAGACTTGCACG	1006-3
1006ppR	GCTTTTTGTTGCCGATCTG	1006-3
CT-1F	GCCACCTTTGGAAATGTCG	CRAL-TRIO domain protein
CT-1R	GCCAGCAACTCAGGATACG	CRAL-TRIO domain protein
BinF	GCCAAAGTCATCAACAAGCG	*cmkB*, amplifying over intron
BinR	AGGTCCGTCACGAGGTAGAG	*cmkB*, amplifying over intron
pBSYT6-2	CCAAGCTGTTTTCCGAGAAG	pBSYT6
pVSsta-f	GCGGCCGCCGAGAATGAACG	pBSYT6
c_1085-1F	CCAAACTCGTCCTCGTATTCG	1085-1
c_1085-1R	CGTATTCCACAGCAGCAAGTC	1085-1
c_1085-2F	CTCCTGGAAAGGCTATCATTG	1085-2
c_1085-2R	TGAAGTGGGGGACTCTACTGG	1085-2
c_1085-3F	GCGAAGTTGAGCAAAGATGTAG	1085-3
c_1085-3R	AAACGAAGGGTGAGCGTCC	1085-3
c_849-2F	GCTCAGCGAAACTACCGTAAG	849-1
c_849-1F	TGGCTTAGTAATGGACGGAAG	Contig 849
c_849-1R	GCTTGGGGGATTTGGGTAG	Contig 849
f-1,6-bpF	TCGTCGAAGCTGCCCATGTA	1085-6
f-1,6-bpR	TTGCCTACCCTGCCGATAAGA	1085-6
icmtF	GGAACAAGGAGCACGATGAG	1085-7
icmtR	GCACAAGTCTGGGCGTATTC	1085-7
pex11-F1	TTCCTCGAGGACGAGGGAAA	1085-5

pex11-R1	TGCGCTACGGTGGGGTGGTA	1085-5
mdm1F2	TCCTTGTGTCGTAGTGAATCG	1085-4
mdm1R2	TCCTGGGGCTATGCTGTAAG	1085-4
mdm1F1	ATTGCGAGGAAGGTTGCCC	1085-4
mdm1R1	GTGAGCACGATGATTACAACG	1085-4
ciao30-F1	CCTGGGACAAGTTCAAGGC	1085-8
ciao30-R1	CAGACATCATCAAGGAATCGC	1085-8
c_1006-3F	TACAGGCTCTTGGACAGCACTC	1006-1
sidR	ACCAAGCAAGGAGCCAATGC	1006-2
sid1FRB	GGTCACAGGCGCGGCAGCATT	1006-2
1006gR1	CATCTCGCTTTTCATATTATC	1006-3
T1	GGTGCGGGAA	Random primer T1
T2	CCAGATGCAC	Random primer T2
T3	GTGACATGCC	Random primer T3
T4	AGATGCAGCC	Random primer T4
T5	TGCGGCTGAG	Random primer T5
T6	GGACCCAACC	Random primer T6
T7	CACCGTATCC	Random primer T7
T8	ACCCGGTCAC	Random primer T8
T9	GGAGCCCAC	Random primer T9
T10	ACGATCGCGG	Random primer T10
RB1	TGCGTTATCCCCTGATTCTGTGGATAA	RB of pBSYT6 and pBSYT7
RB2	CATTAATGCAGCTGGCACGACAG	RB of pBSYT6 and pBSYT7
RB3	CAGCCCGGGGGTTAACGCTA	RB of pBSYT6 and pBSYT7

RB4	TTGCCGGTCTTGCGATGATTA	RB of pBSYT6 and pBSYT7
RB5	ACAAAATATAGCGCGCAAACTAGG	RB of pBSYT6 and pBSYT7
LB1	TCTTCCAGATACAGCTCATC	LB of pBSYT6 and pBSYT7
LB2	CGTCAAGAGACCTACGAGACTG	LB of pBSYT6 and pBSYT7
LB3	GGGTTCGCAAAGATATTG	LB of pBSYT6 and pBSYT7
LB4	ACCCAATACGCCGGCCGA	LB of pBSYT6
LB5	CCCAGATAAGGGAATTAGGGTTCC	LB of pBSYT6
T1.1	GAGAAAATGCGTGAGATTGT	β-tubulin gene
T1.2	TGGTCAACCAGCTCAGCACC	β-tubulin gene
C_532LBR	CCTGCTCACCAGTCAAGCCAAT	contig_532
pII99-2	TTGAGTGAGCTGATACCG	KO construct amplification
pII99-3	GGCTGGCTTAACTATGCG	KO construct amplification
C_532RB1F	CATTCGATCAGATGACTTTGT	Contig_532
C_532RB1R	CGTTCCTTGTCCATTTCTCAA	Contig_532

2.6.1. Standard PCR

Standard PCR amplifications of genomic and plasmid DNA templates were carried out in 25 µl reaction containing: 5 ng genomic DNA or 1 ng plasmid DNA, 1x Taq polymerase commercial buffer supplied with the enzyme, 50 µM each dNTP, 200 nM each primer and 0.5 U Taq polymerase (Roche Diagnostics). The thermocycler conditions used were: 35 cycles, at an annealing temperature of between 55°C and 60°C and elongation time of 50 sec/1 Kb. PCR amplification reported in this thesis were performed using standard PCR, unless otherwise stated.

2.6.2. High fidelity enzymes

PCR products used in the construction of replacement constructs were amplified using the proof-reading high fidelity enzyme *Pfx*50^{TM} DNA polymerase (Invitrogen) according to the manufacturer's instructions. PCR products used as probes in Southern blot analyses or cosmid library screening were generated using Triple Master PCR System (5 PRIME), as per manufacturer's instructions.

2.6.3. Long template

Replacement constructs used for transformation of *E. festucae* protoplasts were amplified using the Expand Long Template reaction mixture (Roche) as per manufacturer's instructions.

2.6.4. cDNA PCR

cDNA (prepared as in Section 2.4.4) was amplified in a 20 µl reactions containing: 1x Taq polymerase buffer, 50 µM each dNTP, 500 nM each primer, 1 U of Taq polymerase and 2 µl of cDNA. Thermocycler conditions were as per standard PCR amplification, except for number of cycles reduced to 29.

2.6.5. TAIL-PCR

Thermal asymmetric interlaced (TAIL)–PCR was used for the recovery of genomic DNA fragments adjacent to the sequences of left border (LB) of T-DNA inserted in the genome of Ag51. TAIL-PCR was done using the method described in (Liu & Whittier, 1995) with modifications described by (Terauchi & Kahl, 2000).

2.7. Plant inoculation and growth analysis

2.7.1. Seed sterilization

Lolium perenne seeds, cultivar Samson, endophyte-free, were surface sterilized before the germination and inoculation with endophyte. Sterilization was achieved by immersion of seeds in 50% sulfuric acid for 30 min, followed by washing three times with milli-Q water. Seeds were then immersed in 50% bleach for 20 min and sterilized seeds washed three times in sterile milli-Q water and air-dried.

2.7.2. Seedling germination and inoculation

Prior to inoculation, surface-sterilized seeds were germinated on WA plates for 7 days, in the dark, at 22°C. The seedlings were then inoculated using the method described by (Latch & Christensen, 1985). After inoculation, the seedlings were incubated for a further 7 days in the dark, at 22°C and then transferred to the light, for a further 7 days at 22°C. Seedlings were then transferred to the greenhouse and planted in root trainers containing potting mix.

2.7.3. Immunoblotting

Four to six weeks after planting, inoculated seedlings were immunoblotted in order to check for the systemic fungal infection. Imunoblotting was performed by cutting tillers close to the base, removing dead leaves and pressing the cut end onto a nitrocellulose

membrane (BDH 0.45 mM Electran). The membrane was soaked in blocking solution (10 mM Tris (hydroxymethyl) methylamine, 50 mM NaCl, 10 mM HCl, 0.5% (w/v) milk powder, pH 7.5) for 2 h at RT which was followed by transfer of the membrane to fresh blocking solution containing primary antibody (1:1000 dilution) and overnight incubation at 4°C. The unbound primary antibody was then removed by several washes with fresh blocking solution. The membrane was then transferred to blocking solution containing secondary antibody (1:2000 dilution) and incubated at RT for 2 h. Several washes with fresh blocking solution were then performed to remove the unbound antibody and the membrane was transferred to fresh chromogen solution (a mixture of 12.5 mg Fast Red in 12.5 ml of 10 mM Tris buffer, pH 8.2, and 12.5 mg naphthol AS-MX phosphate in 12.5 ml of 10 mM Tris buffer, pH 8.2) and incubated at RT for 15 min. The membrane was finally washed with water and allowed to air-dry. The presence of red colour was indicative of a positive reaction.

2.7.4. Aniline blue staining

Fungal hyphae *in planta* were visualized by taking epidermal peels from the inner surfaces of the outer leaf sheaths and mounting them in aniline blue stain (88% lactic acid, 50% glycerol, 0.1% (w/v) aniline blue). The leaf was immersed in aniline blue stain, covered with a cover slip, heated briefly to aid penetration of the stain and remove air bubbles, and then examined by light microscopy.

2.8. Bioinformatics analyses

2.8.1. Sequence comparison and domain analysis

E. festucae sequences were compared with other sequences using the National Centre for Biotechnology Information (NCBI) site (http://www.ncbi.nlm.nih.gov/), using the BLASTn, BLASTp and BLASTx algorithms. Similarity of amino acid sequences was assessed using MacVector™ ClustalW. Intron/exon boundaries were analysed by FGENESH at the Softberry site (http://www.softberry.com/berry.phtml) using *N. crassa*

and *F. graminearum* models as templates. Predicted protein domain structures were analysed using InterProScan (http://www.ebi.ac.uk/Tools/InterProScan/).

2.8.2. Synteny analysis

Synteny between *E. festucae* and *F. graminearum* in the region deleted in Ag212 was examined using the Fungal Genome Initiative (FGI) site (http://www.broad.mit.edu/) and *E. festucae* genome site (http://csurs.csr.uky.edu/biodb-testbed/). Synteny maps were prepared using MacVector™.

2.9. Microscopy

E. festucae culture samples examined by microscopy were either taken directly from the PD agar plates (a 0.25 cm^2 piece of mycelia was excised from the PD agar plate and placed on the microscopic slide) or grown on slides covered with PD agar (slide was placed on the PD plate and covered with an additional 8-10 ml of PD agar). Bright field microscopy was performed using a Zeiss Axiophot light microscope and images recorded using a Leica DCF320 digital camera. Confocal microscopy was performed using a Leica SP5 DM6000B Confocal microscope. Transmission electron microscopy was performed using Philips CM10 transmission electron microscope and images were recorded using a SIS Morada digital camera.

2.9.1. Light microscopy

Light microscopy was used to examine the growth of *E. festucae* strains in culture (bright field and differential interference contrast microscopy), *in planta* samples stained with aniline blue (bright field) and NBT stained *E. festucae* colonies (bright field).

2.9.2. Confocal microscopy

The *in planta* phenotype of EGFP-expressing strains of Fl1 and Ag212 were examined using confocal microscopy. Samples were prepared by cutting 2-week and 5-week-old inoculated seedlings longitudinally, through the meristematic zone.

2.9.3. Transmission electron microscopy (TEM)

Samples for TEM were prepared by cutting 2-week-old seedlings inoculated with EGFP-expressing strains of Fl1 and Ag212 transversely through the inoculation point and ~1 mm on each side of the inoculation point to generate 1 mm thick pieces of pseudostem tissue. Tissues was then fixed in 3% glutaraldehyde and 2% formaldehyde in 0.1 M phosphate buffer, pH 7.2 for 1 h and transverse sections were prepared for TEM as described by (Spiers & Hopcroft, 1993).

2.10. Colony staining

2.10.1. Diaminobenzidine (DAB)

Freshly prepared DAB (1 mg/ml in milli-Q water, ~pH 3.2; Sigma-Aldrich) was poured over colonies grown on PD agar plates. Colonies were then incubated in the dark at RT for ~24 h and transferred to 4°C another ~24 h or until a brick red precipitate was formed.

2.10.2. Nitroblue tetrazolium (NBT)

NBT (0.05% in 50 mM sodium phosphate buffer, pH 7.5; Sigma-Aldrich) was added to the colonies grown on PD agar plates which were then incubated for ~5 h at RT, flooded with 100% ethanol to terminate the reaction and examined by light microscopy.

2.11. Construction of plasmids

2.11.1. pMMI1

The replacement construct for *cmkA*, pMMI1, was prepared by ligating fragments 5' and 3' of the *cmkA* into the Gen^R vector pSF17.8. The 1.9 Kb *XhoI* fragment upstream of the 5' end of *cmkA* was excised from the cosmid clone 36H7 and cloned downstream of the *nptII* resistance gene in pSF17.8. The fragment downstream of the 3' end of *cmkA* was generated by PCR, using forward primer MI59 that introduced a *KpnI* restriction site, and reverse primer MI60. This 2.4 Kb fragment was first cloned into pCR4-TOPO vector and sequenced to confirm that sequence was free of polymerase-induced mutations. This fragment was then subcloned upstream of the *nptII* gene in pSF17.8, generating the final replacement construct pMMI1. The orientation of the flanking fragments was confirmed by sequencing. A linear construct containing the *nptII* gene with *cmkA* flanking sequences was PCR amplified using pMMI1 as a template, Expand Long Template PCR system and primer pair pII99-2/pII99-3. This fragment was concentrated and used for transformation of Fl1 protoplasts.

2.11.2. pMMI2

The flanking fragments used for generation of pMMI2, the replacement construct for *cmkB*, were excised from cosmid clone 41B6. A 2.8 Kb *SalI* fragment 5' of *cmkB* was cloned 3' of the *nptII* cassette in the Gen^R vector pSF17.8. The 2.5 Kb *EcoRV* fragment 3' *cmkB* was cloned 5' of the *nptII* cassette. The orientation of the fragments was confirmed by sequencing. A linear fragment was amplified using Expand Long Template PCR system, primer pair pII99-2/pII99-3 and pMMI2 as a template. Product of this PCR was used for protoplast transformation.

2.11.3. pMMI3

The replacement construct for *cmkC*, pMMI3, was generated by cloning fragments upstream and downstream of the gene into the Hyg^R vector pSF15.15. The fragment 5'

of *cmkC* was generated by PCR using forward primer MI66, which introduced a *PstI* restriction site, and reverse primer MI2. The 2.7 Kb PCR product was A-tailed and cloned into pCR4-TOPO vector and the 1.5 Kb *PstI* fragment was excised from this plasmid and sub-cloned 3' of the *hph* gene in the pSF15.15. The 3.3 Kb *SstI* fragment 3' of *cmkC* was excised from the cosmid clone 15H5 and cloned 5' of *hph* cassette. The orientation of the fragments was confirmed by sequencing. A linear fragment of pMMI3, amplified by Expand Long Template PCR system, using primer pair pII99-2/pII99-3, was used for protoplast transformation.

2.11.4. pMMI4

The calcineurin A gene replacement construct was generated by cloning fragments excised from the cosmid 2C5. The 1.4 Kb *Pst*I/*Bam*HI fragment, 5' of the *cnaA* gene was cloned 3' of the *hph* cassette in the vector pSF15.15. The 2.1 Kb *Eco*RI/*Eco*RV fragment, 3' of the *cnaA* gene, was cloned 5' of the *hph* cassette, generating plasmid pMMI4.

2.11.5. pMMI5

The 3.3 Kb *Hind*III/*Eco*RV fragment containing *cmkB* was excised from cosmid 41B6 and cloned into hygromycin resistance vector pSF13.5, generating pMMI5, plasmid used for complementation tests of Δ*cmkB1.3*.

2.11.6. pMMI6

The 9.2 Kb *Bam*HI fragment containing *cmkB* was excised from cosmid 41B6 and cloned into pUC118 generating pMMI6, plasmid used for complementation tests of Δ*cmkB1.3*, Δ*cmkB10.5* and Δ*cmkAB16*. Since this plasmid carried no fungal resistance markers, pMMI6 was co-transformed with pAN7-1 (Hyg^R) into fungal protoplasts of Δ*cmkB1.3* and Δ*cmkB10.5* protoplasts, and with pAN8-1 for transformation of Δ*cmkAB16* protoplasts.

2.11.7. pMMI7

The 3.3 Kb *Sst*I/*Bam*HI fragment containing *cmkA* was excised from 36H7 and cloned into the hygromycin resistance vector pSF13.5 to generate pMMI5, plasmid used for complementation tests of Δ*cmkA15.2* and Δ*cmkAB16*.

2.11.8. pMMI8

The 11.2 Kb *Sma*I fragment containing *cmkC* was excised from cosmid 15H5 and cloned into pUC118, generating pMMI8. Since this plasmid carried no fungal resistance markers, pMMI8 was co-transformed with pII99 into protoplasts of Δ*cmkC19.2*.

2.11.9. pMMI9

In order to generate the *cmkB* replacement construct containing the hygromycin resistance cassette, *cmkB* flanking sequences, 5' (*SalI* fragment) of and 3' (*EcoRV*) of *cmkB*, were excised from pMMI2 and sub-cloned into vector the pSF15.15, 3' and 5' of *hph* cassette, respectively to generate pMMI9. The 6.8 Kb *Xho*I/*Hpa*I fragment was excised from pMMI9 and transformed into Δ*cmkA15.2* protoplasts.

3. Results

3.1. Identification of *cmkA*, *cmkB* and *cmkC*

Amino acid sequences of Ca^{2+}/calmodulin-dependent protein kinases identified in other filamentous fungi (Yang *et al*., 2001b, Dayton & Means, 1996, Joseph & Means, 2000, Solomon *et al*., 2006) were used in a TBLASTN search of the *E. festucae* genome database (http://csurs.csr.uky.edu/biodb-testbed/). This search identified the respective *E. festucae* homologues of *S. nodorum cpkA*, *cpkB* and *cpkC*. These genes, named *cmkA*, *cmkB* and *cmkC* respectively, were located on contigs 213, 418 and 151 respectively, of the genome map of *E. festucae* strain E2368 (unique gene identifiers given in Appendix 5.10). Virtual translation of these cDNAs using MacVector predicted that CmkA, CmkB and CmkC proteins contain 379, 427 and 677 amino acids, respectively. Amino acid alignments of the *E. festucae* Cmk proteins with homologues from other filamentous fungi showed that they are highly conserved, with CmkB being the most conserved of the three (Figs. 3.1, 3.2 and 3.3). SoftBerry Fgenesh software was used to predict exon-intron structure of *E. festucae cmks* using *F. graminearum* and *N. crassa* gene models as reference. The exon-intron structure identified from this analysis was confirmed experimentally from an *E. festucae* transcriptome sequence analysis (Eaton *et al*., 2010) (Appendices 5.1, 5.2, 5.3, 5.4, 5.5 and 5.6 – Δ*sakA* mutant data included for representation purposes because of a higher coverage). The *cmkA*, *cmkB* and *cmkC* genes were found to have 6, 2 and 6 exons, respectively (Fig. 3.4). InterProScan and Calmodulin Target Database software were used to identify conserved protein domains present in CmkA, CmkB and CmkC. This analysis showed that all three *E. festucae* proteins contain a serine/threonine protein kinase domain, a Ca^{2+}/calmodulin-dependent protein kinase domain and a putative calmodulin binding domain (Fig. 3.4). InterProScan analysis also identified a Ca^{2+}/calmodulin-dependent protein kinase kinase domain in CmkC, confirming that this protein is the homologue of the *S. nodorum* protein kinase kinase, CpkC (overlapping with the Cmk domain in Figure 3.4C).

3.2. *cmkA*, *cmkB* and *cmkC* are differentially expressed in culture and *in planta*

In order to determine weather *cmkA*, *cmkB* and *cmkC* are regulated during symbiosis, RT-PCR was used to compare expression of each gene in culture and *in planta*. Total RNA was isolated from mycelia of *E. festucae* Fl1 grown in culture and from pseudostems of Fl1 infected

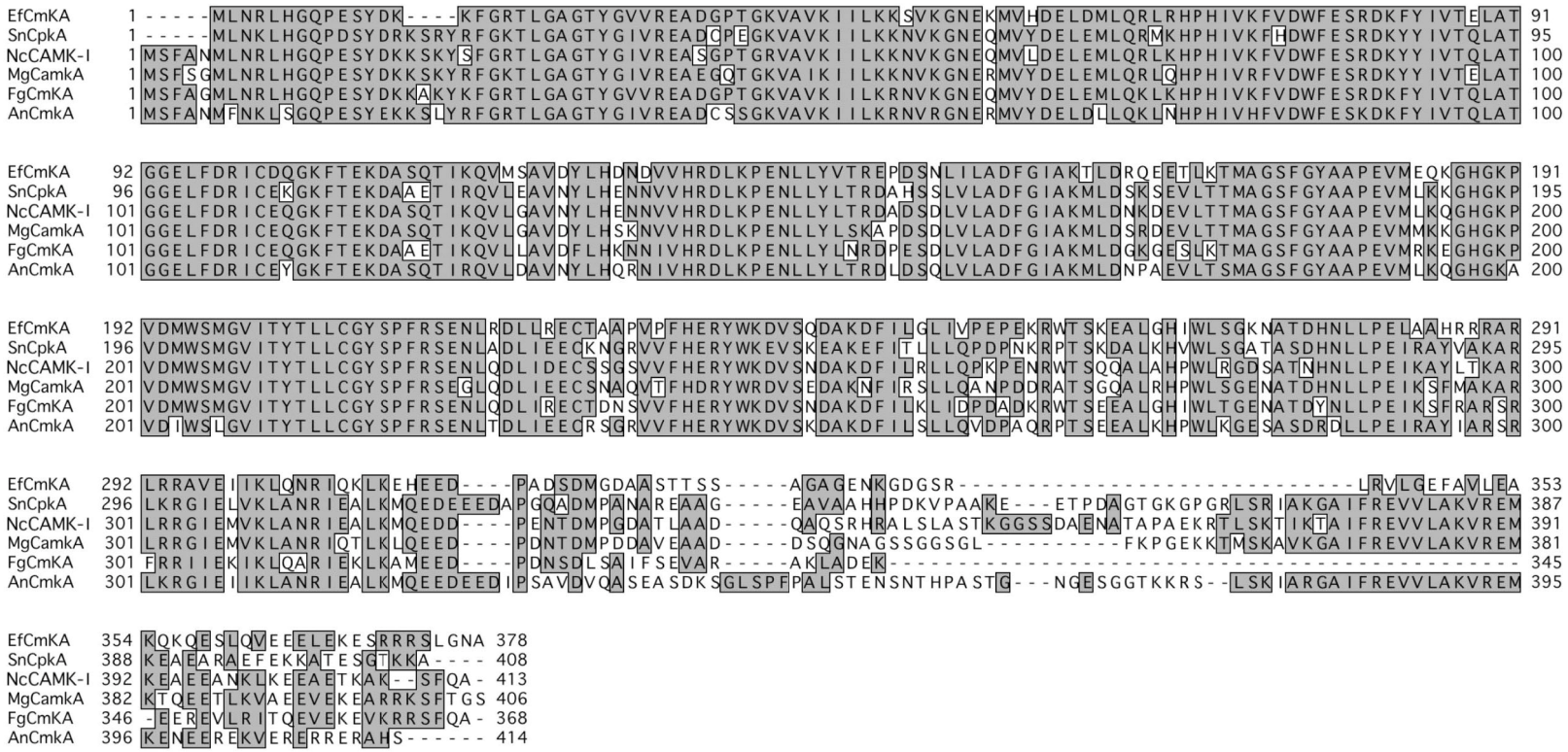

Figure 3.1. Amino acid sequence alignment of fungal Ca^{2+}/Calmodulin-dependent protein kinase A
The predicted amino acid sequence of *E. festucae* CmkA aligned with its homologues from *S. nodorum* (SnCpkA), *N. crassa* (NcCAMK-I), *M. grisea* (MgCaMK1), *F. graminearum* (FgCmkA) and *A. nidulans* (AnCmkA). Identity scores are 60.5%, 63%, 65.8%, 69.3% and 58.4%, respectively. Grey fields correspond to regions of amino acid identity.

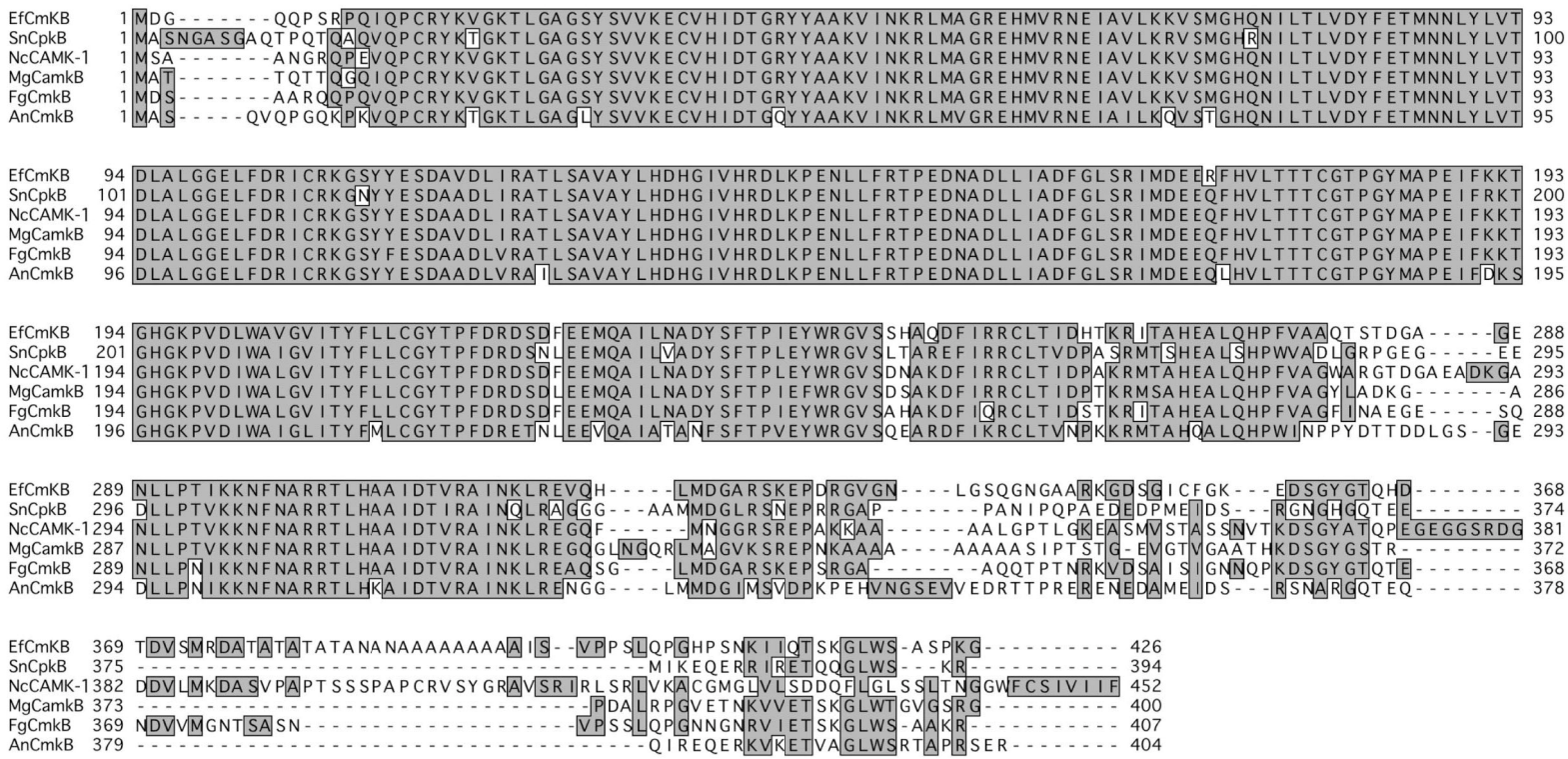

Figure 3.2. Amino acid sequence alignment of fungal Ca^{2+}/Calmodulin-dependent protein kinase B
Predicted amino acid sequence of *E. festucae* CmkB aligned with its homologues from *S. nodorum* (SnCpkB), *N. crassa* (NcCAMK-1), *M. grisea* (MgCaMK), *F. graminearum* (FgCmkB) and *A. nidulans* (AnCmkB). Identity scores are 66.7%, 70%, 73.5%, 79.3% and 64.4%, respectively. Grey fields correspond to regions of amino acid identity.

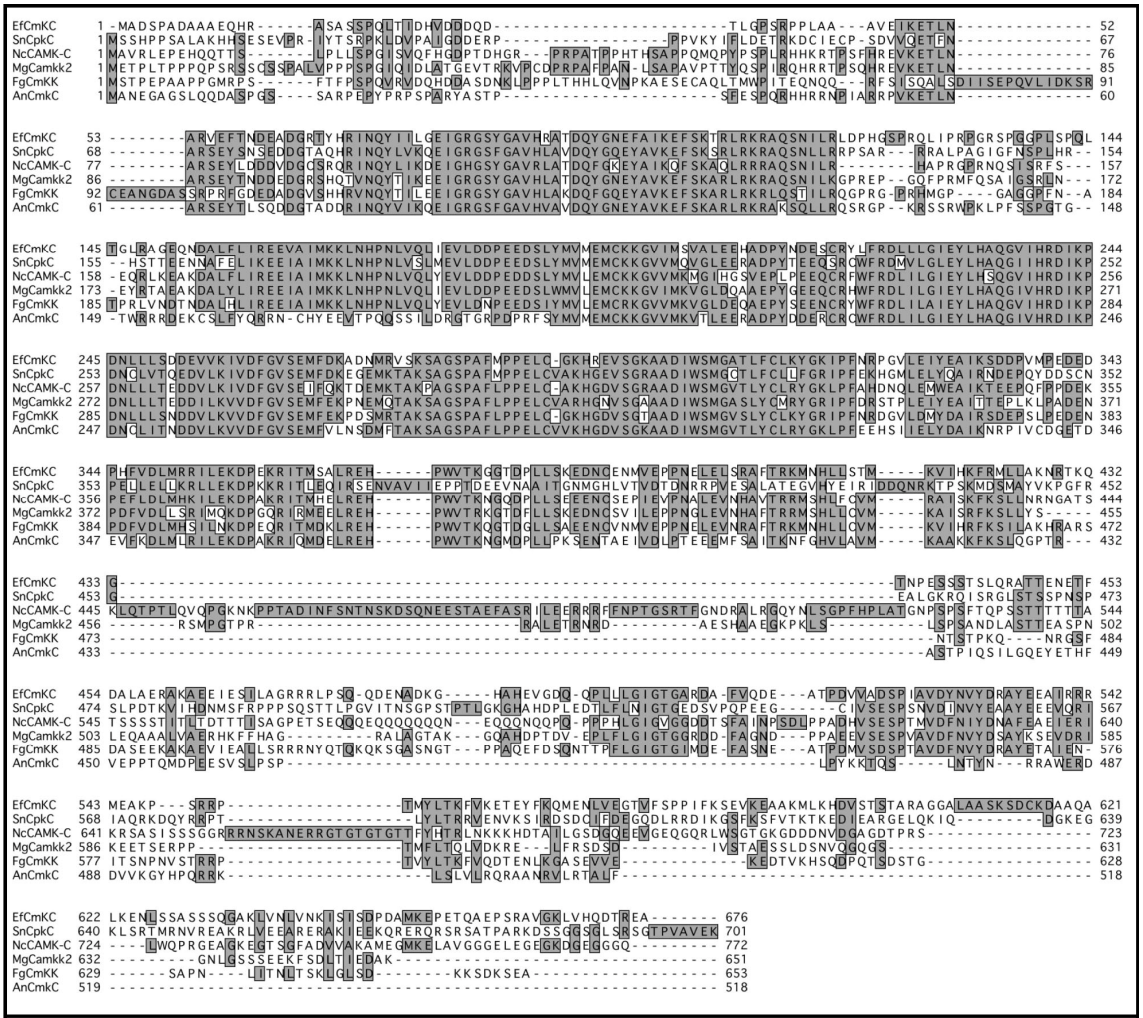

Figure 3.3. Amino acid sequence alignment of fungal Ca^{2+}/Calmodulin-dependent protein kinase C

Predicted amino acid sequence of *E. festucae* CmkC aligned with its homologues from *S. nodorum* (SnCpkC), *N. crassa* (NcCAMK-C), *M. grisea* (MgCamkk2), *F. graminearum* (FgCmKK) and *A. nidulans* (AnCmkC). Identity scores are 39.6%, 38.7%, 43.8%, 49.3% and 34.6%, respectively. Grey fields correspond to regions of amino acid identity.

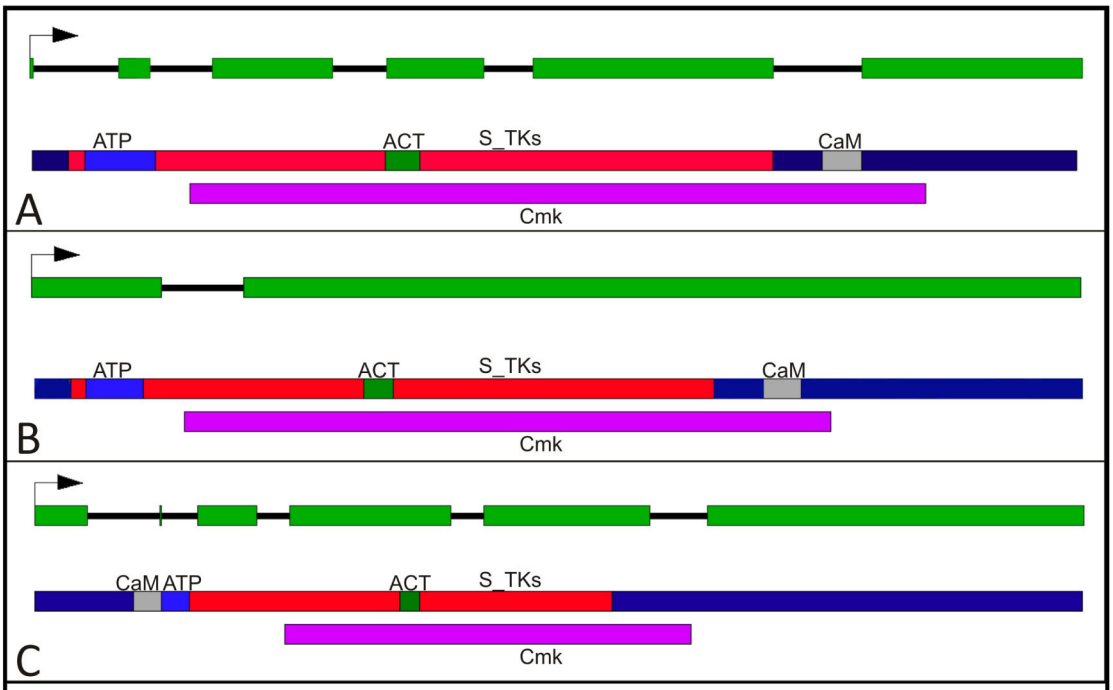

Figure 3.4. Exon-intron structure and protein domains of *E. festucae* CmkA, CmkB and CmkC

Exon-intron structure of *E. festucae cmkA*, *cmkB* and *cmkC* predicted using FGenesh software. **A.** *cmkA* is predicted to have 6 exons, **B.** *cmkB* has 2 exons and **C.** *cmkC* has 6 exons. InterProScan software was used to identify conserved proteins domains. ACT (green) – Serine/threonine protein kinase active site; S_TKs (red) – Serine/threonine protein kinase domain; ATP (blue) – ATP binding site; CaM (grey) – putative calmodulin binding site; Cmk (purple) - Ca^{2+}/Calmodulin-dependent kinase domain.

plants and cDNA was generated by oligo-dT primed RT-PCR. In order to compensate for the differences in fungal biomass between the two samples, serial dilutions of each cDNA sample were used as templates to amplify the housekeeping gene β-tubulin (*tubB*). The 1/10 dilution of the *in planta* sample and the 1/40 dilution of the culture sample appeared to have equal steady state levels of *tubB* transcripts. Therefore, these two dilutions were subsequently used to test expression levels of *cmkA*, *cmkB* and *cmkC* by PCR using primer pairs MI3/MI4, MI5/MI6 and MI1/MI2, specific for each of the genes (Table 2.3). Expression of *cmkA* was greater *in planta* than in culture, while expression of *cmkB* was similar in both samples. The steady-state transcript levels of *cmkC* were greater *in planta* than in culture (Fig. 3.5). These results suggest that *cmkA* and *cmkC* are symbiotically regulated.

3.3. Targeted replacement of *cmkA*, *cmkB* and *cmkC*

To determine whether the *E. festucae cmk* genes are required for growth in culture and the establishment and maintenance of the symbiosis, each gene was deleted by targeted gene replacement.

3.3.1. Design of replacement constructs and screening for replacement mutants.

An *E. festucae* cosmid library (Tanaka *et al.*, 2005) was screened using PCR products specific for *cmkA*, *cmkB* and *cmkC*. Three positive clones were identified in the screen for *cmkA*, 5 for *cmkB* and 10 for *cmkC*. Three clones of each were screened by PCR to confirm the presence of the gene and flanking sequences and one clone of each was used as a source of 5' and 3' sequences to prepare replacement constructs, pMMI1 (*cmkA*), pMMI2 (*cmkB*) and pMMI3 (*cmkC*) (Sections 2.11.1, 2.11.2 and 2.11.3).

In order to generate mutants deleted for *cmkA*, protoplasts of *E. festucae* strain Fl1 were transformed with a linear fragment of KO construct pMMI1, (Section 2.11.1) and transformants were selected by plating on geneticin. Resistant transformants were subsequently subcultured three times on media containing geneticin, in order to isolate monokaryotic, geneticin-resistant, transformants (Young *et al.*, 2005a). To screen for mutants deleted for *cmkA*, PCR was carried out using crude genomic DNA as template

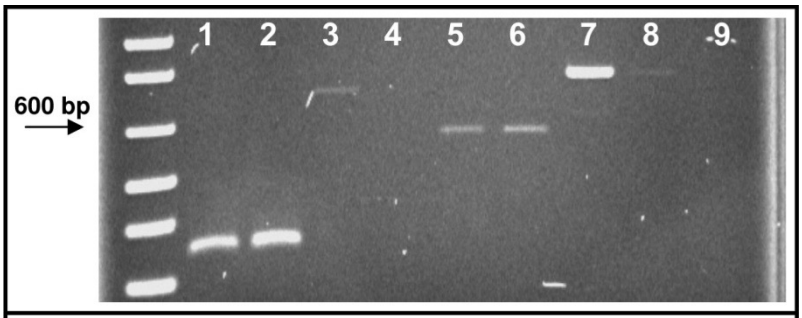

Figure 3.5. Expression analysis of *cmkA*, *cmkB* and *cmkC*.
RT-PCR analysis of steady-state levels of *cmkA*, *cmkB*, *cmkC* and β-tubulin transcripts. cDNA was generated from total RNA isolated from Fl1 in culture and pseudostem of infected plants. 1/40 dilution of culture sample and 1/10 dilution of plant sample were used as templates, to compensate for the endophyte biomass difference between the two samples. Plant sample of β-tubulin (*lane 1*), *cmkA* (*lane 3*), *cmkB* (*lane 5*) and *cmkC* (*lane 7*); culture sample of β-tubulin (*lane 2*), *cmkA* (*lane 4*), *cmkB* (*lane 6*), *cmkC* (*lane 8*); negative control (*lane 9*).

(Section 2.3.3.1) and *cmkA* specific primers, MI3/MI4. From this initial PCR screen three transformants were identified that lacked the PCR product specific for WT. These three putative Δ*cmkA* transformants, together with WT and a transformant with an ectopic integration, were subsequently analyzed by Southern blotting (Fig. 3.6). If replacement of the *cmkA* gene occurs then two bands of 9.5 Kb and 7.3 Kb should be observed for the *Nar*I digest and one band of 7.4 Kb for the *Bgl*II digest, when the blot is hybridized with pMMI1 (Fig. 3.6A and B). For the WT, one band of 16.8 Kb was expected for the *NarI* digest and two bands of 4 Kb and 3.4 Kb for the *Bgl*II digest. Southern analysis revealed, as expected, a single hybridizing band of 7.4 Kb for *Bgl*II digests of Δ*cmkA*8.4, Δ*cmkA*15.2 and Δ*cmkA*15.4, and bands of 4 Kb and 3.4 Kb hybridizing for WT and ectopic. However, in the *NarI* digest, bands of the sizes expected for both a replacement event and a WT gene were observed for Δ*cmkA*8.4, Δ*cmkA*15.2 and Δ*cmkA*15.4 (Fig. 3.6C). There are two possible explanations for this result. Firstly, the 16.8 Kb band, characteristic of WT, could occur in mutants if there was incomplete digestion, as the linear replacement construct and the corresponding WT region are of the same size. Secondly, a band of this size would also occur if the mutants were heterokaryons. However, the latter hypothesis is not supported by the results of the *BglII* digest. To confirm that the 16.8 Kb *Nar*I band is not a WT band, this blot was stripped and reprobed with the PCR product of primers MI3/MI4, corresponding to the *cmkA* gene region that should be deleted by homologous recombination (Fig. 3.6D). Results of this hybridization clearly showed that, in contrast to WT and ectopic, transformants Δ*cmkA*8.4, Δ*cmkA*15.2 and Δ*cmkA*15.4 were deleted for *cmkA*.

In order to generate mutants deleted for *cmkB*, Fl1 protoplasts were transformed with a linear fragment of deletion construct pMMI2 (Section 2.11.2). Transformants were selected for geneticin resistance and taken through the nuclear purification process by subculturing. These geneticin-resistant transformants were screened for the absence of the *cmkB* coding sequence by PCR using crude genomic DNA as a template and *cmkB* specific primers MI5/MI6. Four transformants that lacked the PCR product specific for WT, together with WT and an ectopic transformant, were taken through for Southern analysis. For deletion of *cmkB* (Fig. 3.7A), two bands of 9.6 Kb and 4 Kb were expected for the *Pvu*I digest and two bands of 5 Kb and 4.5 Kb for the *Sph*I digest, when the blot is hybridized with pMMI2. Three bands of 7.8 Kb, 4 Kb and 1.8 Kb

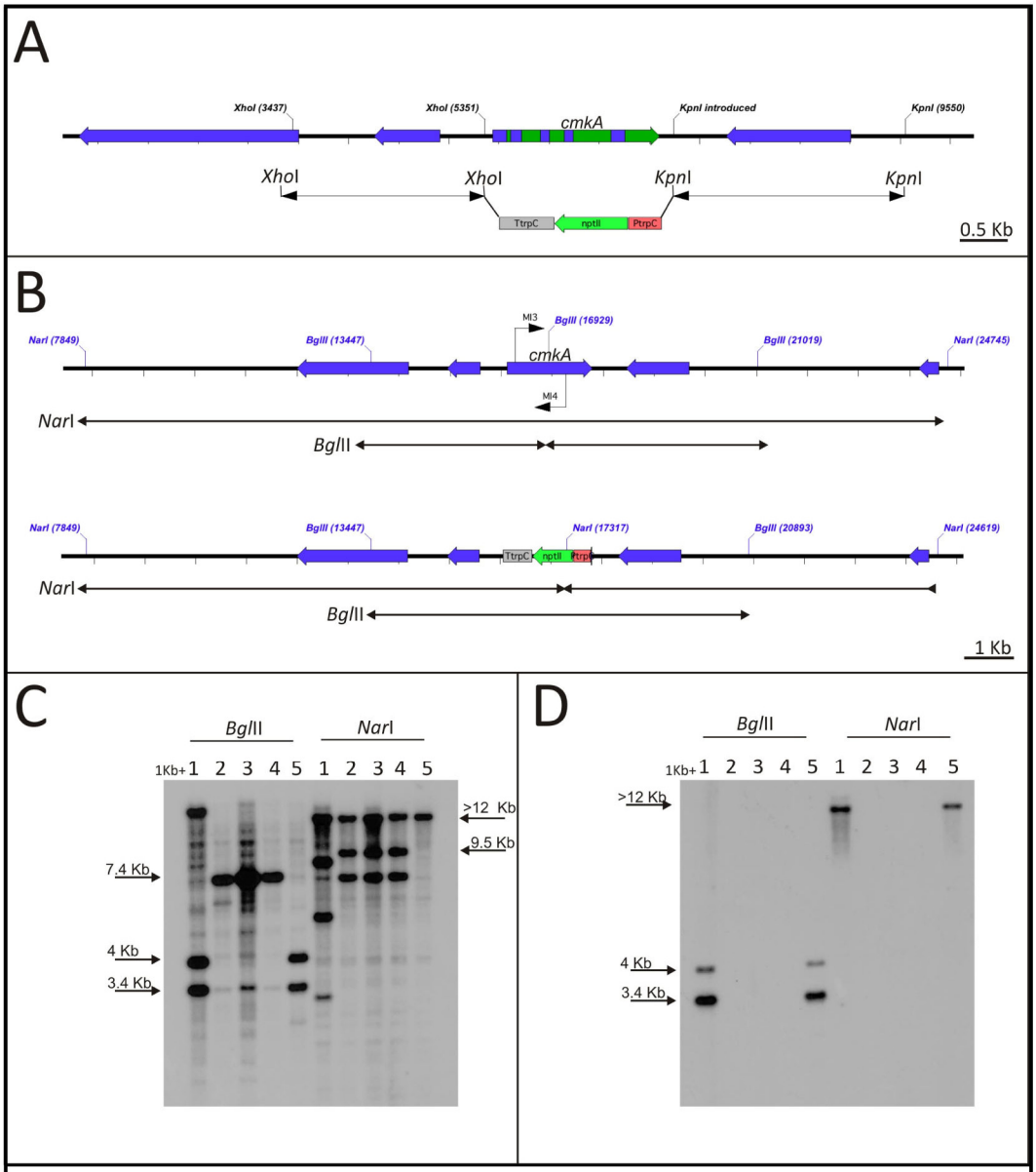

Figure 3.6. Design of *cmkA* replacement construct and screening strategy for identifying gene deletion.
A. Generation of pMMI1, used for deletion of *cmkA*. Flanking fragments were either taken from a cosmid 36H7 (*Xho*I fragment) or generated by PCR, introducing restriction site (*Kpn*I fragment). **B.** Physical map of *cmkA* WT and mutant regions. Expected fragments sizes in Southern analysis for WT: *Nar*I 16.8 Kb; *Bgl*II 4 Kb and 3.4 Kb. Expected fragment sizes for mutant with the gene replacement: *Nar*I 9.5 Kb and 7.3 Kb; *Bgl*II 7.4 Kb **C.** Autoradiograph of Southern blot of *Bgl*II and *Nar*I digests of 1 µg of genomic DNA of WT and mutant, probed with [^{32}P]-labelled pMMI1. Ectopic transformant (*lane 1*), Δ*cmkA8.4* (*lane 2*), Δ*cmkA15.2* (*lane 3*), Δ*cmkA15.4* (*lane 4*) and WT (*lane 5*). **D.** Blot shown in (**C**), re-probed with [^{32}P]-labeled PCR product of MI3/MI4 primer pair (**B**).

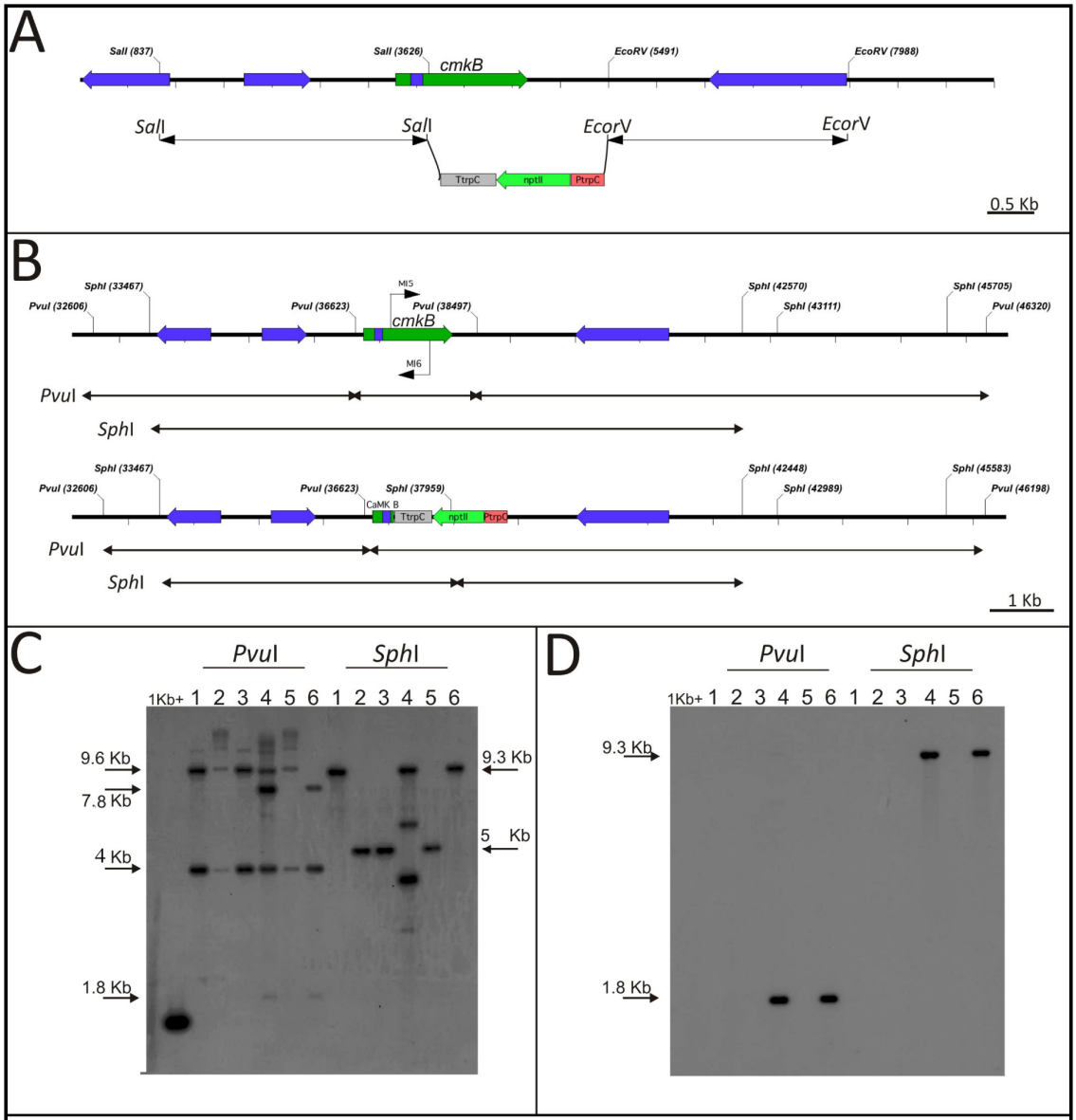

Figure 3.7. Design of *cmkB* replacement construct and screening strategy for identifying gene deletion.

A. Generation of pMMI2, used for deletion of *cmkB* : Flanking fragments (*Sal*I and *Eco*RV) were taken from a cosmid 41B6. **B.** Physical map of *cmkB* WT and mutant with homologues recombination event: Expected fragments sizes in Southern analysis: WT *Sph*I 9.6 Kb; *Pvu*I 1.8 Kb, 4 Kb and 7.8 Kb; mutant *Sph*I 4.5 Kb and 5 Kb; *Pvu*I 4 Kb and 9.6 Kb. **C.** Autoradiograph of blot probed with [^{32}P]-labeled pMMI2. Δ*cmkB1.2* (*lane 1*), Δ*cmkB1.3* (*lane 2*), Δ*cmkB10.5* (*lane 3*), ectopic transformant (*lane 4*), Δ*cmkB14.2* (*lane 5*) and WT (*lane 6*). **D.** Same blot as in (**C**) re-probed with [^{32}P]-labeled PCR product of MI5/MI6 primer pair (**B**).

were expected for the *Pvu*I digest and one band of 9.6 Kb for the *Sph*I digest of WT and ectopic transformants. Southern analysis showed that WT and mutants had bands of the predicted sizes for the *Pvu*I digests (Figs. 3.7B and C), demonstrating that these four transformants have *cmkB* deleted. However, the banding pattern of both WT and transformants observed for the *Sph*I digests did not correspond to the sizes expected, based on maps generated from the *E. festucae* E2368 genome sequence. The observed WT band of ~9.3 Kb was smaller than the expected 9.6 Kb band and the mutants had one band of 5 Kb instead of the two expected bands of 4.5 Kb and 5 Kb. Since the differences between expected and observed bands were found in both transformants as well as in WT, the most likely explanation for these differences is a restriction site polymorphism between the genomes of Fl1 and E2368. In addition, transformant Δ*cmkB1.2* had a *Sph*I band of the same size as WT. Given that the size of the *cmkB* deleted region is identical to the *nptII* replacement cassette in pSF17.8, a possible explanation for this result is a loss or modification of the single *Sph*I site in the *nptII* gene, resulting in a band of the size of WT (Fig. 3.7B). However, this transformant was not analyzed further. To confirm that *cmkB* gene was indeed deleted, the Southern blot was stripped and reprobed with the PCR product of primers MI5/MI6. While this probe hybridized to WT and ectopic insertion mutant, no signal was detected with Δ*cmkB1.2* or any of the other transformants, confirming deletion of *cmkB* gene (Fig. 3.7D).

Transformants deleted for *cmkC* were generated using a linear fragment of pMMI3 KO construct (Fig. 3.8A; Section 2.11.3). Fl1 protoplasts were transformed with this fragment and transformants were selected on plates containing hygromycin. Resistant transformants were taken through three rounds of subculturing on hygromycin containing media in order to obtain homokaryotic colonies. Transformants were screened for the *cmkC* deletion by PCR using crude genomic DNA as a template and a *cmkC* specific primer pair, MI1/MI2. Five transformants, Δ*cmkC10.2,* Δ*cmkC19.2,* Δ*cmkC19.3,* Δ*cmkC30.5* and Δ*cmkC40.3* lacked the PCR product specific for WT and were taken through for Southern analysis. Hybridizing bands expected for deletion of *cmkC* were 5.5 Kb for the *Sac*II digest and 7.4 Kb for the *Xho*I digest when probed with pMMI3. For WT, two bands of 4.3 Kb and 2.3 Kb were expected for the *Sac*II digest and two bands of 4.1 Kb and 3.6 Kb for the *Xho*I digest. Southern analysis revealed that the bands observed for WT corresponded with the sizes expected from the E3268 map. However, for the *Xho*I digests of the transformants, two bands of 6 Kb and 5.1 Kb were

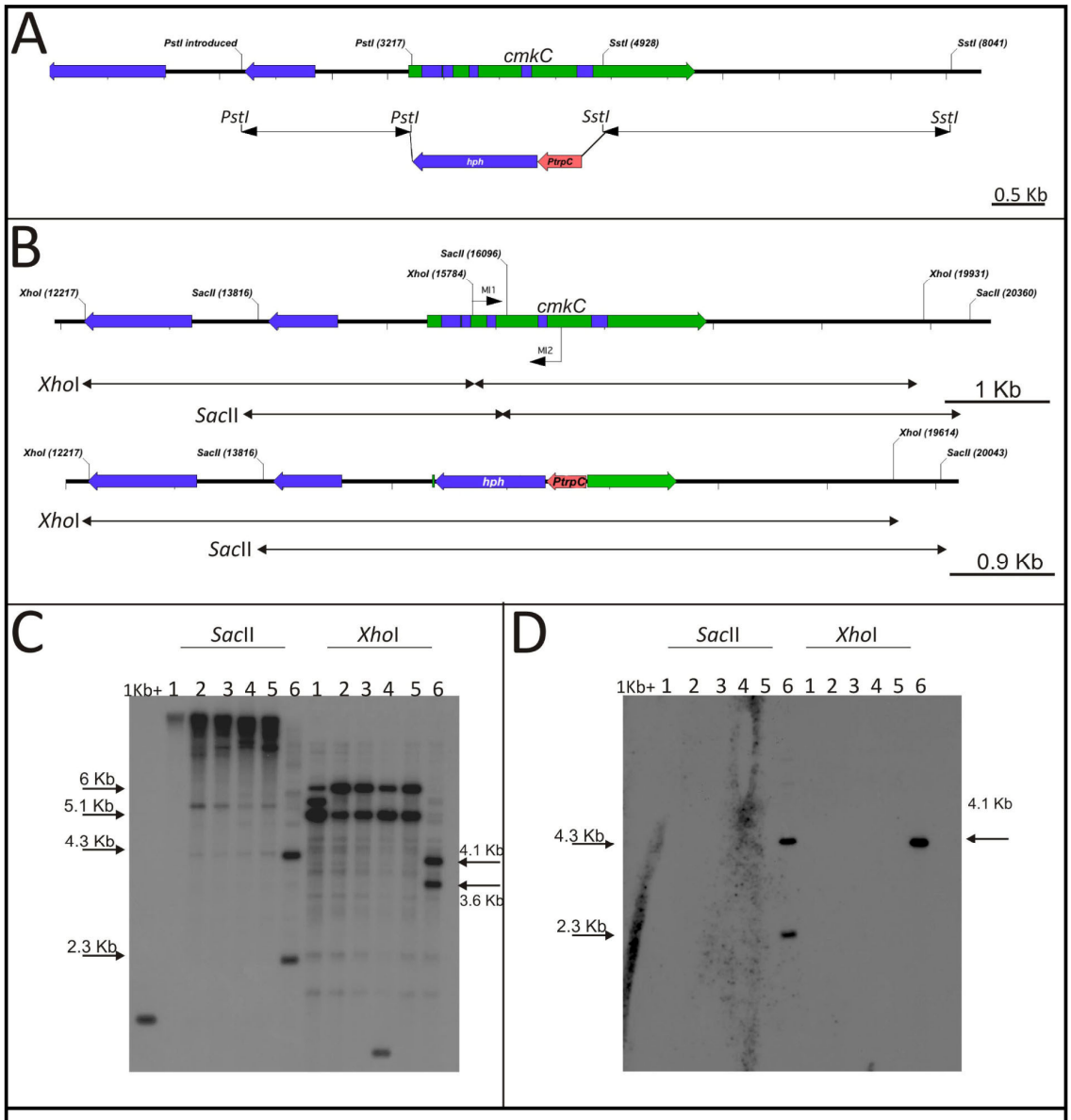

Figure 3.8. Design of *cmkC* replacement construct and screening strategy for identifying gene deletion.

A. Construction of pMMI3, used for deletion of *cmkC*. Flanking fragments were taken from a cosmid clone 15H5 (*Sst*I fragment) or generated by PCR (*Pst*I fragment). **B.** Physical map of WT and transformants with *cmkC* deletion. Expected bands: WT *Sac*II 2.3 Kb and 4.3 Kb, *Xho*I 3.6 Kb and 4.1 Kb; mutant *Sac*II 5.5 Kb, *Xho*I 7.4 Kb **C.** Autoradiograph of blot probed with [^{32}P]-labelled pMMI3.Δ*cmkC10.2* (*lane 1*), Δ*cmkC19.2* (*lane 2*), Δ*cmkC19.3* (*lane 3*), *cmkC30.5* (*lane 4*), Δ*cmkC40.3* (*lane 5*) and WT (*lane 6*). **D.** Same blot as in (**C**) probed with [^{32}P]-labeled PCR product of MI1/MI2 primer pair (**B**).

observed instead of one 7.4 Kb band. In the case of the *Sac*II digests of the transformants, it appears that the genomic DNA had not been completely digested (Fig. 3.8B and C). To confirm that the *cmkC* gene was deleted in all 5 transformants, the blot was stripped and reprobed with the PCR product of *cmkC* specific primers MI1/MI2 (Fig. 3.8D). While this probe hybridized to WT digests, no signal was observed for any of the five transformants, confirming deletion of *cmkC*. The results of the *Xho*I digest for transformants Δ*cmkC10.2* and Δ*cmkC30.5* indicate that an ectopic integration occurred in addition to the homologues recombination event. Hence, these two transformants were excluded from further tests.

3.3.2. Genes *cmkA*, *cmkB* and *cmkC* are not essential for normal growth in culture

Viable transformants for *cmkA*, *cmkB* and *cmkC* were successfully generated, showing that these genes are not essential for the survival of *E. festucae*. A series of tests was done to further functionally characterize these genes.

The colony morphology and growth rate of Δ*cmkA*, Δ*cmkB* and Δ*cmkC* do not differ from WT when grown on PD agar, at 22°C (Fig. 3.9). Furthermore, differential interference contrast (DIC) microscopy showed that hyphal morphology and the branching pattern of the deletion mutants resembles that of WT (Fig. 3.10).

The growth of the deletion mutants was tested under different stress conditions in order to determine if these genes have a role in stress signaling. No difference in sensitivity to either the cell wall destabilizing agent, SDS (Fig. 3.11A), or osmotic stress, caused by high concentrations of NaCl (Fig. 3.12) were observed for all three mutants compared to WT. However, under conditions of oxidative stress, morphological differences were observed between some of the Δ*cmkC* and Δ*cmkA* mutants and WT (Fig. 3.11B). Transformants Δ*cmkC19.2,* Δ*cmkC40.3*, and to a lesser extent Δ*cmkA15.2*, had reduced aerial hyphae, compared with WT and the other Δ*cmkA* and Δ*cmkC* mutants. This phenotype, however, was not highly reproducible. Even greater variation in phenotype among the transformants was seen under conditions of temperature stress. Growth of Δ*cmkA15.2,* Δ*cmkB1.3,* Δ*cmkC19.2* and Δ*cmkC40.3* was severely impaired at 30°C, while growth of the remaining mutants was the same as WT (Fig. 3.11C). Furthermore,

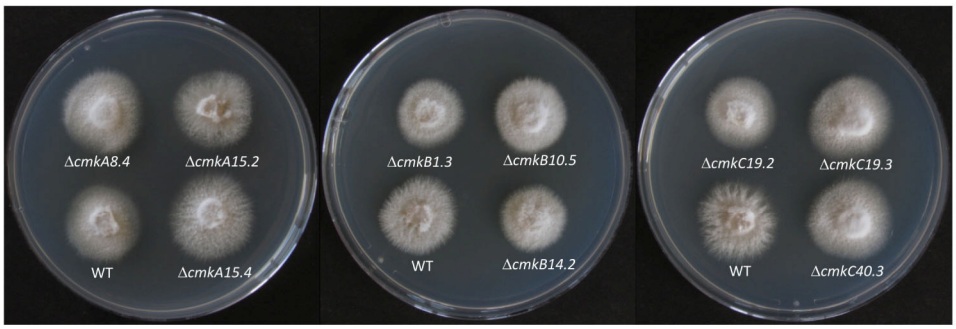

Figure 3.9. Culture phenotype of Δ*cmkA*, Δ*cmkB* and Δ*cmkC* mutants
Colony morphology and growth of WT and mutants grown on PDA, at 22°C.

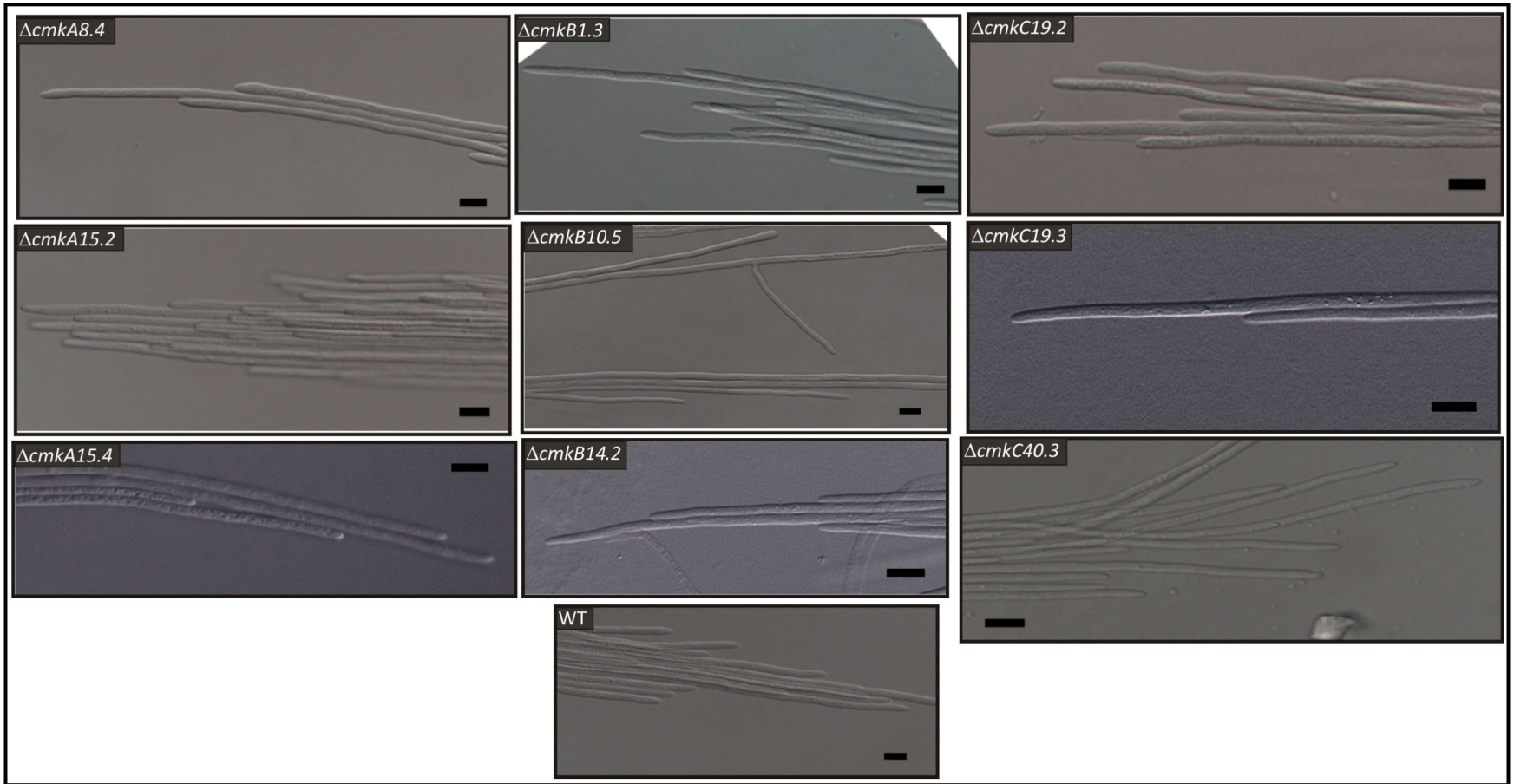

Figure 3.10. Hyphal morphology phenotype of the Δ*cmkA*, Δ*cmkB* and Δ*cmkC*
DIC images of WT and Δ*cmkA*, Δ*cmkB* and Δ*cmkC* hyphae. Colonies were grown on PD agar, for 6 days. Bar: 10 µm.

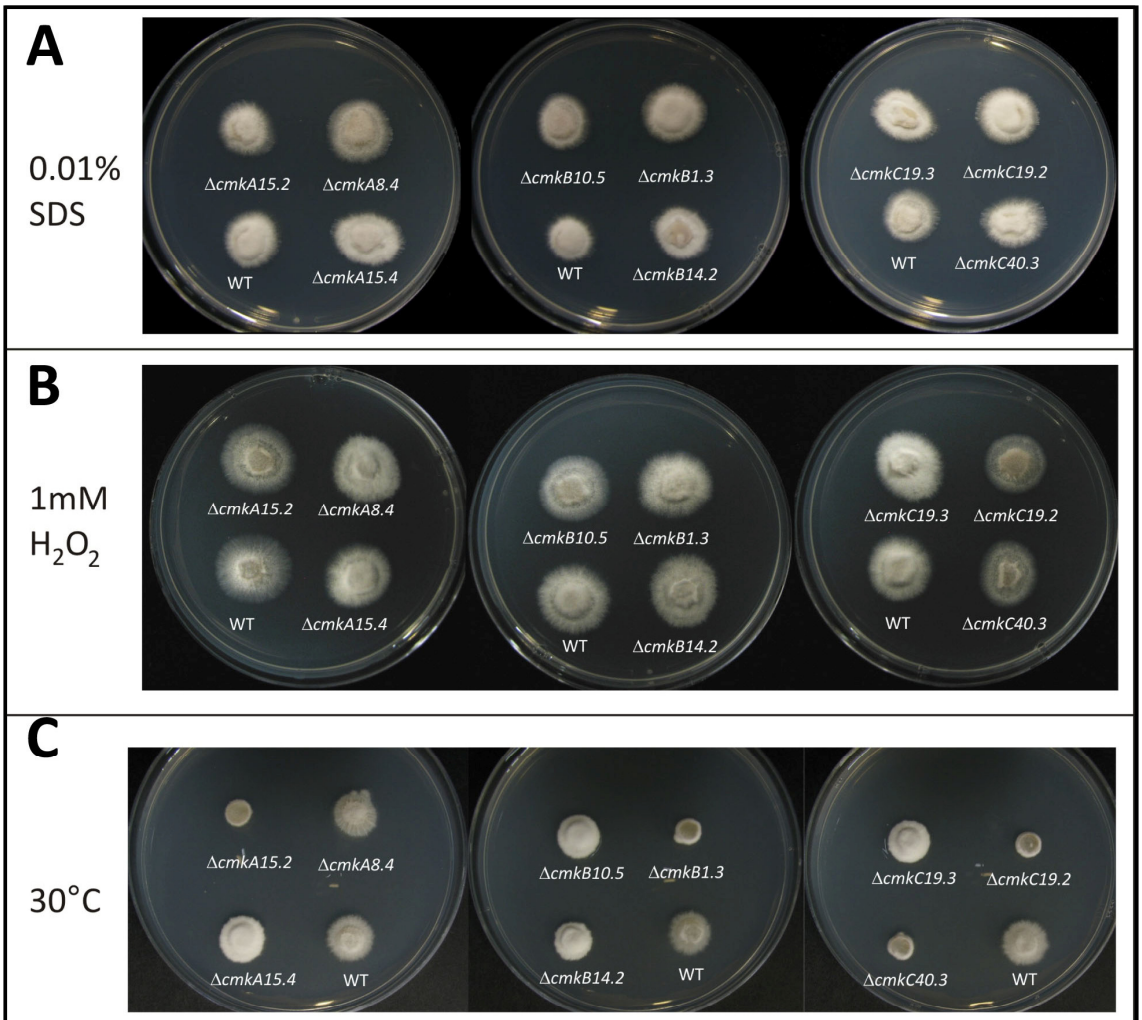

Figure 3.11. Growth of *ΔcmkA*, *ΔcmkB* and *ΔcmkC* under different stress conditions

A. WT and *cmkA*, *cmkB* and *cmkC* mutants tested on PDA plates containing 0.01% SDS (sodium dodecyl sulfate).

B. WT and mutants tested for sensitivity to oxidative stress on PDA plates containing 1 mM H_2O_2.

C. WT and mutants tested for temperature stress, grown on PDA plates at 30°C.

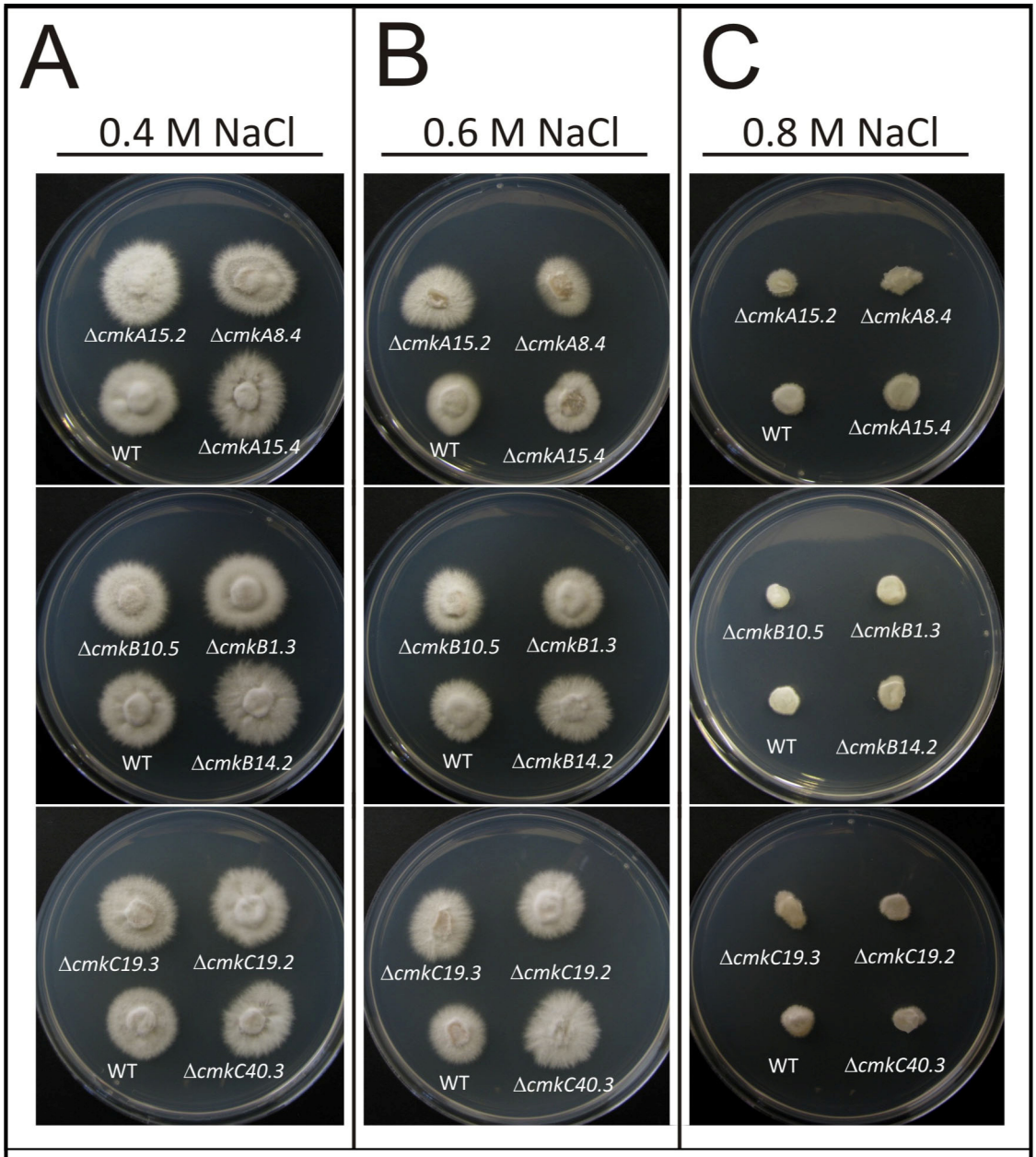

Figure 3.12. Growth of Δ*cmkA*, Δ*cmkB* and Δ*cmkC* under conditions of osmotic stress

The *cmkA*, *cmkB* and *cmkC* mutants were tested for osmotic stress by growing them on PDA plates containing **A.** 0.4 M NaCl, **B.** 0.6 M NaCl and **C.** 0.8 M NaCl.

transformants from each mutant type (except the transformant Δ*cmkA8.4*) that grow the same as WT at 30°C had a 'dense colony' phenotype with more aerial hyphae than WT. Variation in phenotype was also observed in Δ*cmkB* group of mutants for growth under conditions of high concentrations of Mg^{2+} (Fig. 3.13). The degree of variation ranged from severe growth impairment for Δ*cmkB10.5* to growth identical to that of WT.

The variation in growth phenotype observed for mutants carrying the same gene deletion was highly reproducible. One possible explanation for these results was that the colonies tested were heterokaryons rather than homokaryons. However, the results of the Southern analysis shown in Figures 3.6D, 3.7D and 3.8D, taken together with the stable and reproducible nature of the observed phenotype, eliminate this hypothesis. Another possibility is generation of second-site mutations in adjacent genes that comprised the KO constructs. This possibility was ruled out by the complementation experiments (Section 3.4). Some of the variation observed could have occurred if *cmkA*, *cmkB* and *cmkC* were functionally redundant. However, results of tests with double-deletion mutants of *cmkA/cmkB* do not support this hypothesis, at least for the case of high Mg^{2+} sensitivity (Section 3.6). Other explanations include second-site mutations generated by random insertion of small fragments of the replacement construct into the genome and differences in compensatory expression of related genes in the genomes.

3.3.3. Deletion of *cmkA*, *cmkB* or *cmkC* does not affect ROS production in culture

It is well known from the literature that reactive oxygen species play a crucial role in regulating the *E. festucae*-perennial ryegrass symbiosis (Takemoto *et al.*, 2006, Tanaka *et al.*, 2006). ROS production of Δ*cmkA*, Δ*cmkB* or Δ*cmkC* mutants was investigated using 3, 3' diaminobenzidine (DAB) and nitroblue-tetrazolium (NBT) staining. Staining of mutants with both compounds was the same as WT (Figs. 3.14 and 3.15). Both the levels and distribution pattern of staining did not differ from that of WT.

3.3.4. *cmkA*, *cmkB* and *cmkC* are not essential for the symbiotic interaction

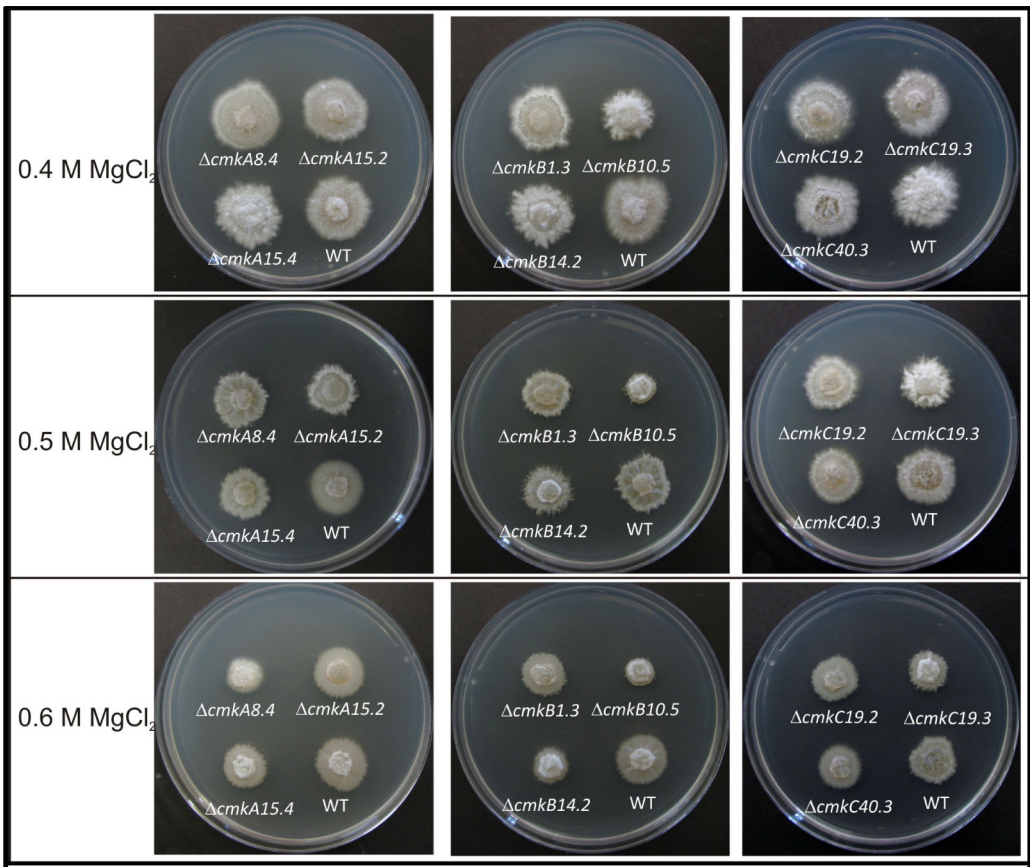

Figure 3.13. Δ*cmkA*, Δ*cmkB* and *Δcmk*C mutants growing on high Mg^{2+} concentrations

Colonies were grown at 22°C, for twelve days, on PDA containing 0.4 M, 0.5 M and 0.6 M $MgCl_2$.

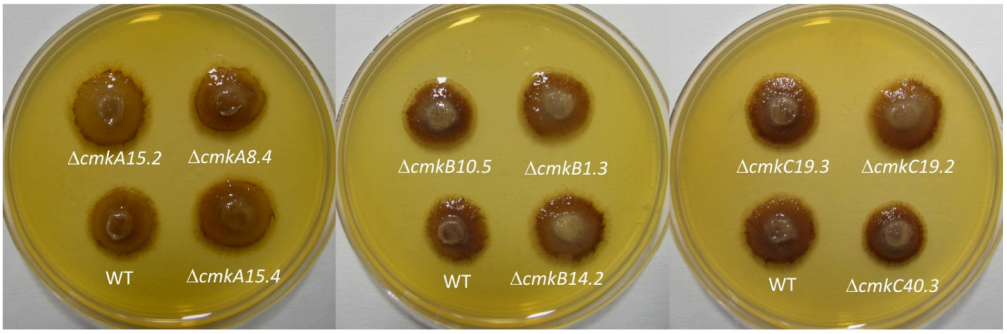

Figure 3.14. H_2O_2 production by Δ*cmkA*, Δ*cmkB* and Δ*cmkC* mutants
Colony production of H_2O_2 by *cmkA*, *cmkB* and *cmkC* mutants was analyzed using DAB (3, 3' diaminobenzidine) staining which forms a brick red precipitate in the presence of H_2O_2. Colonies were stained for 40 h.

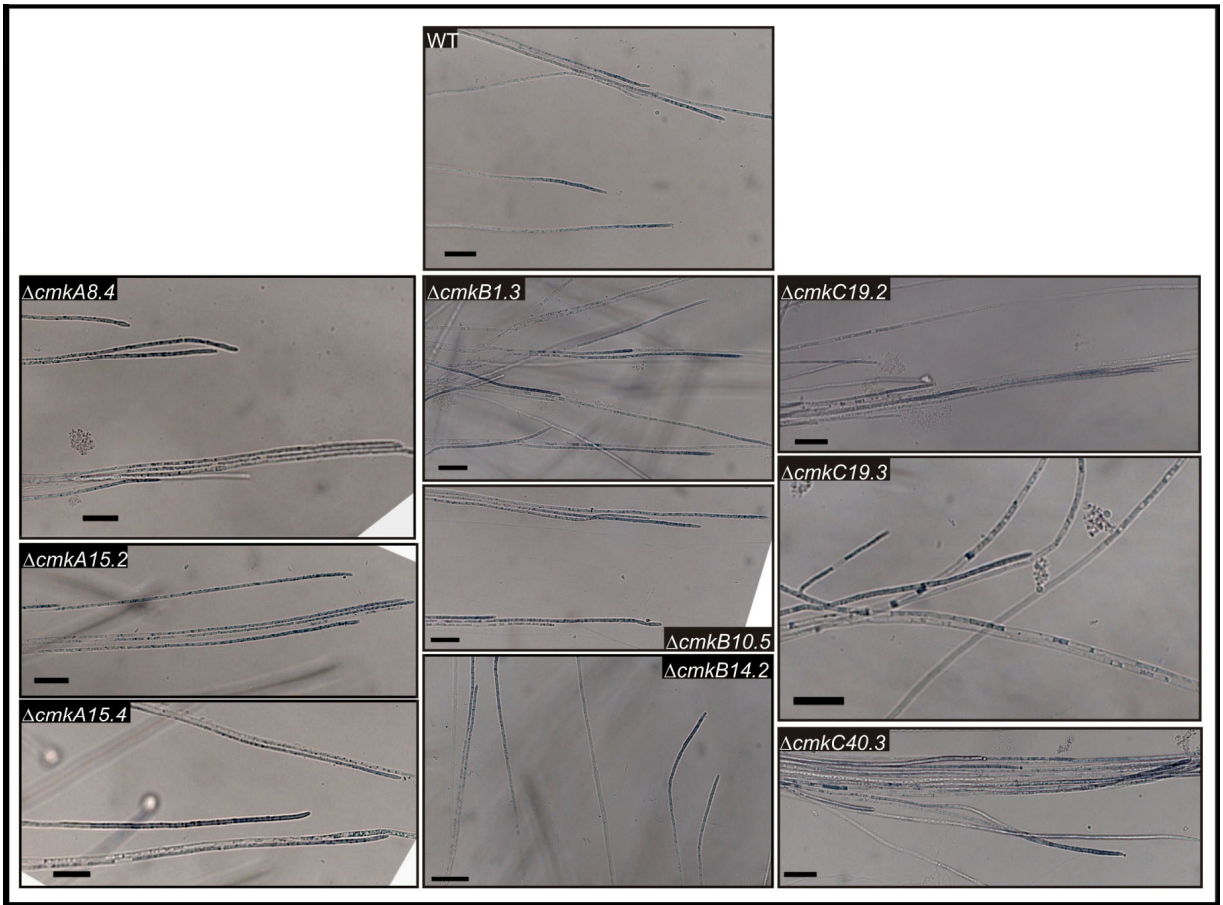

Figure 3.15. Superoxide production of Δ*cmkA*, Δ*cmkB* and Δ*cmkC* mutants
Superoxide anion production of WT and mutants was detected using nitroblue-tetrazolium (NBT). Colonies were grown on slides covered with PDA then incubated with 0.05% (w/v) NBT for 5 h at 22°C. Bar: 20 µm.

In order to determine whether *cmkA*, *cmkB* and *cmkC* are involved in the regulation of the symbiosis, perennial ryegrass seedlings were inoculated with Δ*cmkA*, Δ*cmkB* and Δ*cmkC* mutants and WT. Plants were evaluated for infection after 12 weeks of growth in the greenhouse. Infection rates of mutant strains did not differ from those of WT. No difference was observed in whole plant morphology for plants infected with mutants compared to those infected with WT (Fig. 3.16). Any variations observed in plant size or tiller numbers for mutants were within the range of normal variation observed for WT-infected plants. Plants infected with mutants showed no other detrimental affects such as premature senescence or any other signs of a deregulated symbiotic association. Hyphal morphology *in planta* was examined using aniline-blue stained leaf sheaths of infected plants (Fig. 3.17). No differences in morphology were observed between mutants and WT hyphae. Hyphae of the mutant strains had the same, highly regulated growth pattern observed for WT, where the hyphae grow straight, between the plant intercellular spaces without any signs of increased branching.

These results demonstrate that *cmkA*, *cmkB* and *cmkC* are not essential for establishment and maintenance of the mutualistic interaction between *E. festucae* and perennial ryegrass.

3.4. Complementation of the Δc*mkA*, Δ*cmkB* and Δ*cmkC* mutants

In order to determine whether deletion of *cmkA*, *cmkB* and *cmkC* was responsible for the temperature-sensitive phenotype displayed by *ΔcmkA*, *ΔcmkB* and *ΔcmkC* and the Mg^{2+} sensitive phenotype displayed by Δ*cmkB10.5* (Section 3.3.2), complementation tests were carried out.

Fragments used for complementation experiments were excised from the same cosmid clones used for preparing the deletion constructs (Fig. 3.18) (Sections 2.11.5 to 2.11.8). In order to investigate if the variation in the temperature-sensitive phenotype observed for *ΔcmkA*, *ΔcmkB* and *ΔcmkC* was caused by gene deletion or second-site mutations in adjacent genes, two complementation constructs were prepared for *cmkB*: pMMI5, containing only the *cmkB* gene (Fig. 3.18B) and pMMI6, consisting of a 10 Kb fragment, that included all genes present in the *cmkB* replacement construct (Fig. 3.18C).

Figure 3.16. Symbiotic phenotype of perennial ryegrass plants inoculated with Δ*cmkA*, Δ*cmkB* and Δ*cmkC*.
Seedlings of perennial ryegrass were inoculated with Δ*cmkA,* Δ*cmkB,* Δ*cmkC* mutants and WT, and plants screened for infection after 12 weeks of growth in the greenhouse.

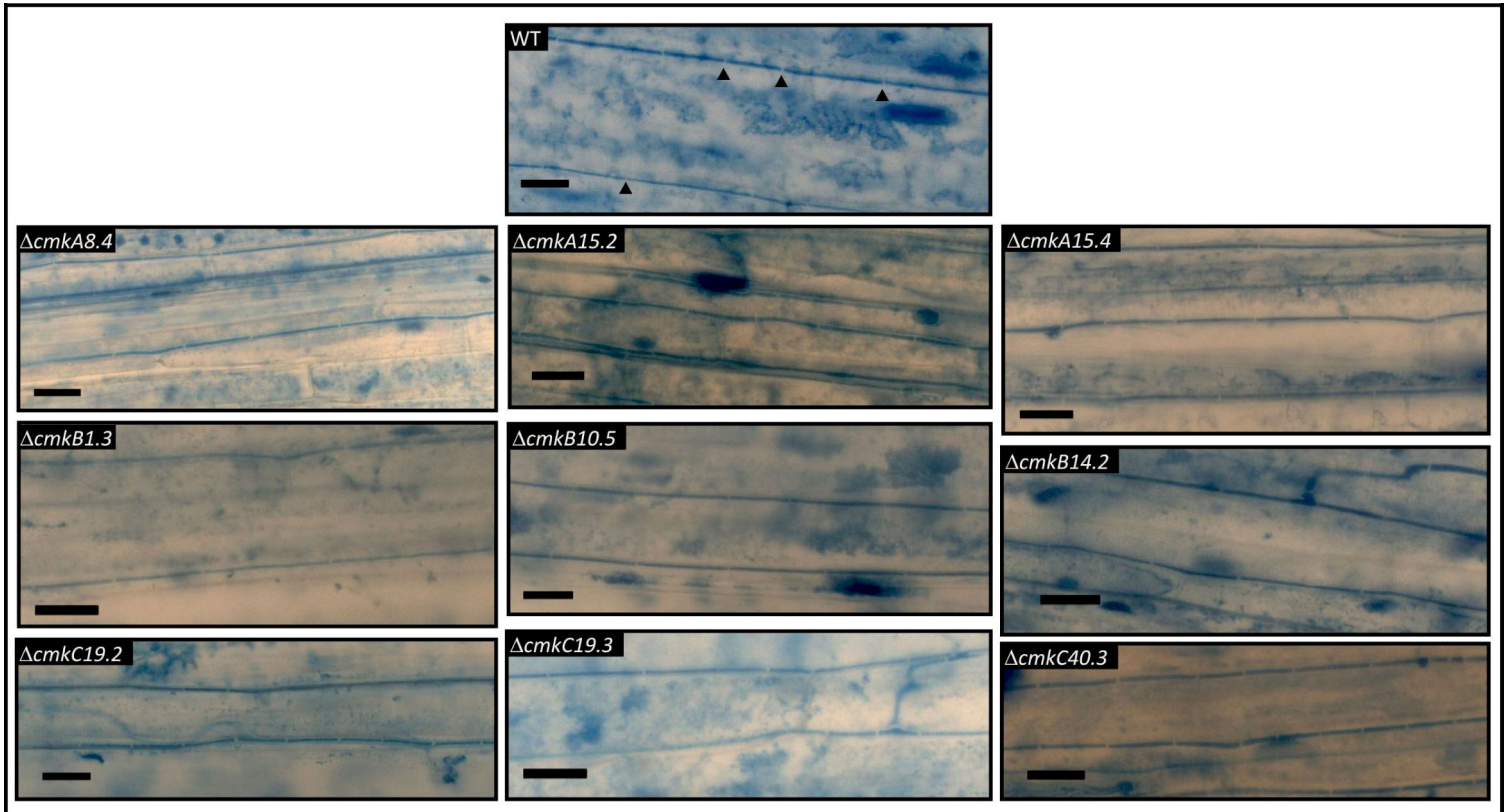

Figure 3.17. *In planta* phenotype of the Δ*cmkA*, Δ*cmkB* and Δ*cmkC* mutants
Light micrographs of aniline-blue stained hyphae of *cmkA*, *cmkB* and *cmkC* mutants in the leaves of perennial ryegrass. Arrows point to septa. Bar: 20 µm.

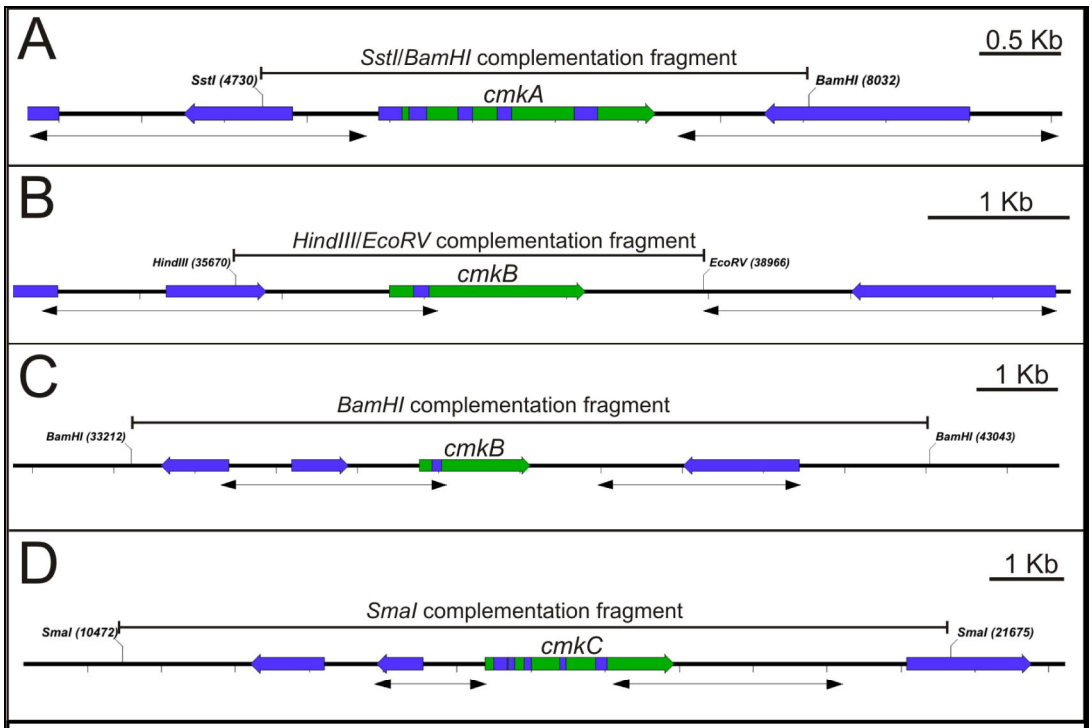

Figure 3.18. Fragments used in complementation tests of Δ*cmkA*, Δ*cmkB* and Δ*cmkC* mutants

Fragments excised from cosmids 36H7 (*cmkA*), 41B6 (*cmkB*) and 15H5 (*cmkC*) were used in complementation tests. **A.** *Sst*I/*Bam*HI fragment with *cmkA* gene used to generate pMMI7. **B.** *Hind*III/*Eco*RV fragment with *cmkB* gene used to generate pMMI5 **C.** *Bam*HI fragment containing *cmkB* and surrounding genes used to generate pMMI6 **D.** *Sma*I fragment with *cmkC* gene used to generate pMMI8. Arrows show flanking fragments used in deletion constructs.

Construct pMMI5 carried a hygromycin resistance gene and was transformed into Δ*cmkB1.3* protoplasts. Construct pMMI6 did not carry any fungal resistance marker and so was co-transformed into Δ*cmkB1.3* protoplasts together with pAN7-1, a hygromycin resistance vector. pMMI6 was also co-transformed into Δ*cmkB10.5*, together with pAN7-1, in order to do a complementation test for the Mg^{2+} sensitivity phenotype of this mutant (Section 3.3.2). The complementation construct for *cmkA*, pMMI7, included only the *cmkA* gene (Fig. 3.18A) and carried a hygromycin resistance gene. This construct was transformed into protoplasts of Δ*cmkA15.2*. The complementation construct for *cmkC*, pMMI8, included all genes present in the *cmkC* replacement construct (Fig. 3.18D). This construct did not carry any fungal resistance marker and was co-transformed into Δ*cmkC19.2* together with the geneticin resistance vector pII99.

PCR analysis of two independent transformants from each complementation group of the temperature-sensitive *cmk* mutants confirmed the presence of the wild-type gene (Figs. 3.19A, B and C). RT-PCR analysis of cDNA from Ba1 and Ba2 (Δ*cmkB1.3*/pMMI5) confirmed that the steady-state levels of *cmkB* were high in both transformants (Fig. 3.19D). However, introduction of the wild-type gene into these mutants failed to suppress the temperature sensitive phenotype (Fig. 3.20A). Similarly, PCR analysis of Δ*cmkB10.5*/pMMI6 complementation transformants confirmed the presence of the wild-type gene in 3 of 4 analyzed transformants (Fig. 3.19E). However, presence of WT gene did not suppress the temperature-induced increased aerial hyphae phenotype (Fig. 3.20B). In contrast, the Mg^{2+} sensitivity of Δ*cmkB10.5* was suppressed in all three *cmkB*-positive transformants (Bc1, Bc2 and Bc3), but not in the *cmkB*-negative transformant (Fig. 3.21). The lack of suppression in *cmkB*-negative transformant (Bc4) is consistent with the absence of the *cmkB* gene in this transformant.

3.5. Generation and analysis of Δ*cmkAB* double-deletion mutants

One possible reason for the variation in colony growth under conditions of high Mg^{2+} observed for the Δ*cmkB* group of mutants and lack of a symbiotic phenotype is functional redundancy among the *cmk*s. To test this hypothesis a *cmkAB* double-deletion mutant was generated.

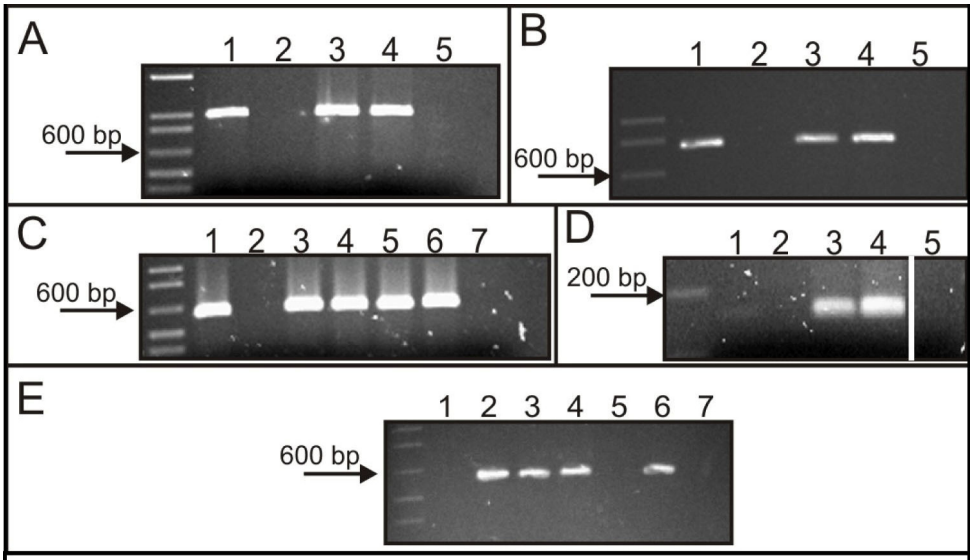

Figure 3.19. PCR analysis of Δ*cmkA*, Δ*cmkB* and Δ*cmkC* complementation transformants

A. Products of *cmkA* specific primer pair MI3/MI4 generated in PCR using as a template genomic DNA of WT (*lane 1*), Δ*cmkA15.2* (*lane 2*), A1(Δ*cmkA15.2*/pMMI7) (*lane 3*) and A2 (Δ*cmkA15.2*/pMMI7) (*lane 4*). Negative control (*lane 5*).

B. Products of *cmkC* specific primer pair MI1/MI2 generated in PCR using as a template genomic DNA of WT (*lane 1*), Δ*cmkC19.2* (*lane 2*), C1 (Δ*cmkC19.2*/pMMI8) (*lane 3*) and C2 (Δ*cmkC19.2*/pMMI8) (*lane 4*). Negative control (*lane 5*).

C. Products of *cmkB* specific primer pair MI5/MI6 generated in PCR using as a template genomic DNA of WT (*lane 1*), Δ*cmkB1.3* (*lane 2*), Ba1 (Δ*cmkB1.3*/pMMI5) (*lane 3*), Ba2 (Δ*cmkB1.3*/pMMI5) (*lane 4*), Bb1(Δ*cmkB1.3*/pMMI6) (*lane 5*), Bb2 (Δ*cmkB1.3*/pMMI6) (*lane 6*). Negative control (*lane 7*).

D. Products of *cmkB* specific primer pair BinF/BinR generated in PCR using as a template cDNA from WT (*lane 1*), Δ*cmkB1.3* (*lane 2*), Ba1 (*lane 3*) and Ba2 (*lane 4*). cDNA was generated by RT-PCR from the total RNA. Negative control (*lane 5*).

E. Products of primer pair MI5/MI6 genrated in PCR using as a template genomic DNA of Δ*cmkB10.5* (*lane 1*), Bc1(Δ*cmkB10.5*/pMMI6) (*lane 2*), Bc2 (Δ*cmkB10.5*/pMMI6) (*lane 3*), Bc3 (Δ*cmkB10.5*/pMMI6) (*lane 4*), Bc4 (Δ*cmkB10.5*/pAN7-1) (*lane 5*) and WT (*lane 6*). Negative control (*lane 7*).

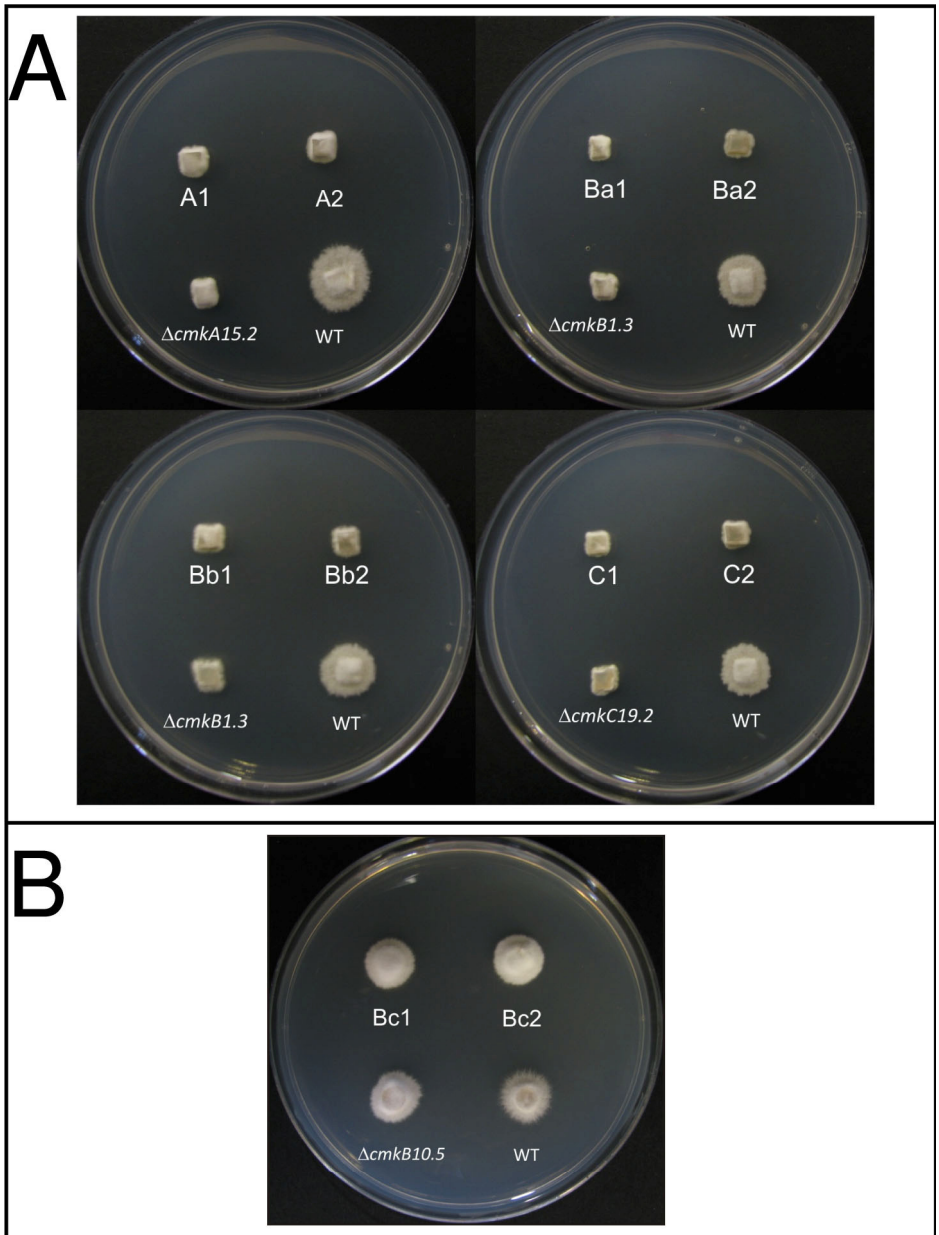

Figure 3.20. Complementation test for temperature-sensitive phenotype of Δ*cmkA*, Δ*cmkB* and Δ*cmkC* mutants
Colonies were grown on PD agar at 30°C for 12 days.
A. Complementation tests for temperature sensitive phenotype. A1 and A2 (Δ*cmkA15.2*/pMMI7), Ba1 and Ba2 (Δ*cmkB1.3*/pMMI5), Bb1 and Bb2 (Δ*cmkB1.3*/pMMI6), C1 and C2 (Δ*cmkC19.2*/pMMI8).
B. Complementation test for temperature induced increase of aerial hyphae. Bc1 and Bc2 (Δ*cmkB10.5*/pMMI6).

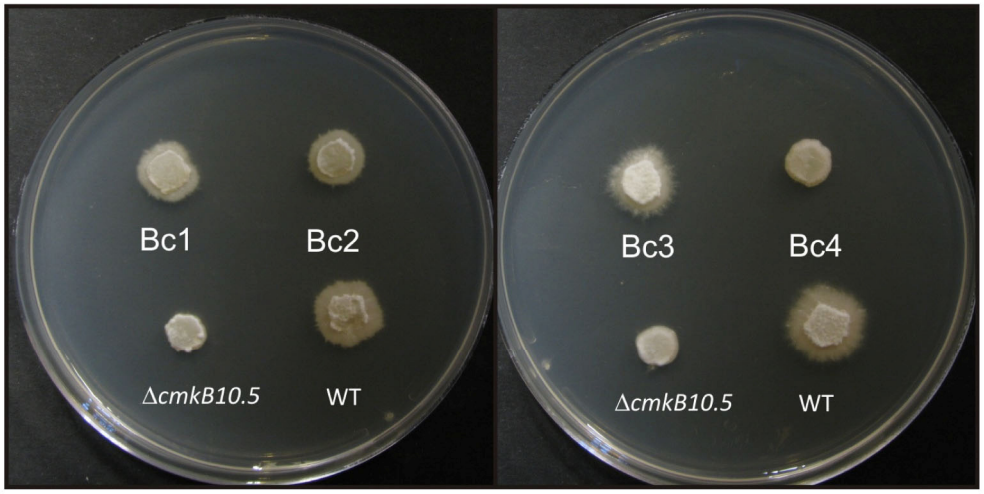

Figure 3.21. Complementation test for Mg^{2+}-sensitive phenotype of *cmkB* mutant
Colonies were grown on PD agar containing 0.6 M $MgCl_2$ for 12 days. Bc1, Bc2 and Bc3 (Δ*cmkB10.5*/pMMI6), Bc4 (Δ*cmkB10.5*/pAN7-1).

The strategy used was to delete the *cmkB* gene in the Δ*cmkA* background. The Δ*cmkB* mutant was not used as the recipient because of the phenotypic variation observed for this group of mutants under conditions of high Mg^{2+}. The goal was to determine whether this phenotypic variation would still be present after deletion of *cmkB* in the Δ*cmkA* background. Transformant Δ*cmkA15.4* was chosen for the generation of Δ*cmkAB* mutants, given that it did not show the temperature sensitive phenotype and had a growth rate similar to the WT under high Mg^{2+} conditions.

Protoplasts of Δ*cmkA15.4* were transformed with a linear fragment excised from pMMI9 (Section 2.11.9) carrying *cmkB* flanking sequences and a *hyg* resistance cassette (Fig. 3.22A). Three out of 52 transformants screened by PCR appeared to lack the *cmkB* gene, and Southern blot analysis using *Bam*HI and *Eco*RV genomic digests confirmed these results. For the *cmkB* deletion, two bands of 5.5 Kb and 3.9 Kb were expected for the *Bam*HI digest and two bands of 5.7 Kb and 2.5 Kb were expected for the *Eco*RV digest, when probed with pMMI9. One band of 9.8 Kb for the *Bam*HI digest and two bands of 6.1 Kb and 2.5 Kb for the *Eco*RV digest were expected for WT (Figs. 3.22B and C). All expected bands were observed in the Southern analysis results (Fig. 3.22D), confirming that transformants *ΔcmkAB16*, *ΔcmkAB28* and *ΔcmkAB31* have the *cmkB* gene replaced by *hph* gene. The phenotypes of these three transformants were then analyzed.

Mutants deleted for both *cmkA* and *cmkB* genes grew as well as WT on PD agar, at 22°C (Fig. 3.23A). The hyphal morphology and branching pattern of the double mutants was the same as WT (Fig. 3.23B). No difference was observed for growth under condition of osmotic stress (Fig. 3.24A). Similarly, growth of mutants at a high temperature, in the presence of SDS or under conditions of oxidative stress, was the same as WT (Fig. 3.24B).

As for the single-deletion mutants, production of ROS was tested using DAB (Fig. 3.25A) and NBT (Fig. 3.25B). These tests showed that ROS production of Δ*cmkAB* did not differ from WT.

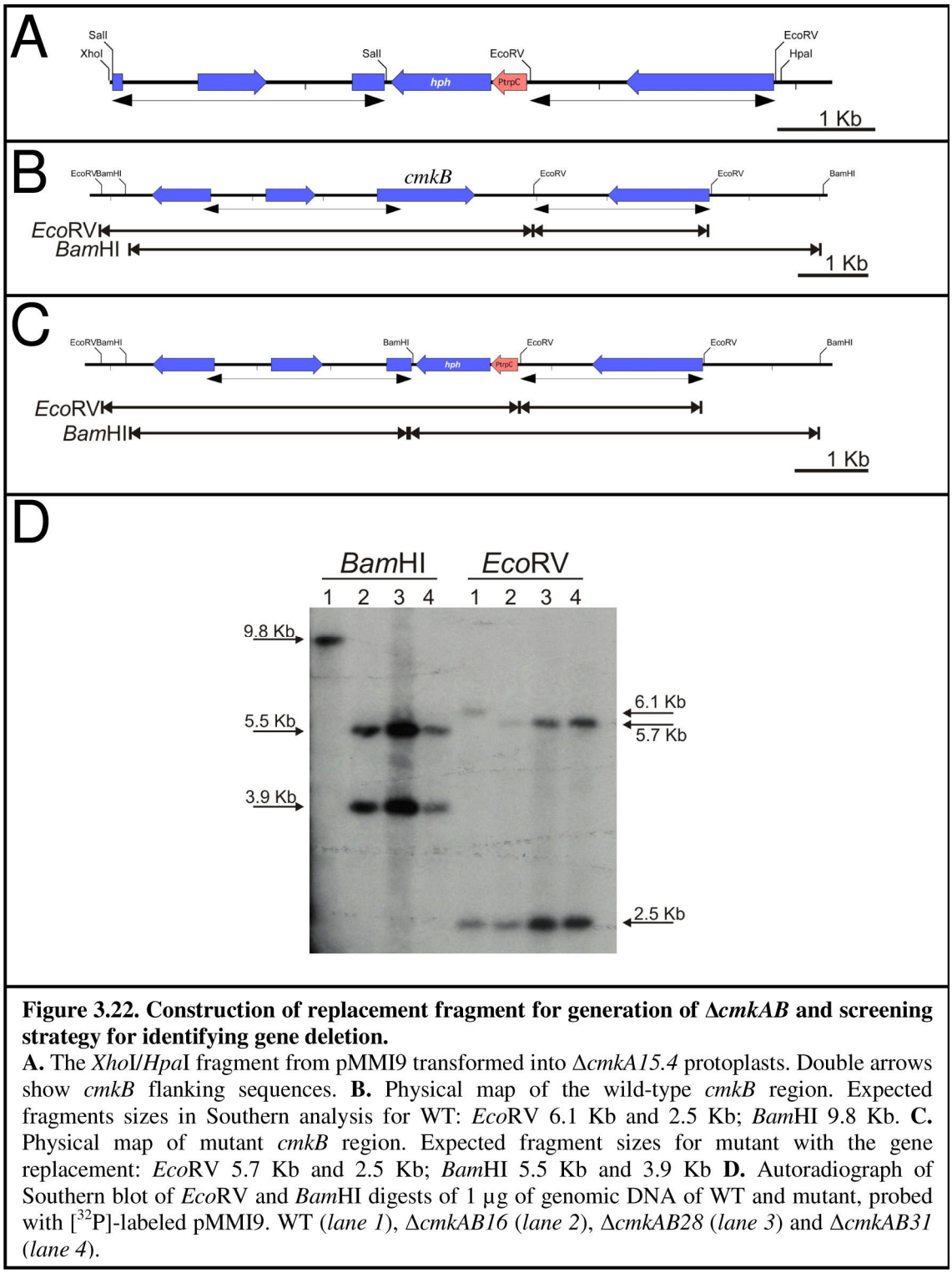

Figure 3.22. Construction of replacement fragment for generation of Δ*cmkAB* and screening strategy for identifying gene deletion.
A. The *Xho*I/*Hpa*I fragment from pMMI9 transformed into Δ*cmkA15.4* protoplasts. Double arrows show *cmkB* flanking sequences. **B.** Physical map of the wild-type *cmkB* region. Expected fragments sizes in Southern analysis for WT: *Eco*RV 6.1 Kb and 2.5 Kb; *Bam*HI 9.8 Kb. **C.** Physical map of mutant *cmkB* region. Expected fragment sizes for mutant with the gene replacement: *Eco*RV 5.7 Kb and 2.5 Kb; *Bam*HI 5.5 Kb and 3.9 Kb **D.** Autoradiograph of Southern blot of *Eco*RV and *Bam*HI digests of 1 µg of genomic DNA of WT and mutant, probed with [^{32}P]-labeled pMMI9. WT (*lane 1*), Δ*cmkAB16* (*lane 2*), Δ*cmkAB28* (*lane 3*) and Δ*cmkAB31* (*lane 4*).

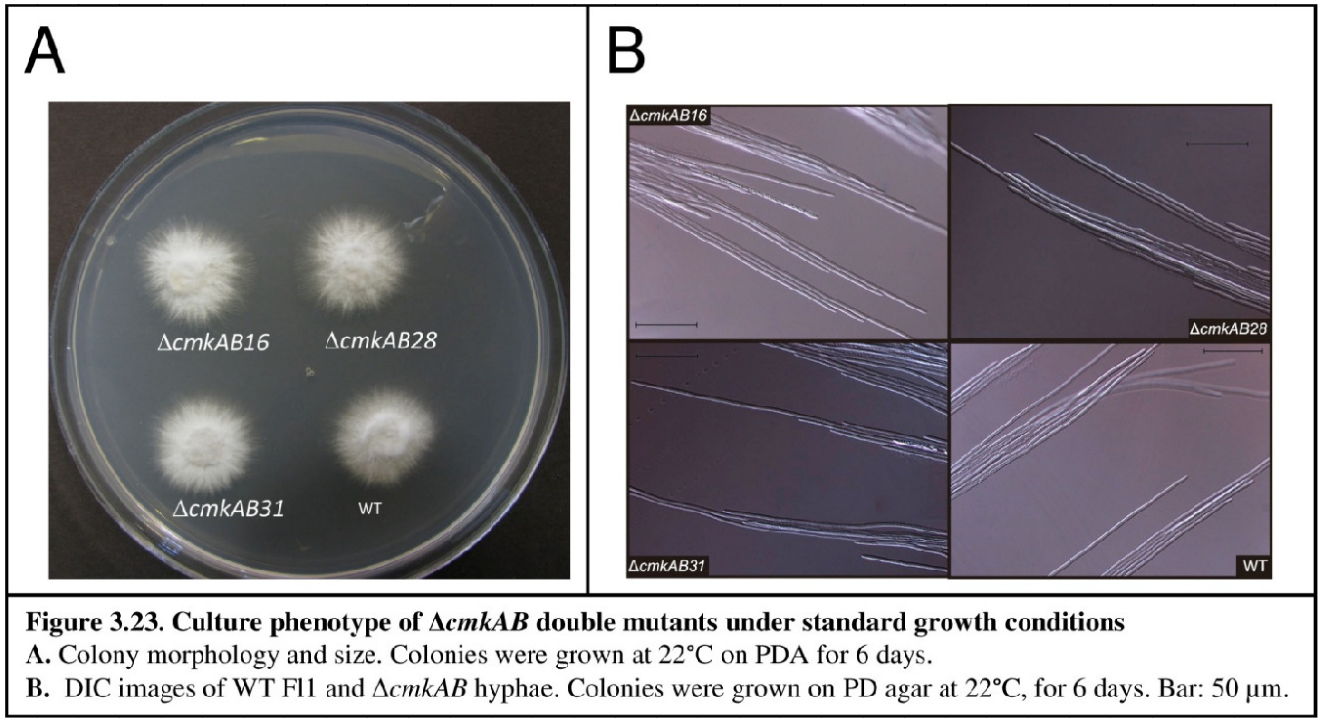

Figure 3.23. Culture phenotype of Δ*cmkAB* double mutants under standard growth conditions
A. Colony morphology and size. Colonies were grown at 22°C on PDA for 6 days.
B. DIC images of WT Fl1 and Δ*cmkAB* hyphae. Colonies were grown on PD agar at 22°C, for 6 days. Bar: 50 µm.

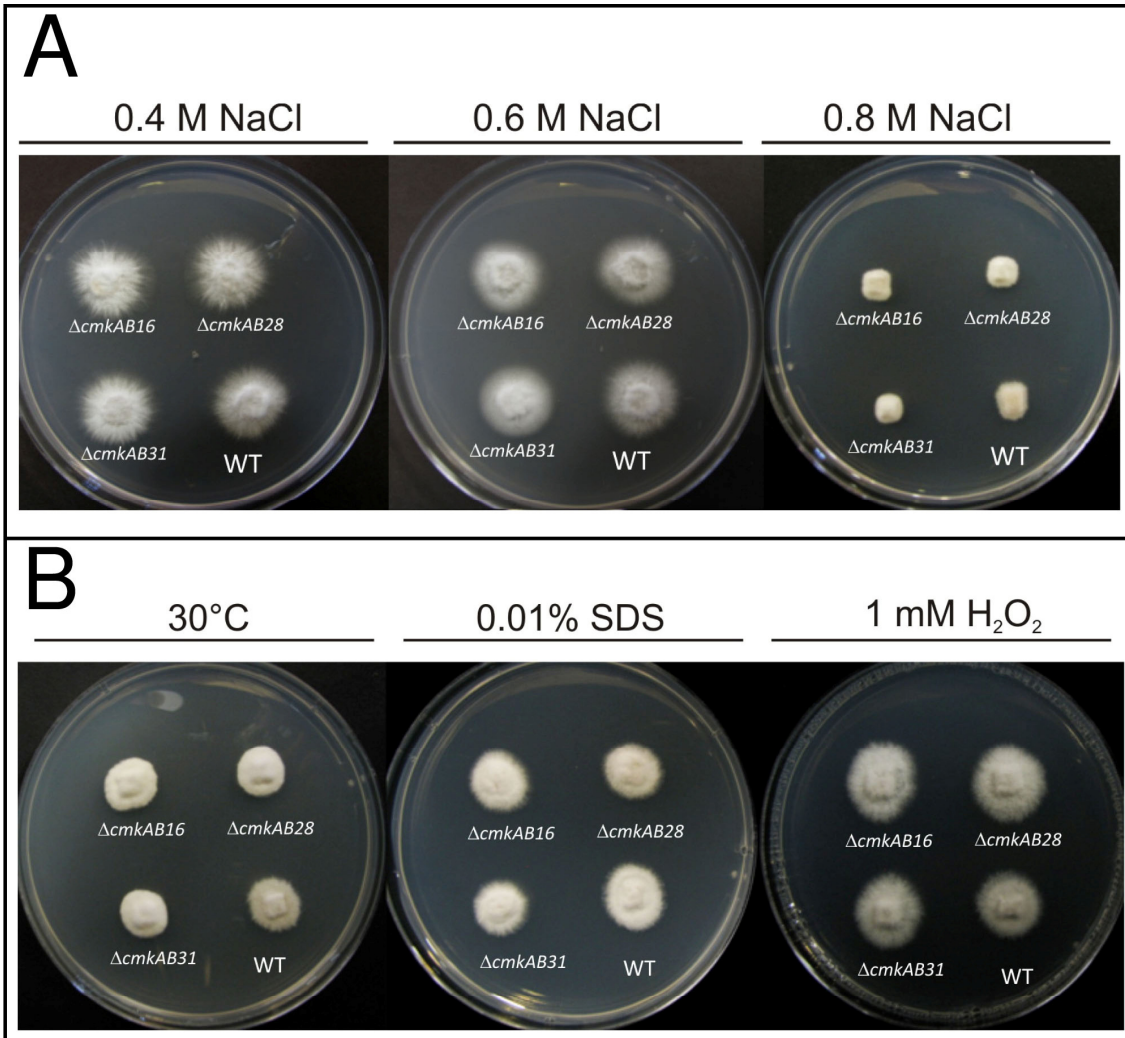

Figure 3.24. Growth phenotype of Δ*cmkAB* mutants under different stress conditions
A. Growth of double-deletion mutants was tested on PDA containing 0.4 M, 0.6 M and 0.8 M NaCl.
B. Growth of Δ*cmkAB* tested under conditions of temperature stress (30°C), cell wall destabilizing agent (SDS) and oxidative stress (H_2O_2).

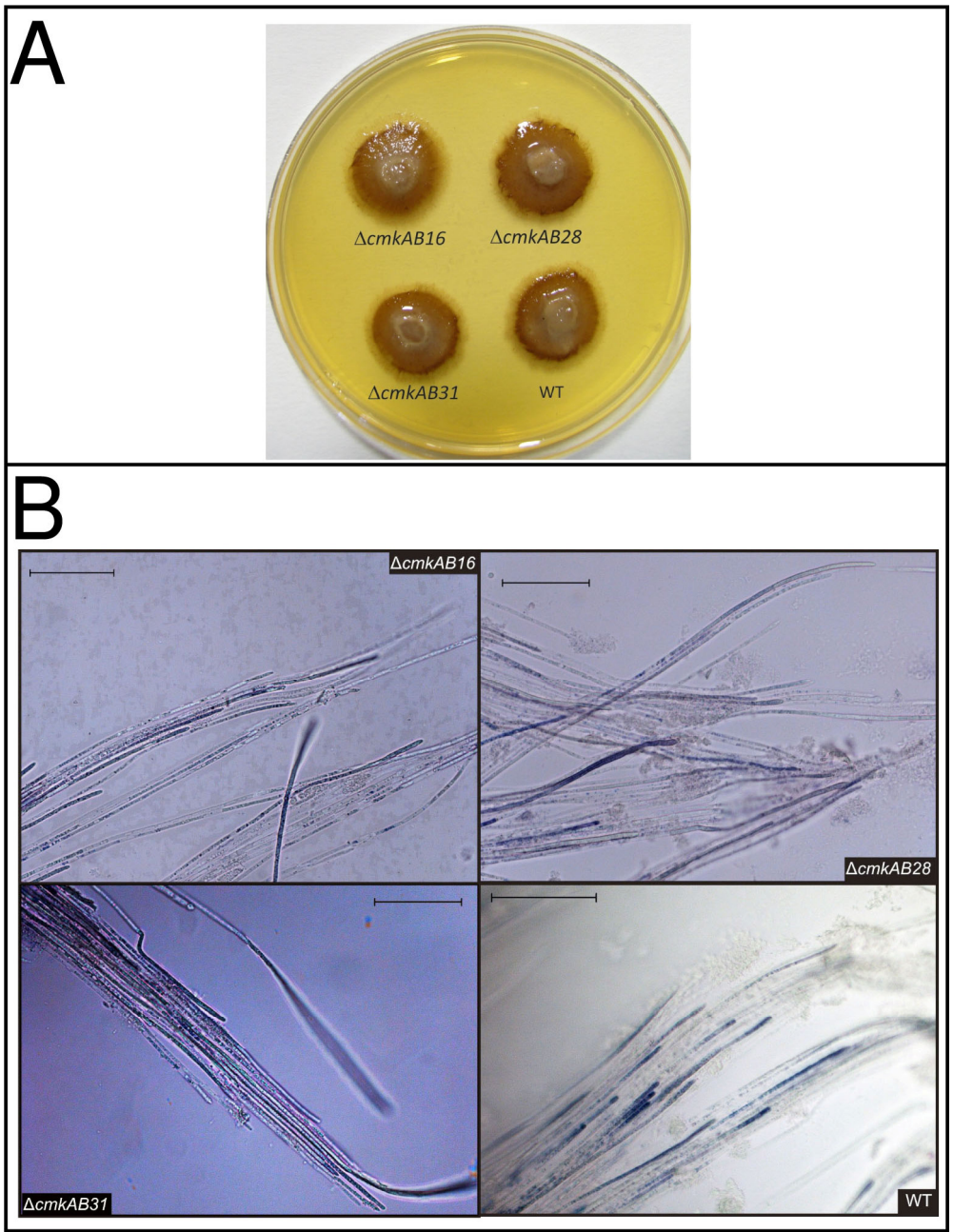

Figure 3.25. ROS production by Δ*cmkAB*
A. DAB staining of 8-day-old colonies of double deletion mutants and WT.
B. NBT staining of hyphae of double deletion mutants and WT. Bar: 50 µm

3.5.1. Growth of Δ*cmkAB* under high extracellular concentrations of Mg^{2+} and Ca^{2+}

Growth of the Δ*cmkAB* mutants was tested in the presence of high concentrations of $MgCl_2$. In contrast to the Δ*cmkA* and Δ*cmkB* single-deletion mutants, the double-deletion mutants showed no variation in phenotypes under the conditions tested. All three independent transformants, Δ*cmkAB16*, Δ*cmkAB28* and Δ*cmkAB31*, showed impaired growth under these conditions. Unlike the Δ*cmkA* and Δ*cmkB* single gene mutants, the Δ*cmkAB* double mutants displayed no variation in phenotype among the independent transformants (Fig. 3.26).

In order to confirm that this effect was specific for magnesium ions and not other divalent ions, growth of Δ*cmkAB* mutants was tested in the presence of high concentrations of $CaCl_2$. The Δ*cmkAB* mutants were less sensitive to very high concentrations of $CaCl_2$ (0.4, 0.5 M and 0.6 M) than WT (Figs. 3.27A and B). However, when grown in the presence of the extracellular Ca^{2+} chelator EGTA, the Δ*cmkAB* mutants had less aerial hyphae than WT (Fig. 3.27C), indicating that they were more sensitive to low extracellular Ca^{2+} concentrations than WT.

Previous work on Ca^{2+} influx into *S. cerevisiae* suggests that unidentified Ca^{2+} transporters are competitively inhibited by elevated extracellular Mg^{2+} concentrations (Cui *et al.*, 2009a). In order to determine whether the Mg^{2+} and Ca^{2+} effects observed for the Δ*cmkAB* mutants are connected, a remediation experiment was conducted using growth media containing equal concentrations of $CaCl_2$ and $MgCl_2$. This experiment showed that in the presence of 0.4 M $MgCl_2$ and 0.4 M $CaCl_2$ Δ*cmkAB* mutants grow as well as WT, suggesting that Ca^{2+} remediates the Mg^{2+} effect (Fig. 3.28). However, WT itself grows slower on these plates than on plates containing only one of the ions, presumably because of the higher (0.8 M) overall concentration of divalent ions.

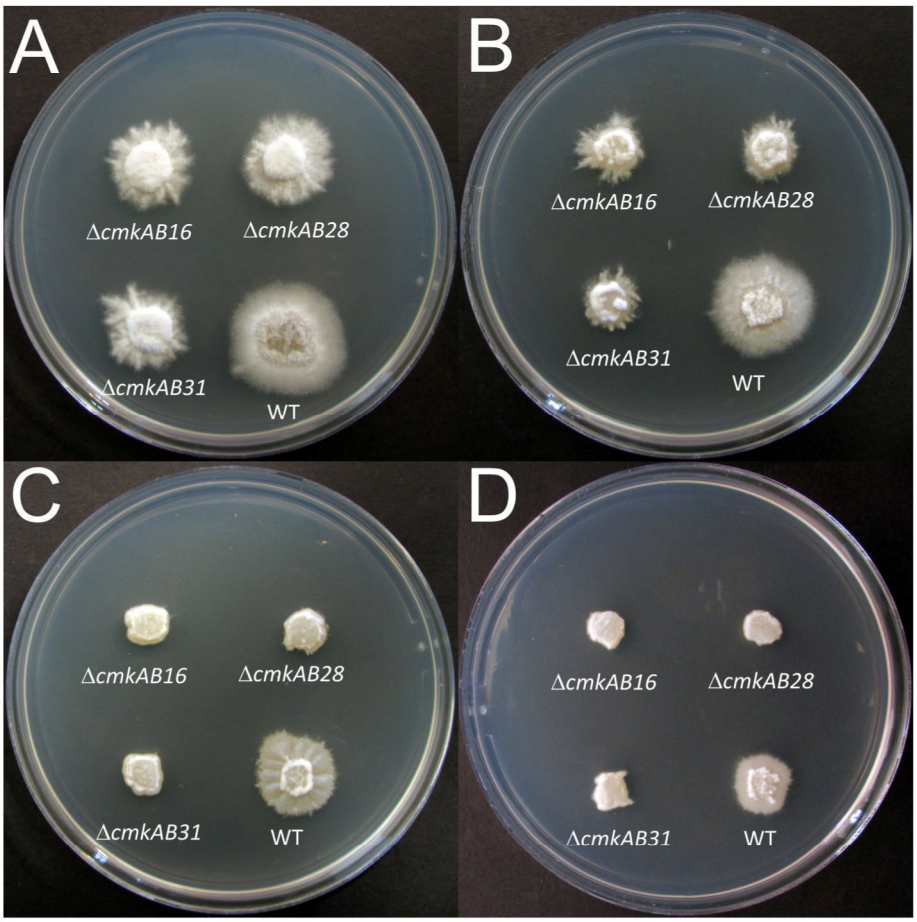

Figure 3.26. Colony morphology phenotype and growth of double-deletion mutants Δ*cmkAB* on high Mg^{2+} concentrations. Growth of Δ*cmkAB* mutants was compared to WT under different concentrations of Mg^{2+}. Colonies were grown for ten days, at 22°C.
A. PD agar containing 0.4 M $MgCl_2$
B. PD agar containing 0.5 M $MgCl_2$
C. PD agar containing 0.6 M $MgCl_2$
D. PD agar containing 0.8 M $MgCl_2$

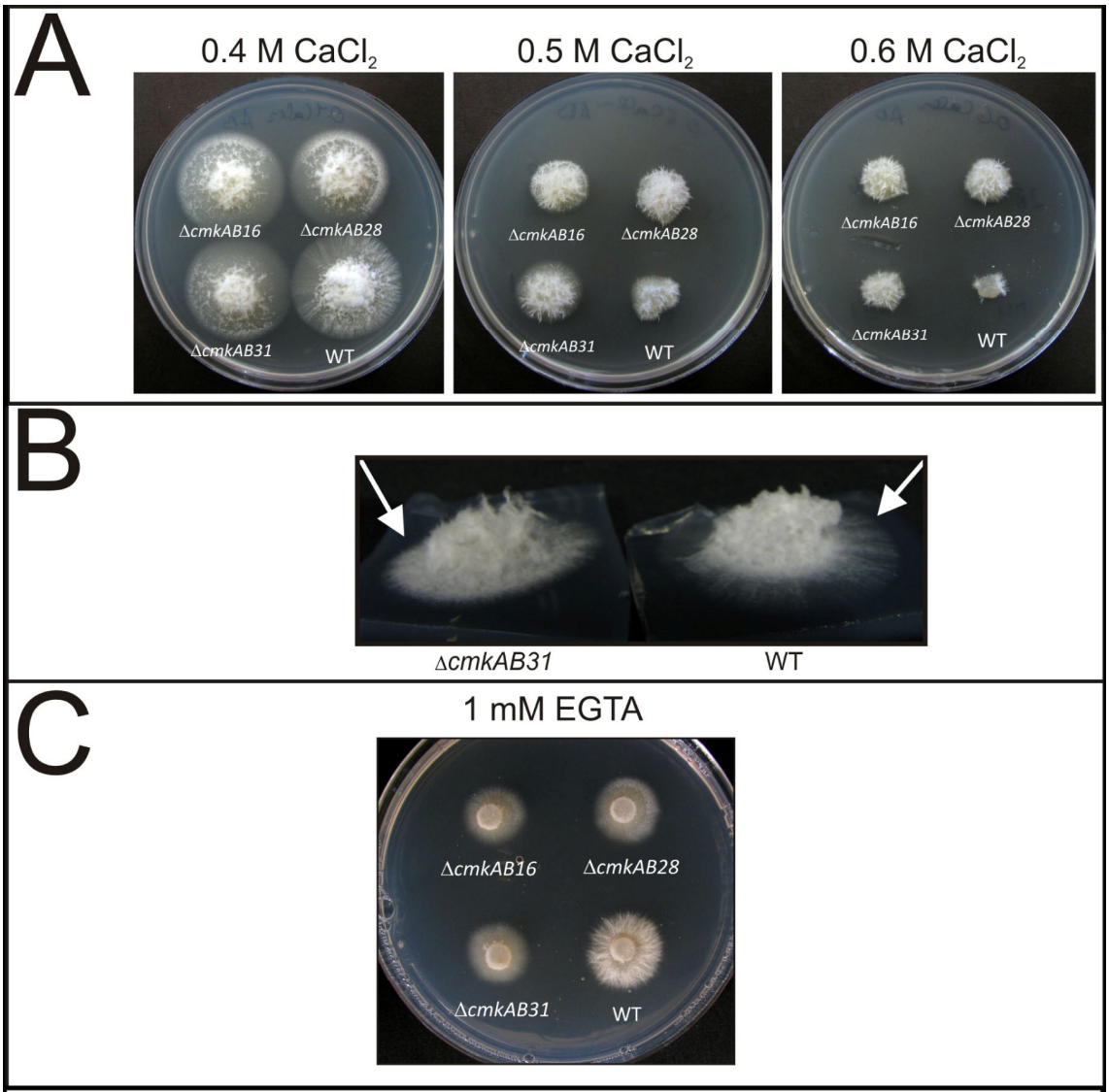

Figure 3.27. Growth of Δ*cmkAB* in the presence of high concentrations of Ca^{2+} and EGTA

A. Colony growth of Δ*cmkAB* mutants on different concentrations of $CaCl_2$. Pictures were taken after 12 days of growth.

B. Loss of aerial hyphae in WT. Pictures were taken after 8 days of growth on 0.4 M $CaCl_2$.

C. Six-day-old colonies of Δ*cmkAB* and WT grown on PDA containing 1 mM EGTA.

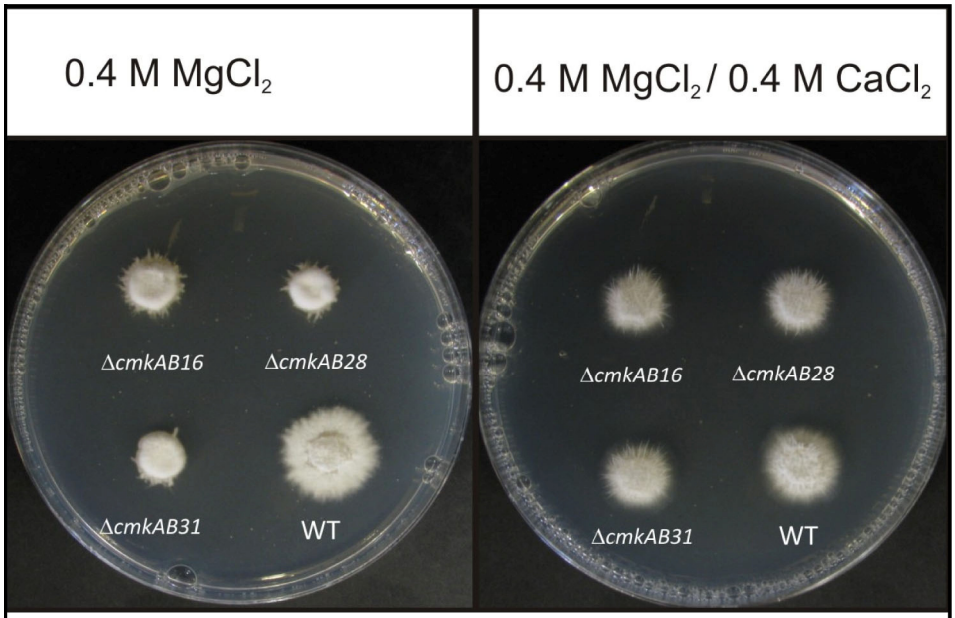

Figure 3.28. Ca^{2+} remediation of Δ*cmkAB* Mg^{2+} sensitivity
Colonies were grown for eight days on PD agar containing 0.4 M $MgCl_2$ alone or 0.4 M $MgCl_2$ together with 0.4 M $CaCl_2$.

3.5.2. Symbiotic phenotype of Δ*cmkAB*

The double-deletion mutants were inoculated into perennial ryegrass seedlings to determine whether they had a symbiotic interaction phenotype. Plants were screened for infection after 10 weeks of growth in the green house. Infection rates of Δ*cmkAB* were similar to that of the WT and plants showed no signs of premature senescence, with the length and colour of the leaves being the same as for WT infected plants (Fig. 3.29). Aniline-blue staining of leaf sheaths of mutant-infected plants showed that the hyphal morphology *in planta* of the Δ*cmkAB* mutants was the same as WT (Fig. 3.30).

3.6. Complementation of double-deletion mutants

To determine whether both the *cmkA* and *cmkB* genes are involved in the Mg^{2+}-sensitive phenotype, complementation experiments were carried out on the Δ*cmkAB* mutants.

Plasmids pMMI6, carrying the *cmkB* gene, and pMMI7, carrying the *cmkA* gene, were used in these complementation experiments. Three different sets of transformants were generated: those containing *cmkA* (Δ*cmkAB*/pMMI7 = AB-A series), those containing *cmkB* (Δ*cmkAB*/pMMI6 = AB-B series) and those containing both *cmkA* and *cmkB* (Δ*cmkAB*/pMMI6,pMMI7 = AB-AB series). All plasmids were co-transformed into Δ*cmkAB16* protoplasts together with pAN8-1, the vector carrying phleomycin/zeocin resistance gene *ble*.

After subculturing the transformants on media containing zeocin (160 μg/ml) twice, transformants were tested by PCR for the presence of the introduced genes (Figs. 3.31B and C). Two PCR positive transformants of each set were tested for Mg^{2+} sensitivity. These tests showed that only *cmkB* had the ability to complement the Mg^{2+} sensitivity phenotype (Fig. 3.31A). The phenotype of Δ*cmkAB*/*cmkB,cmkA* transformants (AB-AB2 and AB-AB3) was the same as the Δ*cmkAB*/*cmkB* (AB-B6 and AB-B7), demonstrating that the phenotypic variation observed for the single-deletion mutants was not due to functional redundancy between *cmkA* and *cmkB*. Total RNA was isolated from Δ*cmkAB*/*cmkA* transformants (AB-A1 and AB-A2) to check expression of *cmkA* from the complementation construct. RT-PCR showed that *cmkA* was expressed in both

Figure 3.29. Plant phenotype of Δ*cmkAB* mutants
Plants infected with WT and double deletion mutants, 12 weeks after inoculation.

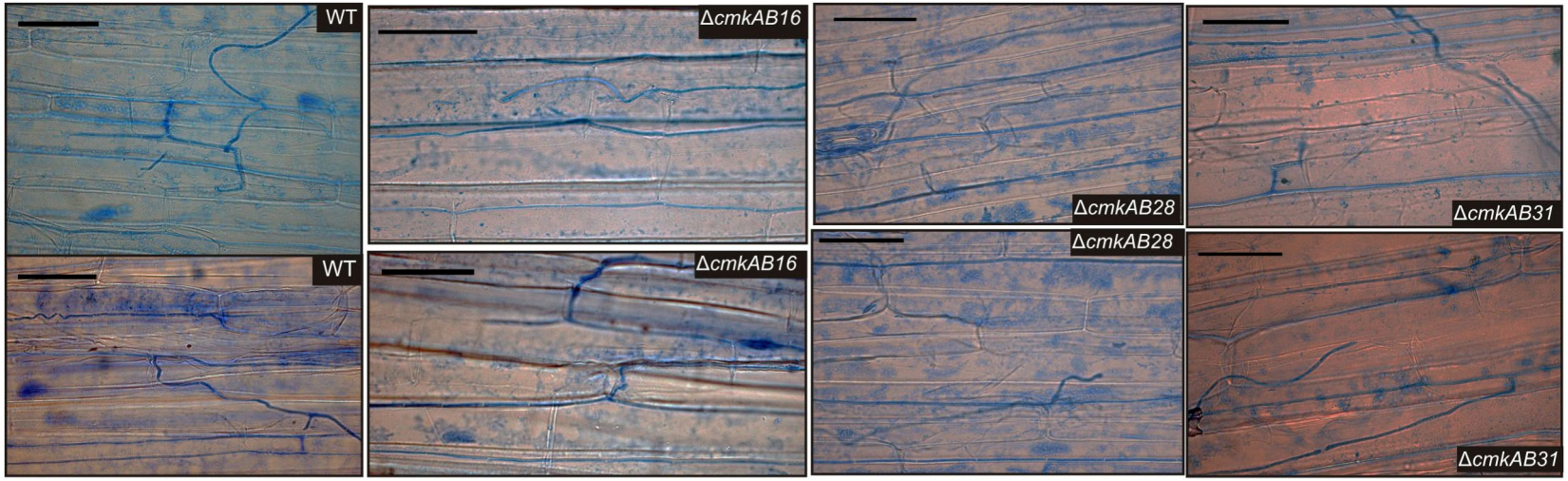

Figure 3.30. *In planta* hyphal morphology phenotype of the Δ*cmkAB* mutants
Micrographs of aniline-blue staining of the pseudostems of plants infected with WT and mutants Δ*cmkAB16*, Δ*cmkAB28*, Δ*cmkAB31*. Bar: 50 µm.

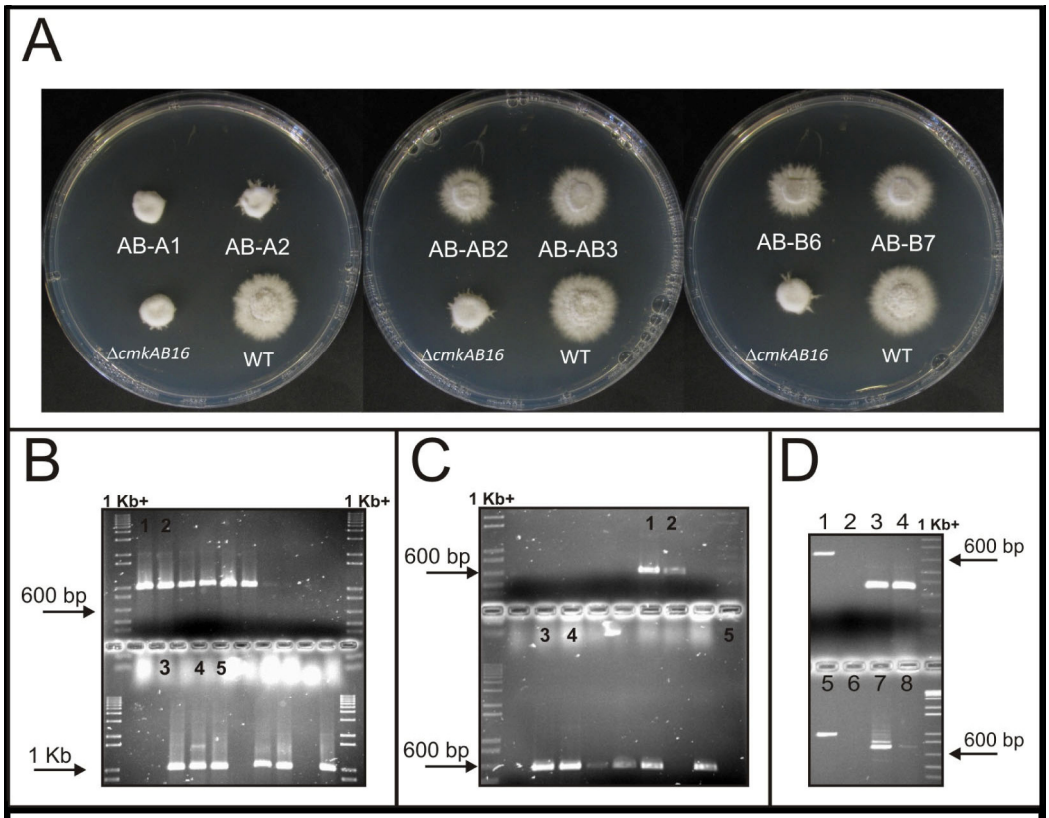

Figure 3.31. Complementation of Δ*cmkAB*

A. Growth of WT, Δ*cmkAB16* and complementation transformants on PD agar containing 0.4 M $MgCl_2$. Growth was assessed 8 days after plating. AB-A1 and AB-A2 (Δ*cmkAB16*/pMMI7), AB-B6 and AB-B7 (Δ*cmkAB16*/pMMI6), AB-AB2 and AB-AB3 (Δ*cmkAB16*/pMMI6, pMMI7).

B. PCR products of primers MI3/MI4 specific for the *cmkA* gene. PCR was performed on genomic DNA of AB-A1 (*lane 1*), AB-A2 (*lane 2*), AB-AB2 (*lane 4*), AB-AB3 (*lane 5*). Negative control (*lane 3*).

C. PCR products of primers MI5/MI6 specific for the *cmkB* gene. PCR was performed on genomic DNA of AB-B6 (*lane 1*), AB-B7 (*lane 2*), AB-AB2 (*lane 3*), AB-AB3 (*lane 4*). Negative control (*lane 5*).

D. PCR products of primers T1.1/T1.2 (*lanes 1, 2, 3 and 4*), specific for β-tubuline gene, and MI3/MI4 (*lanes 5, 6, 7 and 8*), performed using genomic DNA (WT, *lanes 1 and 5*) and cDNA as a template. cDNA was generated by RT-PCR from total RNA isolated from AB-A1 (*lanes 3 and 7*) and AB-A2 (*lanes 4 and 8*). Negative control (*lanes 2 and 6*).

transformants, albeit at different levels (Fig. 3.31D), confirming that expression of *cmkA* did not affect the Mg^{2+}-sensitive phenotype in these transformants.

3.7. Identification *E. festucae* homologue of calcineurin A

In order to identify the *E. festucae* homologue of the gene encoding the calcineurin catalytic subunit, *cnaA*, the genome of *E. festucae* strain E2368 was searched using TBLASTN and protein sequences of calcineurin A from *A. nidulans*, *N. crassa* and *S. cerevisiae*. This search identified two homologues, located on contigs 346 and 1372. PCR performed using primers specific for each copy confirmed that both copies were present in E2368. However, only one copy, on contig 346, was amplified from Fl1 genomic DNA (Figs. 3.32A, C and D). RT-PCR analysis revealed that both copies of *cnaA* from E2368 and the single copy from Fl1 are expressed in culture (Fig. 3.32B).

3.8. Deletion of *cnaA* in *E. festucae* Fl1

In order to study the in culture and symbiotic function of the single-copy *cnaA* of *E. festucae*, deletion mutants for this gene were generated. A cosmid library was screened using the PCR product of primers specific for *cnaA* gene, MI13/MI14. This screening identified 8 positive clones and one of them, 2C5, was used to source fragments for generation of a replacement construct. Fragments, excised from the cosmid using restriction enzymes *Pst*I and *Bam*HI (the 1.4 Kb fragment) and *Eco*RI and *Eco*RV (the 2.1 Kb fragment), were cloned into pSF15.15, a hygromycin resistance vector, to generate plasmid pMMI4 (Fig. 3.33A) (Section 2.11.4). A complete replacement construct was obtained by excising the 5 Kb *Hind*III/*Eco*RV fragment from pMMI4 (Fig. 3.33B) and was transformed into *E. festucae* Fl1 protoplasts. In order to facilitate the process of screening for deletion mutants, a second transformation was conducted using a split selection marker system. The 5' fragment of the split construct was generated by excising the 2.1 Kb *Pst*I/*Pvu*I fragment from pMMI4 and the 3' fragment was obtained by excising the 3 Kb *Sph*I/*Eco*RV fragment from the same plasmid (Fig. 3.33B). These two fragments overlap over a 200bp region within the *hph* gene. The 5' and 3' split marker fragments were cotransformed into WT protoplasts. This transformation generated a smaller number of transformants than the full-length construct transformation but more than what was expected.

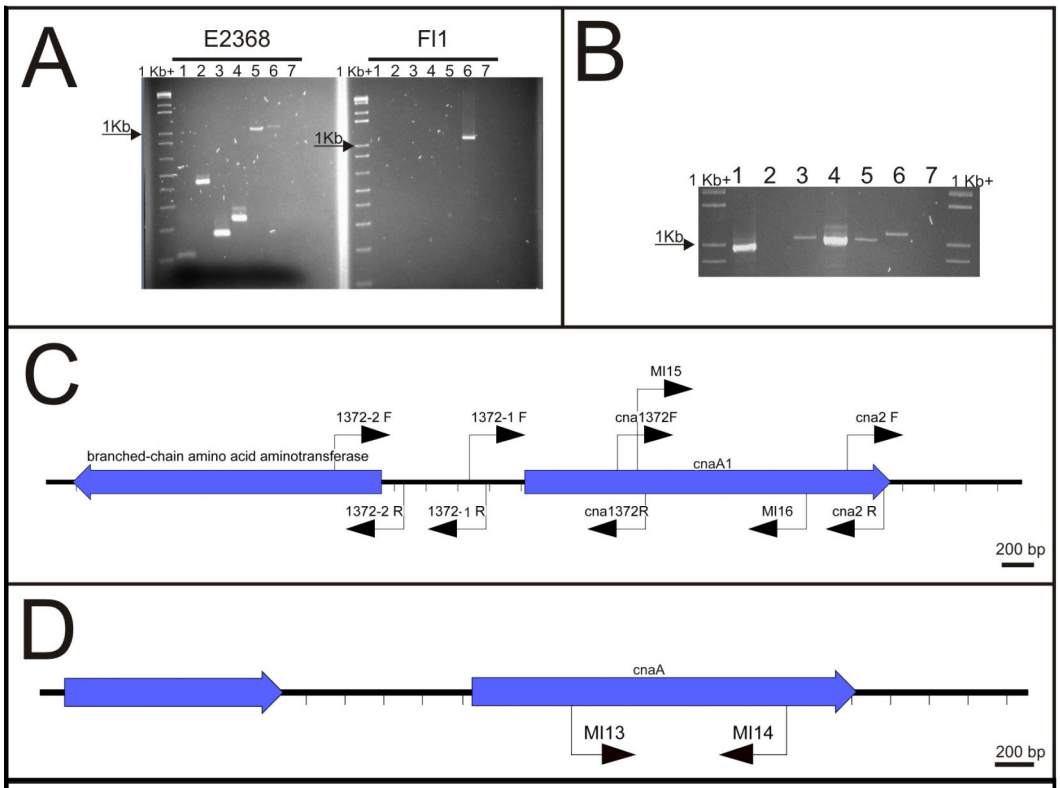

Figure 3.32. ***E. festucae*** **strain E2368 has two copies of calcineurin A gene**
A. PCR analysis of the *cnaA* in strains E2368 and Fl1. Lanes: primer pair 1372-1F/1372-1R (*lane 1*); primer pair 1372-2F/1372-2R (*lane 2*); primer pair cna1372F/cna1372R (*lane 3*); primer pair cna2F/cna2R (*lane 4*); primer pair MI15/MI16 (*lane 5*); primer pair MI13/MI14 (*lane 6*); negative control (*lane* 7).
B. PCR using cDNA generated by RT-PCR from total RNA isolated from E2368 (*lanes 1* and *4*) and Fl1 (*lanes 2* and *5*) and E2368 genomic DNA (*lanes 3* and *6*). Primers: MI15/MI16 (*lanes 1*, *2* and *3*) and MI13/MI14 (*lanes 4*, *5* and *6*). Negative control (*lane 7*).
C. Physical map of contig 1372 derived from the E2368 genome sequence, showing primers used in the PCR analysis (**A**).
D. Physical map of contig 346 region that contains *cnaA* gene.

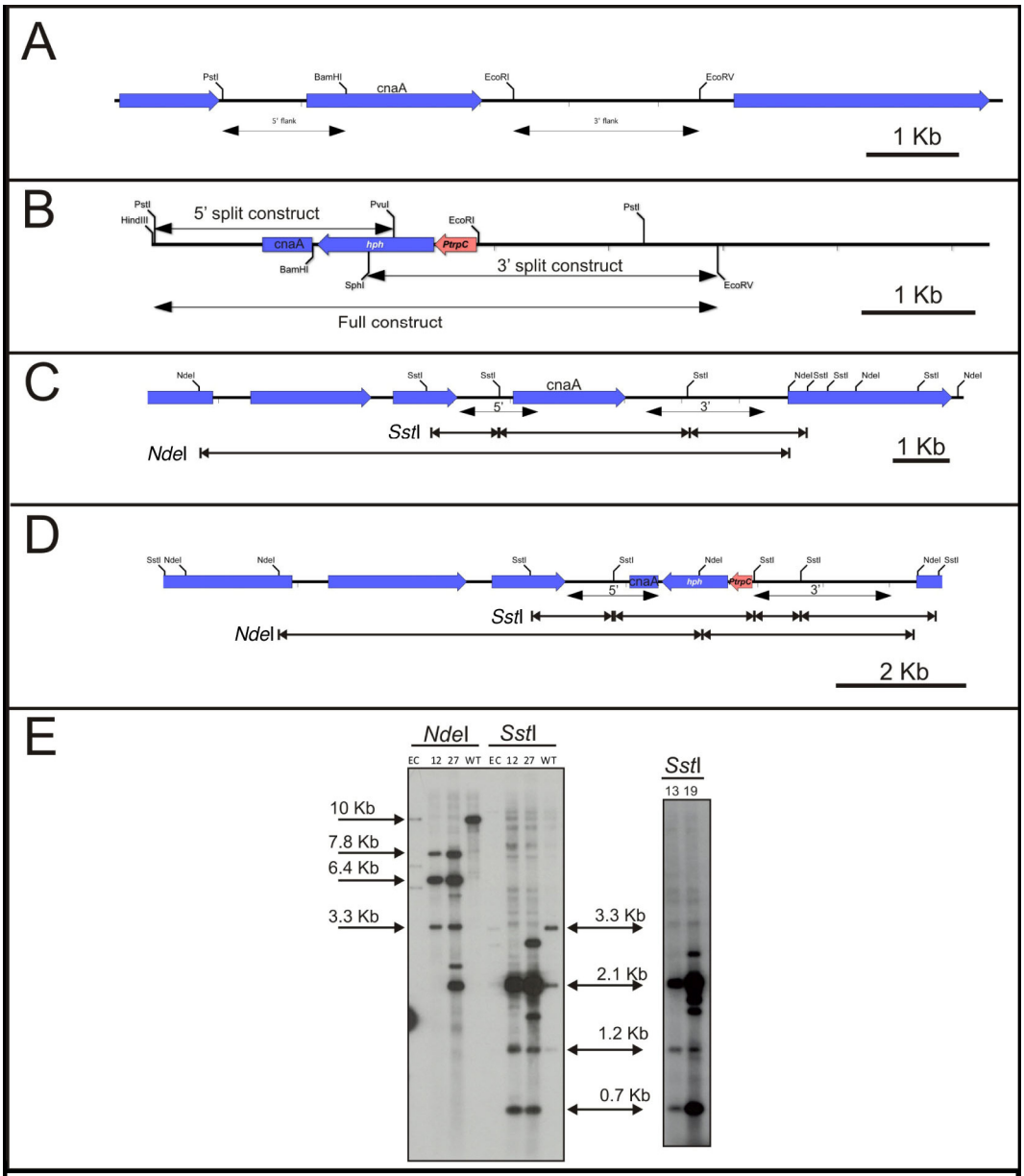

Figure 3.33. Construction of *cnaA* replacement mutants
A. Physical map of *cnaA* genomic region, showing 5' and 3' flanking sequences.
B. Physical map of pMMI4 showing the replacement fragments.
C. Physical map of the WT region with the *cnaA* gene, showing bands expected to be observed in the Southern analysis for *Nde*I and *Sst*I digests, when probed with [^{32}P]-dCTP-labeled pMMI4.
D. Physical map of the mutant region with the replacement of *cnaA* gene, showing bands expected to be observed in the Southern analysis for *Nde*I and *Sst*I digests, when probed with [^{32}P]-dCTP-labeled pMMI4.
E. Autoradiographs of Southern blots containing WT and mutant digests, probed with [^{32}P]-dCTP-labeled pMMI4. Lanes: Transformant with an ectopic integration (EC); Δ*cnaA12* (12); Δ*cnaA27* (27); wild-type (WT); Δ*cnaA13* (13); Δ*cnaA19* (19).

The explanation for the relatively high number of transformants could be the self-annealing of the two bands generated from the *Pst*I/*Pvu*I digestion of pMMI4, which are approximately the same size and were difficult to separate when excising from the gel. All transformants from the split-marker transformation, 165 in total, and the 75 transformants from the full construct transformation plates were subcultured onto plates containing hygromycin and subsequently subcultured three times to generate homokaryotic colonies. Sixteen transformants from the split-marker transformation pool and 15 transformants from the full construct transformation pool showed highly reduced growth in culture and secretion of a yellow pigment into the growth media. Two of these transformants, Δ*cnaA*12 from the full construct pool and Δ*cnaA*27 from the split-marker pool, were screened by Southern blot in order to confirm that they were deleted for *cnaA* gene. Genomic DNA of these transformants, together with WT and a transformant carrying an ectopic integration, was digested using restriction enzymes *Nde*I and *Sst*I. For the *Nde*I digest, two bands of 3.3 Kb and 6.4 Kb were expected to hybridize for a *cnaA* gene replacement, while one band of 10 Kb was expected for WT, when digests were probed with pMMI4. For the *Sst*I digests, four bands of 0.7 Kb, 1.2 Kb, 2.1 Kb and 2.14 Kb were expected for replacement mutants and three bands of 1.2 Kb, 2.1 Kb and 3.3 Kb were expected for WT, when probed with pMMI4 (Figs. 3.33C and D). Upon hybridization, the expected bands for both WT and mutants were observed, confirming deletion of *cnaA* in Δ*cnaA12* and Δ*cnaA27* (Fig. 3.33E). Additional bands were observed in transformant Δ*cnaA27*, suggesting that this transformant also had an ectopic integration. The additional band of 7.8 Kb hybridized in the *Nde*I digests of the mutants corresponded to the size of an incomplete digested fragment 5' of *cnaA*. To further confirm that the dramatic culture phenotype is caused by deletion of *cnaA* gene, two more transformants displaying the same phenotype, Δ*cnaA13* from the full construct pool and Δ*cnaA19* from the split construct pool, were investigated by Southern blot analysis, using *Sst*I digest. The observed banding pattern was consisted with the deletion of *cnaA* and showed that Δ*cnaA19* also has an ectopic integration (Fig. 3.33E).

3.8.1. Culture and symbiotic phenotypes of Δ*cnaA*

The four *cnaA* mutants displayed highly reduced growth in culture and secretion of a yellow pigment (Fig. 3.34A). The hyphae of the mutants were shorter than those of WT, had increased and irregular branching, and were frequently surrounded by debris

indicative of cell lysis (Fig. 3.34B). This morphology suggests that the mutants might have impaired cell wall synthesis and that the yellow pigment could be the result of extensive cell lysis.

The four Δ*cnaA* mutants and two other putative knock-out mutants were inoculated into perennial ryegrass seedlings (20 seedlings each) to examine the symbiotic phenotype. The seedlings inoculated with the *ΔcnaA* mutants displayed a strong hypersensitive response, characterized by a brown colouration that spread from the inoculation point (Fig. 3.35A). In some seedlings the HR was strong enough to lead to the death of the seedling within two weeks. Seedlings that survived were planted and checked for infection after 8 weeks. Of all the plants inoculated with the Δ*cnaA* mutants, only three plants were infected, one inoculated with Δ*cnaA27* and two inoculated with Δ*cnaA12*. The plant infected with Δ*cnaA27* was small compared with WT and died immediately after the screening. Two plants inoculated with Δ*cnaA12* displayed a similar growth phenotype to the WT (Fig. 3.35B). Aniline-blue staining of leaf sheaths showed that the hyphal growth pattern of the Δ*cnaA* mutants resembled that of WT. However, the cytoplasm of the Δ*cnaA* mutant hyphae was highly vacuolated, compared with WT (Figs. 3.35C, D and E).

These experiments show that calcineurin is important for *E. festucae* growth in culture and for establishment of a symbiosis with *L. perenne*.

3.9. Analysis of two symbiotic mutants of *Epichloë festucae* generated by Agrobacterium-mediated mutagenesis

Agrobacterium-mediated mutagenesis (AMT) of *E. festucae* strain Fl1 was performed using an *A. tumefaciens* strain EHA105/pBSYT6 (PN1975) containing plasmid pBSYT6. Strain EHA105 (PN1828), containing the disarmed agropine plasmid pTiBo542, was used as a control (Section 2.5.3).

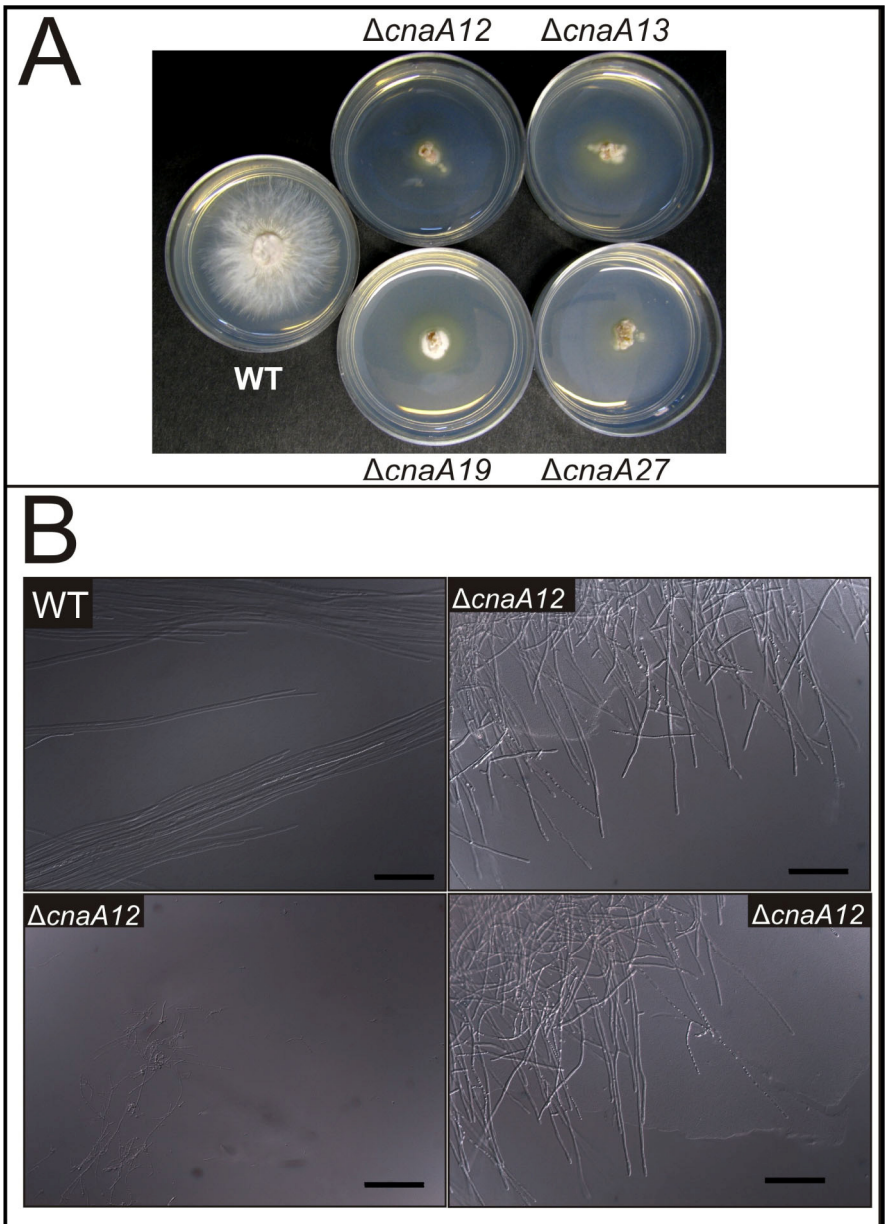

Figure 3.34. Culture phenotype of Δ*cnaA* mutants.
A. Colony size and morphology of Δ*cnaA* mutants compared with WT. Colonies were grown on PD agar for 8 days.
B. Hyphal morphology and branching pattern of Δ*cnaA12* and WT. DIC micrographs of 8-day-old colonies. Bar 50 µm.

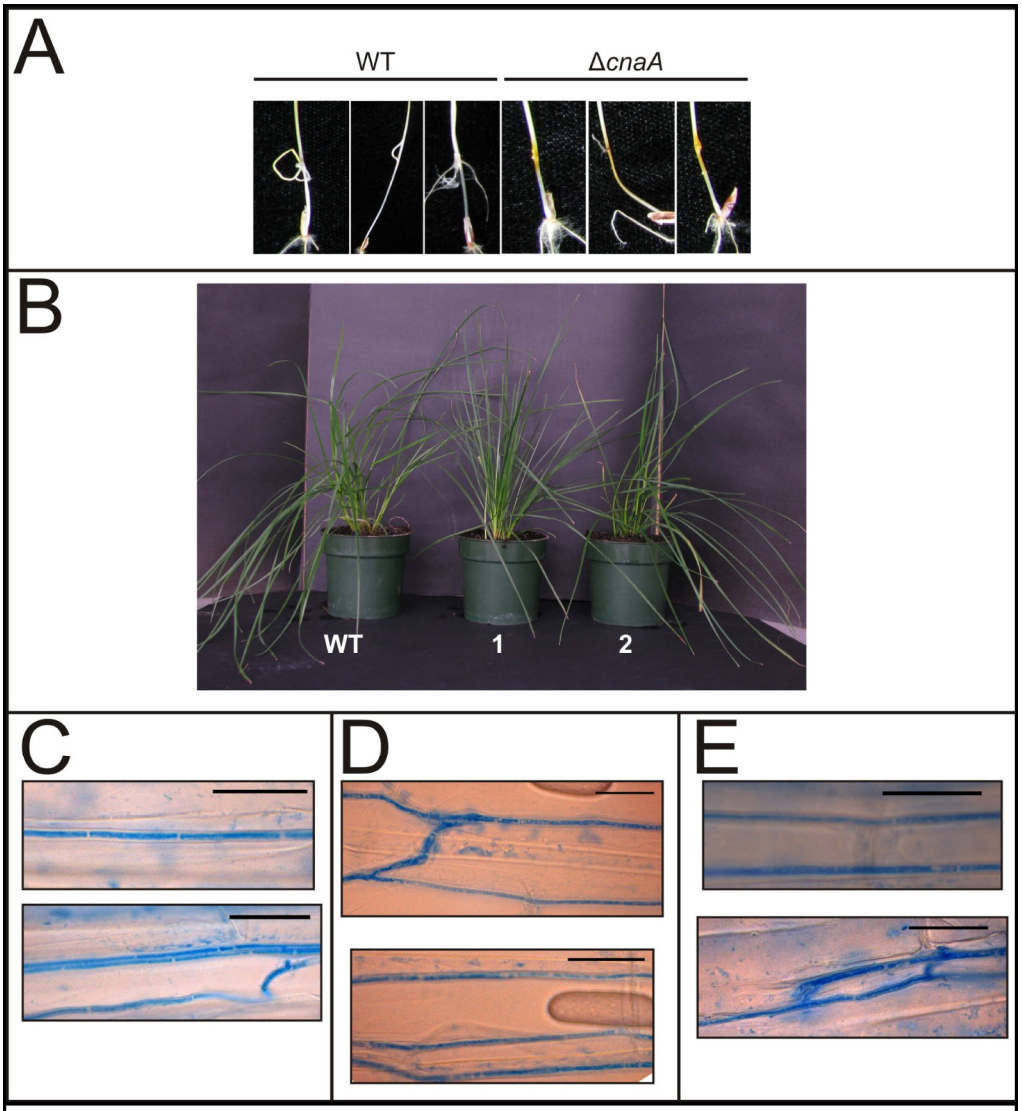

Figure 3.35. Symbiotic phenotype of Δ*cnaA* mutants
A. Hypersensitive reaction in 11-day-old seedlings inoculated with Δ*cnaA* mutants, compared with seedlings inoculated with WT.
B. Morphology of two plants infected with Δ*cnaA12* compared to WT. Plants were grown in growth room for 12 weeks.
C. Micrographs of aniline-blue stained leaf sheaths of plants infected with WT. Bar: 50 µm.
D. Micrographs of aniline-blue stained leaf sheaths of plant 1 infected with Δ*cnaA12*. Bar: 50 µm.
E. Micrographs of aniline-blue stained leaf sheaths of plant 2 infected with Δ*cnaA12*. Bar: 50 µm.

One hundred and eighty hygromycin-resistant mutants were generated and taken through three rounds of subculturing on media containing hygromycin in order to achieve homokaryotic hygromycin-resistant transformants. After nuclear purification, mutants were grown on PD agar without hygromycin, at 22°C, together with wild-type colonies, in order to screen for the growth phenotype in culture. The symbiotic phenotype was assessed by inoculating transformants and WT into perennial ryegrass seedlings and screening for stunting or lack of infection. Those transformants that had an altered symbiotic phenotype were further inoculated into more seedlings in order to confirm the initial results. Out of 180 mutants, two transformants, Ag51 and Ag212, had a culture and *in planta* phenotype.

3.9.1. In culture phenotype of mutants Ag51 and Ag212

When grown on PD agar at 22°C, both Ag51 and Ag212 grow slower than WT (Fig. 3.36A). In repeated rounds of screening, mutant Ag51 showed variable degrees of secretion of a yellow pigment into the growth media (Fig. 3.36B). The secretion appeared to be greater under conditions of stress, such as prolonged storage at 4°C or when hygromycin was present in the growth media.

The hyphal morphology and branching pattern were examined using DIC microscopy. Both Ag51 and Ag212 displayed a hyphal morphology the same as WT (Fig. 3.37). Compared with WT, Ag51 showed increased branching in regions further away from the hyphal tip.

3.9.2. Symbiotic phenotype of mutants Ag51 and Ag212

Perennial ryegrass seedlings inoculated with Ag51 showed signs of a hypersensitive reaction, manifested as a brown colouration of the seedling around the inoculation point (Fig. 3.38). This kind of reaction has never been observed for WT or Ag212. Out of a total of 65 plants inoculated with Ag51 from multiple screens, only two plants were positive for infection. At the time of screening (8 weeks post-inoculation) these two plants were small and did not survive the screening procedure.

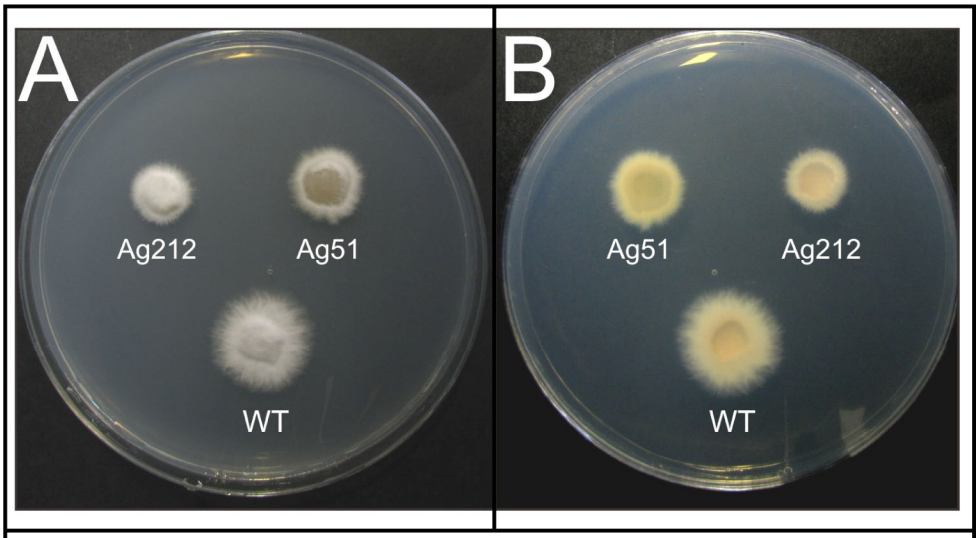

Figure 3.36. Colony morphology and growth of T-DNA mutants Ag212 and Ag51 in culture
Cultures were grown for 6 days on PD agar plates at 22°C. **A.** View from the top. **B.** View from the bottom of the plate.

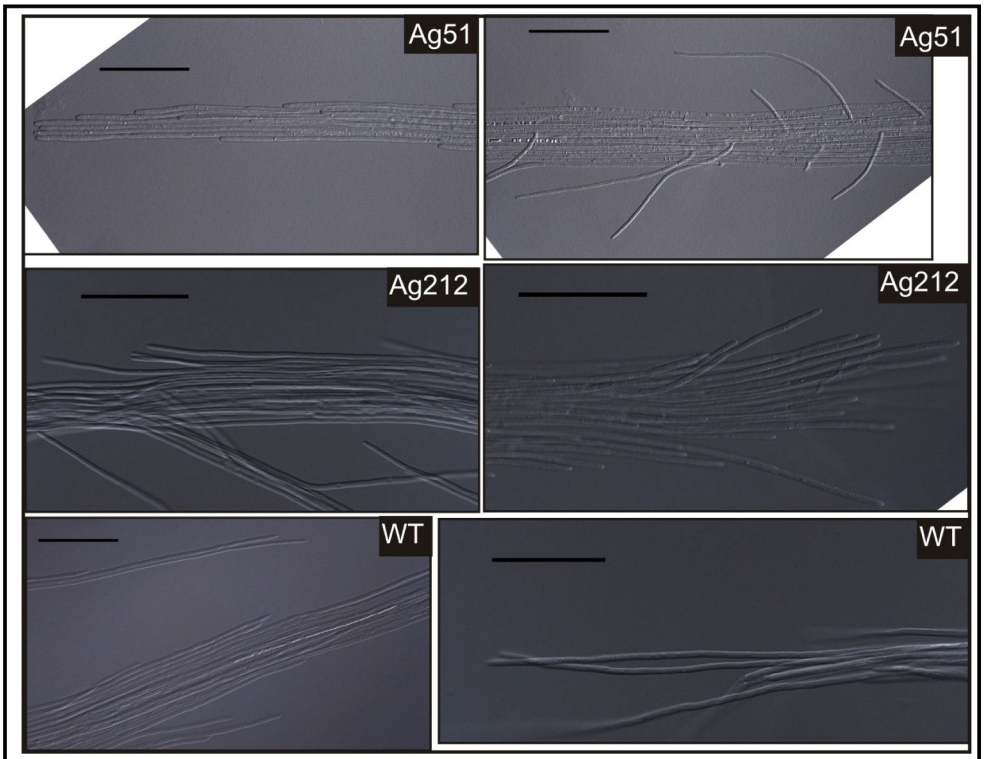

Figure 3.37. Hyphal morphology of Ag212 and Ag51
Hyphal morphology and branching pattern of six-day-old colonies grown on PD agar were examined using DIC. Bar 50 µm.

Figure 3.38. Ag51 induces a hypersensitive response in perennial ryegrass seedlings
Seedling inoculated with Ag51 compared to seedlings inoculated with Ag212 and WT. Pictures were taken 10 days after inoculation. Arrows point to the inoculation point.

Ag212 was inoculated into 91 seedlings in total in repeated screens. No infected plants were detected in these screens, suggesting that Ag212 is a colonization mutant, unable to establish infection.

3.10.Identification of insertion locus in Ag51

3.10.1. Copy number

In order to determine the number of T-DNA copies integrated in the Ag51 genome, this mutant was taken through a Southern analysis using *Sst*I, *Xho*I and *Bam*HI genomic digests. Since there are no *Bam*HI restriction sites inside the T-DNA, one band should be observed for a single-copy integration when a Southern blot of this digest is probed with pBSYT6. *Sst*I and *Xho*I cut once inside the T-DNA, so two bands should be observed for single-copy integration, for each of these digests, when probed with pBSYT6. *Sst*I genomic digest of WT was included in the analysis as a control for nonspecific binding of the probe. After probing with pBSYT6, 3 bands were observed for *Sst*I and *Xho*I digests of Ag51 with one 6 Kb band in each digest (Fig. 3.39B). This result can be explained by the presence of a head-to-tail tandem insertion of the T-DNA at a single locus (Fig. 3.39A). The *Sst*I and *Xho*I digests of such insertion will result in a 6 Kb T-DNA fragment being excised from the insertion. This result, however, does not provide any information about the number of tandem-inserted copies of T-DNA. The band observed for the *Bam*HI digest was of a very high molecular weight, confirming that there are more than two copies of T-DNA present at the site of tandem insertion.

3.10.2. Identification of LB insertion site in Ag51 by TAIL-PCR

TAIL-PCR (Section 2.6.5) was used to identify the insertion site of the T-DNA left border (LB) in Ag51. Two random primers, T1 and T4, gave the expected 'ladder pattern' of PCR products when used with the LB region primers LB3, LB4 and LB5 (Fig. 3.40A). The largest PCR products of each group, T1/LB3 and T4/LB3, were cloned into pCRII-TOPO vector and sequenced using M13F/M13R primers (Appendices 5.11 and 5.12). Sequencing of the PCR product of primers T1/LB3 revealed that the LB insertion site is located on contig 532, immediately upstream from

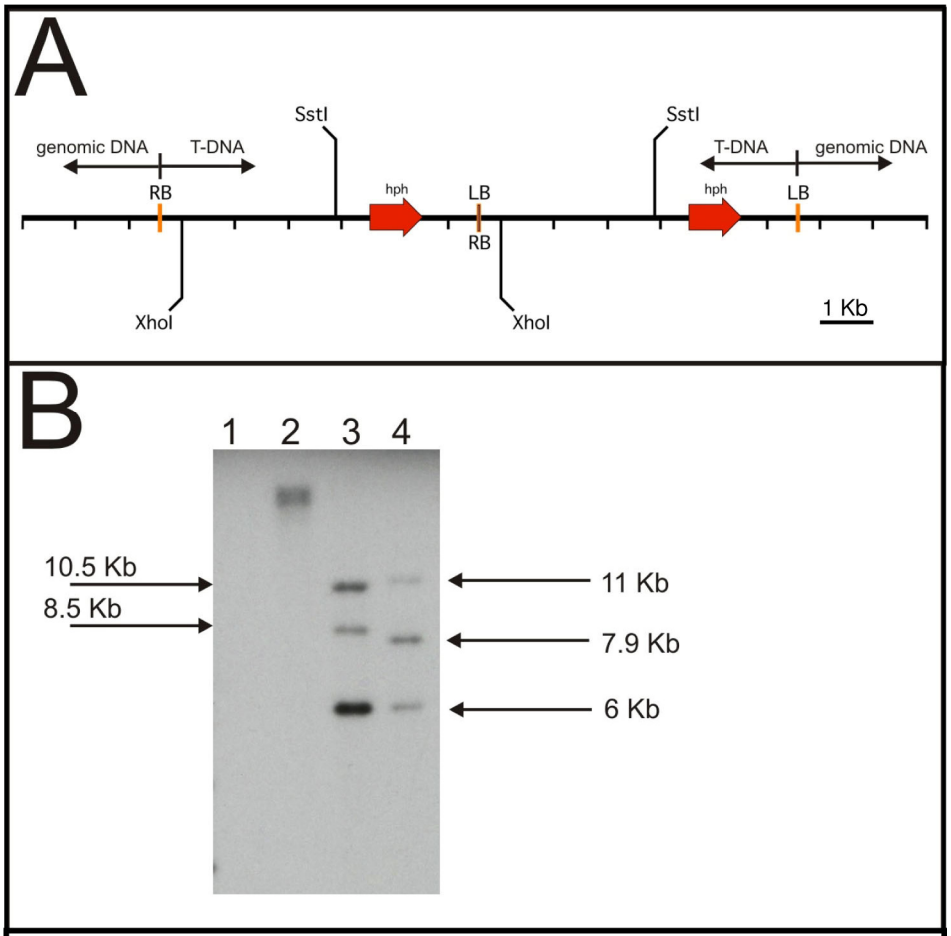

Figure 3.39. Tandem insertion of T-DNA copies in the genome of Ag51

A. Physical map showing tandem insertion of T-DNA in the genomic region. Restriction enzyme sites for *Xho*I and *Sst*I are also shown.

B. Autoradiograph of a Southern blot of WT and Ag51 genomic DNA (1 µg), probed with [^{32}P]-labeled pBSTY6. WT *Sst*I digest (*lane 1*); Ag51 *Bam*HI digest (*lane 2*); Ag51 *Sst*I digest (*lane 3*); Ag51 *Xho*I digest (*lane 4*).

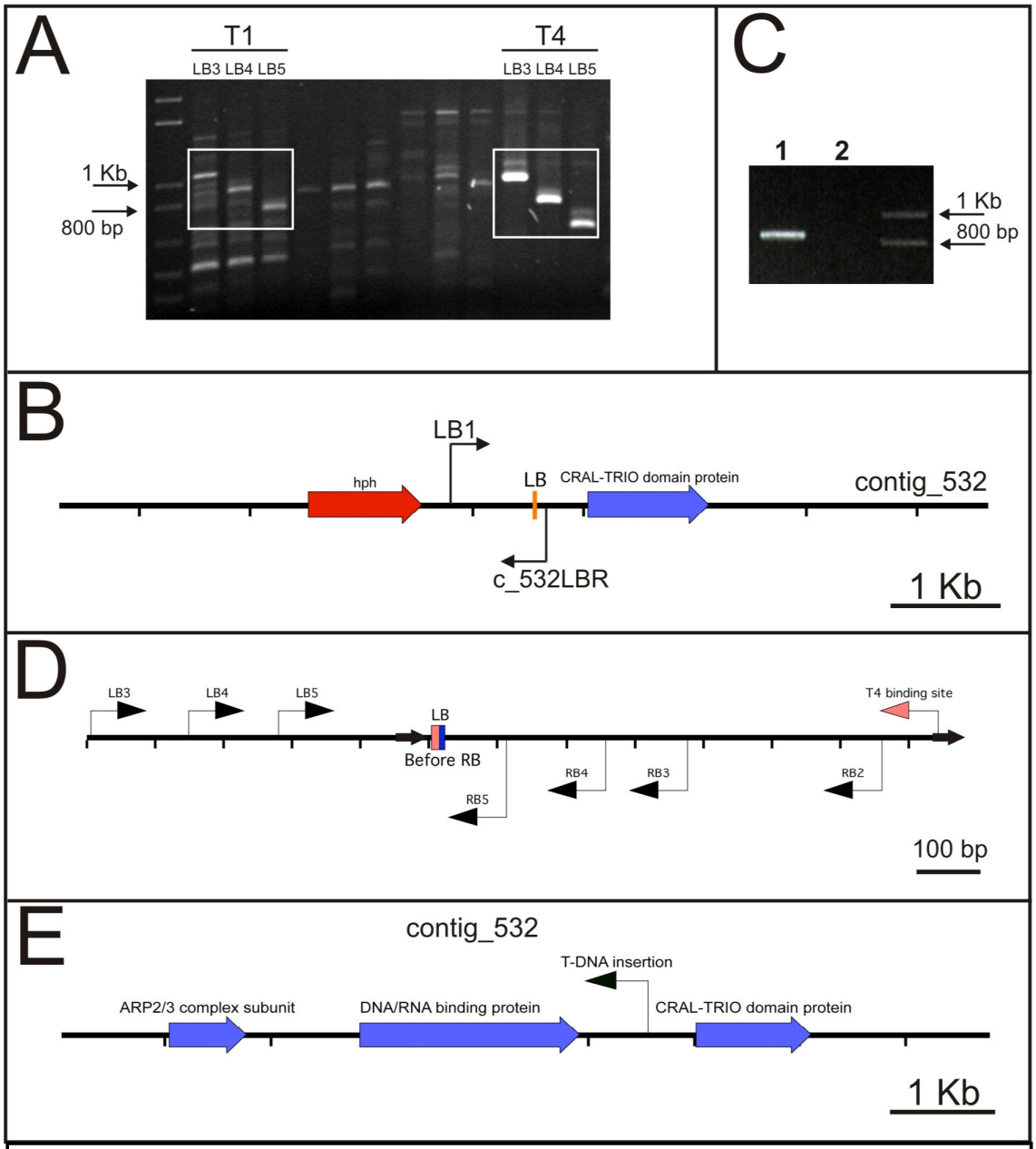

Figure 3.40. Identification of the T-DNA LB insertion site in Ag51 using TAIL-PCR
A. PCR products generated by TAIL-PCR using primer T1 with primers LB3, LB4, LB5 and primer T4 with primers LB3, LB4, LB5. Standard: 1 Kb+ ladder.
B. Physical map of the T-DNA LB insertion in the Fl1 genome, as deduced from sequence derived from T1/LB3 TAIL-PCR product. LB – left border.
C. PCR product generated with primers LB1 within T-DNA and c_532LBR designed using sequence from contig_532 (see map in **B**). Ag51 genomic DNA was used as template.
D. Physical map of TAIL-PCR product of primers T4 and LB3 obtained by sequencing. Ten base pairs region before the RB (blue) of one T-DNA copy recombined with the sequence within the LB (red) generating head-to-tail tandem insertion.
E. Wild type region of the contig_532, showing locus of the T-DNA insertion.

the gene encoding a CRAL-TRIO domain protein. PCR of Ag51 genomic DNA using primers LB1 (designed for inside T-DNA) and c_532LBR (designed for sequence of contig 532) generated a 0.9 Kb fragment confirming the insertion site (Fig. 3.40B and C). A physical map of the wild-type region of the LB insertion site is shown on the Figure 3.40E. Sequencing of the T4/LB3 product (Fig 3.40D) further confirmed that Ag51 contained a tandem T-DNA insertion. Unexpectedly, the random primer T4 bound to the sequence inside the T-DNA, in the region before the right border (RB). In the case of a head-to-tail tandem insertion, when used with primers LB3, LB4 and LB5, this primer will generate the 'ladder conformation' of PCR products, amplifying across the junction of the two T-DNA copies.

3.10.3. Attempts to locate the right border of Ag51

In order to identify the insertion locus of the T-DNA right border, TAIL-PCR was attempted using different RB specific primers. However, none of these attempts was successful. Plasmid rescue (Section 2.3.16) was also tried using *Bam*HI and *Sst*I digests. No colonies were obtained with ligated products of *Bam*HI digests and in the case of the *Sst*I digests, 46 colonies were produced but all of them contained the 6 Kb plasmid which was a circularly-permutated T-DNA that was excised from the tandem insertion. A possible reason for the lack of success in identifying the RB insertion site is the potential rearrangement that could have occurred in the tandem insertion end opposite to the identified LB. This rearrangement could have made the RB end of T-DNA insertion inaccessible for the PCR primers and could have eliminated the selection marker (Amp^R) necessary for plasmid rescue.

3.10.4. Southern blot analysis of Ag51

Since TAIL-PCR and plasmid rescue were not successful in identifying the RB insertion site in Ag51, Southern analysis was used to assess whether the T-DNA insertion caused a deletion in the Ag51 genome. *Sst*I and *Xho*I genomic digests of Ag51 were used together with the *Sst*I WT digest as a control. Two PCR products were used as probes, designed so that they hybridize to the regions immediately upstream (c_532RB1F/c_532RB1R) and downstream (CT-1F/CT-1R) from the T-DNA insertion (Fig. 3.41A). In the case of the CT-1F/CT-1R probe, bands expected to be observed in

mutant are 8.5 Kb for *Sst*I digest and 7.9 Kb for *Xho*I digest (Fig. 3.41B). The band expected for the *Sst*I digest of WT when probed with CT-1F/CT-1R is 7.4 Kb. Upon hybridization, the banding pattern observed for mutant digests showed bands expected for both mutant and WT (Fig. 3.41C). A band of 3 Kb observed in mutant *Xho*I digests corresponds to the band expected for WT *Xho*I digest. The bands of 8.5 Kb and 7.9 Kb correspond to the bands observed when the same digests were probed with pBSYT6 (Fig. 3.39B), indicating that these two bands represent the LB region of the insertion. If the region covered by the c_532RB1F/c_532RB1R probe is not deleted, the observed bands should be of a size different from WT, as this region is located immediately next to the T-DNA insertion, but expected sizes could not be predicted as the physical map of RB region is not known. If this region is deleted no signal would be expected.

Upon hybridization with the c_532RB1F/c_532RB1R probe, the banding pattern observed for digests of mutant corresponded to the bands expected for WT (Fig. 3.41D). Bands of 10.5 Kb and 11 Kb, observed when the same digests were probed with pBSYT6 (Fig. 3.39B), that correspond to the RB region, were not present.

There are three possible explanations for this unexpected result. Firstly, the genomic region of the T-DNA insertion in Ag51 could be duplicated in Fl1. Secondly, Ag51 could be a heterokaryon. Thirdly, the T-DNA insertion itself could have caused a chromosomal rearrangement of this region in Ag51. Given the complexity of this insertion and the inability to identify the right border, work on this mutant was discontinued.

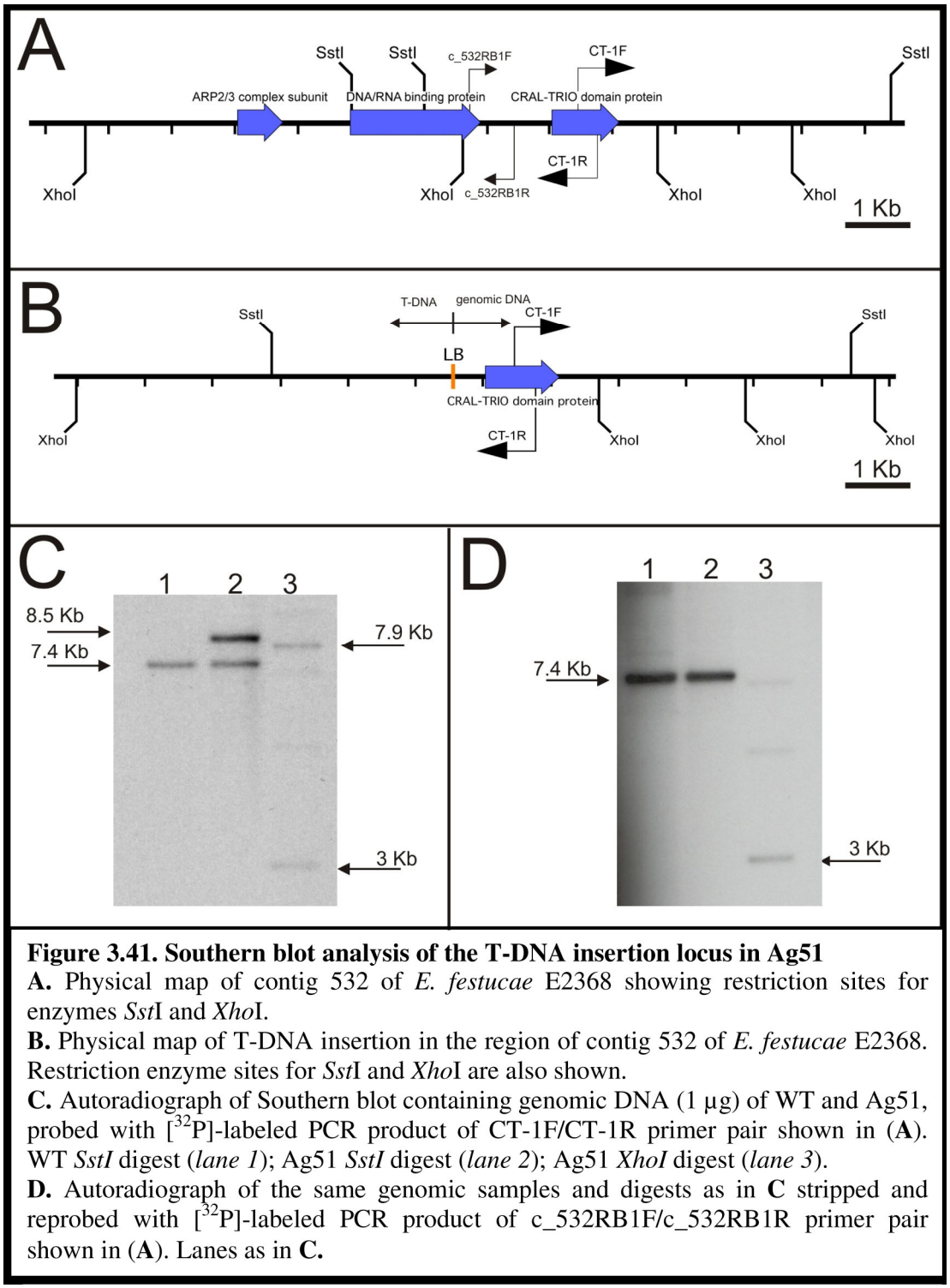

Figure 3.41. Southern blot analysis of the T-DNA insertion locus in Ag51
A. Physical map of contig 532 of *E. festucae* E2368 showing restriction sites for enzymes *Sst*I and *Xho*I.
B. Physical map of T-DNA insertion in the region of contig 532 of *E. festucae* E2368. Restriction enzyme sites for *Sst*I and *Xho*I are also shown.
C. Autoradiograph of Southern blot containing genomic DNA (1 µg) of WT and Ag51, probed with [^{32}P]-labeled PCR product of CT-1F/CT-1R primer pair shown in (**A**). WT *SstI* digest (*lane 1*); Ag51 *SstI* digest (*lane 2*); Ag51 *XhoI* digest (*lane 3*).
D. Autoradiograph of the same genomic samples and digests as in **C** stripped and reprobed with [^{32}P]-labeled PCR product of c_532RB1F/c_532RB1R primer pair shown in (**A**). Lanes as in **C.**

3.11.Identification of insertion locus in Ag212

3.11.1. Copy number

The number of T-DNA copies present in the genome of Ag212 was examined using Southern blot analysis. *Sst*I, *Xho*I and *Bam*HI genomic DNA digests of mutant and *Sst*I genomic digest of WT were probed with the T-DNA plasmid pBSYT6. One band observed for the *Bam*HI digest and two bands observed for the *Sst*I and *Xho*I digests of Ag212 suggests that only one copy of the T-DNA is inserted into the Ag212 genome (Fig 3.42).

3.11.2. Identification of LB and RB using plasmid rescue

Insertion sites of the T-DNA left and right borders in Ag212 were identified using the plasmid rescue technique. In order to identify the LB insertion site, genomic DNA of Ag212 was digested with *Xho*I, ligated and transformed into *E. coli*. One *E. coli* colony, carrying an 8.5 Kb plasmid (pMMI10), was obtained from the transformation (Fig. 3.43A). The size of pMMI10 corresponds to the size of the *Xho*I band that hybridized with pBSYT6 (Fig. 3.42). Sequencing of pMMI10 revealed that the T-DNA LB was inserted into the 3' end of a gene arbitrary named 1006-3, located on contig 1006 (Fig. 3.43D) of the E2368 genome (Appendix 5.13). PCR amplification using primers LB5/1006gR1 confirmed that T-DNA is linked to gene 1006-3 (Fig. 3.43B and C). Sequencing analysis revealed that a short sequence of the pBSYT6 vector itself, adjacent to the LB, was also transferred and inserted together with the T-DNA. The T-DNA RB insertion site was identified by plasmid rescue of an *Sst*I ligated product. Eight Amp^R *E. coli* colonies were obtained, each of them carrying an 11 Kb plasmid (Fig. 3.44A). The size of the plasmid corresponded with the band observed for the Ag212 genomic DNA *SstI* digest (Fig 3.42). Sequencing of the plasmid pMMI11 (Appendix 5.14), isolated from one of the colonies, placed the insertion site of the RB on contig 849, which was confirmed by PCR (Fig. 3.44B and C). T-DNA together with the short sequence of pBSYT6 adjacent to the RB was inserted close to the end of the contig, downstream of a gene named 849-1 (Fig. 3.44D).

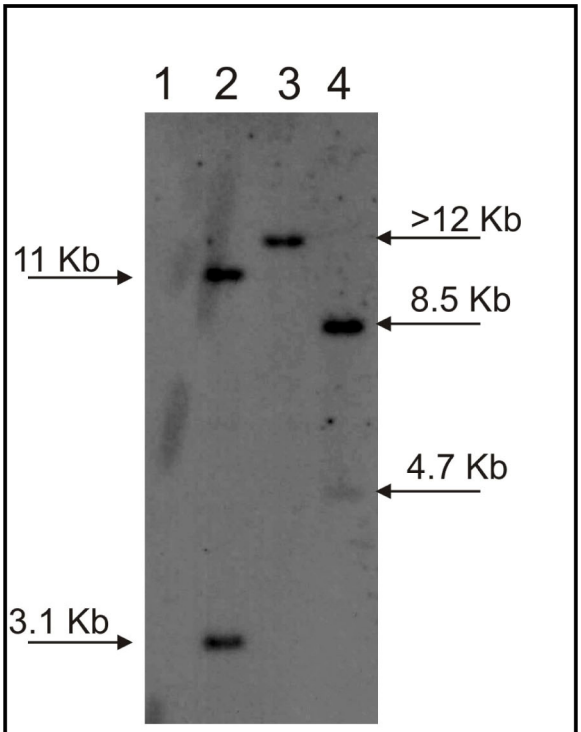

Figure 3.42. Analysis of T-DNA copy number in Ag212
Autoradiograph of Southern blot containing genomic DNA of WT and Ag212, probed with [^{32}P]-dCTP-labeled pBSYT6. WT *SstI* digest (*lane 1*); Ag212 *SstI* digest (*lane 2*); Ag212 *BamHI* digest (*lane 3*); Ag212 *XhoI* digest (*lane 4*).

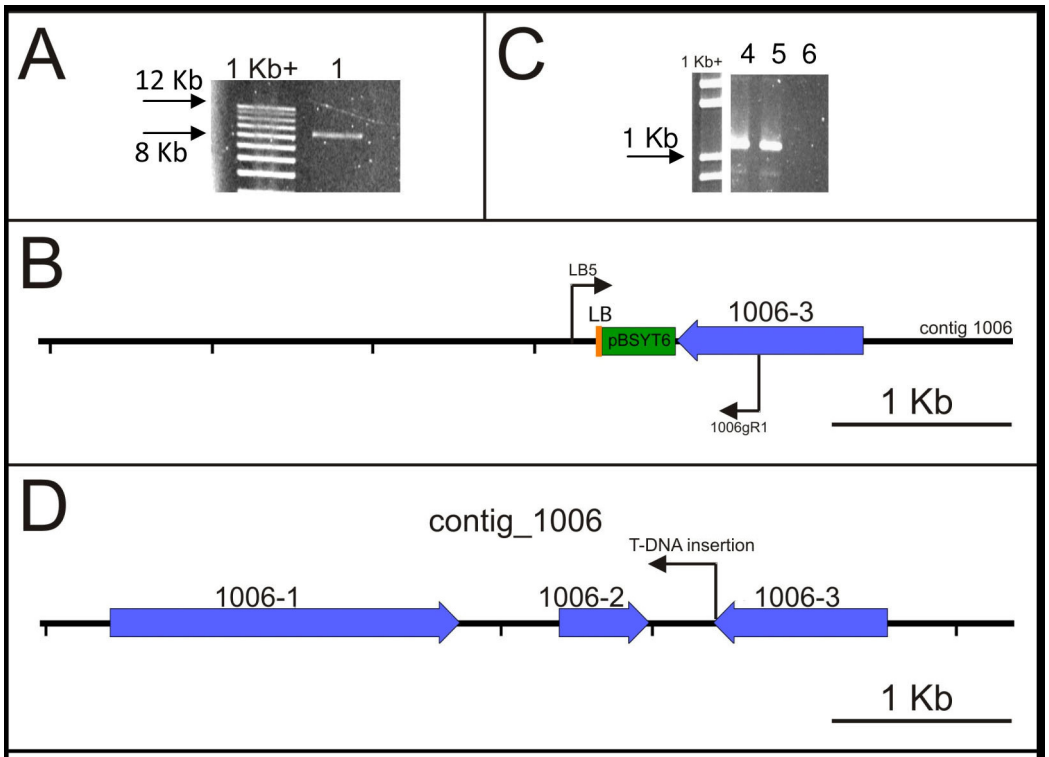

Figure 3.43. Identification of the T-DNA LB insertion site in Ag212 using plasmid rescue

A. *Xho*I digest of 8.5 Kb plasmid pMMI10, obtained by plasmid rescue.

B. Physical map of the T-DNA LB insertion site in Ag212 genome, deduced from the sequence of pMMI10. The T-DNA is inserted within gene 1006-3 on contig_1006. A piece of pBSYT6 (green) after the LB was also inserted.

C. PCR product of primers LB5 (designed for T-DNA) and 1006gR1 (designed for contig_1006), as shown in (**B**). PCR product (duplicate) (*lane 4 and 5*); negative control (*lane 6*).

D. Physical map of the wild type region of contig_1006. Arrow shows the place of T-DNA insertion.

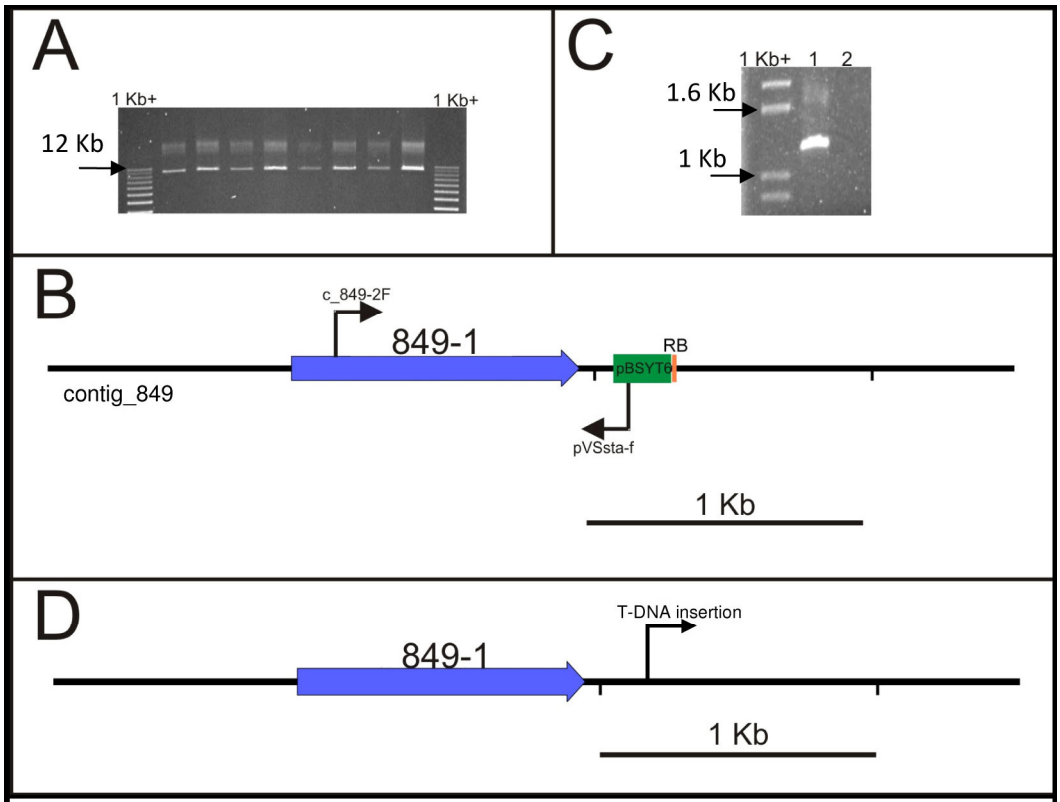

Figure 3.44. Identification of the RB locus of T-DNA in Ag212 using plasmid rescue

A. *Sst*I digests of plasmids isolated from eight *E. coli* colonies transformed with ligated products of *Sst*I digestion.

B. Physical map of the T-DNA RB insertion site in Ag212 genome, deduced from sequence of the pMMI11, isolated from one of the colonies. The T-DNA is inserted on contig_849. A piece of pBSYT6 after the RB was also inserted.

C. PCR product of primers pVSsta-f (designed for pBSYT6) and c_849-2F (designed for contig_849), as shown in (**B**), using Ag212 genomic DNA as a template. pVSsta-f/ c_849-2F PCR product (*lane 1*); negative control (*lane 2*).

D. Physical map of the wild type region of contig 849. Arrow shows the place of T-DNA insertion.

This result suggested that the two genes, named 1006-1 and 1006-2 and shown in Figure 3.43D are deleted in Ag212.

3.11.3. Identification of the size of the deletion in Ag212

The insertion sites of the T-DNA left and right borders of Ag212 were shown to be on two different contigs according to the *E. festucae* E2368 genome map. At least two genes appeared to be deleted according to the genome map. This suggested that Ag212 contains a deletion of unknown size, as a result of the T-DNA insertion.

3.11.3.1. *Synteny analysis*

In order to determine the size of the deletion and identity of missing genes in Ag212, synteny analysis was carried out with the corresponding regions of *F. graminearum*. Homologues of *E. festucae* genes 849-1 (Fig. 3.44) and 1006-1 (Fig. 3.43) were identified using BLASTP. This analysis identified genes FGSG_09277.3 and FGSG_09286.3 as homologues of 849-1 and 1006-1, respectively, suggesting that the two *E. festucae* genes might be linked, as found for *F. graminearum*. *E. festucae* homologues of genes located between FGSG_09277.3 and FGSG_09286.3 were identified using BLASTP, revealing that these genes are all located on the *E. festucae* contig 1085, genes 1085-1 to 1085-6, suggesting that these genes are deleted in Ag212. Results of the synteny analysis are presented in the Table 3.1 and Figure 3.45. Since the *F. graminearum* homologue of gene 1006-2 was not located next to the homologue of 1006-1 and *E. festucae* gene 1006-3 did not have a homologue in *F. graminearum*, PCR was used to confirm the linkage and predicted order of these genes in *E. festucae* (Fig. 3.46)

Table 3.1 Synteny between *F. graminearum* and *E. festucae* regions affected in Ag212.

[a]as in the Fungal Genome Initiative database

***E. festuacae* gene name**	***F. graminearum* locus / gene name[a]**
849-1	FGSG_09277.3 / conserved hypothetical protein
1085-6	FGSG_09280.3 / fructose-1,6-bisphosphatase
1085-5	FGSG_09281.3 / hypothetical protein similar to peroxin-11
1085-4	FGSG_13543.3 / hypothetical protein similar to intermediate filament protein Mdm1
1085-3	FGSG_13544.3 / tRNA
1085-2	FGSG_09284.3 / homoserine dehydrogenase
1085-1	FGSG_09285.3 / conserved hypothetical protein
1006-1	FGSG_09286.3 / conserved hypothetical protein
1006-2	FGSG_09302.3 /conserved hypothetical protein
1006-3	no hits

http://www.broadinstitute.org/annotation/genome/fusarium_group/MultiHome.html

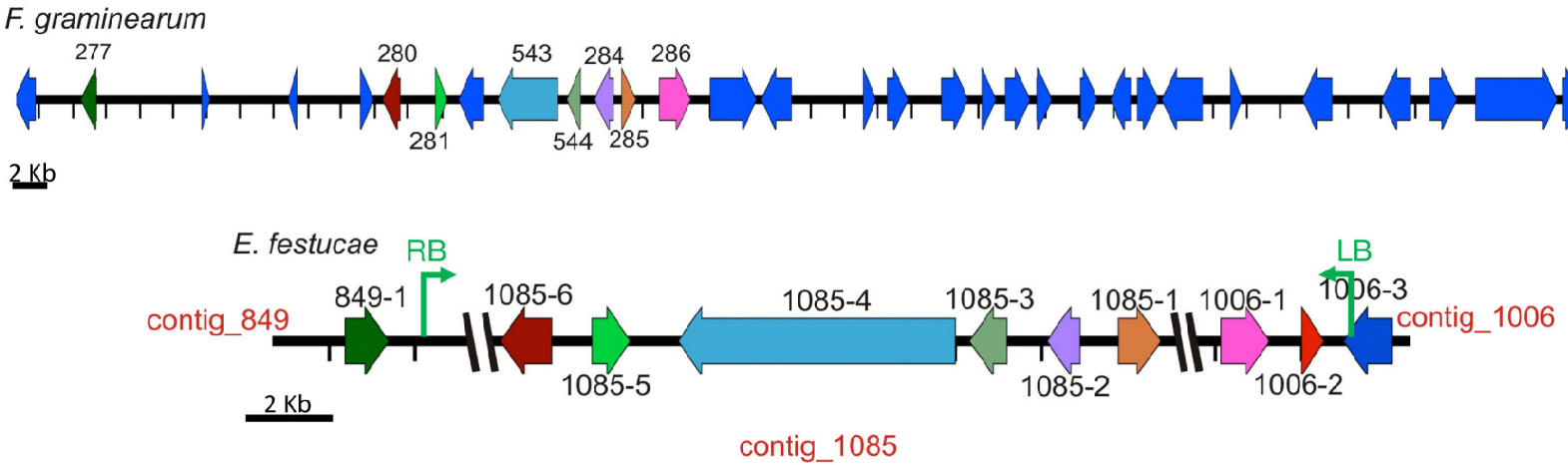

Figure 3.45. Synteny between regions of *E. festucae* and *F. graminearum*.
Physical maps of the *F. graminearum* region of the Supercontig 6, chromosome 4, and *E. festucae* contigs 849, 1085 and 1006. *F. graminearum* genes: FGSG_09277.3 (277), FGSG_09280.3 (280), FGSG_09281.3 (281), FGSG_13543.3 (543), FGSG_13544.3 (544), FGSG_09284.3 (284), FGSG_09285.3 (285), FGSG_09286.3 (286) and FGSG_09302.3 (302). RB – right border; LB - left border;

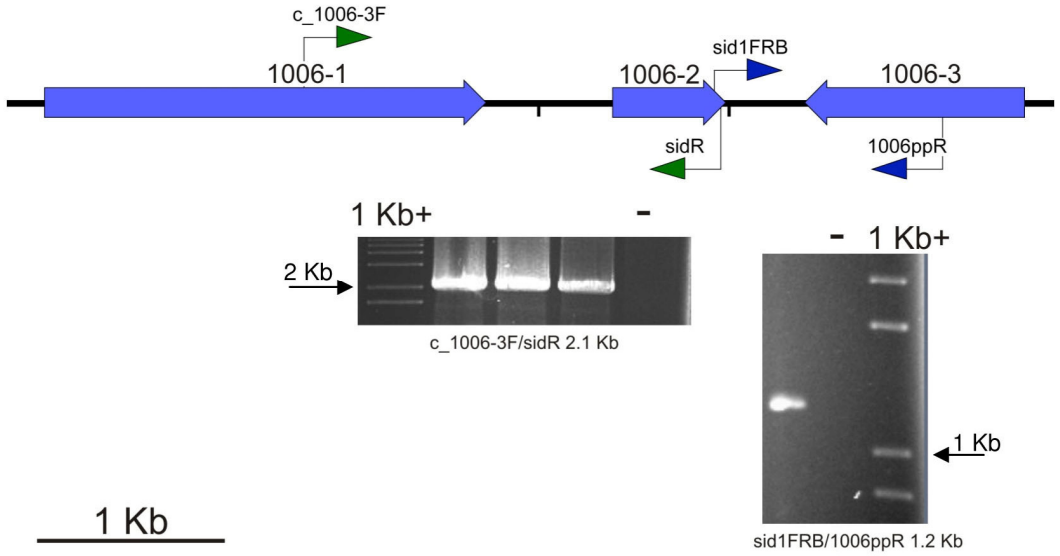

Figure 3.46. Confirmation of predicted positions of genes 1006-1, 1006-2 and 1006-3 by PCR

Physical map of genes on contig 1006, as predicted by the genome assembly of *E. festucae* E2368. PCR products of primer pairs c_1006-3F/sidR and sid1FRB/1006ppR. Primer pair and expected product size given under the picture of the gel.

- - negative control.

3.11.3.2. *Screening of the cosmid library and Southern analysis of deletion in Ag212*

Southern blot analysis was used to further investigate the deletion in Ag212. Genomic digests of WT and Ag212 were hybridized using five different probes located on contigs 849, 1085 and 1006, and representative digests are shown in Figure 3.47. Autoradiographs of Southern blots are given in the Appendix 5.7. Absence of bands in Ag212 digests for probes 2, 3 and 4 suggests deletion of the corresponding regions. These results confirm linkage of contigs 849, 1085 and 1006. The *E. festucae* Fl1 cosmid library was then screened using probes specific for genes located on contigs 1006 and 1085. The library was first screened using a PCR product specific for gene 1006-3, but this screen identified two false positive clones, 8B1 and 46D1, as shown by Southern analysis, Appendix 5.8. Subsequent screening of the cosmid library with the PCR product specific for gene 1085-6 identified cosmids 12G8 and 17G5 as positive clones. In order to investigate which genes are present on these clones, DNA digests of the cosmids were Southern blotted and probed using the same probes as in the genomic DNA analysis (Fig. 3.48). This analysis showed that cosmid 12G8 contains regions of contigs 849 and 1085 while cosmid 17G5 contain regions of all three contigs. Autoradiographs of Southern blots are presented in Appendix 5.8.

Given that cosmid clone 17G5 included the entire region of the deletion in Ag212, this cosmid was sequenced to obtain the full sequence of the deleted region (Section 2.3.15). Sequence analysis of cosmid 17G5 (Appendix 5.15) further confirmed linkage of contigs 849, 1085 and 1006 and identified two more genes deleted in Ag212, named 1085-7 and 1085-8 (Fig. 3.49A). These results, together with the PCR confirmation of the linkage of genes on contig 1006, show that Ag212 has a 25.2 Kb deletion, which includes 10 genes, presented in Table 3.2 (Fig. 3.49B).

3.12. Complementation of Ag212 in culture and *in planta* phenotype

In order to confirm that the Ag212 deletion is responsible for the culture and symbiotic phenotypes of this mutant, a complementation test was carried out using cosmid clones 17G5 and 12G8. Each cosmid was co-transformed into Ag212 together with the

Table 3.2 Genes deleted in *E. festucae* mutant Ag212

E. festucae gene	Identified conserved domain[a]	*F. graminearum* homologue gene name[b]
1085-1	No hits	conserved hypothetical protein
1085-2	Homoserine dehydrogenase, catalytic, Aspartate/homoserine dehydrogenase, NAD-binding	homoserine dehydrogenase
1085-3	tRNA (guanine-N-7) methyltransferase	tRNA
1085-4	Regulator of G protein signaling, Phox-like, Sorting nexin, C-terminal, RNA recognition motif, RNP-1	hypothetical protein similar to intermediate filament protein Mdm1
1085-5	Peroxisomal biogenesis factor 11	hypothetical protein similar to peroxin-11
1085-6	Fructose-1,6-bisphosphatase	fructose-1,6-bisphosphatase
1085-7	3-oxo-5-alpha-steroid 4-dehydrogenase, C-terminal	No hit
1085-8	NADH:ubiquinone oxidoreductase intermediate-associated protein 30	conserved hypothetical protein
1006-1	Basic-leucine zipper (bZIP) transcription factor	conserved hypothetical protein
1006-2	signal-peptide	conserved hypothetical protein

[a]domains identified using InterProScan software
[b]as in the Fungal Genome Initiative database http://www.broadinstitute.org/annotation/genome/fusarium_group/MultiHome.html

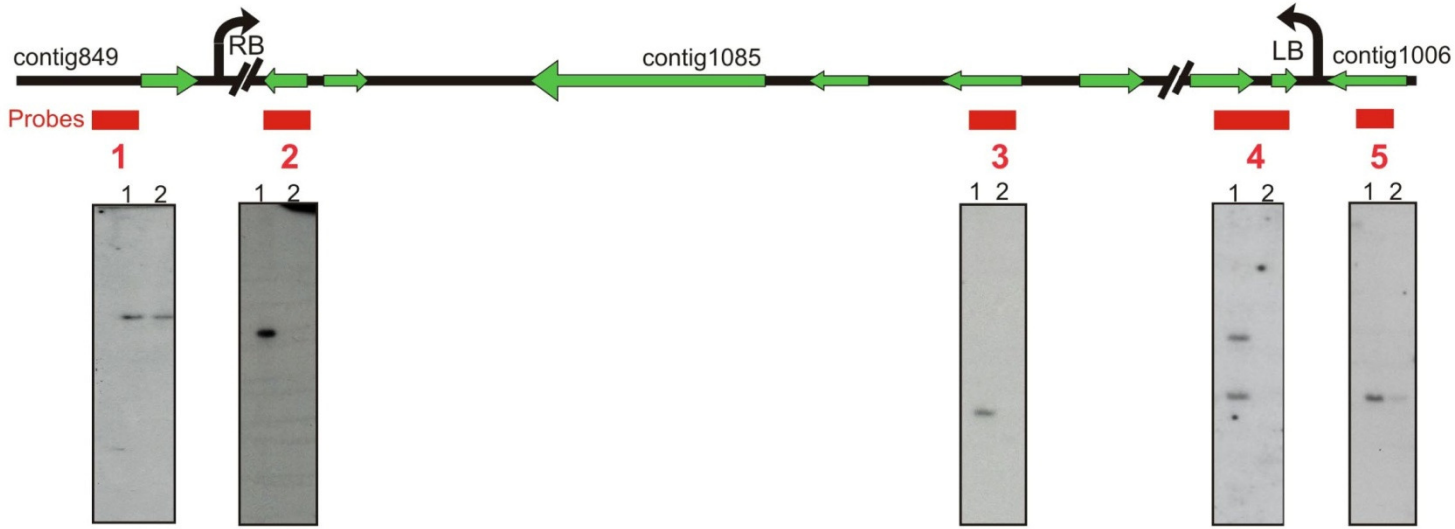

Figure 3.47. Southern blot analysis of the deletion in Ag212
Representative digests of genomic DNA (Lanes: WT (*lane 1*); Ag212 (*lane 2*)) probed with [^{32}P]-dCTP-labeled PCR products from the different regions of contig 849, contig 1085 and contig 1006. Primers used for probe generation: c_849-1F/R (Probe 1); f-1,6-bpF/R (Probe 2); c_1085-2F/R (Probe 3); c_1006-3F/sidR (Probe 4); 1006ppF/R (Probe 5). Autoradiographs of Southern blots are shown in Appendix 5.7. RB – right border; LB – left border.

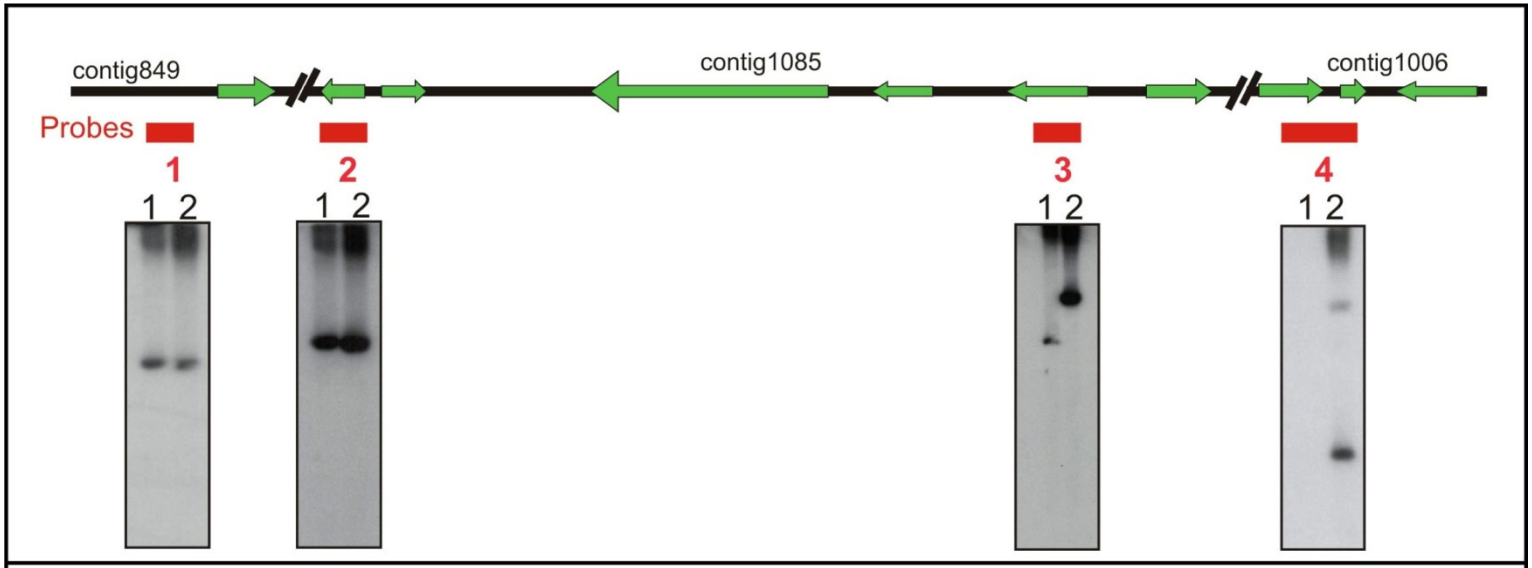

Figure 3.48. Southern blot analysis of genes present on *E. festucae* cosmids 12G8 and 17G5
Representative digests of cosmid DNA (Lanes: 12G8 (*lane 1*); 17G5 (*lane 2*)) probed with [^{32}P]-dCTP-labeled PCR products from the different regions of contig 849, contig 1085 and contig 1006. Primers used for probe generation: c_849-1F/R (Probe 1); f-1,6-bpF/R (Probe 2); c_1085-2F/R (Probe 3); c_1006-3F/sidR (Probe 4); 1006ppF/R (Probe 5). Autoradiographs of Southern blots are shown in the Appendix 5.8.

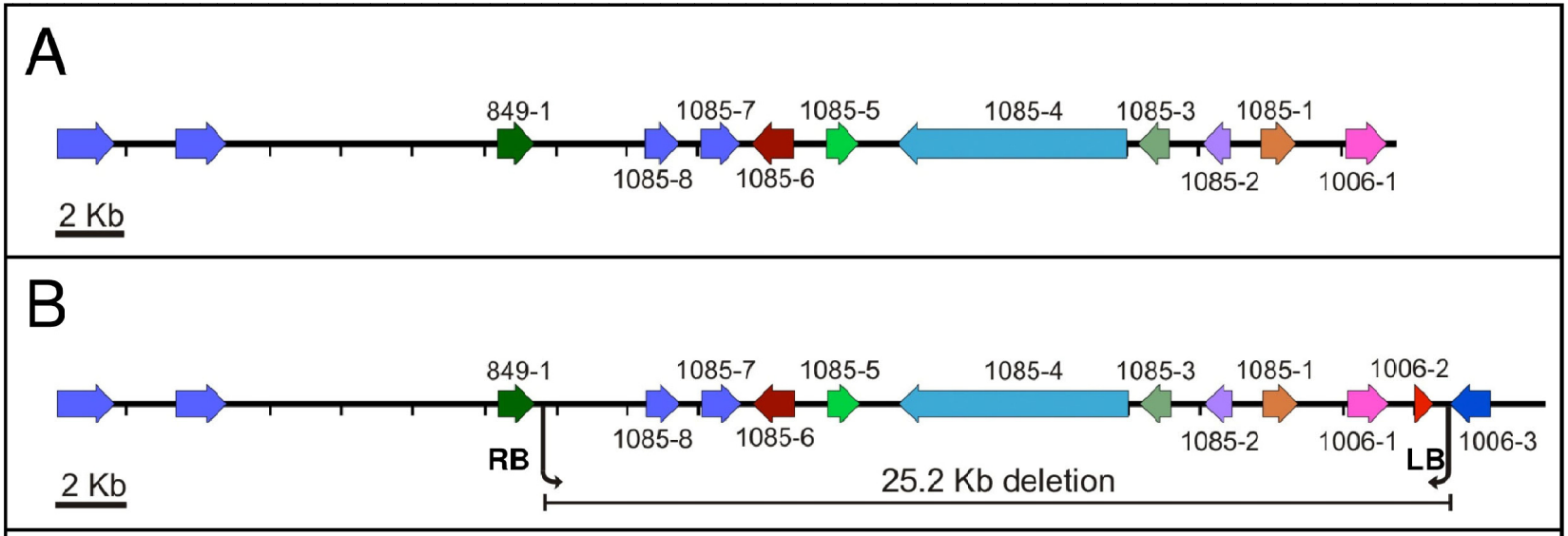

Figure 3.49. Map of deletion locus in Ag212
A. Gene map of cosmid 17G5 as derived from Illumina sequencing.
B. Physical map of WT region showing region deleted in Ag212. The deletion is 25.2 Kb long and includes 10 genes. RB – T-DNA right border; LB – T-DNA left border.

geneticin resistance vector pII99. Gen^R transformants were taken through three rounds of subculturing on media containing geneticin and 3 transformants of each cosmid (12-1, 12-2, 12-7, 17-1, 17-4 and 17-11) were further tested. All 6 transformants had a WT growth phenotype when grown on PD agar, at 22°C, confirming complementation with both cosmids (Fig. 3.50A). This result revealed that genes 1006-1 and 1006-2, absent from the cosmid 12G8, are not required to restore the growth phenotype. PCR analysis of cosmid genes present in each transformant showed that transformants 12-1, 12-2, 12-7, 17-4 and 17-11 contain all genes from 1085-1 to 1085-8. However, transformant 17-1 contained only genes 1085-3, 1085-4 and 1085-5, suggesting loss of the other genes upon integration of this cosmid into the genome (Fig. 3.50B). This result also suggests that the three genes present in 17-1 are sufficient for complementation of the culture growth phenotype. All six transformants were inoculated into perennial ryegrass seedlings (20 plants of each) in order to check for restoration of the plant phenotype. Plants were screened for infection 10 weeks after planting. Infected plants were detected for 12-1 (12 infected/20 inoculated), 12-2 (12/20), 12-7 (10/20), 17-4 (10/20) and 17-11 (11/20), with an infection rate similar to WT (13/20). However, no infected plants were detected for 17-1, suggesting that genes 1085-3, 1085-4 and 1085-5 are not sufficient for complementation of the symbiotic phenotype of Ag212. Plants infected with the other 5 transformants had a phenotype similar to those infected with WT and no difference was observed in the hyphal morphology or branching pattern of the endophyte strains within the host (Fig. 3.51).

3.13. Detailed analysis of *Ag212 in planta* phenotype

It has been proposed that during the colonization process, hyphae of *E. festucae* grow inside the meristematic zone of the seedlings in an unrestricted manner (Christensen *et al*., 2008). However, once the hyphae start colonizing the leaf blade, they switch to a restricted growth form in the intercellular spaces, and seldom branch. In the case of Ag212, according to the former hypothesis, there are two potential stages where the colonization breaks down: colonization of the meristem and colonization of the leaves. In order to determine whether Ag212 is able to colonize the plant meristem, strains expressing GFP were generated by transforming Ag212 protoplasts with the GFP expressing vector pPN83 (no selectable marker) and pII99 (Gen^R). One transformant, 212GFP, that expressed GFP and had the same culture phenotype as Ag212,

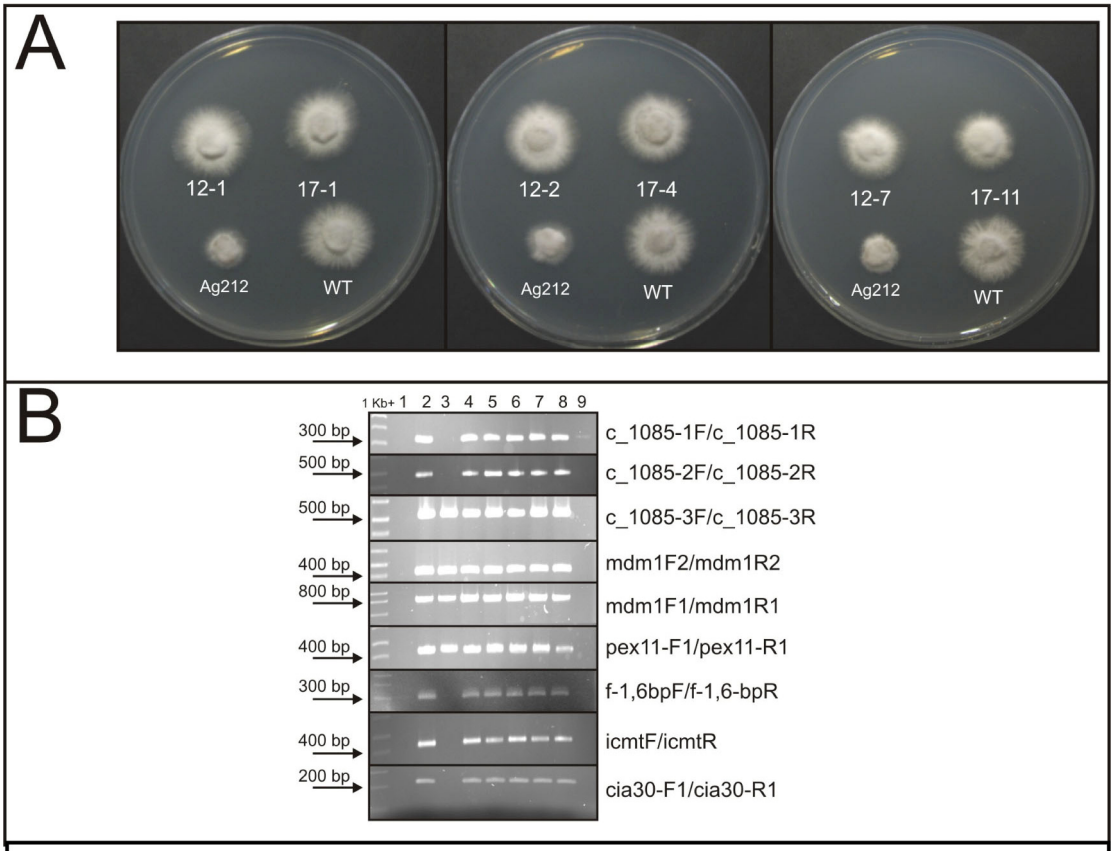

Figure 3.50. Complementation of culture phenotype of Ag212 using cosmids 12G8 and 17G5

A. Three independent transformants carrying cosmid 12G8 (12-1, 12-2 and 12-7) and three independent transformants carrying cosmid 17G5 (17-1, 17-4 and 17-11) grown on PD agar at 22°C, compared to WT and Ag212.

B. PCR analysis of genes present in complementation transformants. Lanes: Ag212 (*lane 1*); 12-1 (*lane 2*); 17-1 (*lane 3*); 12-2 (*lane 4*); 17-4 (*lane 5*); 12-7 (*lane 6*); 17-11 (*lane 7*); WT (*lane 8*); negative control (*lane 9*). PCR was done on genomic DNA using primers specific for genes deleted in Ag212: 1085-1 (primers c_1085-1F/c_1085-1R); 1085-2 (primers c_1085-2F/c_1085-2R); 1085-3 (primers c_1085-3F/c_1085-3R); 1085-4 (primers mdm1F2/mdm1R2); 1085-4 (primers mdm1F2/mdm1R2); 1085-5 (primers pex11-F1/pex11-R1); 1085-6 (primers f-1,6bpF/f-1,6-bpR); 1085-7 (primers icmtF/icmtR); 1085-8 (primers cia30-F1/cia30-R1). Primer pair indicated next to the gel picture.

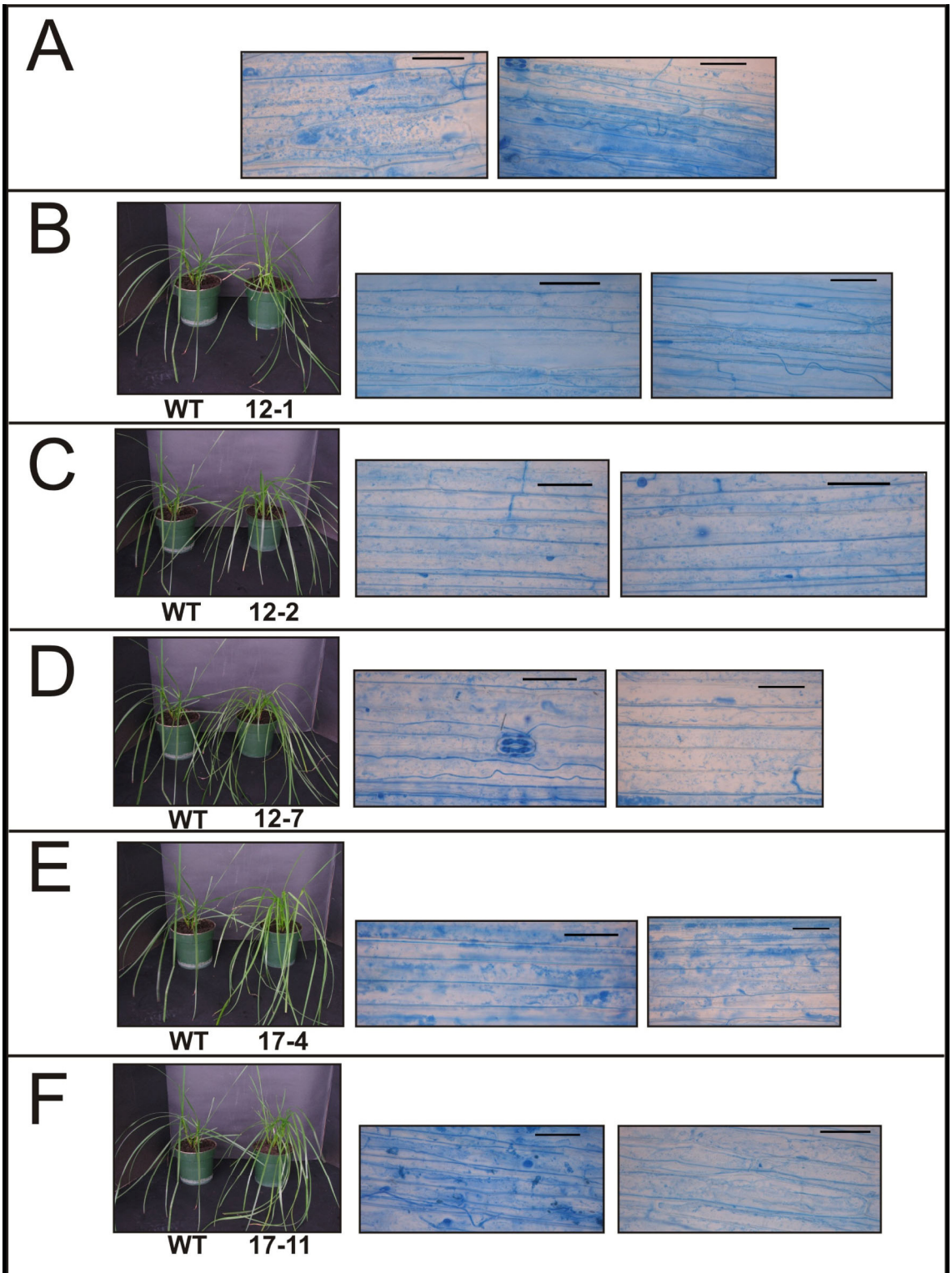

Figure 3.51. Complementation of Ag212 plant phenotype with cosmids 12G8 and 17G5
A. Micrographs of aniline-blue stained pseudostems of wildtype-infected plants.
B to **F.** Plants infected with the complementation transformants (compared to WT) and the aniline blue staining of transformant-infected plants. Transformants: **B.** 12-1; **C.** 12-2; **D.** 12-7; **E.** 17-4; **F.** 17-11; Bar: 50 µm.

was inoculated into perennial ryegrass seedlings. A GFP-expressing WT strain (WG11) was inoculated as a control.

Sections were prepared by cutting seedlings longitudinally through the meristematic zone. Examination of seedlings 2 weeks post inoculation (pi) (Fig. 3.52A) and 5 weeks pi (Fig. 3.52B) using confocal microscopy showed that the mutant is unable to colonize the plant meristem and thereby grow into the leaves. In two weeks pi seedlings, mutant hyphae were present on the surface of the plant or at the site of inoculation. However, 5 weeks pi, hyphae could not be seen in plants inoculated with the mutant, suggesting that Ag212 cannot survive for long either inside or outside the plant.

In order to more closely investigate colonization of the host, ~1 mm thick transverse sections of seedlings inoculated with WT and mutant were prepared 2 weeks pi by cutting through the inoculation point, and examined using light and confocal microscopy. These experiments revealed that hyphae of both mutant and WT proliferate inside the plant forming a hyphal matrix that fills the inoculation cut (Figs. 3.53A, B, D, E and 3.54B and C) (Originals of confocal images given in Appendix 5.16). This matrix was not observed with WT samples after infection of the host extracellular spaces had been widely established in the form of a hyphal network (Figs. 3.53F and 3.54D, E and F). However, the remains of the hyphal matrix were visible on the surface of some such samples (Fig. 3.53F). Furthermore, it was noticed that both mutant and WT occasionally colonize host cells located around the inoculation cut (Figs. 3.53A and 3.54C and F). One possible reason for this is damage of the plant cells by the inoculation cut which could create an entry point for the hyphae. Mutant hyphae were also observed in the aerial spaces between the young leaf and the meristem (Fig. 3.53C) and on the surface of the seedlings (Fig. 3.54A), but were never observed in extracellular spaces, between host cells, forming the hyphal network characteristic of WT.

Results of light and confocal microscopy were further confirmed using transmission electron microscopy (TEM). WT samples contained individual hyphae between the host cells (Figs. 3.55A, E and F) as well as remains of the hyphal matrix on the leaf surface (Fig. 3.55B). TEM demonstrated close contact of the hyphal matrix and the surrounding plant cells (Fig. 3.55D). Although the WT samples that retained the hyphal matrix had a

low rate of infection, individual hyphae were observed between the plant cells surrounding the site of the inoculation cut (Fig. 3.55F). There were no obvious differences in morphology of the hyphae in the hyphal matrix for WT (Fig. 3.55C) and mutant (Fig. 3.55G). Close observation of colonization of host cells by mutant hyphae (Figs. 3.55H, I and J) revealed deformations of the plant cell wall of colonized cells. As for WT, mutant hyphae were found in close contact with the leaf surface (Fig. 3.55K).

These results suggest that, although mutant colonizes site of the inoculation cut as well as WT, it is unable to establish a specific hyphae-plant cell interaction that leads to the colonization of the meristematic zone and systemic infection.

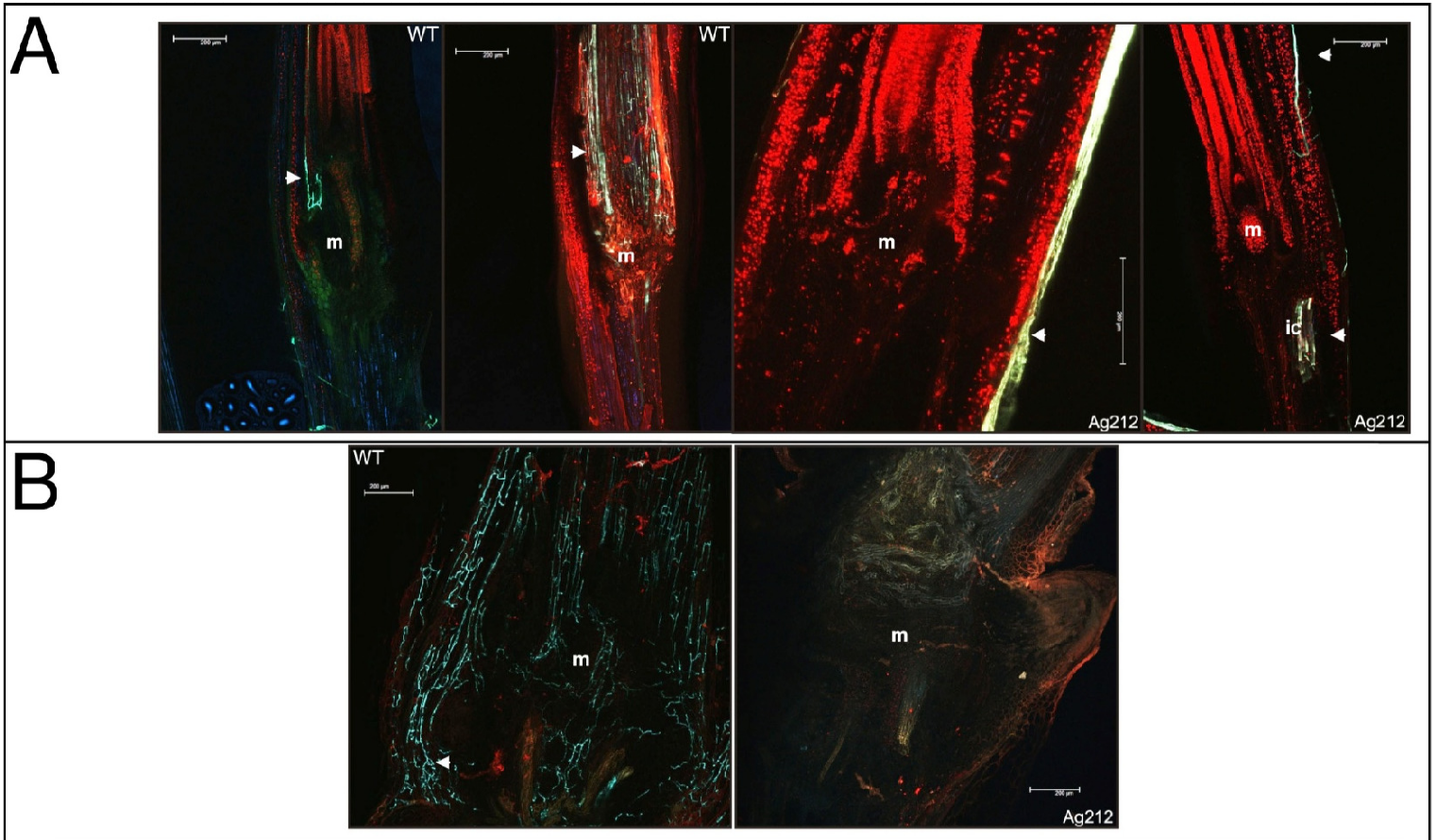

Figure 3.52. Colonization of host plant by WT and Ag212 – longitudinal sections
Confocal microscopy images of seedlings 2 weeks (**A**) and 5 weeks post inoculation (**B**) inoculated with WT or Ag212. Longitudinal sections, cut through the meristematic zone (**m**). Arrows point to hyphae. **ic** – inoculation cut. Bar: 200 µm.

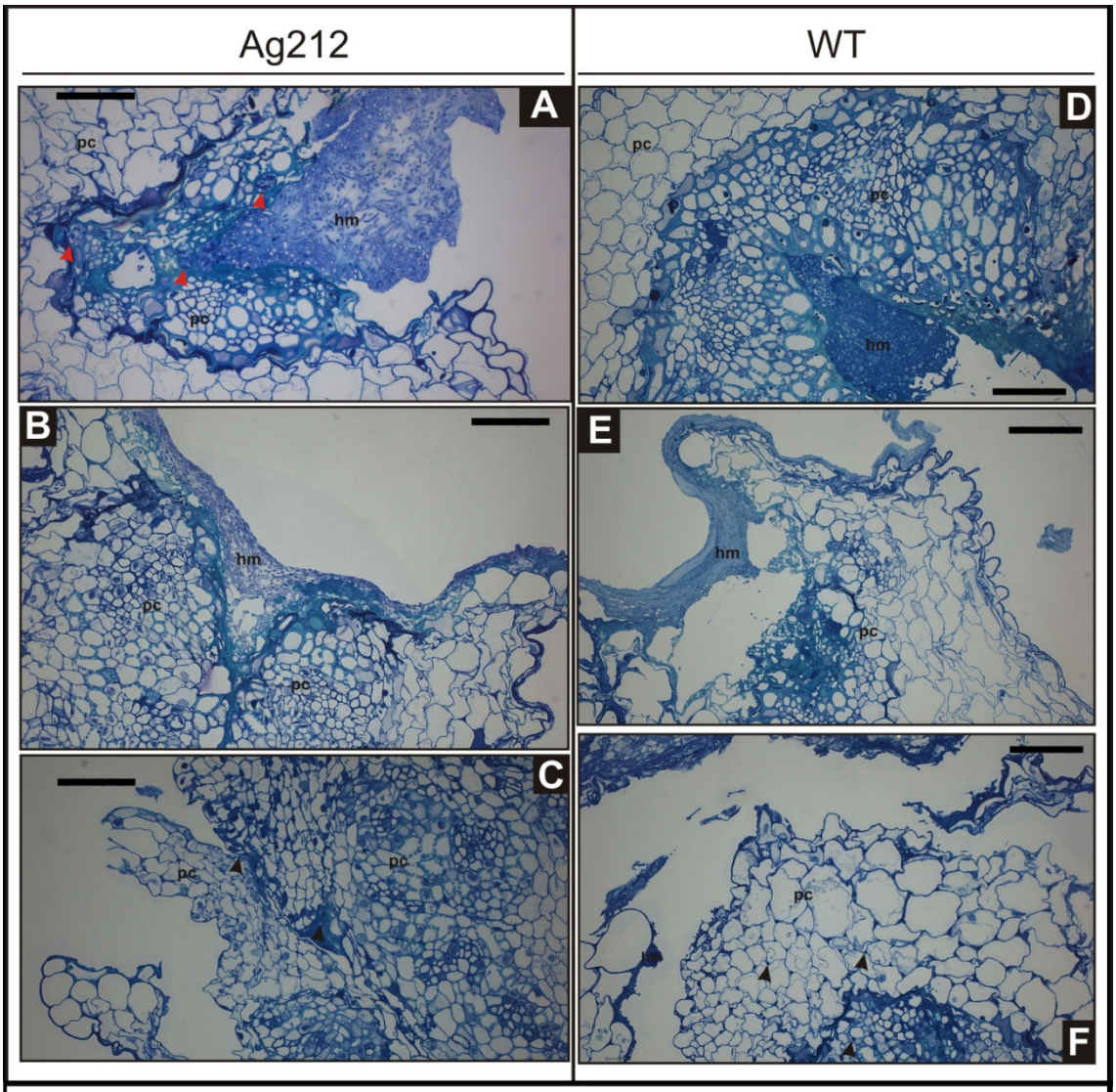

Figure 3.53. Colonization of host plant by WT and Ag212: light micrographs of transverse sections

Light micrographs of transverse sections through the inoculation point of seedlings inoculated with WT or Ag212, two weeks pi. **A, B, D** and **E.** Sites of inoculation filled with hyphae to form hyphal matrix (**hm**). Red arrows point to the host cells colonized by mutant hyphae. **C.** Arrows pointing to mutant hyphae colonizing aerial space between the meristem and the new leaf. **F.** WT hyphae growing in the intercellular spaces of plant cells (arrows). The remains of the hyphal matrix are present on the surface of the first leaf. **pc** – plant cells. Samples stained with toulidin-blue. Bar: 50 µm.

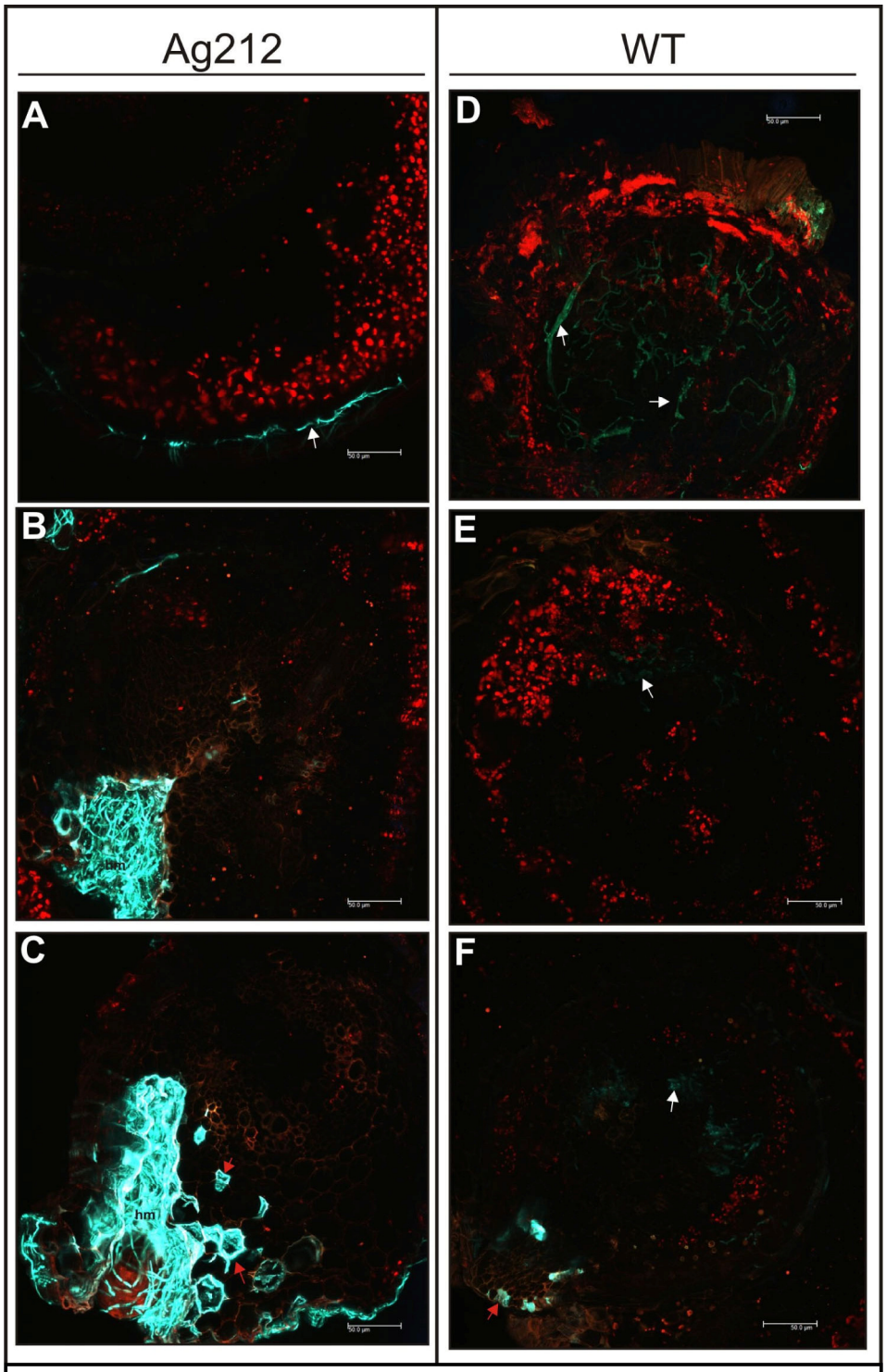

Figure 3.54. Colonization of host plant by WT and Ag212: confocal microscopy of transverse sections
Confocal micrographs of transverse sections through the inoculation point of seedlings inoculated with GFP expressing WT or Ag212, two weeks pi. White arrows point to hyphae. Red arrows point to colonized host cells. **hm** – hyphal matrix Bar: 50 µm.

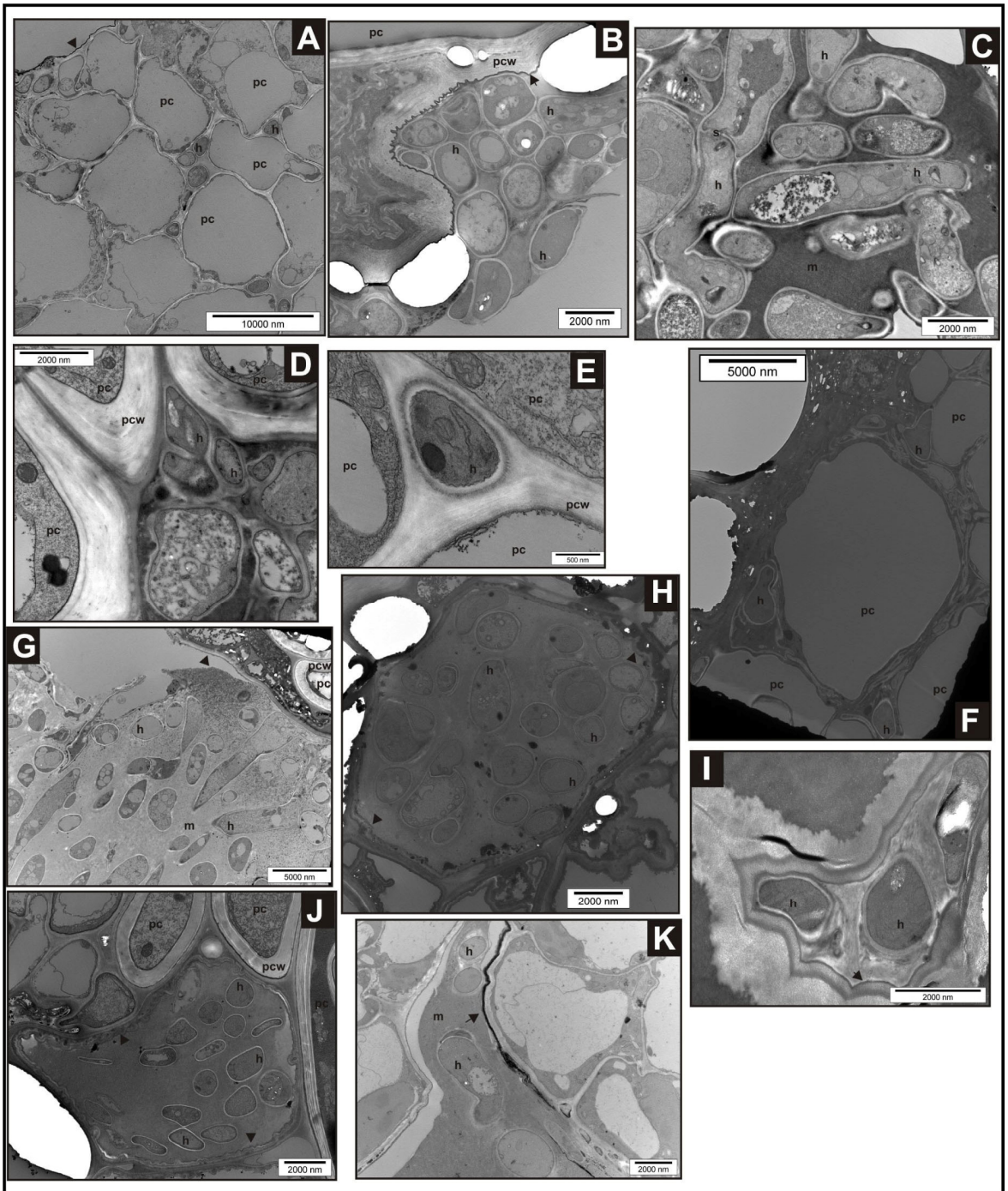

Figure 3.55. Colonization of host plant by WT and Ag212: TEM of transverse sections
A, **B** and **E.** TE micrographs of seedling inoculated with WT (Fig. 3.53F), showing hyphae in the extracellular spaces of host cells (**A** and **E**) and hyphal matrix on the leaf surface (**B**); arrows point to leaf surface. **C**, **D** and **F.** TEM of WT sample (Fig. 3.53D) showing hyphal matrix (**C**), tip of the hyphal matrix in close contact with plant cells (**D**) and individual hyphae between plant cells (**F**). **G**, **H**, **I** and **J.** TEM of mutant sample (Fig. 3.53A) showing hyphal matrix (**G**) and host cells colonized by hyphae (**H**, **I** and **J**); arrows point to the plant cell wall in direct contact with the hyphal matrix. **K.** Mutant sample (Fig. 3.53C) showing hyphae in the aerial space between meristem and young leaf; arrows point to the leaf surface. **h** – hyphae; **pc** – plant cell; **pcw** – plant cell wall; **m** – matrix; **s**-septa.

4. Discussion

4.1. Functional analysis of *E. festucae cmkA, cmkB and cmkC*

This study describes the identification and functional characterization of three *E. festucae* genes encoding Ca^{2+}/calmodulin-dependent protein kinases, *cmkA*, *cmkB* and *cmkC*. An analysis of the protein domain amino acid sequences encoded by these genes showed that, as in other fungi, CmkC has a Ca^{2+}/calmodulin-dependent kinase kinase domain. This protein has been shown to activate CmkB in *A. nidulans* and *S. pombe* (Joseph & Means, 2000, Rasmussen, 2000), as is the case for their homologues in the mammalian Ca^{2+}/CaM cascade. However, recent biochemical characterization of CmkA and CmkB homologues in *M. oryzae*, MgCaMK1 and MgCaMK2 respectively, showed that, while MgCaMK1 acts in a Ca^{2+}/CaM dependent manner, MgCaMK2 acts in a Ca^{2+}-dependent manner, suggesting that these kinases might have different mechanisms of regulation within fungi (Ma *et al.*, 2010). Semi-quantitative RT-PCR analysis showed that the expression of *E. festucae cmkA* and *cmkC* was increased *in planta*. In *S. nodorum* all three *cmk* genes were increased *in planta* when expression levels were measured 4 and 8 days after inoculation (Solomon *et al*., 2006). The preferential expression of *cmkA* and *cmkC in planta* suggests that these genes may have a role in regulation of the symbiosis.

Disruption of *cmkA*, *cmkB* and *cmkC* genes, as well as deletion of both *cmkA/cmkB*, demonstrated that these genes are not essential for viability of *E. festucae*, as is the case in all other fungi reported so far, with the exception of *A. nidulans cmkA* and *cmkB* (Solomon *et al*., 2006, Yang *et al*., 2001b, Rasmussen, 2000, Joseph & Means, 2000, Dayton & Means, 1996, Pausch *et al.*, 1991). Furthermore, the growth rate and morphology of *E. festucae* single and double-deletion mutants under standard growth conditions did not differ from WT. Colony growth rate, presence of aerial hyphae and hyphal morphology of all four mutant strains were identical to WT. In contrast, all other filamentous fungi examined to date show growth alterations when some of the *cmk* homologues are disrupted. In *S. nodorum*, the Δ*cpkA* mutant has reduced growth and changed colony pigmentation, depending on the light conditions (Solomon *et al*., 2006). *M. oryzae* mutants deleted for MoCMK1 have a lower density of aerial hyphae (Liu *et al*., 2009b). The *N. crassa* Δ*camk1* mutant has a transient slow growth phenotype and fewer aerial hyphae when grown from spores. Through some unknown mechanism, the mutant reverts to full WT growth after two transfers to fresh media (Yang *et al*., 2001b).

It is important to note, however, that most genetic and biochemical studies report defects in sporulation and spore germination. In *S. cerevisiae*, Δ*cmk2* mutants had a reduced rate of spore germination (Pausch *et al*., 1991). In *N. crassa*, the transient growth defect is accompanied by a low conidiation rate (Yang *et al*., 2001b). Lower conidial production and slower germination were reported for *M. oryzae* MoCMK1 mutants. In *Colletotrichum gloeosporioides*, spore germination is reduced in the presence of CaMK inhibitors (Kim *et al*., 1998). In *S. nodorum*, Δ*cpkA* mutants had reduced sporulation both on plates and during the infection process while Δ*cpkC* mutants displayed delayed sporulation during the infection process (Solomon *et al*., 2006). However, screening for changes in both asexual and sexual reproduction in *E. festucae* is difficult because sporulation is sparse. Colonies in culture do not produce sufficient numbers of conidia to study the effect of *cmk* mutations on spore development and germination, and development of a stroma, the first stage of the sexual cycle, has not been reported in perennial ryegrass plants infected with *E. festucae*. Therefore, the possibility remains that *cmkA*, *cmkB* and *cmkC* mutants might be defective in either conidiation and ascospore development and/or germination, as has been reported for other fungi. Furthermore, neither single nor double *cmk* deletion mutants had altered production of reactive oxygen species either at a colony or at a hyphal level, showing that *cmkA*, *cmkB* and *cmkC* have no role in regulation of ROS production in axenic culture of *E. festucae*.

Not much is known about the role of fungal CaMKs in response to specific stress conditions. Data from *S. cerevisiae* studies indicate that these kinases are involved in regulation of induced thermotolerance (Iida *et al*., 1995) but *cmk* mutants do not exhibit differential growth under various temperature (Pausch *et al*., 1991). *E. festucae cmk* mutant strains were tested under conditions of oxidative, temperature, osmotic and cell wall integrity stress. Both single and double-deletion mutants grew as well as wild-type suggesting that these genes are not involved in the regulation of growth under these conditions. However, tests for growth at different temperatures revealed an unusual result. When grown at 30°C, transformants Δ*cmkA15.2*, Δ*cmkB1.3*, Δ*cmkC19.2* and Δ*cmkC40.3* displayed a stable and reproducible reduction in growth rate. Additionally, transformants from all three groups of knock-outs had an increase in aerial hyphae, resulting in more dense-looking colonies than WT, and this phenotype was retained in the double-deletion Δ*cmkAB* mutant. Neither of these phenotypes were complemented

by introduction of WT *cmk* genes. Because some of the constructs used for complementation contained a full-length sequence of adjacent genes, the possibility that secondary mutations in adjacent genes caused the temperature sensitive phenotypes was ruled out. It is important to note that the *E. festucae* p21-activated kinase deletion mutant, Δ*pakA*, also had a slow-growth phenotype under conditions of temperature stress which could not be complemented by reintroduction of the WT gene (Eaton, C., personal communication). One possible explanation for these phenotypes are genetic or epigenetic processes, such as transposon activation, which might be induced by cell manipulations during protoplasting and transformation. Another possible explanation would involve random insertion of small fragments of KO constructs in the fungal genome, generated during transformation and homologous recombination processes. Such insertions could cause phenotype changes unrelated to CaMK gene deletion. However, given that the slow-growth phenotype was observed in four independent transformants and the 'dense colony' phenotype was present in four independent transformants, the latter explanation seems unlikely.

While *cmk* mutants did not show sensitivity to increased concentrations of NaCl, SDS or H_2O_2, Δ*cmkB* mutants as well as Δ*cmkAB* double mutants were sensitive to high concentrations of Mg^{2+}. Under these conditions, three Δ*cmkB* transformants had different phenotypes which were stable and reproducible. Growth of Δ*cmkB1.3* resembled that of WT while Δ*cmkB10.5* had a highly reduced growth rate, with Δ*cmkB14.2* displaying an intermediate phenotype. However, Δ*cmkAB* mutants, which were generated as independent *cmkB* deletion mutants in the Δ*cmkA* background, did not show any variation, with all three transformants being highly sensitive to increased Mg^{2+}. One possible explanation for these results is redundancy between *cmkA* and *cmkB* but this hypothesis was not supported by complementation experiments. While reintroduction of WT *cmkB* gene in both single and double-deletion mutants restored the WT phenotype, introduction of *cmkA* into Δ*cmkAB* mutants did not complement the Mg^{2+} sensitivity phenotype. Expression analysis suggests that the lack of complementation is not due to a lack of expression of *cmkA* gene from the complementation constructs, although the possibility remains that, in order to complement, a high level of expression of *cmkA* is required, which was not achieved in the complementation transformants analyzed, due to positional effects. This result leaves completely open the question of the origin of the variation in Δ*cmkB*

transformants. One unlikely possibility is that *cmkA* has no effect on Mg^{2+} sensitivity and the results obtained for the single and double mutants are due to stochastic events. Another possible explanation is that *cmkA* and *cmkB* interact through a complex process that involves mutual regulation of expression and activity. There is also the possibility that the cause of the variation is due to formation or the lack thereof of suppressor mutations which are reported to be frequently generated in some fungi, for example *U. maydis* (Egan *et al.*, 2009). If the presence of *cmkA* triggers a higher frequency of suppressor mutations, this would explain why double mutants do not show this variation.

Beside Mg^{2+} sensitivity, Δ*cmkAB* mutants were also affected by changes in the extracellular Ca^{2+} concentrations. Mg^{2+} and Ca^{2+} show a complex relationship in various types of cells. In *S. cerevisiae*, Mg^{2+} starvation induces a Ca^{2+} signaling response (Wiesenberger *et al.*, 2007). Also, an increase in Mg^{2+} concentration decreases Ca^{2+} accumulation in the vacuole (Beeler *et al.*, 1994). *S. cerevisiae* mutants deficient in PMR1, a Ca^{2+}-ATPase, are sensitive to elevated Mg^{2+} concentrations (Szigeti *et al.*, 2005). This study indicated that Ca^{2+} and Mg^{2+} influence the growth of the mutant in a competitive manner, probably due to competition for transport across the plasma membrane. In fact, the presence of increased Ca^{2+} concentration suppressed the growth defect of the *E. festucae* Δ*cmkAB* mutants under conditions of high Mg^{2+}. However, unlike the *S. cerevisiae* PMR1 mutant, Δ*cmkAB* mutants did not show increased sensitivity to high Ca^{2+} concentrations. Interestingly, Δ*cmkAB* mutants were less sensitive to high concentration of Ca^{2+} ions than WT colonies, losing aerial hyphae at a slower rate than WT. In contrast, these mutants were more sensitive to depletion of Ca^{2+} by EGTA than WT. There are two possible explanations for these results. Firstly, Δ*cmkAB* might be impaired for Ca^{2+} uptake, resulting in reduced susceptibility to high Ca^{2+} concentrations in the media compared to WT, and greater sensitivity than WT to a lack of Ca^{2+} in the presence of EGTA. The detailed mechanisms of fungal Ca^{2+} uptake are yet to be fully understood. In yeast there is evidence for two calcium influx systems: a high-affinity Ca^{2+} influx system (HACS) and a low-affinity Ca^{2+} influx system (LACS) (Muller *et al.*, 2001). The HACS is regulated by calcineurin and involves the Cch1pMid1p calcium channel. The LACS remains to be characterized, but activation of this system requires genes involved in cell cycle arrest and polarized morphogenesis during the mating process. A recent study of a mathematical model for dynamics of cytosolic Ca^{2+} changes in yeast, using aequorin, a calcium reporter protein successfully

used for studying of Ca^{2+} concentrations, identified a calcineurin signalling-independent Ca^{2+} transporter which is competitively inhibited by Mg^{2+} (Cui *et al.*, 2009a). An interpretation of the *E. festucae* results on the basis of this model would suggest that Δ*cmkAB* mutants are deficient in a calcineurin signalling-dependent Ca^{2+} import system and rely only on a calcineurin signalling-independent system, which is inhibited by high concentrations of Mg^{2+}, resulting in growth arrest. A second explanation for the Δ*cmkAB* phenotype could be 'calcium auxotrophy' where the Ca^{2+} uptake systems are intact but the mutant itself requires higher Ca^{2+} concentrations than WT for growth. Such a condition was recently reported in *A. nidulans*, where the basis of calcium auxotrophy was shown to be due to expansion of the vacuolar membrane and overexpression of vacuolar Ca^{2+} pumps Pmc1 and Pmc2 (Findon *et al.*, 2010).

A full understanding of how *cmkB* regulates Ca^{2+} ion homeostasis in *E. festucae* would require the use of techniques that allow measurement of Ca^{2+} uptake by the mutant compared with WT in order to distinguish between the two possible explanations: impaired Ca^{2+} uptake and Ca^{2+} auxotrophy. Such measurements are still not routinely performed in filamentous fungi but in recent years a codon-optimized aequorin reporter system has been established as a useful tool for investigating Ca^{2+} homeostasis in filamentous fungi (Nelson *et al.*, 2004, Bencina *et al.*, 2005, Binder *et al.*, 2010).

An analysis of the phenotype of perennial ryegrass plants infected with single or double mutants showed that *cmkA*, *cmkB* and *cmkC* are dispensable for the establishment and maintenance of the mutualistic symbiotic interaction. In other fungi, these genes have well-established roles in plant interactions. In *M. oryzae,* disruption of MoCMK1 leads to a delay in appressoria formation as well as reduced appressorial turgor (Liu *et al*., 2009b). Appressoria formation was also affected in *C. gloeosporioides* when treated with CaMK inhibitors (Kim *et al*., 1998). In *S. nodorum*, *cpkA* and *cpkC* mutants are disrupted in sporulation and, consequently, are impaired in infection (Solomon *et al*., 2006). These phenotypes establish functional roles for CaMKs in the processes of host cuticle penetration and other early stages of infection. It is reasonable to assume then, because epichloë endophytes are predominantly vertically transmitted, that the role of the CaMKs in the establishment and maintenance of fungal-plant interaction has been lost. However, as for the culture phenotype, it is possible that *E. festucae* CaMKs might

still have an important role in the establishment of the symbiosis through horizontal transmission, a process that involves sporulation and spore germination.

4.2. Role of *E. festucae* calcineurin in fungal growth and symbiosis

PCR and RT-PCR analyses identified two copies of *cnaA* in the genome of *E. festucae* E2368 that were expressed in culture. In contrast, strain Fl1 has only one copy of *cnaA*. While *S. cerevisiae* contains two copies of the calcineurin A gene (Cyert *et al.*, 1991), all studies of filamentous fungi reported to date show the presence of only one copy in these organisms.

Disruption of the single copy of *cnaA* gene present in the genome of *E. festucae* Fl1 demonstrated that, while this gene is not essential for viability, it is important for normal fungal growth. In other fungi, deletion of calcineurin A gene has diverse effects on growth under normal conditions. Disruption of *cnaA* in *A. nidulans* is lethal (Rasmussen *et al.*, 1994). In *S cerevisiae* disruption of both copies of calcineurin A gene had no effect on growth under normal conditions, but mutants displayed sensitivity to high salt concentration and pH >8.0 (Nakamura *et al.*, 1993). However, deletion of both CNA1 and CNA2 in a Δ*pkc1* (protein kinase C) background leads to lethality. Δ*pkc1* mutants have a cell wall integrity defect and undergo lethal cell lysis unless grown in the presence of osmotic stabilizers. Deletion of calcineurin genes abolished the rescue of the phenotype, indicating that calcineurin perform functions that are related to regulation of cell integrity (Garrett-Engele *et al.*, 1995). A study of genes involved in chitin synthesis in *C. albicans* confirms the importance of calcineurin for this process. *C. albicans* chitin synthesis genes *chs2* and *chs8* respond to Ca^{2+} changes through the action of Crz1p (Munro *et al.*, 2007). Data from other fungi indicate a crucial role for calcineurin in polarity and elongation of filamentous cells. In *C. neoformans*, calcineurin is required for growth at 37°C and formation of conjugation tubes in response to pheromones as well as for filamentation of heterokaryons (Cruz *et al.*, 2001). A role in cell polarity was also established for *S. pombe* where deletion of calcineurin caused a branched cell phenotype (Yoshida *et al.*, 1994). Studies in *M. oryzae* and *N. crassa* using gene silencing showed that disruption of calcineurin function affects hyphal branching and elongation (Choi *et al*., 2009b, Prokisch *et al*., 1997). Disruption

of calcineurin A in *U. maydis* results in a multiple-budding phenotype and disruption of the mating process (Egan *et al.*, 2009). An extensive functional characterization of *cnaA* gene was conducted in *A. fumigatus* where deletion of the *cnaA* gene was shown not to be lethal (Da Silva Ferreira *et al.*, 2007). *A. fumigatus* Δ*cnaA* mutants had a dramatic reduction of colony edge extension resulting in small, compact-looking colonies. The hyphae had altered morphology with hyperbranching, loss of polarity and reduced filamentation which caused the hyphae to look more 'bulged' than WT (Steinbach *et al.*, 2006). In *E. festucae*, disruption of *cnaA* gene led to similar colony morphology as observed for *A. fumigatus* mutants. Colonies were small and compact, with a dramatically reduced growth rate. As in other filamentous fungi, hyphae of the *E. festucae* Δ*cnaA* mutant are extensively hyperbranched. However, hyphal morphology itself was less severely affected than in *A. fumigatus*. Apart from being short and occasionally wobbly, hyphae and hyphal tips did not differ strikingly from WT. Another feature of the *E. festucae* Δ*cnaA* mutants was the presence of a yellow pigment on the growth plate, probably because of cell exudation as a result of cell lysis. The presence of hyphal debris around the intact hyphae suggests that the cell wall integrity of these mutants is impaired.

Disruption of *cnaA* in *E. festucae* also led to a dramatic symbiotic interaction phenotype. Seedlings inoculated with the mutant showed a strong hypersensitive response. A brown colouration was present at the point of inoculation and in some cases spread to the entire seedling, leading to loss of chlorophyll and death of the seedling shortly after inoculation. This type of response is never observed for WT. Of the plants that survived just three plants were infected, one of which showed signs of an impaired symbiosis and died soon after screening. Given that the mutant strain used for inoculation of this plant has an additional copy of the KO construct integrated into the genome, the phenotype observed may not be entirely due to deletion of *cnaA*. The other two infected plants showed no signs of an antagonistic interaction that is typically observed for *E. festucae* mutants such as Δ*noxA* and Δ*sakA*. Furthermore, the hyphal growth and branching pattern *in planta* resembled that of WT. However, hyphae of the mutant showed an increased presence of vesicles in the cytoplasm.

The strong hypersensitive response of seedlings inoculated with Δ*cnaA* suggests that the mutant is recognized by the host as a pathogen. Recognition of plant pathogens and

activation of the first layer of the plant immune response depends on recognition of so called pathogen-associated molecular patterns (PAMPs). PAMPs represent conserved molecules characteristic for one class of pathogens such as bacteria or fungi. Perception of PAMPs by the plant activates PAMP-triggered immunity (PTI) which, among other responses, includes rapid ion fluxes across the membrane, ROS production, changes of gene expression and cell wall reinforcement (Zipfel, 2008). Chitin is an important PAMP of fungal pathogens and suppression of a gene encoding a chitin receptor in rice, *CEBiP*, leads to suppression of the oxidative burst and gene expression characteristic of plant immune response (Kaku *et al.*, 2006). Fungal pathogens employ various mechanisms in order to prevent plant perception of chitin. The effector protein Avr4 of the tomato pathogen *Cladosporium fulvum* binds to the chitin of the fungus cell wall during the infection process, protecting the fungus from plant chitinases (van den Burg *et al.*, 2006). In the same organism, protein Ecp6 sequesters chitin molecules released from the fungal cell wall during the infection process, preventing elicitation of host immunity (de Jonge *et al.*, 2010). Disruption of chitin synthesis itself can induce plant immunity against the pathogen. In *F. oxysporum* and *B. cinerea* disruption of genes encoding class V and class III chitin synthases, respectively, induces stimulation of host immunity (Arbelet *et al.*, 2010, Pareja-Jaime *et al.*, 2010). Given that calcineurin regulates chitin synthases in filamentous fungi, as was shown in *A. fumigatus* (Fortwendel *et al.*, 2010), it is possible that HR in seedlings inoculated with Δ*cnaA* is triggered by disrupted chitin synthesis. If this is the case, maybe *E. festucae* avoids elicitation of the plant immune response by successful prevention of chitin recognition by the host. This raises an interesting question as to how the initial host response was overcome by mutant in two infected plants where functional symbiosis was established. Nothing is known about the mechanisms behind the hyphal cell wall-plant cell wall attachment during the establishment of the *E. festucae*-perennial ryegrass symbiosis. One possibility to explain the results above is that attachment to the plant cell wall and switch to intercalary growth might stabilize otherwise impaired hyphal cell wall synthesis in the Δ*cnaA* mutants. Further investigation of the Δ*cnaA* symbiotic phenotype, including detailed microscopic studies, is needed in order to fully understand these results, although the very low rate of infection by the mutant will make this difficult.

4.3. T-DNA mutagenesis generates mutants defective in growth and symbiosis

This study used Agrobacterium-mediated T-DNA mutagenesis in order to identify new genes involved in regulation of the symbiosis. Large scale T-DNA mutagenesis in phytopathogenic fungi has established AMT as a useful tool to identify new pathogenicity loci. In *M. oryzae* and *Leptosphaeria maculans* 0.95% and 1.9% of insertions were in pathogenicity loci (Jeon *et al.*, 2007, Blaise *et al*., 2007). Out of 180 T-DNA mutants generated in this study, 2 were identified to have a disrupted symbiotic interaction and for one of them, Ag212, the T-DNA insertion was confirmed to be linked to the symbiotic phenotype. Although this study was conducted on a small number of mutants, the results confirmed that AMT represents a useful tool for finding symbiotically important genes.

Mutant Ag51 had both an in culture and *in planta* phenotype. Like the calcineurin mutant, Ag51 had increased secretion of a yellow pigment into the agar which is most likely due to an increase in cell lysis. The *E. festucae* Δ*sakA* mutant has a similar phenotype, consistent with the loss of cell wall integrity (Eaton, 2009). Ag51 also elicits an HR when inoculated into seedlings. As for the Δ*cnaA* mutant, the reason for this could be the exposure of fungal PAMPs. Furthermore, the ability of Ag51 to infect plants was dramatically reduced and infected plants died soon after planting, showing loss of a mutualistic interaction. Southern blot and plasmid rescue analysis showed that Ag51 possesses a tandem insertion of T-DNA with at least two head-to-tail copies. One end of the insertion appeared to be truncated or rearranged, as neither TAIL-PCR nor plasmid rescue techniques were useful for the identification of the insertion locus. Furthermore, Southern analysis suggests the presence of chromosomal rearrangement in the genome of Ag51. Induction of chromosomal rearrangements by T-DNA insertion is well documented in plants (Castle *et al.*, 1993). Studies in Arabidopsis and rice report chromosomal rearrangements accompanied by tandem insertion of T-DNA in both head-to-head and head-to-tail configurations (Zhu *et al.*, 2010, Nacry *et al.*, 1998). In filamentous fungi, both head-to-tail tandem insertions of T-DNA (Meng *et al.*, 2007) and chromosomal rearrangements (Choi *et al.*, 2007) were reported in systematic studies of T-DNA insertion sites in *M. oryzae*. Another possibility is that Ag51 is a heterokaryon, containing both mutant and WT nuclei. Given the complexity of the

insertion, high throughoutput sequencing analysis would be required in order to fully characterize the T-DNA insertion.

The second T-DNA mutant, Ag212, had slow growth in culture and was reproducibly shown to be unable to colonize inoculated plants, failing to establish infection. In the artificial symbiosis used in the *E. festucae* model system, this suggests that this mutant is potentially defective in one of two primary steps: sensing of the inner plant environment and/or colonization of the plant meristem. This mutant is therefore very useful for identification of genes involved in the early stages of colonization. Given that the T-DNA LB and RB in Ag212 were localized on non-linked contigs in the *E. festucae* genome, a combination of synteny analysis and Southern analysis was used to characterize the extent of the deletion. A large (25 Kb) deletion was identified in this mutant. Large deletions (>75 Kb) have been reported as a consequence of T-DNA insertion in Arabidopsis (Kaya *et al.*, 2000). Deletions of adjacent genomic sequences have also been reported in fungi including *M. oryzae* (Meng *et al*., 2007). However, the largest deletion reported in this study was just 2.5 Kb. Ten genes were identified to be deleted in Ag212 and complementation experiments narrowed down the candidate genes responsible for the symbiotic phenotype to eight genes. Analysis of cosmid transformants identified one that was complemented for the culture growth defect but had lost all but 3 of the 8 candidate genes. Like the original mutant, this transformant was not able to infect the host, suggesting that the three genes present in this transformant were not sufficient for restoration of the symbiotic phenotype. The fact that restoration of the culture phenotype was not sufficient to restore plant infection suggests that Ag212 is disrupted in some molecular process specific for plant colonization. This was further confirmed by microscopic analysis of the colonization process of WT and mutant. This analysis showed that the mutant colonizes the space of the inoculation cut in a manner similar to WT, showing that the mutant senses the inner plant environment. However, individual mutant hyphae were never found among plant cells or closely attached to the plant cell wall, suggesting that Ag212 lacks the ability to form a specific hyphal-plant cell wall interaction. It is important to note that plant tissue in contact with the hyphae did not differ between mutant and WT, suggesting that this mutant is not recognized by the host as a pathogen. Since hyphae were also absent from older plants, it seems likely that the development of new leaves in the meristematic zone

pushes the hyphae towards the outside of the plant resulting in eventual death of the fungus.

Bioinformatic analysis of the 8 candidate genes identified in Ag212 suggests potential functions for these genes. Gene 1085-1 encodes a conserved hypothetical protein that lacks any known conserved protein domain. Another gene, 1085-7, also encodes a hypothetical conserved protein. However, a 3-oxo-5-α-steroid 4-dehydrogenase domain as well as seven transmembrane domains were identified in this protein. It is interesting to note that, although not a homologue of 1085-7, a protein from *U. maydis*, Udh1, containing the same 5α-steroid reductase domain and six transmembrane domains, was transcriptionally upregulated during the process of host infection (Basse *et al.*, 2002). Homologues of the six other genes identified have been studied in other fungi. The homologue of 1085-2, a putative homoserine dehydrogenase, is synthetically lethal in *S. cerevisiae* (Arevalo-Rodriguez *et al.*, 2004). Deletion of the homologue of 1085-3, *trm8*, a putative tRNA methyl transferase, in the phytopathogenic fungus *Colletotrichum lagena* resulted in dramatically reduced pathogenicity. Mutants form WT-looking appressoria and penetration hyphae on the cellophane but fail to develop intracellular penetration hyphae *in planta*. This defect, however, was overcome on plants whose defence system was partially impaired by heat-shock, suggesting that *trm8* plays an important role in overcoming environmental stress induced by the plant defence system (Takano *et al.*, 2006). The 1085-4 gene encodes a putative intermediate filament protein 1, which is an important component of the fungal cytoskeleton. In *S. cerevisiae*, intermediate filament protein 1 (MDM1) is an essential gene (McConnell & Yaffe, 1992) that plays a role in organelle inheritance (Fisk & Yaffe, 1997). Given that Ag212 is viable, the *mdm1* homologue in *E. festucae* is not essential for growth. 1085-5 encodes a putative peroxisomal biogenesis protein, PEX11, which in *A. oryzae* regulates the function of the Woronin body (Escano *et al.*, 2009). 1085-6 encodes a putative fructose-1,6-biphosphatase (*FBP1*), a key enzyme for gluconeogenesis. In yeast, FBP1 regulates DNA damage by the DNA methylating agent methyl methanesulfonate (MMS). Expression of FBP1 was up-regulated in the presence of MMS. Deletion of FBP1 resulted in elevated production of ROS and caused cells to become less sensitive to MMS (Kitanovic & Wolfl, 2006). 1085-8 belongs to the CIA30 family of proteins, which are required for the assembly of mitochondrial complex 1 (Schulte, 2001).

Complementation experiments identified genes 1085-3, 1085-4 and 1085-5 as candidates for the culture phenotype of Ag212. However, further experiments, including single gene complementations and gene disruptions will be required to fully understand the phenotype of Ag212. It is also possible that more than one gene is responsible for both culture and plant phenotypes.

4.4. Conclusions

This study identified a novel function of fungal *cmkB* in regulation of ion homeostasis and provides an insight into the importance of fungal CaMKs for mutualistic fungal-plant interactions. Genetic analysis of *E. festucae* calcineurin A gene established this gene as important for both culture growth and symbiosis. Induction of HR in seedlings infected with Δ*cnaA* mutant highlights the potential importance of functional cell integrity pathways for *E. festucae* to avoid a host immune response during establishment of the mutualistic interaction. Investigation of T-DNA Ag51 mutant supports this hypothesis. Genetic and molecular analysis of Ag212 identified new gene candidates for the regulation of processes required for establishing a mutualistic interaction of *E. festucae* and its host. Detailed analysis of this mutant provided valuable insights into the plant colonization process. Taken together, the results of the investigations of *cnaA* and T-DNA mutants lead to a conclusion that avoidance of the plant immune response, perception of plant inner environment and attachment of the hyphae to the plant cell walls are crucial processes in the early stages of the *E. festucae*–perennial ryegrass symbiotic interaction.

5. Appendices

5.1. Appendix 5.1 WT transcriptome data for *cmkA*

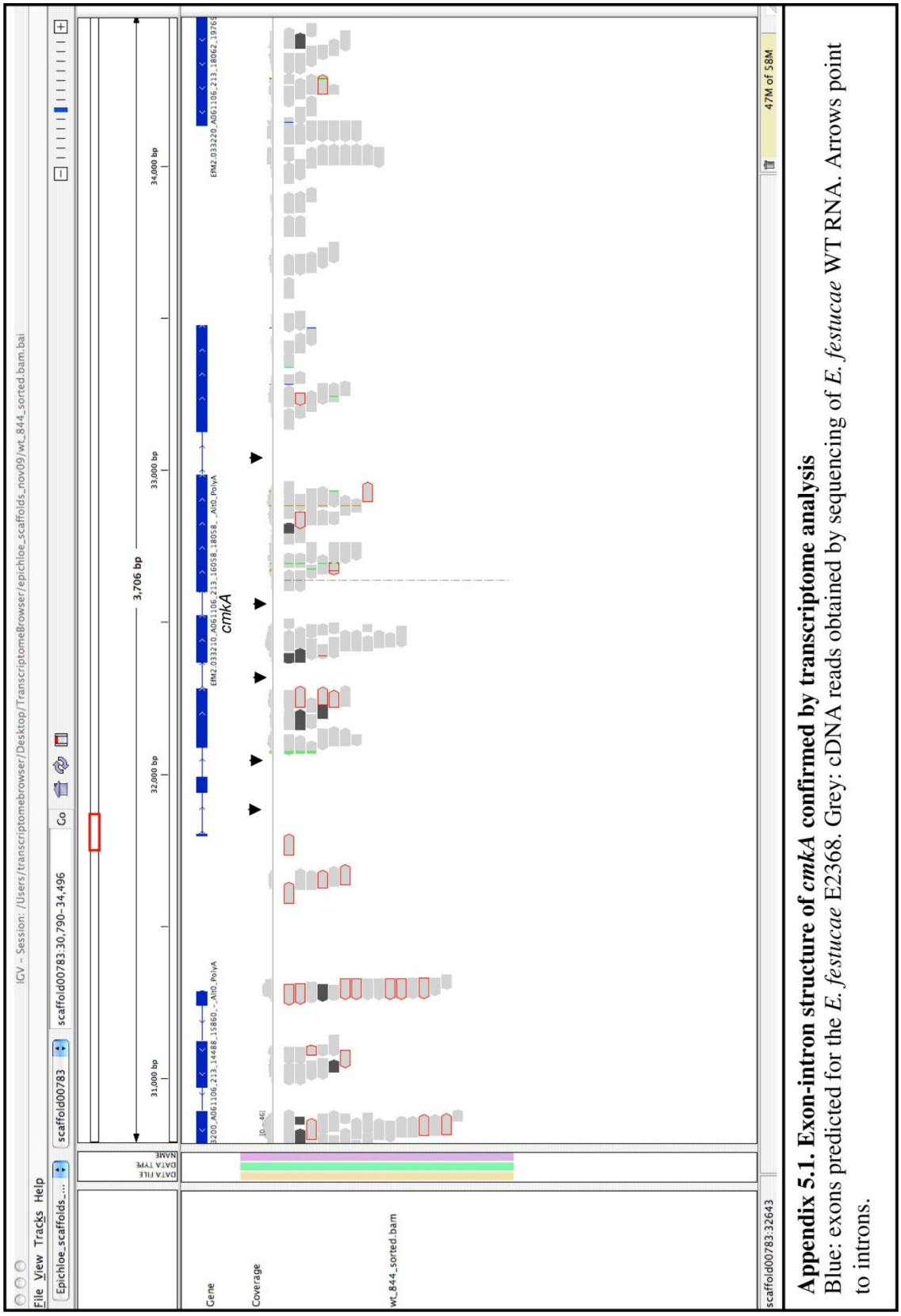

Appendix 5.1. Exon-intron structure of *cmkA* confirmed by transcriptome analysis
Blue: exons predicted for the *E. festucae* E2368. Grey: cDNA reads obtained by sequencing of *E. festucae* WT RNA. Arrows point to introns.

5.2. Appendix 5.2 Δ*sakA* transcriptome data for *cmkA*

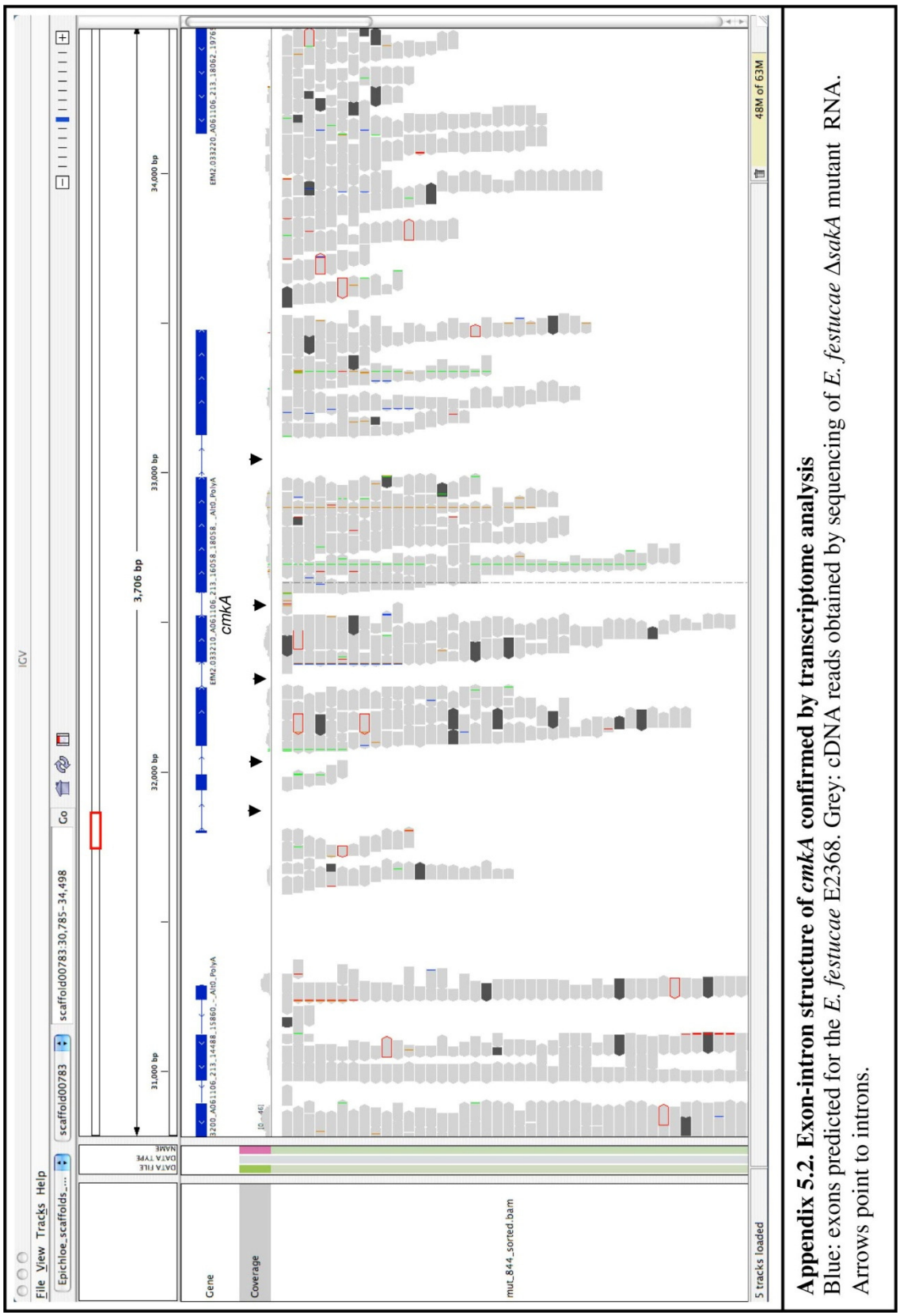

Appendix 5.2. Exon-intron structure of *cmkA* confirmed by transcriptome analysis
Blue: exons predicted for the *E. festucae* E2368. Grey: cDNA reads obtained by sequencing of *E. festucae* Δ*sakA* mutant RNA. Arrows point to introns.

5.3. Appendix 5.3 WT transcriptome data for *cmkB*

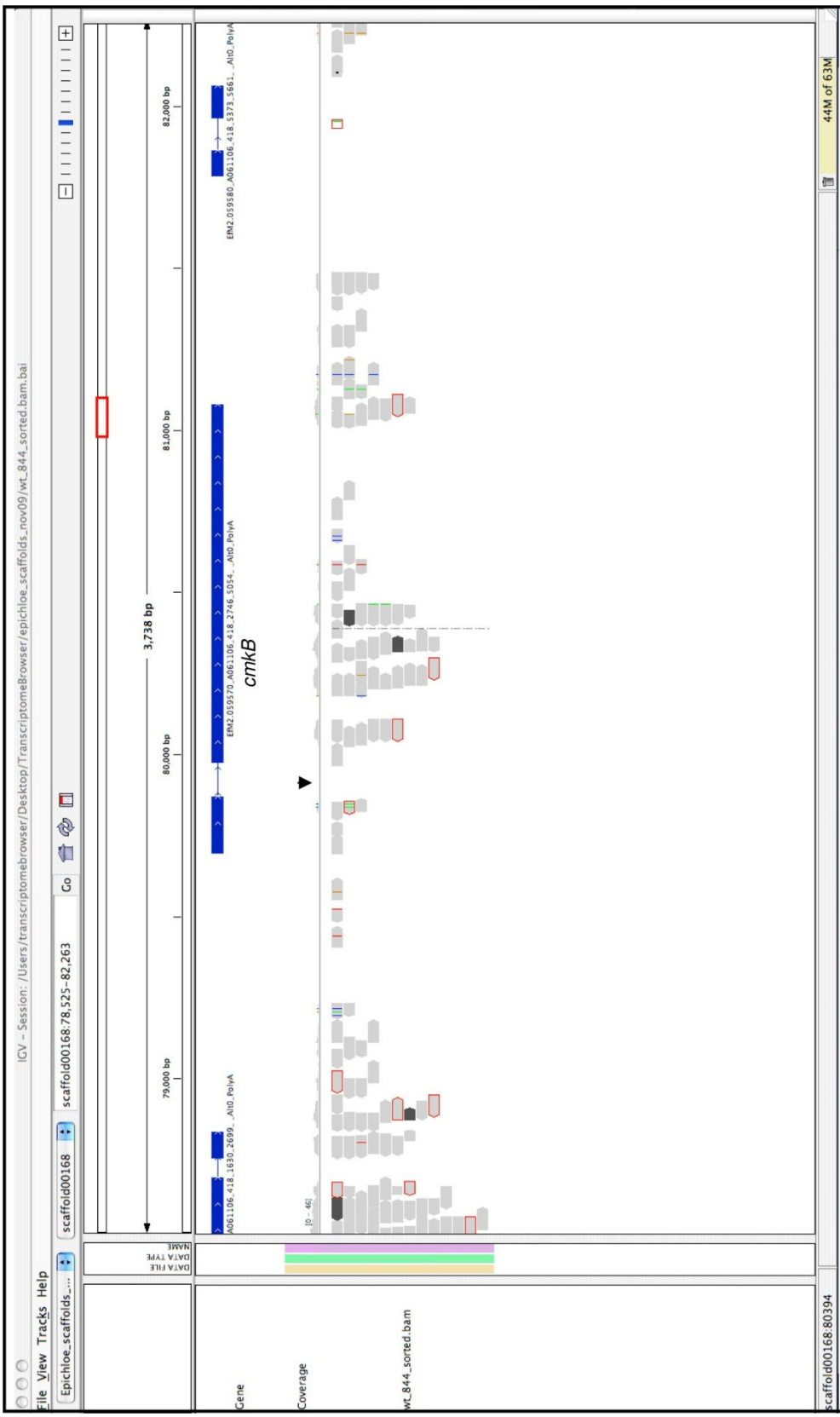

Appendix 5.3. Exon-intron structure of *cmkB* confirmed by transcriptome analysis
Blue: exons predicted for the *E. festucae* E2368. Grey: cDNA reads obtained by sequencing of *E. festucae* WT RNA. Arrow points to intron.

5.4. Appendix 5.4 Δ*sakA* transcriptome data for *cmkB*

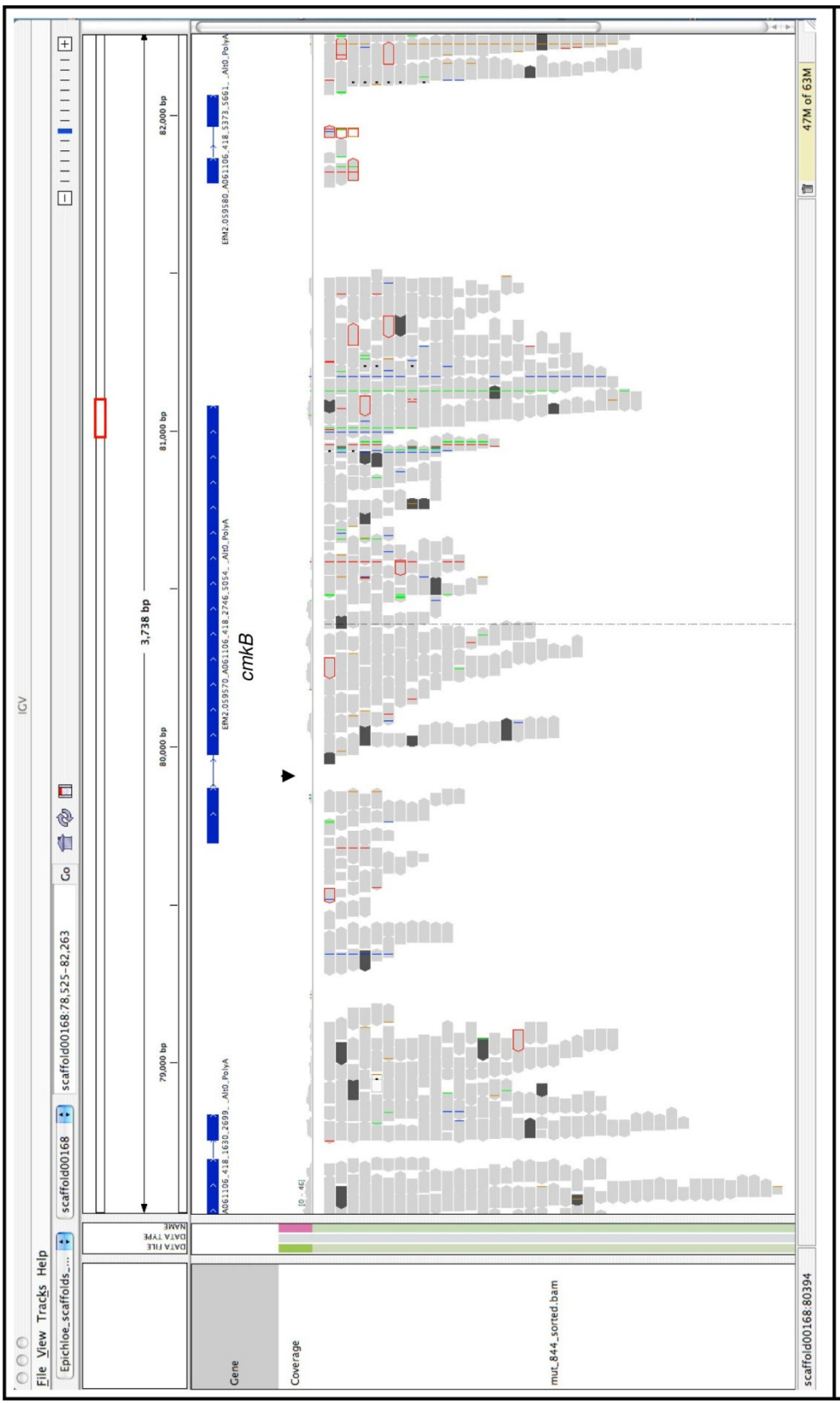

Appendix 5.4. Exon-intron structure of *cmkB* confirmed by transcriptome analysis
Blue: exons predicted for the *E. festucae* E2368. Grey: cDNA reads obtained by sequencing of *E. festucae* Δ*sakA* mutant RNA. Arrow points to intron.

5.5. Appendix 5.5 WT transcriptome data for *cmkC*

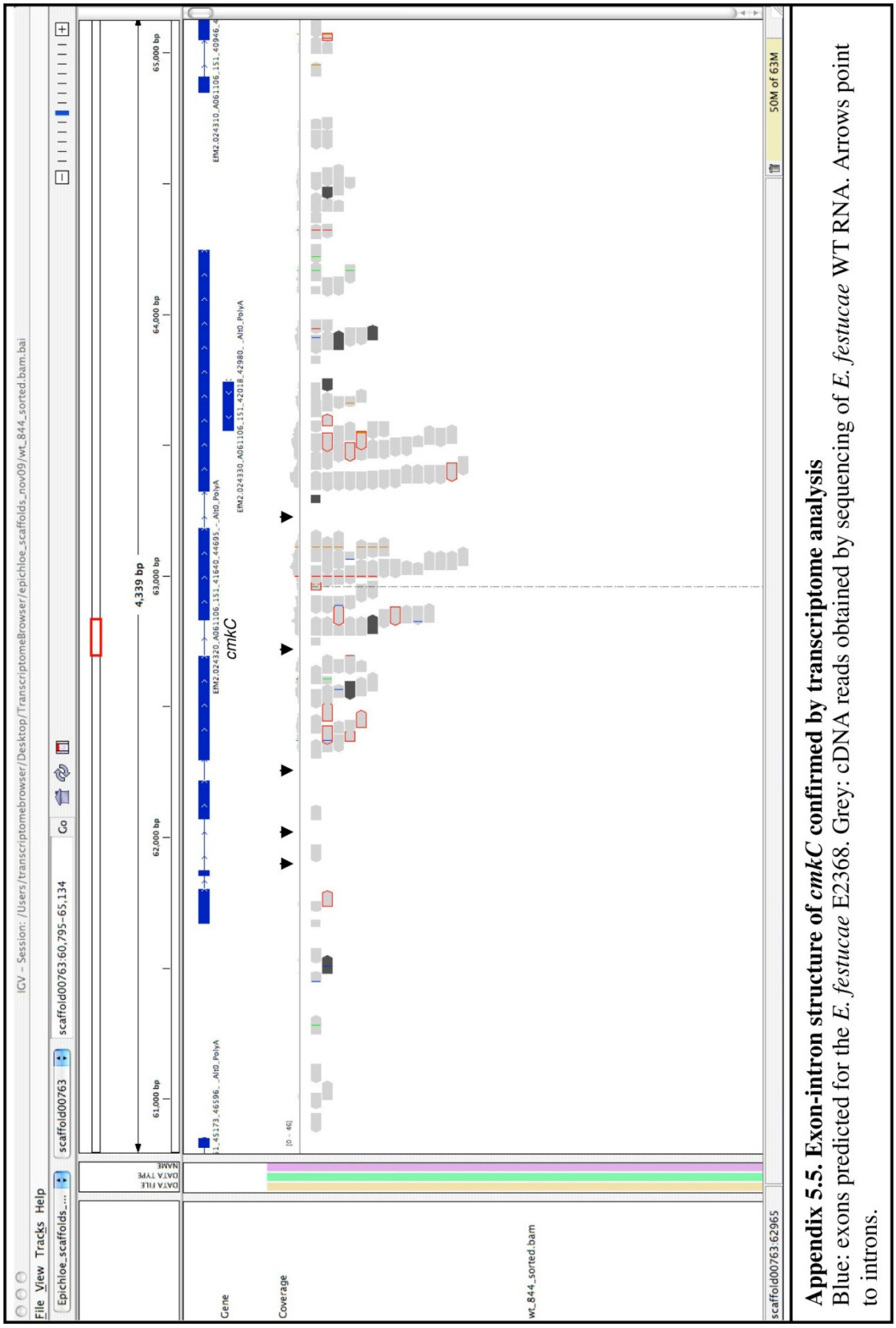

Appendix 5.5. Exon-intron structure of *cmkC* confirmed by transcriptome analysis
Blue: exons predicted for the *E. festucae* E2368. Grey: cDNA reads obtained by sequencing of *E. festucae* WT RNA. Arrows point to introns.

5.6. Appendix 5.6 Δ*sakA* transcriptome data for *cmkC*

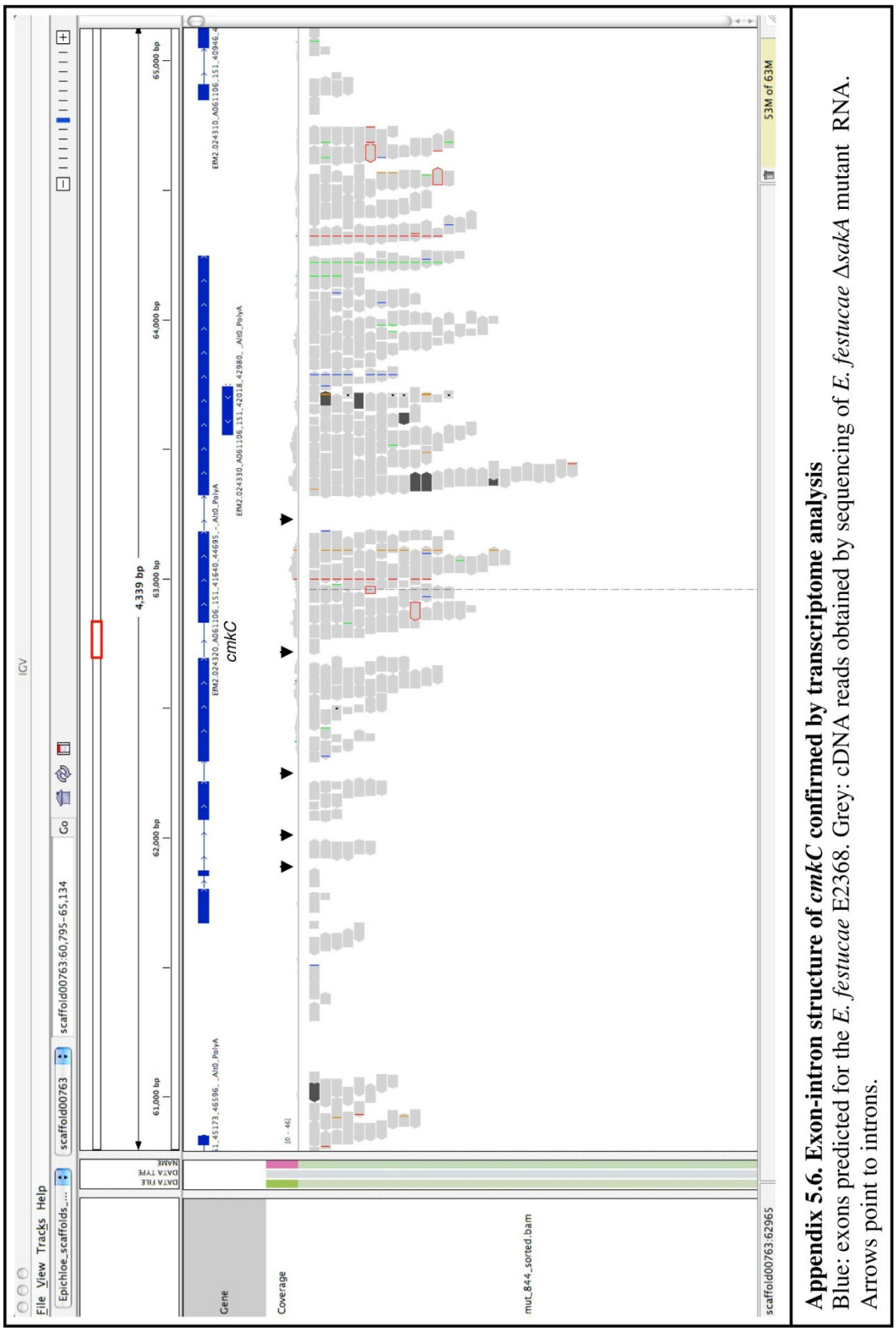

Appendix 5.6. Exon-intron structure of *cmkC* confirmed by transcriptome analysis
Blue: exons predicted for the *E. festucae* E2368. Grey: cDNA reads obtained by sequencing of *E. festucae* Δ*sakA* mutant RNA. Arrows point to introns.

5.7. Appendix 5.7 Southern blot analysis of T-DNA induced deletion in Ag212 – genomic digests

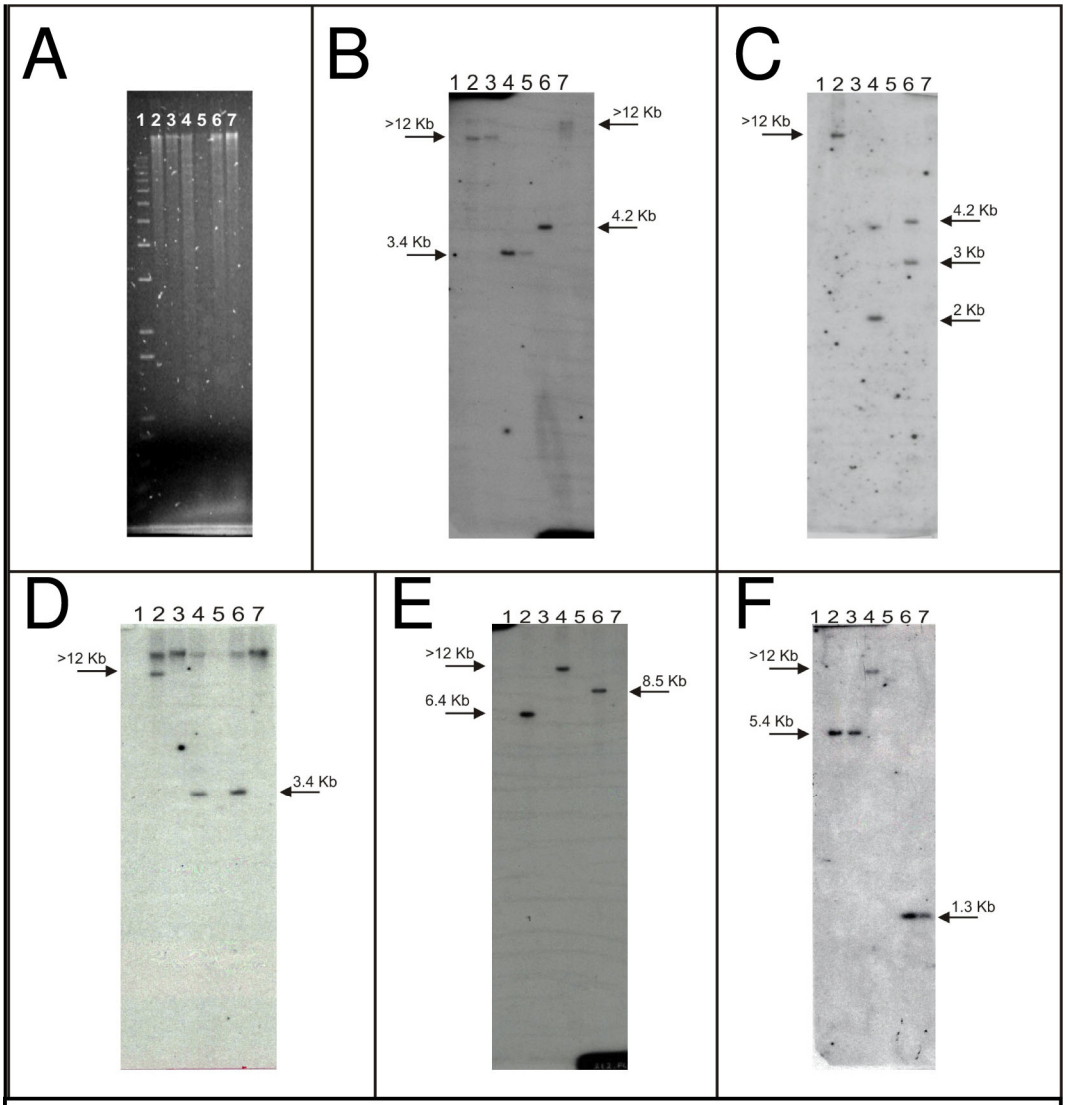

Appendix 5.7. Southern blot analysis of T-DNA induced deletion in Ag212
Autoradiographs of Southern blots containing genomic DNA digests of WT and Ag212. Lanes: 1 Kb+ ladder (*lane 1*); Fl1 *BamHI* digest (*lane 2*); Ag212 *BamHI* digest (*lane 3*); Fl1 *SstI* digest (*lane 4*); Ag212 *SstI* digest (*lane 5*); Fl1 *XhoI* digest (*lane 6*); Ag212 *XhoI* digest (*lane 7*); **A.** Ethidium bromide stained gel of genomic digests. **B.** Autoradiograph of the Southern blot probed with [^{32}P]-labeled PCR product of 1006ppF/R primer pair. **C.** Autoradiograph of the Southern blot probed with [^{32}P]-labeled PCR product of c_1006-3F/sid1R primer pair. **D.** Autoradiograph of the Southern blot probed with [^{32}P]-labeled PCR product of c_1085-2F/R primer pair. **E.** Autoradiograph of the Southern blot probed with [^{32}P]-labeled PCR product of f-1,6-bpF/R primer pair. **F.** Autoradiograph of the Southern blot probed with [^{32}P]-labeled PCR product of c_849-1F/R primer pair. A map of the region, with primer pairs, is shown in Appendix 5.9.

5.8. Appendix 5.8 Southern blot analysis of T-DNA induced deletion in Ag212 – cosmid digests

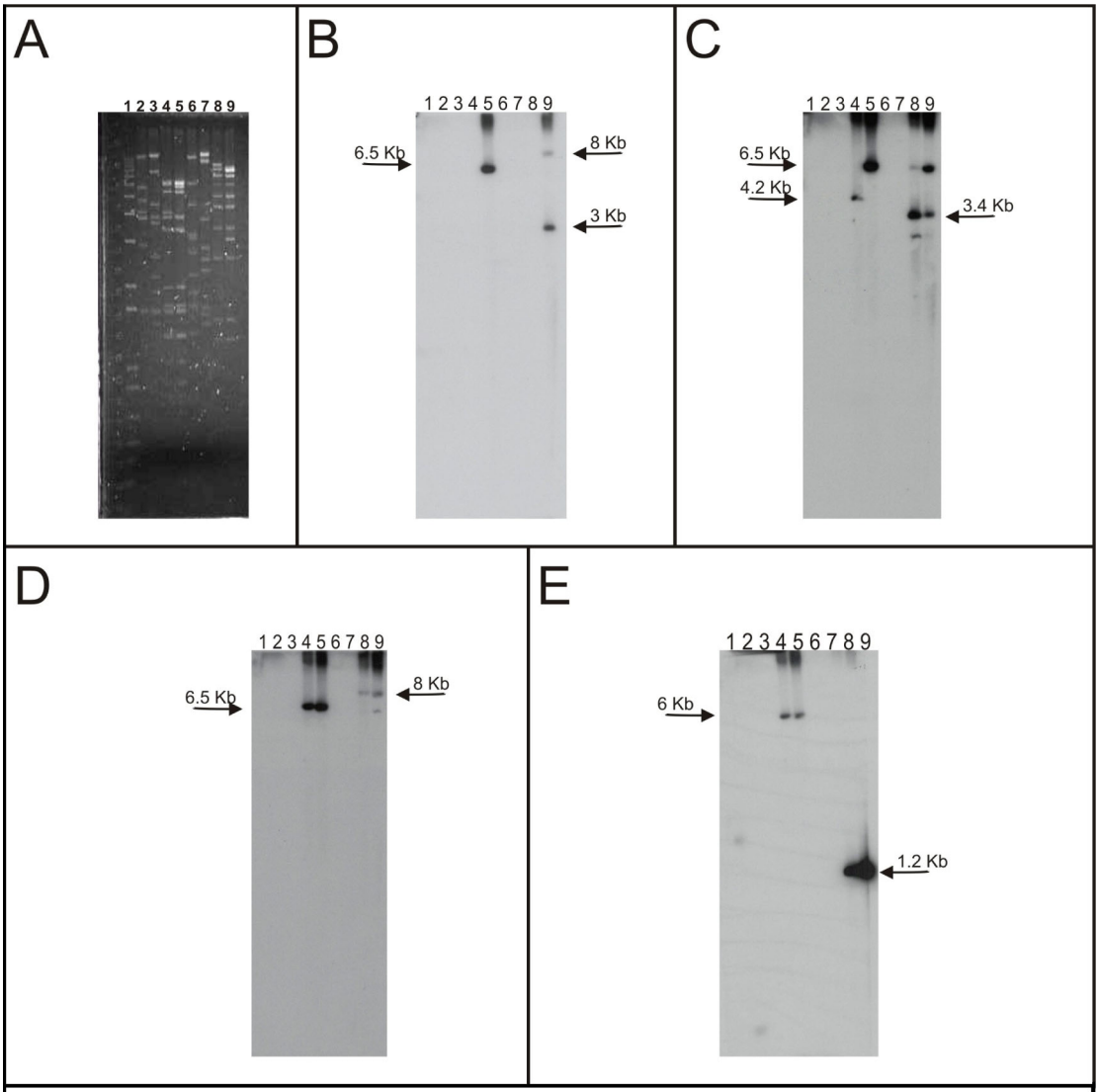

Appendix 5.8. Southern blot analysis of genes present on cosmids 12G8 and 17G5
Autoradiographs of Southern blots containing cosmid DNA digests. Lanes: 1 Kb+ ladder (*lane 1*); cosmid 46D1 *BamHI* diges (*lane 2*); cosmid 8B1 *BamHI* digest (*lane 3*); cosmid 12G8 *BamHI* digest (*lane 4*); cosmid 17G5 *BamHI* digest (*lane 5*); cosmid 46D1 *XhoI* digest (*lane 6*); cosmid 8B1 *XhoI* digest (*lane 7*); cosmid 12G8 *XhoI* digest (*lane* 8); cosmid 17G5 *XhoI* digest (*lane 9*). **A.** Ethidium bromide stained gel of cosmid digests. **B.** Autoradiograph of the Southern blot probed with [^{32}P]-labeled PCR product of c_1006-3F/sid1R primer pair. **C.** Autoradiograph of the Southern blot probed with [^{32}P]-labeled PCR product of c_1085-2F/R primer pair. **D.** Autoradiograph of the Southern blot probed with [^{32}P]-labeled PCR product of f-1,6-bpF/R primer pair. **E.** Autoradiograph of the Southern blot probed with [^{32}P]-labeled PCR product of c_849-1F/R primer pair. A map of cosmid 17G5 obtained by sequencing and primer pairs is shown in Appendix 5.9.

5.9. Appendix 5.9 Southern blot analysis of T-DNA induced deletion in Ag212

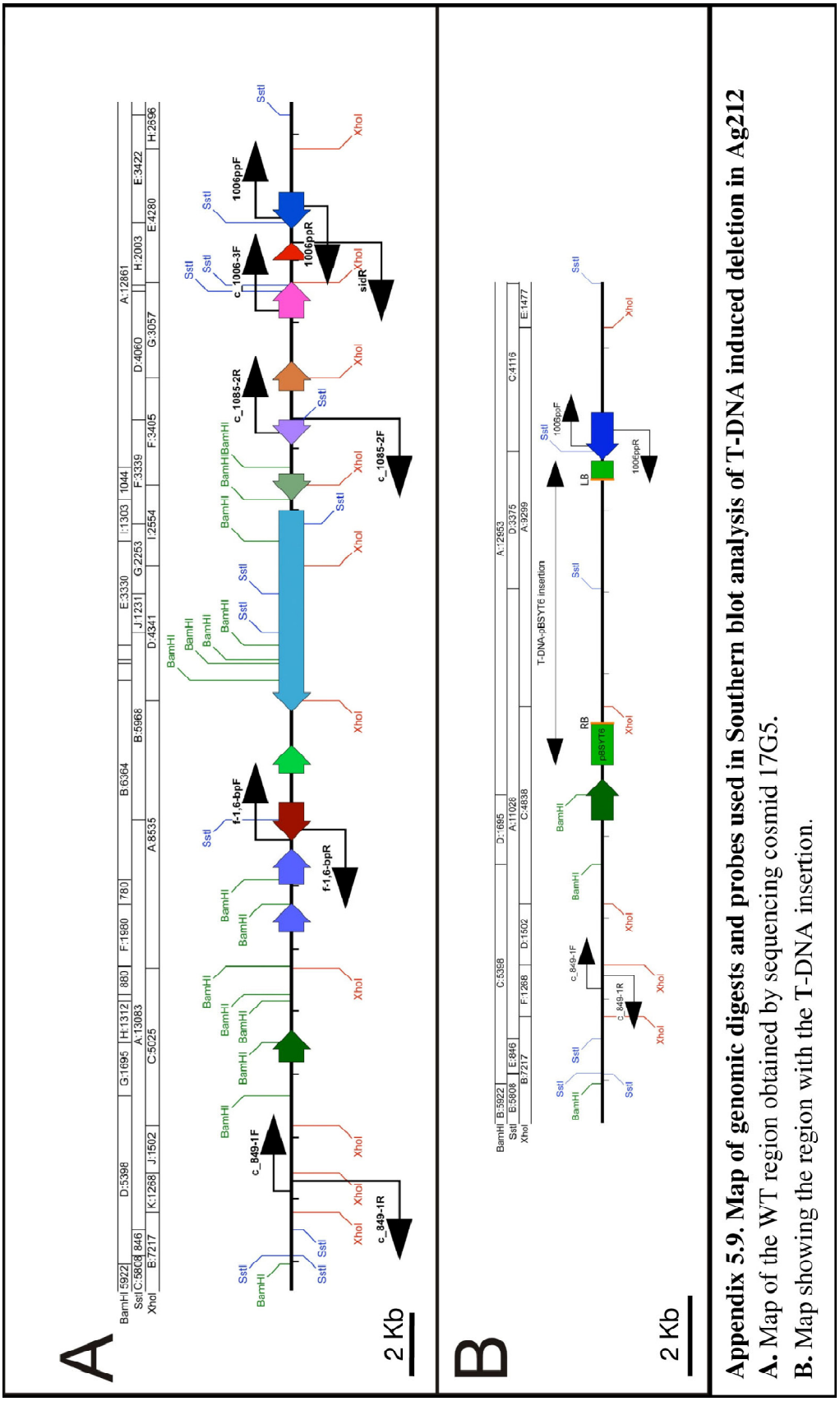

Appendix 5.9. Map of genomic digests and probes used in Southern blot analysis of T-DNA induced deletion in Ag212
A. Map of the WT region obtained by sequencing cosmid 17G5.
B. Map showing the region with the T-DNA insertion.

5.10. Appendix 5.10 E2368 genome database unique gene identifiers of genes used in this study

Table 5.1 *E. festucae* unique gene identifiers of genes mentioned in this study

***E. festucae* gene name**	**Unique gene identifier in the *E. festucae* E2368 genome browser**
cmkA	EfM2.033210_A061106_213_16058_18058_+_Alt0_PolyA
cmkB	EfM2.059570_A061106_418_2746_5054_+_Alt0_PolyA
cmkC	EfM2.024320_A061106_151_41640_44695_-_Alt0_PolyA
cnaA	EfM2.051620_A061106_346_10485_13074_+_Alt0_PolyA
cnaA1	EfM2.114340_A061106_1372_2271_6038_+_Alt0_PolyA
1085-1	EfM2.107560_A061106_1085_268_1483_-_Alt0_PolyA
1085-2	EfM2.107570_A061106_1085_1779_3310_+_Alt0_PolyA
1085-3	EfM2.107590_A061106_1085_3300_4987_+_Alt0_PolyA
1085-4	EfM2.107600_A061106_1085_4957_9279_+_Alt0_PolyA
1085-5	EfM2.107610_A061106_1085_12357_13595_-_Alt0_PolyA
1085-6	EfM2.107630_A061106_1086_1_1066_+_Alt0_noPA
1085-7	Missing in E2368 genome assembly
1085-8	EfM2.118440_A061106_2020_78_927_+_Alt0_PolyA
1006-1	EfM2.104610_A061106_1006_1417_3734_+_Alt0_PolyA
1006-2	EfM2.104620_A061106_1006_4191_5013_+_Alt0_PolyA
1006-3	EfM2.104630_A061106_1006_5233_7616_-_Alt0_PolyA
849-1	EfM2.096250_A061106_849_26645_28222_+_Alt0_PolyA
CRAL-TRIO domain protein	EfM2.069560_A061106_532_10040_11922_+_Alt0_PolyA

6. Bibliography

Arbelet, D., P. Malfatti, E. Simond-Cote, T. Fontaine, L. Desquilbet, D. Expert, C. Kunz & M. C. Soulie, (2010) Disruption of the Bcchs3a Chitin Synthase Gene in *Botrytis cinerea* Is Responsible for Altered Adhesion and Overstimulation of Host Plant Immunity. *Mol Plant Microbe Interact* **23**: 1324-1334.

Arechavaleta, M., C. W. Bacon, C. S. Hoveland & D. E. Radcliffe, (1989) Effect of the tall fescue endophyte on plant response to environmental stress. *Agron J* **81**: 83-90.

Arevalo-Rodriguez, M., X. Pan, J. D. Boeke & J. Heitman, (2004) FKBP12 controls aspartate pathway flux in *Saccharomyces cerevisiae* to prevent toxic intermediate accumulation. *Eukaryot Cell* **3**: 1287-1296.

Basse, C. W., C. Kerschbamer, M. Brustmann, T. Altmann & R. Kahmann, (2002) Evidence for a *Ustilago maydis* steroid 5alpha-reductase by functional expression in Arabidopsis det2-1 mutants. *Plant Physiol* **129**: 717-732.

Beeler, T., K. Gable, C. Zhao & T. Dunn, (1994) A novel protein, CSG2p, is required for Ca^{2+} regulation in *Saccharomyces cerevisiae*. *J Biol Chem* **269**: 7279-7284.

Bencina, M., M. Legisa & N. D. Read, (2005) Cross-talk between cAMP and calcium signalling in *Aspergillus niger*. *Mol Microbiol* **56**: 268-281.

Berridge, M. J., M. D. Bootman & H. L. Roderick, (2003) Calcium signalling: dynamics, homeostasis and remodelling. *Nat Rev Mol Cell Biol* **4**: 517-529.

Binder, U., M. Chu, N. D. Read & F. Marx, (2010) The antifungal activity of the *Penicillium chrysogenum* protein PAF disrupts calcium homeostasis in *Neurospora crassa*. *Eukaryot Cell* **9**: 1374-1382.

Blaise, F., E. Remy, M. Meyer, L. Zhou, J. P. Narcy, J. Roux, M. H. Balesdent & T. Rouxel, (2007) A critical assessment of *Agrobacterium tumefaciens*-mediated transformation as a tool for pathogenicity gene discovery in the phytopathogenic fungus *Leptosphaeria maculans*. *Fungal Genet Biol* **44**: 123-138.

Bootman, M. D., T. J. Collins, C. M. Peppiatt, L. S. Prothero, L. MacKenzie, P. De Smet, M. Travers, S. C. Tovey, J. T. Seo, M. J. Berridge, F. Ciccolini & P. Lipp, (2001) Calcium signalling--an overview. *Semin Cell Dev Biol* **12**: 3-10.

Bormann, J. & P. Tudzynski, (2009) Deletion of Mid1, a putative stretch-activated calcium channel in *Claviceps purpurea*, affects vegetative growth, cell wall synthesis and virulence. *Microbiology* **155**: 3922-3933.

Brand, A., S. Shanks, V. M. Duncan, M. Yang, K. Mackenzie & N. A. Gow, (2007) Hyphal orientation of *Candida albicans* is regulated by a calcium-dependent mechanism. *Curr Biol* **17**: 347-352.

Brown, J. S. & D. W. Holden, (1998) Insertional mutagenesis of pathogenic fungi. *Curr Opin Microbiol* **1**: 390-394.

Bultman, T. L., J. F. White, T. I. Bowdish, A. M. Welch & J. Johnston, (1995) Mutualistic transfer of Epichloë spermatia by Phorbia flies. *Mycologia* **87**: 182-189.

Buscot, F., J. C. Munch, J. Y. Charcosset, M. Gardes, U. Nehls & R. Hampp, (2000) Recent advances in exploring physiology and biodiversity of ectomycorrhizas highlight the functioning of these symbioses in ecosystems. *FEMS Microbiol Rev* **24**: 601-614.

Byrd, A. D., C. L. Schardl, P. J. Songlin, K. L. Mogen & M. R. Siegel, (1990) The beta-tubulin gene of *Epichloe typhina* from perennial ryegrass (*Lolium perenne*). *Curr Genet* **18**: 347-354.

Castle, L. A., D. Errampalli, T. L. Atherton, L. H. Franzmann, E. S. Yoon & D. W. Meinke, (1993) Genetic and molecular characterization of embryonic mutants identified following seed transformation in Arabidopsis. *Mol Gen Genet* **241**: 504-514.

Chayakulkeeree, M., T. C. Sorrell, A. R. Siafakas, C. F. Wilson, N. Pantarat, K. J. Gerik, R. Boadle & J. T. Djordjevic, (2008) Role and mechanism of phosphatidylinositol-specific phospholipase C in survival and virulence of *Cryptococcus neoformans*. *Mol Microbiol* **69**: 809-826.

Cheng, H. & W. J. Lederer, (2008) Calcium sparks. *Physiol Rev* **88**: 1491-1545.

Chi, M. H., S. Y. Park, S. Kim & Y. H. Lee, (2009) A novel pathogenicity gene is required in the rice blast fungus to suppress the basal defenses of the host. *PLoS Pathog* **5**: e1000401.

Chin, D. & A. R. Means, (2000) Calmodulin: a prototypical calcium sensor. *Trends Cell Biol* **10**: 322-328.

Choi, J., Y. Kim, S. Kim, J. Park & Y. H. Lee, (2009a) MoCRZ1, a gene encoding a calcineurin-responsive transcription factor, regulates fungal growth and pathogenicity of *Magnaporthe oryzae*. *Fungal Genet Biol* **46**: 243-254.

Choi, J., J. Park, J. Jeon, M. H. Chi, J. Goh, S. Y. Yoo, J. Park, K. Jung, H. Kim, S. Y. Park, H. S. Rho, S. Kim, B. R. Kim, S. S. Han, S. Kang & Y. H. Lee, (2007)

Genome-wide analysis of T-DNA integration into the chromosomes of *Magnaporthe oryzae*. *Mol Microbiol* **66**: 371-382.

Choi, J. H., Y. Kim & Y. H. Lee, (2009b) Functional analysis of MCNA, a gene encoding a catalytic subunit of calcineurin, in the rice blast fungus *Magnaporthe oryzae*. *J Microbiol Biotechnol* **19**: 11-16.

Choquer, M., E. Fournier, C. Kunz, C. Levis, J. M. Pradier, A. Simon & M. Viaud, (2007) *Botrytis cinerea* virulence factors: new insights into a necrotrophic and polyphageous pathogen. *FEMS Microbiol Lett* **277**: 1-10.

Christensen, M. J., R. J. Bennet & J. Schmid, (2002) Growth of Epichloë/Neotyphodium and p-endophytes in leaves of Lolium and Festuca grasses. *Mycol Res* **106**: 93-106.

Christensen, M. J., R. J. Bennett, H. A. Ansari, H. Koga, R. D. Johnson, G. T. Bryan, W. R. Simpson, J. P. Koolaard, E. M. Nickless & C. R. Voisey, (2008) Epichloë endophytes grow by intercalary hyphal extension in elongating grass leaves. *Fungal Genet Biol* **45**: 84-93.

Cruz, M. C., D. S. Fox & J. Heitman, (2001) Calcineurin is required for hyphal elongation during mating and haploid fruiting in *Cryptococcus neoformans*. *EMBO J* **20**: 1020-1032.

Cui, J., J. A. Kaandorp, O. O. Ositelu, V. Beaudry, A. Knight, Y. F. Nanfack & K. W. Cunningham, (2009a) Simulating calcium influx and free calcium concentrations in yeast. *Cell Calcium* **45**: 123-132.

Cui, J., J. A. Kaandorp, P. M. Sloot, C. M. Lloyd & M. V. Filatov, (2009b) Calcium homeostasis and signaling in yeast cells and cardiac myocytes. *FEMS Yeast Res* **9**: 1137-1147.

Cunningham, K. W. & G. R. Fink, (1996) Calcineurin inhibits VCX1-dependent H^+/Ca^{2+} exchange and induces Ca^{2+} ATPases in *Saccharomyces cerevisiae*. *Mol Cell Biol* **16**: 2226-2237.

Cyert, M. S., R. Kunisawa, D. Kaim & J. Thorner, (1991) Yeast has homologs (CNA1 and CNA2 gene products) of mammalian calcineurin, a calmodulin-regulated phosphoprotein phosphatase. *Proc Natl Acad Sci U S A* **88**: 7376-7380.

Da Silva Ferreira, M. E., T. Heinekamp, A. Hartl, A. A. Brakhage, C. P. Semighini, S. D. Harris, M. Savoldi, P. F. de Gouvea, M. H. de Souza Goldman & G. H. Goldman, (2007) Functional characterization of the *Aspergillus fumigatus* calcineurin. *Fungal Genet Biol* **44**: 219-230.

Davis, T. N., M. S. Urdea, F. R. Masiarz & J. Thorner, (1986) Isolation of the yeast calmodulin gene: calmodulin is an essential protein. *Cell* **47**: 423-431.

Dayton, J. S. & A. R. Means, (1996) Ca^{2+}/calmodulin-dependent kinase is essential for both growth and nuclear division in *Aspergillus nidulans*. *Mol Biol Cell* **7**: 1511-1519.

Dayton, J. S., M. Sumi, N. N. Nanthakumar & A. R. Means, (1997) Expression of a constitutively active Ca^{2+}/calmodulin-dependent kinase in *Aspergillus nidulans* spores prevents germination and entry into the cell cycle. *J Biol Chem* **272**: 3223-3230.

de Jonge, R., H. P. van Esse, A. Kombrink, T. Shinya, Y. Desaki, R. Bours, S. van der Krol, N. Shibuya, M. H. Joosten & B. P. Thomma, (2010) Conserved fungal LysM effector Ecp6 prevents chitin-triggered immunity in plants. *Science* **329**: 953-955.

Denis, V. & M. S. Cyert, (2002) Internal Ca(2+) release in yeast is triggered by hypertonic shock and mediated by a TRP channel homologue. *J Cell Biol* **156**: 29-34.

Dower, W. J., J. F. Miller & C. W. Ragsdale, (1988) High efficiency transformation of *E. coli* by high voltage electroporation. *Nucleic Acids Res* **16**: 6127-6145.

Dunican, D. J. & P. Doherty, (2000) The generation of localized calcium rises mediated by cell adhesion molecules and their role in neuronal growth cone motility. *Molecular Cell Biology Research Communications* **3**: 255-263.

Eaton, C. J., (2009) Investigation of signalling involved in maintaining the mutually beneficial association between *Epichloë festucae* and perennial ryegrass. In: IMBS. Palmerston North: PhD thesis, Massey University, pp. 158.

Eaton, C. J., M. P. Cox, B. Ambrose, M. Becker, U. Hesse, C. L. Schardl & B. Scott, (2010) Disruption of signaling in a fungal-grass symbiosis leads to pathogenesis. *Plant Physiol* **153**: 1780-1794.

Egan, J. D., M. D. Garcia-Pedrajas, D. L. Andrews & S. E. Gold, (2009) Calcineurin is an antagonist to PKA protein phosphorylation required for postmating filamentation and virulence, while PP2A is required for viability in *Ustilago maydis*. *Mol Plant Microbe Interact* **22**: 1293-1301.

Escano, C. S., P. R. Juvvadi, F. J. Jin, T. Takahashi, Y. Koyama, S. Yamashita, J. Maruyama & K. Kitamoto, (2009) Disruption of the Aopex11-1 gene involved

in peroxisome proliferation leads to impaired Woronin body formation in *Aspergillus oryzae*. *Eukaryot Cell* **8**: 296-305.

Feijo, J. A., J. Sainhas, T. Holdaway-Clarke, M. S. Cordeiro, J. G. Kunkel & P. K. Hepler, (2001) Cellular oscillations and the regulation of growth: the pollen tube paradigm. *BioEssays* **23**: 86-94.

Findon, H., A. M. Calcagno-Pizarelli, J. L. Martinez, A. Spielvogel, A. Markina-Inarrairaegui, T. Indrakumar, J. Ramos, M. A. Penalva, E. A. Espeso & H. N. Arst, Jr., (2010) Analysis of a novel calcium auxotrophy in *Aspergillus nidulans*. *Fungal Genet Biol* **47**: 647-655.

Fisk, H. A. & M. P. Yaffe, (1997) Mutational analysis of Mdm1p function in nuclear and mitochondrial inheritance. *J Cell Biol* **138**: 485-494.

Flick, J. S. & J. Thorner, (1993) Genetic and biochemical characterization of a phosphatidylinositol-specific phospholipase C in *Saccharomyces cerevisiae*. *Mol Cell Biol* **13**: 5861-5876.

Foreman, J., V. Demidchik, J. H. Bothwell, P. Mylona, H. Miedema, M. A. Torres, P. Linstead, S. Costa, C. Brownlee, J. D. Jones, J. M. Davies & L. Dolan, (2003) Reactive oxygen species produced by NADPH oxidase regulate plant cell growth. *Nature* **422**: 442-446.

Fortwendel, J. R., P. R. Juvvadi, B. Z. Perfect, L. E. Rogg, J. R. Perfect & W. J. Steinbach, (2010) Transcriptional regulation of chitin synthases by calcineurin controls paradoxical growth of *Aspergillus fumigatus* in response to caspofungin. *Antimicrob Agents Chemother* **54**: 1555-1563.

Fukami, K., (2002) Structure, regulation, and function of phospholipase C isozymes. *J Biochem* **131**: 293-299.

Gallagher, R. T., A. D. Hawkes, P. S. Steyn & R. Vleggaar, (1984) Tremorgenic neurotoxins from perennial ryegrass causing ryegrass staggers disorder of livestock: Structure elucidation of lolitrem B. *J Chem Soc Chem Comm* **1984**: 614-616.

Garrett-Engele, P., B. Moilanen & M. S. Cyert, (1995) Calcineurin, the Ca^{2+}/calmodulin-dependent protein phosphatase, is essential in yeast mutants with cell integrity defects and in mutants that lack a functional vacuolar H^{+}-ATPase. *Mol Cell Biol* **15**: 4103-4114.

Gelvin, S. B., (2003) Agrobacterium-mediated plant transformation: the biology behind the "gene-jockeying" tool. *Microbiol Mol Biol Rev* **67**: 16-37, table of contents.

Glenn, A. E., C. W. Bacon, R. Price & R. T. Hanlin, (1996) Molecular phylogeny of Acremonium and its taxonomic implications. . *Mycologia* **88**: 369-383.

Hahn, H., M. T. McManus, K. Warnstorff, B. J. Monahan, C. A. Young, E. Davies, B. A. Tapper & B. Scott, (2008) Neotyphodium fungal endophytes confer physiological protection to perennial ryegrass (*Lolium perenne L.*) subjected to a water deficit. *Environ Exp Bot* **63**: 183-199.

Halachmi, D. & Y. Eilam, (1989) Cytosolic and vacuolar Ca^{2+} concentrations in yeast cells measured with the Ca^{2+}-sensitive fluorescence dye indo-1. *FEBS Lett* **256**: 55-61.

Hallen, H. E. & F. Trail, (2008) The L-type calcium ion channel cch1 affects ascospore discharge and mycelial growth in the filamentous fungus *Gibberella zeae* (anamorph *Fusarium graminearum*). *Eukaryot Cell* **7**: 415-424.

Iida, H., H. Nakamura, T. Ono, M. S. Okumura & Y. Anraku, (1994) MID1, a novel *Saccharomyces cerevisiae* gene encoding a plasma membrane protein, is required for Ca^{2+} influx and mating. *Mol Cell Biol* **14**: 8259-8271.

Iida, H., Y. Ohya & Y. Anraku, (1995) Calmodulin-dependent protein kinase II and calmodulin are required for induced thermotolerance in *Saccharomyces cerevisiae*. *Curr Genet* **27**: 190-193.

Jackson, S. L. & I. B. Heath, (1993) Roles of calcium ions in hyphal tip growth. *Microbiol Rev* **57**: 367-382.

Jagnandan, D., J. E. Church, B. Banfi, D. J. Stuehr, M. B. Marrero & D. J. Fulton, (2007) Novel mechanism of activation of NADPH oxidase 5. calcium sensitization via phosphorylation. *J Biol Chem* **282**: 6494-6507.

Jeon, J., S. Y. Park, M. H. Chi, J. Choi, J. Park, H. S. Rho, S. Kim, J. Goh, S. Yoo, J. Choi, J. Y. Park, M. Yi, S. Yang, M. J. Kwon, S. S. Han, B. R. Kim, C. H. Khang, B. Park, S. E. Lim, K. Jung, S. Kong, M. Karunakaran, H. S. Oh, H. Kim, S. Kim, J. Park, S. Kang, W. B. Choi, S. Kang & Y. H. Lee, (2007) Genome-wide functional analysis of pathogenicity genes in the rice blast fungus. *Nat Genet* **39**: 561-565.

Joseph, J. D. & A. R. Means, (2000) Identification and characterization of two Ca^{2+}/CaM-dependent protein kinases required for normal nuclear division in *Aspergillus nidulans*. *J Biol Chem* **275**: 38230-38238.

Kaku, H., Y. Nishizawa, N. Ishii-Minami, C. Akimoto-Tomiyama, N. Dohmae, K. Takio, E. Minami & N. Shibuya, (2006) Plant cells recognize chitin fragments

for defense signaling through a plasma membrane receptor. *Proc Natl Acad Sci U S A* **103**: 11086-11091.

Kawahara, T., M. T. Quinn & J. D. Lambeth, (2007) Molecular evolution of the reactive oxygen-generating NADPH oxidase (Nox/Duox) family of enzymes. *BMC Evol Biol* **7**: 109-130.

Kawano, C. Y. & S. Said, (2005) Hyperbranching induced by cold-shock or snow-flake mutation in *Neurospora crassa* is prevented by addition of exogenous calcium. *J Basic Microbiol* **45**: 199-206.

Kaya, H., S. Sato, S. Tabata, Y. Kobayashi, M. Iwabuchi & T. Araki, (2000) hosoba toge toge, a syndrome caused by a large chromosomal deletion associated with a T-DNA insertion in Arabidopsis. *Plant Cell Physiol* **41**: 1055-1066.

Kemppainen, M., A. Circosta, D. Tagu, F. Martin & A. G. Pardo, (2005) Agrobacterium-mediated transformation of the ectomycorrhizal symbiont *Laccaria bicolor* S238N. *Mycorrhiza* **16**: 19-22.

Kim, Y. K., D. Li & P. E. Kolattukudy, (1998) Induction of Ca^{2+}-calmodulin signaling by hard-surface contact primes *Colletotrichum gloeosporioides* conidia to germinate and form appressoria. *J Bacteriol* **180**: 5144-5150.

Kitanovic, A. & S. Wolfl, (2006) Fructose-1,6-bisphosphatase mediates cellular responses to DNA damage and aging in *Saccharomyces cerevisiae*. *Mutat Res* **594**: 135-147.

Kubler, E., F. Schimmoller & H. Riezman, (1994) Calcium-independent calmodulin requirement for endocytosis in yeast. *EMBO J* **13**: 5539-5546.

Kuldau, G. A., H. F. Tsai & C. L. Schardl, (1999) Genome sizes of *Epichloë* species and anamorphic hybrids. *Mycologia* **91**: 776-782.

Kunze, D., I. Melzer, D. Bennett, D. Sanglard, D. MacCallum, J. Norskau, D. C. Coleman, F. C. Odds, W. Schafer & B. Hube, (2005) Functional analysis of the phospholipase C gene CaPLC1 and two unusual phospholipase C genes, CaPLC2 and CaPLC3, of *Candida albicans*. *Microbiology* **151**: 3381-3394.

Lambeth, J. D., (2004) NOX enzymes and the biology of reactive oxygen. *Nat Rev Immunol* **4**: 181-189.

Lardy, B., M. Bof, L. Aubry, M. H. Paclet, F. Morel, M. Satre & G. Klein, (2005) NADPH oxidase homologs are required for normal cell differentiation and morphogenesis in *Dictyostelium discoideum*. *BBA-Mol Cell Res* **1744**: 199-212.

Lassegue, B. & R. E. Clempus, (2003) Vascular NAD(P)H oxidases: specific features, expression, and regulation. *Am J Physiol Regul Integr Comp Physiol* **285**: R277-297.

Latch, G. C. M. & M. J. Christensen, (1985) Artificial infection of grasses with endophytes. *Ann Appl Biol* **107**: 17-24.

Leclerque, A., H. Wan, A. Abschutz, S. Chen, G. V. Mitina, G. Zimmermann & H. U. Schairer, (2004) Agrobacterium-mediated insertional mutagenesis (AIM) of the entomopathogenic fungus *Beauveria bassiana*. *Curr Genet* **45**: 111-119.

Leonard, K. J. & L. J. Szabo, (2005) Stem rust of small grains and grasses caused by *Puccinia graminis*. *Mol Plant Pathol* **6**: 99-111.

Li, G., Z. Zhou, G. Liu, F. Zheng & C. He, (2007) Characterization of T-DNA insertion patterns in the genome of rice blast fungus *Magnaporthe oryzae*. *Curr Genet* **51**: 233-243.

Liu, M., P. Du, G. Heinrich, G. M. Cox & A. Gelli, (2006) Cch1 mediates calcium entry in *Cryptococcus neoformans* and is essential in low-calcium environments. *Eukaryot Cell* **5**: 1788-1796.

Liu, P., R. L. Li, L. Zhang, Q. L. Wang, K. Niehaus, F. Baluska, J. Samaj & J. X. Lin, (2009a) Lipid microdomain polarization is required for NADPH oxidase-dependent ROS signaling in *Picea meyeri* pollen tube tip growth. *Plant J* **60**: 303-313.

Liu, X. H., J. P. Lu, B. Dong, Y. Gu & F. C. Lin, (2009b) Disruption of MoCMK1, encoding a putative calcium/calmodulin-dependent kinase, in *Magnaporthe oryzae*. *Microbiol Res* **165**: 402-410.

Liu, Y. G. & R. F. Whittier, (1995) Thermal asymmetric interlaced PCR: automatable amplification and sequencing of insert end fragments from P1 and YAC clones for chromosome walking. *Genomics* **25**: 674-681.

Liu, Z. M. & P. E. Kolattukudy, (1999) Early expression of the calmodulin gene, which precedes appressorium formation in *Magnaporthe grisea*, is inhibited by self-inhibitors and requires surface attachment. *J Bacteriol* **181**: 3571-3577.

Lohar, D. P., S. Haridas, J. S. Gantt & K. A. VandenBosch, (2007) A transient decrease in reactive oxygen species in roots leads to root hair deformation in the legume-rhizobia symbiosis. *New Phytol* **173**: 39-49.

Ma, Z.-b., L.-j. Sun, J.-x. Zhao, J. Liu & L.-a. Wang, (2010) Two CaMK genes with different biochemical characteristics exist in *Magnaporthe oryzae*. *European Journal of Plant Pathology* **127**: 545-556.

Ma, Z. B., J. X. Zhao, L. A. Wang & X. B. Zheng, (2009) Cloning, prokaryotic expression, and bioactivity of the calmodulin gene of *Magnaporthe grisea*. *FEMS Microbiol Lett* **300**: 107-114.

Malinowski, D. P. & D. P. Belesky, (1999) *Neotyphodium coenophialum*-endophyte infection affects the ability of tall fescue to use sparingly available phosphorus. *J Plant Nutr* **222**: 835-853.

Mattson, M. P., (1999) Establishment and plasticity of neuronal polarity. *J Neurosci Res* **57**: 577-589.

McConnell, S. J. & M. P. Yaffe, (1992) Nuclear and mitochondrial inheritance in yeast depends on novel cytoplasmic structures defined by the MDM1 protein. *J Cell Biol* **118**: 385-395.

Meng, Y., G. Patel, M. Heist, M. F. Betts, S. L. Tucker, N. Galadima, N. M. Donofrio, D. Brown, T. K. Mitchell, L. Li, J. R. Xu, M. Orbach, M. Thon, R. A. Dean & M. L. Farman, (2007) A systematic analysis of T-DNA insertion events in *Magnaporthe oryzae*. *Fungal Genet Biol* **44**: 1050-1064.

Michielse, C. B., P. J. Hooykaas, C. A. van den Hondel & A. F. Ram, (2005) Agrobacterium-mediated transformation as a tool for functional genomics in fungi. *Curr Genet* **48**: 1-17.

Michielse, C. B., R. van Wijk, L. Reijnen, B. J. Cornelissen & M. Rep, (2009) Insight into the molecular requirements for pathogenicity of *Fusarium oxysporum f. sp. lycopersici* through large-scale insertional mutagenesis. *Genome Biol* **10**: R4.

Miller, J., (1972) Experiments in molecular genetics. *Cold Spring Harbor Laboratory Press, New York.*

Moon, C. D., K. D. Craven, A. Leuchtmann, S. L. Clement & C. L. Schardl, (2004) Prevalence of interspecific hybrids amongst asexual fungal endophytes of grasses. *Mol Ecol* **13**: 1455-1467.

Mori, I. C. & J. I. Schroeder, (2004) Reactive oxygen species activation of plant Ca^{2+} channels. A signaling mechanism in polar growth, hormone transduction, stress signaling, and hypothetically mechanotransduction. *Plant Physiol* **135**: 702-708.

Moser, M. J., J. R. Geiser & T. N. Davis, (1996) Ca^{2+}-calmodulin promotes survival of pheromone-induced growth arrest by activation of calcineurin and Ca^{2+}-calmodulin-dependent protein kinase. *Mol Cell Biol* **16**: 4824-4831.

Moy, M., F. Belanger, R. Duncan, A. Freehoff, C. Leary, W. Meyer, R. Sullivan & J. F. White, (2000) Identification of epiphyllous mycelial nets on leaves of grasses infected by clavicipitaceous endophytes. *Symbiosis* **28**: 291-302.

Muller, E. M., E. G. Locke & K. W. Cunningham, (2001) Differential regulation of two Ca^{2+} influx systems by pheromone signaling in *Saccharomyces cerevisiae*. *Genetics* **159**: 1527-1538.

Munch, S., U. Lingner, D. S. Floss, N. Ludwig, N. Sauer & H. B. Deising, (2008) The hemibiotrophic lifestyle of *Colletotrichum species*. *J Plant Physiol* **165**: 41-51.

Munro, C. A., S. Selvaggini, I. de Bruijn, L. Walker, M. D. Lenardon, B. Gerssen, S. Milne, A. J. Brown & N. A. Gow, (2007) The PKC, HOG and Ca^{2+} signalling pathways co-ordinately regulate chitin synthesis in *Candida albicans*. *Mol Microbiol* **63**: 1399-1413.

Nacry, P., C. Camilleri, B. Courtial, M. Caboche & D. Bouchez, (1998) Major chromosomal rearrangements induced by T-DNA transformation in Arabidopsis. *Genetics* **149**: 641-650.

Nakamura, T., Y. Liu, D. Hirata, H. Namba, S. Harada, T. Hirokawa & T. Miyakawa, (1993) Protein phosphatase type 2B (calcineurin)-mediated, FK506-sensitive regulation of intracellular ions in yeast is an important determinant for adaptation to high salt stress conditions. *EMBO J* **12**: 4063-4071.

Namiki, F., M. Matsunaga, M. Okuda, I. Inoue, K. Nishi, Y. Fujita & T. Tsuge, (2001) Mutation of an arginine biosynthesis gene causes reduced pathogenicity in *Fusarium oxysporum* f. sp. *melonis*. *Mol Plant Microbe Interact* **14**: 580-584.

Nelson, G., O. Kozlova-Zwinderman, A. J. Collis, M. R. Knight, J. R. S. Fincham, C. P. Stanger, A. Renwick, J. G. M. Hessing, P. J. Punt, C. A. M. J. J. van den Hondel & N. D. Read, (2004) Calcium measurement in living filamentous fungi expressing codon-optimized aequorin. *Mol Microbiol* **52**: 1437-1450.

Nguyen, Q. B., N. Kadotani, S. Kasahara, Y. Tosa, S. Mayama & H. Nakayashiki, (2008) Systematic functional analysis of calcium-signalling proteins in the genome of the rice-blast fungus, *Magnaporthe oryzae*, using a high-throughput RNA-silencing system. *Mol Microbiol* **68**: 1348-1365.

Ohya, Y., H. Kawasaki, K. Suzuki, J. Londesborough & Y. Anraku, (1991) Two yeast genes encoding calmodulin-dependent protein kinases. Isolation, sequencing and bacterial expressions of CMK1 and CMK2. *J Biol Chem* **266**: 12784-12794.

Oldroyd, G. E. D. & J. A. Downie, (2004) Calcium, kinases and nodulation signalling in legumes. *Nature Reviews Molecular Cell Biology* **5**: 566-576.

Paidhungat, M. & S. Garrett, (1997) A homolog of mammalian, voltage-gated calcium channels mediates yeast pheromone-stimulated Ca^{2+} uptake and exacerbates the cdc1(Ts) growth defect. *Mol Cell Biol* **17**: 6339-6347.

Palmer, C. P., X. L. Zhou, J. Lin, S. H. Loukin, C. Kung & Y. Saimi, (2001) A TRP homolog in *Saccharomyces cerevisiae* forms an intracellular Ca^{2+}-permeable channel in the yeast vacuolar membrane. *Proc Natl Acad Sci U S A* **98**: 7801-7805.

Pareja-Jaime, Y., M. Martin-Urdiroz, M. I. Roncero, J. A. Gonzalez-Reyes & C. Roldan Mdel, (2010) Chitin synthase-deficient mutant of *Fusarium oxysporum* elicits tomato plant defence response and protects against wild-type infection. *Mol Plant Pathol* **11**: 479-493.

Park, S. Y., S. B. Seo, S. J. Lee, J. G. Na & Y. J. Kim, (2001) Mutation in PMR1, a Ca^{2+}-ATPase in Golgi, confers salt tolerance in *Saccharomyces cerevisiae* by inducing expression of PMR2, an Na^{+}-ATPase in plasma membrane. *J Biol Chem* **276**: 28694-28699.

Parniske, M., (2008) Arbuscular mycorrhiza: the mother of plant root endosymbioses. *Nat Rev Microbiol* **6**: 763-775.

Pausch, M. H., D. Kaim, R. Kunisawa, A. Admon & J. Thorner, (1991) Multiple Ca^{2+}/calmodulin-dependent protein kinase genes in a unicellular eukaryote. *EMBO J* **10**: 1511-1522.

Peiter, E., M. Fischer, K. Sidaway, S. K. Roberts & D. Sanders, (2005) The *Saccharomyces cerevisiae* Ca^{2+} channel Cch1pMid1p is essential for tolerance to cold stress and iron toxicity. *FEBS Lett* **579**: 5697-5703.

Perfect, S. E. & J. R. Green, (2008) Infection structures of biotrophic and hemibiotrophic fungal plant pathogens. *Mol Plant Pathol* **2**: 101-108.

Permyakov, E. A. & R. H. Kretsinger, (2009) Cell signaling, beyond cytosolic calcium in eukaryotes. *J Inorg Biochem* **103**: 77-86.

Piers, K. L., J. D. Heath, X. Liang, K. M. Stephens & E. W. Nester, (1996) *Agrobacterium tumefaciens*-mediated transformation of yeast. *Proc Natl Acad Sci U S A* **93**: 1613-1618.

Pinchai, N., P. R. Juvvadi, J. R. Fortwendel, B. Z. Perfect, L. E. Rogg, Y. G. Asfaw & W. J. Steinbach, (2010) The *Aspergillus fumigatus* P-type Golgi apparatus Ca^{2+}/Mn^{2+} ATPase PmrA is involved in cation homeostasis and cell wall integrity but is not essential for pathogenesis. *Eukaryot Cell* **9**: 472-476.

Prokisch, H., O. Yarden, M. Dieminger, M. Tropschug & I. B. Barthelmess, (1997) Impairment of calcineurin function in *Neurospora crassa* reveals its essential role in hyphal growth, morphology and maintenance of the apical Ca^{2+} gradient. *Mol Gen Genet* **256**: 104-114.

Punt, P. J., R. P. Oliver, M. A. Dingemanse, P. H. Pouwels & C. A. van den Hondel, (1987) Transformation of Aspergillus based on the hygromycin B resistance marker from *Escherichia coli*. *Gene* **56**: 117-124.

Punt, P. J. & C. A. van den Hondel, (1992) Transformation of filamentous fungi based on hygromycin B and phleomycin resistance markers. *Methods Enzymol* **216**: 447-457.

Putney, J. W. & G. S. Bird, (2008) Cytoplasmic calcium oscillations and store-operated calcium influx. *J Physiol* **586**: 3055-3059.

Rasmussen, C., C. Garen, S. Brining, R. L. Kincaid, R. L. Means & A. R. Means, (1994) The calmodulin-dependent protein phosphatase catalytic subunit (calcineurin A) is an essential gene in *Aspergillus nidulans*. *EMBO J* **13**: 2545-2552.

Rasmussen, C. D., (2000) Cloning of a calmodulin kinase I homologue from *Schizosaccharomyces pombe*. *J Biol Chem* **275**: 685-690.

Rho, H. S., J. Jeon & Y. H. Lee, (2009) Phospholipase C-mediated calcium signalling is required for fungal development and pathogenicity in *Magnaporthe oryzae*. *Mol Plant Pathol* **10**: 337-346.

Rusnak, F. & P. Mertz, (2000) Calcineurin: form and function. *Physiol Rev* **80**: 1483-1521.

Sanders, D., J. Pelloux, C. Brownlee & J. F. Harper, (2002) Calcium at the crossroads of signaling. *Plant Cell* **14** S401-417.

Schardl, C. L., (1996) Epichloë species: fungal symbionts of grasses. *Annu Rev Phytopathol* **34**: 109-130.

Schardl, C. L., (2001) *Epichloë festucae* and related mutualistic symbionts of grasses. *Fungal Genet Biol* **33**: 69-82.

Schardl, C. L. & K. D. Craven, (2003) Interspecific hybridization in plant-associated fungi and oomycetes: a review. *Mol Ecol* **12**: 2861-2873.

Schardl, C. L., A. Leuchtmann & M. J. Spiering, (2004) Symbioses of grasses with seedborne fungal endophytes. *Annu Rev Plant Biol* **55**: 315-340.

Schmid, J. & F. M. Harold, (1988) Dual roles for calcium ions in apical growth of *Neurospora crassa*. *J Gen Microbiol* **134**: 2623-2631.

Schmid, J., M. J. Spiering & M. J. Christensen, (2000) Metabolic activity, distribution and propagation of grass endophytes *in planta*. Investigations using the GUS system. In: Microbial Endophytes. J. F. White & C. W. Bacon (eds). New York: Marcel Dekker, pp. 295-322.

Schmitz, H. P. & J. J. Heinisch, (2003) Evolution, biochemistry and genetics of protein kinase C in fungi. *Curr Genet* **43**: 245-254.

Schulte, U., (2001) Biogenesis of respiratory complex I. *J Bioenerg Biomembr* **33**: 205-212.

Schumacher, J., I. F. de Larrinoa & B. Tudzynski, (2008a) Calcineurin-responsive zinc finger transcription factor CRZ1 of *Botrytis cinerea* is required for growth, development, and full virulence on bean plants. *Eukaryot Cell* **7**: 584-601.

Schumacher, J., M. Viaud, A. Simon & B. Tudzynski, (2008b) The G-alpha subunit BCG1, the phospholipase C (BcPLC1) and the calcineurin phosphatase co-ordinately regulate gene expression in the grey mould fungus *Botrytis cinerea*. *Mol Microbiol* **67**: 1027-1050.

Scott, B. & C. Schardl, (1993) Fungal symbionts of grasses: evolutionary insights and agricultural potential. *Trends Microbiol* **1**: 196-200.

Scott, D. B., D. Takemoto, A. Tanaka, C. A. Young, M. K. Bryant & K. J. May, (2007) Functional analysis of the *Epichloë festucae*-perennial ryegrass symbiosis. In: New Zealand Grassland Association: Endophyte Symposium 433-441. pp.

Semighini, C. P. & S. D. Harris, (2008) Regulation of apical dominance in *Aspergillus nidulans* hyphae by reactive oxygen species. *Genetics* **179**: 1919-1932.

Shirai, Y. & N. Saito, (2002) Activation mechanisms of protein kinase C: maturation, catalytic activation, and targeting. *J Biochem* **132**: 663-668.

Silverman-Gavrila, L. B. & R. R. Lew, (2002) An IP3-activated Ca^{2+} channel regulates fungal tip growth. *J Cell Sci* **115**: 5013-5025.

Silverman-Gavrila, L. B. & R. R. Lew, (2003) Calcium gradient dependence of *Neurospora crassa* hyphal growth. *Microbiology* **149**: 2475-2485.

Solomon, P. S., K. Rybak, R. D. Trengove & R. P. Oliver, (2006) Investigating the role of calcium/calmodulin-dependent protein kinases in *Stagonospora nodorum*. *Mol Microbiol* **62**: 367-381.

Spiers, A. G. & D. H. Hopcroft, (1993) Black canker and leaf spot of Salix in New Zealand caused by *Glomerella miyabeana* (*Colletotrichum gloeosporioides*). *Eur J Forest Pathol* **23**: 92-102.

Steinbach, W. J., R. A. Cramer, Jr., B. Z. Perfect, Y. G. Asfaw, T. C. Sauer, L. K. Najvar, W. R. Kirkpatrick, T. F. Patterson, D. K. Benjamin, Jr., J. Heitman & J. R. Perfect, (2006) Calcineurin controls growth, morphology, and pathogenicity in *Aspergillus fumigatus*. *Eukaryot Cell* **5**: 1091-1103.

Stie, J. & D. Fox, (2008) Calcineurin regulation in fungi and beyond. *Eukaryot Cell* **7**: 177-186.

Swulius, M. & M. Waxham, (2008) Ca^{2+}/calmodulin-dependent protein kinases. *Cellular and Molecular Life Sciences* **65**: 2637-2657.

Szigeti, R., A. Miseta & R. Kellermayer, (2005) Calcium and magnesium competitively influence the growth of a PMR1 deficient *Saccharomyces cerevisiae* strain. *FEMS Microbiol Lett* **251**: 333-339.

Takano, Y., N. Takayanagi, H. Hori, Y. Ikeuchi, T. Suzuki, A. Kimura & T. Okuno, (2006) A gene involved in modifying transfer RNA is required for fungal pathogenicity and stress tolerance of *Colletotrichum lagenarium*. *Mol Microbiol* **60**: 81-92.

Takemoto, D., A. Tanaka & B. Scott, (2006) A p67Phox-like regulator is recruited to control hyphal branching in a fungal-grass mutualistic symbiosis. *Plant Cell* **18**: 2807-2821.

Takemoto, D., A. Tanaka & B. Scott, (2007) NADPH oxidases in fungi: diverse roles of reactive oxygen species in fungal cellular differentiation. *Fungal Genet Biol* **44**: 1065-1076.

Tanaka, A., M. J. Christensen, D. Takemoto, P. Park & B. Scott, (2006) Reactive oxygen species play a role in regulating a fungus-perennial ryegrass mutualistic interaction. *Plant Cell* **18**: 1052-1066.

Tanaka, A., M. J. Christensen, D. Takemoto & B. Scott, (2007a) Endophyte production of rective oxygen specias is critical for maintaining the mutualistic interaction

between *Epichloë festucae* and Pooid grasses. In: New Zealand Grassland Association: Endophyte Symposium. pp. 185-188.

Tanaka, A., D. Takemoto, G. S. Hyon, P. Park & B. Scott, (2008) NoxA activation by the small GTPase RacA is required to maintain a mutualistic symbiotic association between *Epichloë festucae* and perennial ryegrass. *Mol Microbiol* **68**: 1165-1178.

Tanaka, A., B. A. Tapper, A. Popay, E. J. Parker & B. Scott, (2005) A symbiosis expressed non-ribosomal peptide synthetase from a mutualistic fungal endophyte of perennial ryegrass confers protection to the symbiotum from insect herbivory. *Mol Microbiol* **57**: 1036-1050.

Tanaka, A., R. E. Wrenn, D. Takemoto & D. B. Scott, (2007b) *Agrobacterium tumefaciens* T-DNA mediated transformation of *Epichloë festucae*. In: The 6th International Symposium on Fungal Endophytes of Grasses. E. S. Popay A. (ed). pp. 469-472.

Terauchi, R. & G. Kahl, (2000) Rapid isolation of promoter sequences by TAIL-PCR: the 5'-flanking regions of Pal and Pgi genes from yams (Dioscorea). *Mol Gen Genet* **263**: 554-560.

Tisi, R., S. Baldassa, F. Belotti & E. Martegani, (2002) Phospholipase C is required for glucose-induced calcium influx in budding yeast. *FEBS Lett* **520**: 133-138.

Torralba, S. & I. B. Heath, (2001) Cytoskeletal and Ca^{2+} regulation of hyphal tip growth and initiation. *Curr Top Dev Biol* **51**: 135-187.

Torres, M. A., H. Onouchi, S. Hamada, C. Machida, K. E. Hammond-Kosack & J. D. Jones, (1998) Six *Arabidopsis thaliana* homologues of the human respiratory burst oxidase (gp91phox). *Plant J* **14**: 365-370.

Valle-Aviles, L., S. Valentin-Berrios, R. R. Gonzalez-Mendez & N. Rodriguez-Del Valle, (2007) Functional, genetic and bioinformatic characterization of a calcium/calmodulin kinase gene in *Sporothrix schenckii*. *BMC Microbiol* **7**: 107.

van den Burg, H. A., S. J. Harrison, M. H. Joosten, J. Vervoort & P. J. de Wit, (2006) *Cladosporium fulvum* Avr4 protects fungal cell walls against hydrolysis by plant chitinases accumulating during infection. *Mol Plant Microbe Interact* **19**: 1420-1430.

Vieira, J. & J. Messing, (1987) Production of single-stranded plasmid DNA. *Methods Enzymol* **153**: 3-11.

Walton, F. J., A. Idnurm & J. Heitman, (2005) Novel gene functions required for melanization of the human pathogen *Cryptococcus neoformans*. *Mol Microbiol* **57**: 1381-1396.

Watts, H. J., A. A. Very, T. H. Perera, J. M. Davies & N. A. Gow, (1998) Thigmotropism and stretch-activated channels in the pathogenic fungus *Candida albicans*. *Microbiology* **144** 689-695.

Wei, C., X. Wang, M. Chen, K. Ouyang, L. S. Song & H. Cheng, (2009) Calcium flickers steer cell migration. *Nature* **457**: 901-905.

Wiesenberger, G., K. Steinleitner, R. Malli, W. F. Graier, J. Vormann, R. J. Schweyen & J. A. Stadler, (2007) Mg^{2+} deprivation elicits rapid Ca^{2+} uptake and activates Ca^{2+}/calcineurin signaling in *Saccharomyces cerevisiae*. *Eukaryot Cell* **6**: 592-599.

Wymer, C. L., T. N. Bibikova & S. Gilroy, (1997) Cytoplasmic free calcium distributions during the development of root hairs of *Arabidopsis thaliana*. *Plant J* **12**: 427-439.

Yan, Y., C. L. Wei, W. R. Zhang, H. P. Cheng & J. Liu, (2006) Cross-talk between calcium and reactive oxygen species signaling. *Acta Pharmacologica Sinica* **27**: 821-826.

Yang, J., H. A. Kang, S. M. Ko, S. K. Chae, D. D. Ryu & J. Y. Kim, (2001a) Cloning of the *Aspergillus niger pmrA* gene, a homologue of yeast PMR1, and characterization of a *pmrA* null mutant. *FEMS Microbiol Lett* **199**: 97-102.

Yang, Y., P. Cheng, G. Zhi & Y. Liu, (2001b) Identification of a calcium/calmodulin-dependent protein kinase that phosphorylates the *Neurospora* circadian clock protein FREQUENCY. *J Biol Chem* **276**: 41064-41072.

Yang, Z., (1998) Signaling tip growth in plants. *Curr Opin Plant Biol* **1**: 525-530.

Yoko-o, T., Y. Matsui, H. Yagisawa, H. Nojima, I. Uno & A. Toh-e, (1993) The putative phosphoinositide-specific phospholipase C gene, PLC1, of the yeast *Saccharomyces cerevisiae* is important for cell growth. *Proc Natl Acad Sci U S A* **90**: 1804-1808.

Yoshida, T., T. Toda & M. Yanagida, (1994) A calcineurin-like gene ppb1+ in fission yeast: mutant defects in cytokinesis, cell polarity, mating and spindle pole body positioning. *J Cell Sci* **107**: 1725-1735.

Young, C. A., M. K. Bryant, M. J. Christensen, B. A. Tapper, G. T. Bryan & B. Scott, (2005a) Molecular cloning and genetic analysis of a symbiosis-expressed gene

cluster for lolitrem biosynthesis from a mutualistic endophyte of perennial ryegrass. *Mol Genet Genomics* **274**: 13-29.

Young, C. A., M. K. Bryant, M. J. Christensen, B. A. Tapper, G. T. Bryan & B. Scott, (2005b) Molecular cloning and genetic analysis of a symbiosis-expressed gene cluster for lolitrem biosynthesis from a mutualistic endophyte of perennial ryegrass. *Mol Gen Genom (submitted).*

Zelter, A., M. Bencina, B. J. Bowman, O. Yarden & N. D. Read, (2004) A comparative genomic analysis of the calcium signaling machinery in *Neurospora crassa*, *Magnaporthe grisea*, and *Saccharomyces cerevisiae*. *Fungal Genet Biol* **41**: 827-841.

Zhang, H., Q. Zhao, K. Liu, Z. Zhang, Y. Wang & X. Zheng, (2009) MgCRZ1, a transcription factor of *Magnaporthe grisea*, controls growth, development and is involved in full virulence. *FEMS Microbiol Lett* **293**: 160-169.

Zhou, X. L., A. F. Batiza, S. H. Loukin, C. P. Palmer, C. Kung & Y. Saimi, (2003) The transient receptor potential channel on the yeast vacuole is mechanosensitive. *Proc Natl Acad Sci U S A* **100**: 7105-7110.

Zhu, C., J. Wu & C. He, (2010) Induction of chromosomal inversion by integration of T-DNA in the rice genome. *J Genet Genomics* **37**: 189-196.

Zipfel, C., (2008) Pattern-recognition receptors in plant innate immunity. *Curr Opin Immunol* **20**: 10-16.